

SKB

**TECHNICAL
REPORT**

91-12

**Numerical groundwater flow
calculations at the Finnsjön site**

Björn Linddom, Anders Boghammar, Hans Lindberg,
Jan Bjelkås

KEMAKTA Consultants CO., Stockholm

February 1991

SVENSK KÄRNBRÄNSLEHANTERING AB

SWEDISH NUCLEAR FUEL AND WASTE MANAGEMENT CO

BOX 5864 S-102 48 STOCKHOLM

TEL 08-665 28 00 TELEX 13108 SKB S

TELEFAX 08-661 57 19

NUMERICAL GROUNDWATER FLOW CALCULATIONS AT THE FINNSJÖN
SITE

Björn Lindbom, Anders Boghammar, Hans Lindberg,
Jan Bjelkås

Kemakta Consultants Co., Stockholm

February 1991

This report concerns a study which was conducted for SKB. The conclusions and viewpoints presented in the report are those of the author(s) and do not necessarily coincide with those of the client.

Information on SKB technical reports from 1977-1978 (TR 121), 1979 (TR 79-28), 1980 (TR 80-26), 1981 (TR 81-17), 1982 (TR 82-28), 1983 (TR 83-77), 1984 (TR 85-01), 1985 (TR 85-20), 1986 (TR 86-31), 1987 (TR 87-33), 1988 (TR 88-32) and 1989 (TR 89-40) is available through SKB.

Numerical Groundwater Flow Calculations

at the Finnsjön Site

by

Björn Lindbom
Anders Boghammar
Hans Lindberg
Jan Bjelkås

Kemakta Consultants Co., Stockholm, Sweden

Abstract

The Swedish Nuclear Fuel and Waste Management Company (SKB) has initiated a research project called SKB 91, which is related to performance assessment of repositories for high level waste from nuclear power plants. Specifically the Finnsjön site is of concern. As part of this research project, the present report describes groundwater flow calculations at the Finnsjön site, located in northern Uppland, approximately 150 km north of Stockholm. The calculations have been performed with the finite element method applying the porous media approach. The project comprises three steps, the first of which is concerned with the presence of salt below a hydraulically significant structure. This step was modelled in two dimensions in a semi-generic fashion, while the two following steps comprised three-dimensional modelling of the site at a semi-regional and a local scale.

The semi-regional model covered approximately 43 km² while the area of the local model was roughly 6.6 km². The semi-regional model included well expressed regional fracture zones that were explicitly modelled in a deterministic manner. Apart from a few of these regional fracture zones present on the semi-regional scale, the local model also consisted of some minor, less expressed local fracture zones. These were implicitly modelled in a manner so that their hydraulic properties were averaged over the elements that were crossed by these zones. In order not to have the fracture properties averaged over too large distances, the mesh on the local scale was extremely fine discretised.

The modelling was performed with the finite element code NAMMU, used together with the program-package HYPAC. The latter was used for pre- and postprocessing purposes. The modelling was performed with 8-noded brick elements for the three-dimensional calculations, and the two-dimensional model involved the use of 8-noded rectangular elements. NAMMU and HYPAC are both implemented on a Convex computer, model C-210.

The present report is a revised version of a report previously published as a working report. The difference between the present report and the previous one, is that the present report describes the conclusions more site-specifically, the presentation of a number of the cases tackled has been pruned down, some editorial effort has been put into having the volume of the report reduced, and finally the Summary has been edited and cut down.

The project has been carried out under contract from SKB. The background data has been supplied by the Swedish Geological Company (SGAB).

Stockholm, February, 1991.

Summary

The Swedish Nuclear Fuel and Waste Management Company (SKB) has initiated a research project called SKB 91, which is related to performance assessment of repositories for high level waste from nuclear power plants. Specifically the Finnsjön site is of concern. As part of this research project, the present report describes deterministic groundwater flow calculations at the Finnsjön site, located in northern Uppland, approximately 150 km north of Stockholm. The calculations have been performed with the use of the NAMMU-code which is based on the finite element method. The flow in both the fracture zones and the interlying rock mass is assumed to obey Darcy's law, i.e. the medium in which the flow takes place is regarded as porous. The project comprised three steps, the first of which is concerned with the presence of salt below a hydraulically significant structure. This step was modelled in two dimensions in a semi-generic fashion, while steps two and three comprised three-dimensional modelling of the site at a semi-regional and a local scale, respectively.

Modelling of Saline Water (2D)

Saline groundwater has been encountered in and below the hydraulically significant subhorizontal fracture zone 2. The presence of salt was modelled as an increased density where occurring. Since the modelling was performed in a semi-generic fashion with little or no knowledge about the boundary conditions in nature, the results from the two-dimensional modelling of the saline water have to be regarded and evaluated in a qualitative manner as a result of "scoping" calculations.

Two sets of lateral boundary conditions were prescribed, so that they were regarded either as no-flow or hydrostatic boundaries. The increased density caused by the presence of salt together with the inclination of zone 2, created a density-dependent flow below zone 2, whereas the flow above the zone was seemingly unaffected by the higher density below zone 2. The flow below zone 2 thus mainly depends on the salinity of the groundwater and the inclination of zone 2, which implies that the groundwater would have been stagnant below zone 2, had the zone been horizontal.

The saline groundwater below zone 2 is flowing in the opposite direction if compared to the fresh-water case, due to the fact that zone 2 has an inclination opposite to the regional gradient. This implies that the discharge at the lateral boundary in the fresh-water cases has been moved downwards through the domain resulting in stagnation points for the flow paths studied. The fluxes below zone 2 were increased with roughly a factor of ten when saline water was considered. Typical flux values are in the order of 30-300 ml/m²/year at z=-500 m in the middle of the domain. However, the density-dependent flow is not yet fully understood, since the lateral boundary conditions are uncertain and the spatial distribution of salt is unknown in the area. The presence of salt was therefore not considered for the following three-dimensional calculations.

Modelling on the Semi-regional Scale (3D)

The semi-regional model covered approximately 43 km² and included well expressed regional fracture zones that were explicitly modelled. The intention of the modelling of the semi-regional scale, was to analyse the impact on the overall flow system of different assumptions with regard to the hydraulic conductivities of the rock mass and the fracture zones. This was achieved by means of parameter variations of the hydraulic conductivities of the rock mass and the fracture zones. Furthermore, the calculated pressure distribution was intended to be used for a transfer of boundary conditions to the local scale model.

The natural groundwater flow in zone 2 had been estimated using the results from field measurements. The calculated flow rates in zone 2 were to be calibrated in a rough sense against the estimated natural ones. To this end, zone 2 was modelled according to a base case concept, and optionally as extended southward to intersect with Lake Finnsjön. The calculations indicated that the model set-up for a base case with reference values could be considered calibrated, since the amount of water estimated as the natural flow through zone 2 was achieved with this case.

The general flow was directed from south-west to north-east with rather gentle fluctuations in the topographic gradient. The results on the semi-regional scale indicated that the model seemed to be rather insensitive to the different assumptions with regard to the hydraulic conductivities. It was also shown that the fracture zones are important for the flow on the semi-regional scale. This was particularly indicated by the generated particle tracks for a case when the entire domain was treated as rock mass. The calculated flowpaths indicated a strong clustering at the same discharge point for all cases, except for the latter case.

The flux distribution within the potential repository indicated that values of about 100 ml/m²/year were representative for the base case formulation. The different cases differ internally more or less only by a scaling factor corresponding to the changes introduced in terms of hydraulic conductivities for the rock mass. The importance of the fracture zones were also shown by the fact that about 99% of the infiltrating water entered the model through the top surfaces of the fracture zones.

Modelling on the Local Scale (3D)

The areal coverage of the local scale model was approximately 6.6 km². Apart from the bounding fracture zones that were present on the semi-regional scale, a set of local fracture zones were included in the model. These were modelled in an implicit manner by averaging their properties over the finite elements, the positions of which do not necessarily correspond to the strikes and inclinations of the fracture zones. The flow on the local scale was governed by the topography, and the major flow pattern was directed towards the intersection between three fracture zones in the upper north-east corner.

Five cases were studied. Two of these involved lateral boundary conditions that were transferred from the semi-regional scale, while the three remaining cases had no-flow lateral boundaries. The sensitivity of the model to different representations of the upper boundary conditions were examined for two of the latter cases.

The model appeared to be rather insensitive to the type of boundary condition applied along the top surface for this specific project. The differences in the description of the groundwater topography between the regional and local scale (in terms of local fluctuations on the local scale) were not large enough to affect the flow situation on the local scale, and should be seen as an evidence of that the flow also on the local scale was governed by the underlying regional topography. On the other hand, the model appeared to be extremely sensitive to the artificially introduced vertical gradient stemming from the way in which the transferred boundary conditions were calculated. These gradients were introduced since pressure values in the semi-regional model at nodes located outside the local domain also contributed to the pressure to be prescribed to the nodes located at the very confinement of the local model. This effect was analysed and found not to affect the flow situation in the inner part of the domain.

The particle tracks, that were released in the northern block at the position corresponding to the potential repository, indicated that the overall flow pattern is similar to that on the semi-regional scale. The transfer of boundary pressure seemed to yield pathlines that had exit points that corresponded to those on the semi-regional scale. The flowpaths for the cases with no-flow boundaries had, due to the boundary condition, their exit points at the top surface or close to it.

It could be noticed that none of the released particle tracks crossed zone 1 on their way to the exit point, i.e. all the pathlines that were studied had their release points and exit points in the northern block, or at the border between the northern and the southern block.

The calculated flux distribution indicated that the fluxes were increased in the area due to the presence of the local fracture zones. The increased fluxes occurred preferably in the vicinity of the fracture zones. Representative values were about 100 ml/m²/year in the rock mass at repository level. About 90 % of the area at 500 m below ground surface had flux values lower than 300 ml/m²/year when the local fracture zones were omitted. Corresponding value for the cases when local fracture zones were modelled was 65-70 %. It was also shown that three cases with either transferred or no-flow lateral boundaries and either semi-regional or local topography prescribed, had flux distributions that were in almost perfect agreement. This would imply that neither the type of lateral boundary, nor the type of upper boundary is as important as the local fracture zones for this study, as far as fluxes at repository level are concerned. An average hydraulic gradient of about 0.009 was at hand at repository level.

Water balance calculations in zone 2 showed that regardless of which case that was studied, the calculated flow rate was within the range that was specified as the natural groundwater flow through zone 2. Zone 2 was recharged with roughly 165000 m³/year (corresponding to about 40 mm/year) through its top confinement, while it was recharged with about half that amount of water from its surrounding fracture zones. These values are valid for the base case formulation where implicitly modelled local fracture zones contributed to the recharge through the top boundary of zone 2 by roughly 65000 m³/year.

Generally, the results have indicated that there are rather modest deviations internally between the cases in terms of pressure distribution, flow paths, and flow rates in zone 2. The similarity between all the cases thus offers a possibility to appoint either of the cases as the most suitable model for future use within the framework of SKB 91. If there is a wish for bringing in as much detailed knowledge as possible into future modelling exercises, there would be a preference to appoint the case with no-flow lateral boundaries and the local topography for these purposes.

General Remarks

A number of uncertainty sources were pointed at in this study. These can be referred to either as site-specific or as model-specific. The three main sources are:

- The hydraulic conductivities of the fracture zones in general, and for zone 2 in particular. The hydraulic significance of zone 2 is indisputable, but there is a need for further investigations as to whether or not an alternative interpretation of the conductivities of zone 2 affects the results to a significant degree. It is still uncertain if the conductivity of zone 2 is depth dependent or not. The hydraulic conductivity of zone 2 affects the amount of water to be discharged at the north-western corner; the major discharge point within the domain. The conductivities for the remaining zones affect the flow by the amount of water to be infiltrated through their top surfaces.
- The upper boundary condition. This was represented differently on the two scales. It is of major concern to find out to what degree the semi-regional topography affected the results on the local scale when applied at the top of the local mesh.
- The lateral boundary conditions. It was elucidated in the report, that the results suffer from uncertainties to some extent by the use of transferred lateral boundary conditions. It was shown within this study that these uncertainties affect the flow situation in a local sense just by the boundaries. However, a quantitative statement in this context would be of utmost use; not only for this project but also for future studies involving modelling at different scales with a transfer of boundary conditions.

The three main sources of uncertainty mentioned above all have an impact on the flow situation within the present study. If sensitivity analyses are to be performed for the results presented here, it would be useful if these could be oriented towards investigations of the impact on the fluxes at repository level, and towards the calculated groundwater flow in zone 2 against which the model results were calibrated in a rough sense.

Table of Contents

Page

ABSTRACT	i
SUMMARY	iii
1. INTRODUCTION	1
1.1 Background	1
1.2 Purpose and Scope of the Project	2
2. MATHEMATICAL MODEL	4
2.1 General	4
2.2 Brief Description of NAMMU	6
2.3 Brief Description of HYPAC	7
3. GEOHYDROLOGY AT THE FINNSJÖN SITE	8
3.1 General	8
3.2 Division of the Domain into a Semi-Regional and a Local Scale	8
3.3 Brief Description of the Hydrology	13
3.4 Hydraulic Properties of the Rock Mass	13
3.5 Hydraulic Properties of the Fracture Zones	14
3.6 Presence of Salt	17
4. MODELLING STRATEGY	18
4.1 General	18
4.2 Modelling of the Presence of Salt in Two Dimensions	18
4.3 Modelling in Three Dimensions of the Semi-Regional Area	19
4.4 Modelling in Three Dimensions of the Local Area	19
5. TWO-DIMENSIONAL MODELLING OF THE PRESENCE OF SALT	20
5.1 Introduction	20
5.2 Discretisation of the Domain	20
5.3 Case Definitions – Nomenclature, Hydraulic Properties, and Boundary Conditions	20
5.4 Modelling Results	22
5.4.1 Flux Distribution	22
5.4.2 Particle Tracking	26
5.5 Conclusions	28

6.	THREE-DIMENSIONAL MODELLING ON THE SEMI-REGIONAL SCALE	29
6.1	Introduction	29
6.2	Discretisation of the Domain	29
6.3	Case Definitions – Nomenclature, Hydraulic Properties, and Boundary Conditions	30
6.4	Modelling Results	31
6.4.1	General	31
6.4.2	Pressure Distribution	32
6.4.3	Particle Tracking	36
6.4.4	Flux Distribution in the Potential Repository	39
6.4.5	Evaluation of the Extension of Zone 2 Towards Lake Finnsjön	41
6.5	Summing up	45
7.	THREE-DIMENSIONAL MODELLING ON A LOCAL SCALE	46
7.1	Introduction	46
7.2	Discretisation of the Domain	48
7.3	Case Definitions – Nomenclature, Hydraulic Properties, and Boundary Conditions	49
7.4	Modelling Results	51
7.4.1	General	51
7.4.2	Pressure Distribution	52
7.4.3	Particle Tracking	59
7.4.4	Flux Distribution in the Potential Repository	63
7.4.5	Mass Balance Calculation Around Zone 2	68
7.4.6	Investigation of Transferred Lateral Boundary Conditions	72
7.4.7	Global Mass Balance	73
7.5	Summing up	73
8.	SUMMING UP OF TECHNICAL ASPECTS	76
9.	CONCLUSIONS	78

REFERENCES

LIST OF SYMBOLS

- APPENDIX A** Evaluation figures associated with the modelling on the semi-regional scale.
- APPENDIX B** Evaluation figures associated with the modelling on the local scale.
- APPENDIX C** List of files created and processed during the course of the project.
- APPENDIX D** Description of the technique for modelling fracture zones implicitly.

1. Introduction

1.1 Background

The Swedish Nuclear Fuel and Waste Management Company (SKB) has initiated a research project called SKB 91, which is related to safety assessment of potential disposal sites for spent nuclear fuel, and more specifically to the Finnsjön site. These deposits will be located in crystalline bed-rock. The most plausible transport for radio-nuclides to reach the accessible environment is by migration with the groundwater. To analyse the impact that could be expected from different scenarios with respect to the significance of fracture zones, assumptions regarding conservative estimates of hydraulic properties of the rock-mass and the fracture zones etc, one part of the SKB 91 research programme is devoted to groundwater flow modelling on a far-field scale relative to a potential repository.

The present report forms part of SKB 91 in terms of numerical groundwater flow modelling at the Finnsjön site, which is located about 100 km north of Stockholm. Figure 1.1 displays the approximate location of the site, along with an indication of the division of the region into three scales, which will be discussed further on in the report. The site has been thoroughly investigated in the context of radio-active waste disposal research. The evaluations from investigations conducted at the site have been compiled and put together in a report by /Andersson, J-E et al, 1989/, which forms the entire background material for the present report. The former report will from now on be referred to as the "Background report". Data relevant to the present project have been extracted from the Background report. Further, supplementary information needed has been made available through personal conversations and discussions with the authors of the Background report.

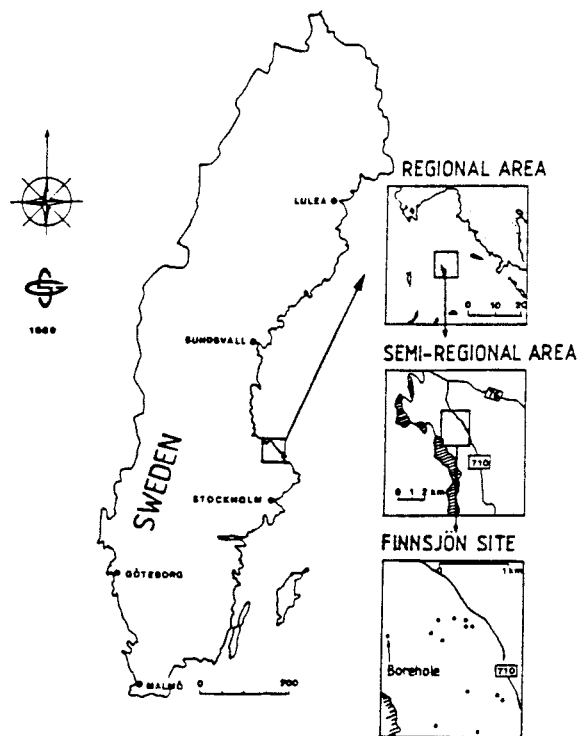


Figure 1.1 Map of Sweden indicating the location of the Finnsjön research area. (From /Ahlbom, K., et al, 1989/)

1.2 Purpose and Scope of the Project

The purpose of the present project is primarily to obtain increased knowledge of the flow situation at the Finnsjön site by the termination of the field activities, and to develop the numerical tools to properly handle the extensive data base available from the investigations carried out at the site.

The Finnsjön research area has been divided into three scales on geological grounds. The scales are referred to as regional, semi-regional, and local, respectively; the division is roughly indicated in Figure 1.1. Figure 1.2 shows the areal extent of the regional area with major geological lineaments indicated, while Figure 1.3 illustrates the extent of the semi-regional and the local scale.

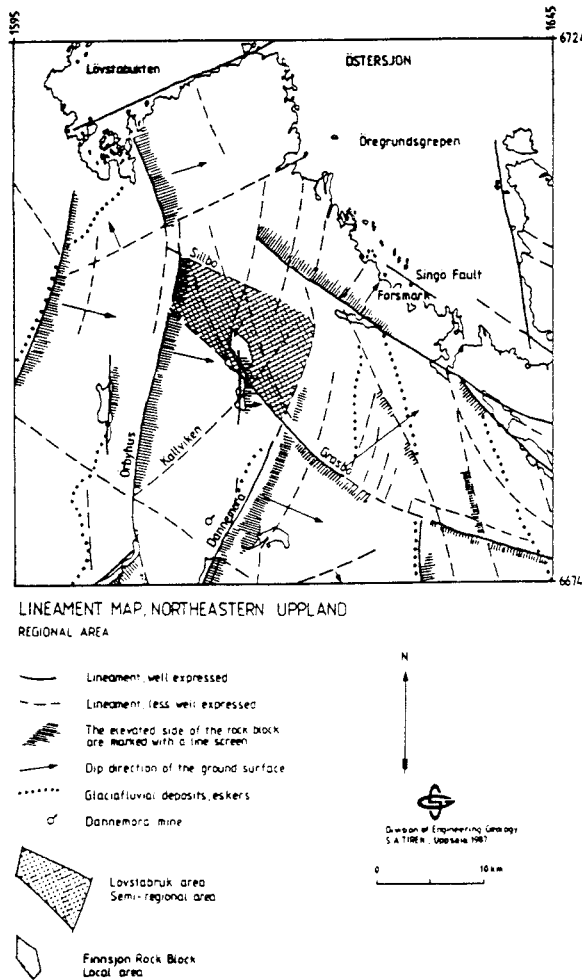


Figure 1.2 The extent of the regional area of the Finnsjön study site. (From the Background report.)

It is recommended in the Background report, that the division of the domain shown in Figures 1.2 and 1.3 should be maintained also for the groundwater flow modelling described in the present report. However, the regional area will not be considered in this project. The modelling will be performed at the semi-regional and the local scale; both in three dimensions. The reason for omitting the regional scale from groundwater flow modelling is further discussed in Chapter 3. Moreover, for modelling purposes, the areal extent of the semi-regional area as suggested in the Background Report will be reduced; the reason for this is further discussed in the report.

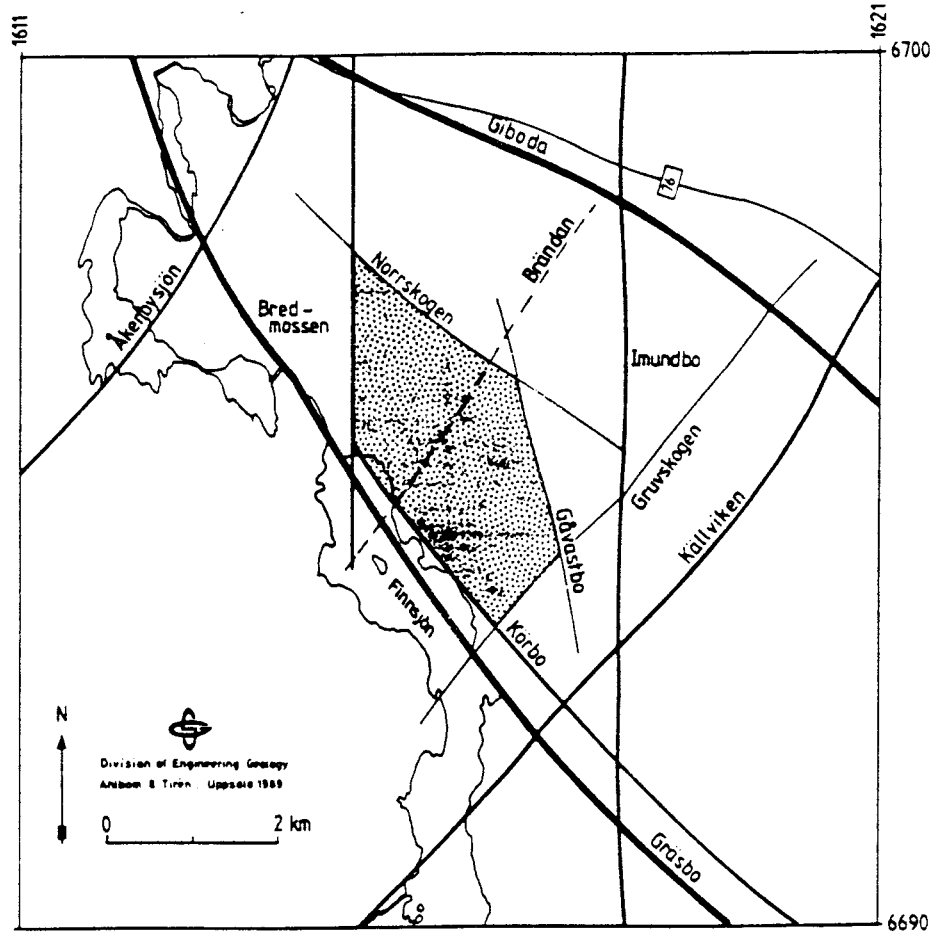


Figure 1.3 The extent of the semi-regional and the local area of the Finnsjön study site. The local area is shaded. (From the Background report.)

The modelling of the groundwater flow at Finnsjön will be carried out with the computer code NAMMU, which is based on the finite-element method applying the porous media approach. Fracture zones on a regional scale are modelled in a deterministic way, whereas minor local fracture zones are modelled in an implicit manner where fracture zone properties were averaged over finite elements not necessarily coinciding with the positions of the fracture zones. For pre- and postprocessing purposes, the program package HYPAC will be used. Further details with regard to these packages are given in Chapter 2.

One feature that causes additional analyses apart from the pure transport of groundwater, is the occurrence of salt water at some depth below a sub-horizontal fracture zone on the local scale. The saline groundwater probably stems from the Lithorina basin, and is very old. The analysis concerned with the salinity of the groundwater, will be carried out in two dimensions - initially in a semi-generic fashion in order to investigate the influence on the groundwater flow caused by the presence of salt.

The coordinate system used is the RAK-system, with offset in $y=1600000$ m and $x=6600000$, the same offset as used in the Background report.

This report is a revised version of a report previously published /Lindbom, B., et al, 1990/. The difference between the present report and the previous one, is that the present report describes the conclusions more site-specifically, the presentation of a number of the cases tackled has been pruned down, and some editorial effort has been put into having the volume of the report reduced.

2. Mathematical Model

2.1 General

This section deals with the different steps involved in the numerical modelling of groundwater flow in a general sense. A more detailed description specific for the present project with regard to the overall strategy and methodology is given in Chapter 4. Specific issues like assignment of boundary conditions and material properties or evaluation of the calculated results are given in Chapters 5-7, which are concerned with the different modelling steps within the present project.

NAMMU is within this project applied to the stated problem for solving an equation system numerically for the distribution of pressure. Apart from this application, a substantial amount of pre- and post-processing is required.

The pre-processing mainly consists of construction of a mesh representing the domain to be modelled, checks of the geometrical correctness of the mesh (orientation, connectivity etc.), and assignment of boundary conditions and material properties. After solving the equation system, rather a large effort needs to be put into evaluation and presentation of the results; the so called post-processing. The post-processing routines are mainly concerned with calculations of the resulting pressure distributions, tracking of water particles, checking the relevance of the results etc.

The general working scheme is outlined below and sketched in Figure 2.1. It should be pointed out though, that all the steps presented below are not necessarily run through for all applications.

- The topography (i.e. the elevation of the groundwater table) is digitised.
- The elevation contours are interpolated on to a grid of equally spaced points.
- Location of fracture zones and the bounds for the model are defined and digitised, (mesh pre-processing). In many cases, the lateral boundary conditions and the top boundary conditions are fixed already at this stage.
- Construction and generation of the finite element mesh.
- Check of the geometrical correctness of the mesh (mesh post-processing), such as numbering sequence of the nodal points, connectivity of the mesh etc.
- Optimisation of the numbering sequence of the finite-element mesh in order to reduce the required computer memory space when the active front of the equation system is stored in the computer.
- Adjusting top most layer(s) of the finite element mesh to the digitised topography.
- Assignment of hydraulic properties. This is normally done element-wise.
- Assignment of boundary conditions, which normally is done node-wise. If steady-state conditions are assumed, the elevation of the groundwater table is often considered as the boundary condition at the top surface.
- Finite Element Model is applied, (here NAMMU is used).
- Evaluation and presentation of the results, the so called post-processing.

NAMMU contains rather a large amount of pre- and post-processing routines. However, for both pre- and post-processing purposes, the program package HYPAC /Grundfelt B., 1983/, has been utilised within this project. This program package was initially designed to be associated to the groundwater flow code GWHRT /Thunvik R., et al, 1980; Thunvik R., et al, 1988 /, but some routines have been altered and added to HYPAC in order to create a necessary interface between HYPAC and NAMMU, see Figure 2.2. Brief descriptions of NAMMU and HYPAC are given in the following sections.

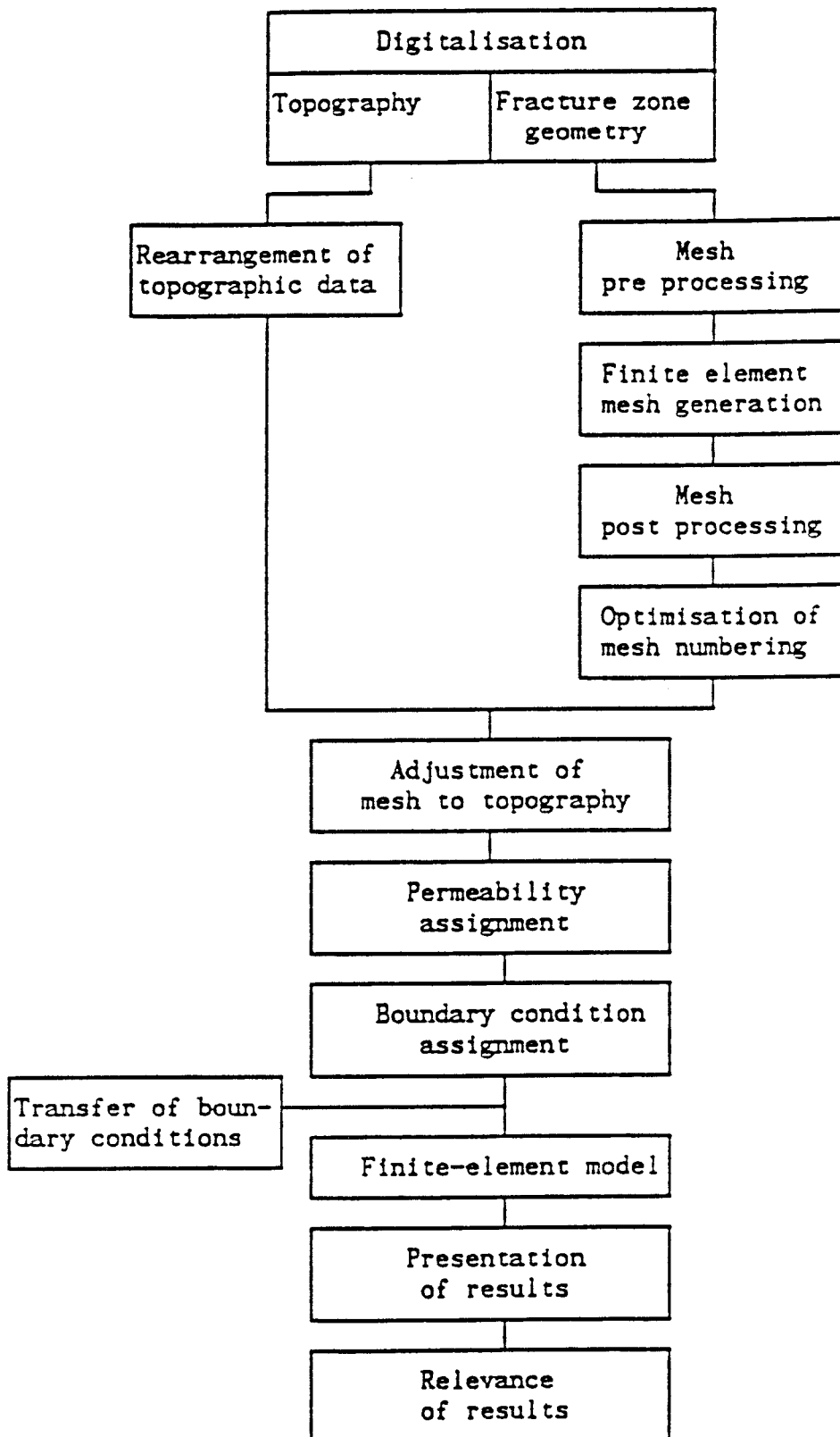


Figure 2.1

Flow sheet showing the general working scheme. It should be noted that all steps are not run through for all applications, the sketch rather illustrates the general and possible flow of information.

2.2 Brief Description of NAMMU

The flow system at the site is solved numerically with the computer code NAMMU /Atkinson R., et al, 1985; Rae J., et al, 1979 /. NAMMU is a computer code developed to simulate coupled heat and groundwater flow in either one, two or three dimensions. It is a finite-element model with the continuum approach based on the flow equation (flow through porous media). The two dependent variables to be determined in NAMMU are the non-hydrostatic pressure and the temperature. The two coupled partial differential equations being solved are:

$$\frac{\partial}{\partial t} (\epsilon \rho^f) + \nabla \cdot (\rho^f \bar{q}) = 0 , \quad (2.1)$$

and

$$(\rho c_p)_s \frac{\partial T}{\partial t} + \rho^f c_p^f \bar{q} \cdot \nabla T - \Gamma_s \nabla^2 T = H , \quad (2.2)$$

where $(\rho c_p)_s$ is given by

$$(\rho c_p)_s = \epsilon \rho^f c_p^f + (1 - \epsilon) \rho^s c_p^s . \quad (2.3)$$

The Darcy velocity \bar{q} is given by

$$\bar{q} = -\frac{k}{\eta} (\nabla p_d - (\rho^f - \rho_s^f) \bar{g}) . \quad (2.4)$$

A list of the symbols used is given at the end of the report.

Some applications within the present project involve saline groundwater. This is dealt with under steady-state conditions accounting for the density gradient caused by the salinity. The density depending on the salt concentration is expressed according to Eq 2.5 below:

$$\rho_s^f = 998.3 + 41.3 \cdot 10^{-3} \cdot C_{\text{NaCl}} , \quad (2.5)$$

where C_{NaCl} is the concentration of NaCl expressed in mole/m³.

The equations are discretised in space using the Galerkin finite-element method, discretised in time by backward finite-difference schemes with time-stepping using Gear's method. The resulting non-linear algebraic equations are generally linearised by the Newton-Raphson method and then solved by a direct frontal solver.

NAMMU is implemented on a Convex, model C-210, on which the FEM-model described above is run. The calculations performed within this project are carried out with 8-noded elements for both the two-dimensional and the three-dimensional modelling, which means that the interpolation scheme between element corners is quadratic for the 2D-modelling and linear for the 3D-modelling. NAMMU version 4S has been used within the present project.

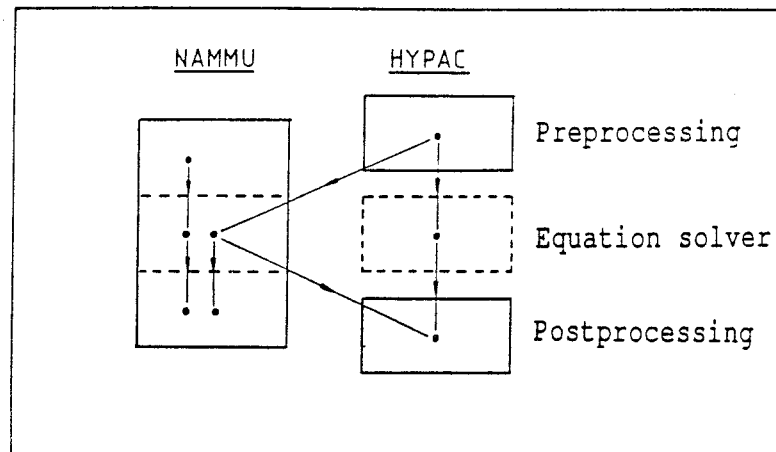


Figure 2.2 Possible routes for information flow between NAMMU and HYPAC.

2.3 Brief Description of HYPAC

HYPAC version 5.3 has been used within this project. The pre-processing normally carried out in HYPAC is divided into two parts, which are designed for processing of the mesh, and assignment of boundary conditions and material properties respectively, see below:

Pre-processing:

- definition of the geometry of geological features (fractures etc.), and design of the finite element mesh using the commercially available program FEMGEN /FEMPROG AB, 1987/
- minimising the frontal width of the equation system to reduce the demand of computer memory space
- checking the distortion of the elements in order to detect future poor numerical solutions.
- assignment of hydraulic properties and boundary conditions.

Post-processing:

TRG (Trajectory Generator) generates flow lines and can also be used for calculation of potentials and fluxes in an arbitrarily selected cross-section or for calculation of potentials and fluxes along a straight line. TRG is the postprocessing routine which mainly has been used within the present project for the evaluation of the results.

Furthermore, a couple of programs designed for testing the accuracy and relevance of the computed results are applied to the solution obtained with NAMMU. These checks that the calculated potentials lie within the range that is limited by the potentials of the boundary conditions, and the local mass conservation of the numerical solution, respectively.

The commercially available program packages Grapher and Surfer /Golden Software Inc./ have also been used for part of the graphical presentation within this project. HYPAC is implemented on the Convex computer. However, the major part of the graphical output from the evaluation is run on PC-s with enhancement cards.

3. Geohydrology at the Finnsjön Site

3.1 General

As mentioned earlier, the data base available for modelling purposes is rather extensive. A number of core drillings and percussion drillings have been performed on the local scale. Furthermore, a large number of investigations, including for instance single-hole packer tests as well as interference tests have been carried out. The results from these tests have been used to estimate the hydraulic conductivities of the different geological units.

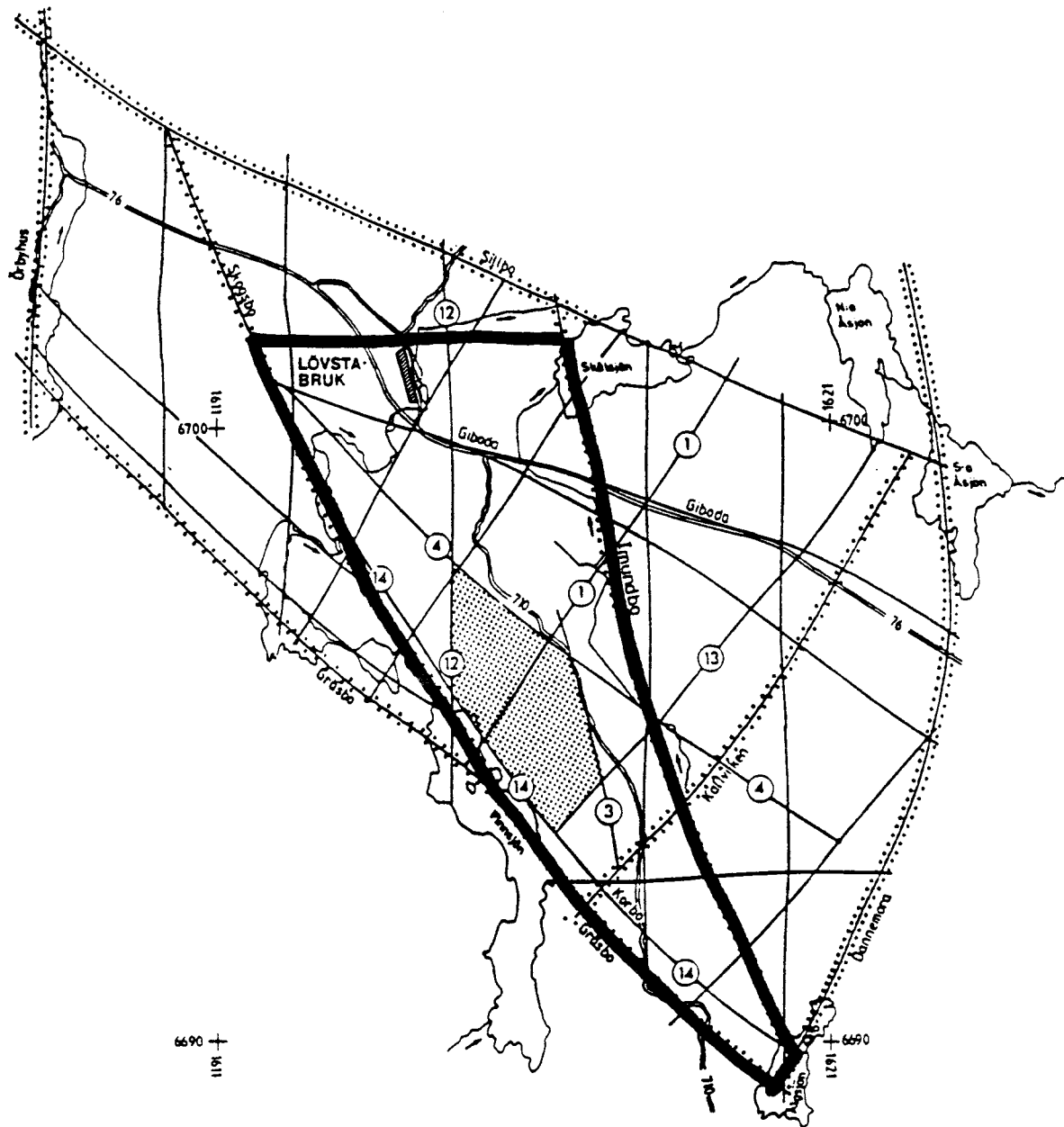
In order to establish a conceptual model of the Finnsjön area and its surroundings, the hydraulic conductivity data have been classified in two hydraulic units. A unit has been classified either as being rock mass with fracture zones excluded, or as fracture zones of different orders.

3.2 Division of the Domain into a Semi-Regional and a Local Scale

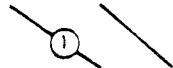
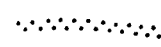

The Background Report suggests a division of the Finnsjön area into three scales for purposes of groundwater flow modelling. This division is based on geological grounds, such as classifications of major regional lineaments with regard to age and significance. The areal coverage of the regional area is approximately 2500 km². It is suggested that the regional scale may be discarded since the knowledge of the hydraulic properties on such a large scale is extremely limited. Moreover, modelling on such large scales are of limited value, since the discretisation by necessity has to be coarse. This in turn leads to far too large blocks to imply an increased understanding of the flow system on the scales of primary concern.

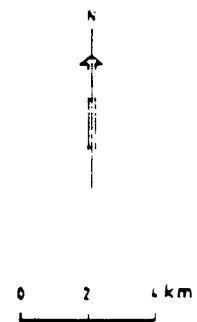
On the other hand, proposed boundaries for a model on a semi-regional and a local scale are presented in the Background Report. The extension of the semi-regional area as proposed in the Background Report is shown in Figure 3.1a along with major lineaments. The elevation of the groundwater table in the semi-regional area is shown in Figure 3.1b. The extension of the semi-regional area has been deemed to be possible to reduce. The validity of this reduction is based on the assumption that the west-most and east-most parts, located outside the reduced area of the domain, most likely do not take part in the flow system of concern, i.e. the flow on the local scale. The omitted areas are rather regarded as two separate flow cells, cut off from the area of interest by the two discharge areas aligning with the positions of the boundaries of the reduced domain. This is clear if Figures 3.1a and 3.1b are superimposed. Thus, the area within the thick solid lines as shown in Figure 3.1a is the one considered for the semi-regional model within the present project.

The areal coverage of the local area as proposed in the Background Report is shown in Figure 3.2a, along with the local fracture zones. The elevation of the groundwater table on the local scale is shown in Figure 3.2b. The areal coverage of the local scale as suggested in the Background Report coincides with the one that will be considered for the present project.



SIMPLIFIED ROCK BLOCK MAP , LÖVSTABRUK AREA

-  Fracture zones
-  Position of lineaments interpreted on regional scale
-  Finnsjön Rock Block



The glacial striation is north-south

Figure 3.1a

Areal coverage of the semi-regional area as suggested in the Background Report. Thick solid lines correspond to the boundaries of the semi-regional area considered for groundwater flow modelling in the present project. The local model is indicated as a shaded area

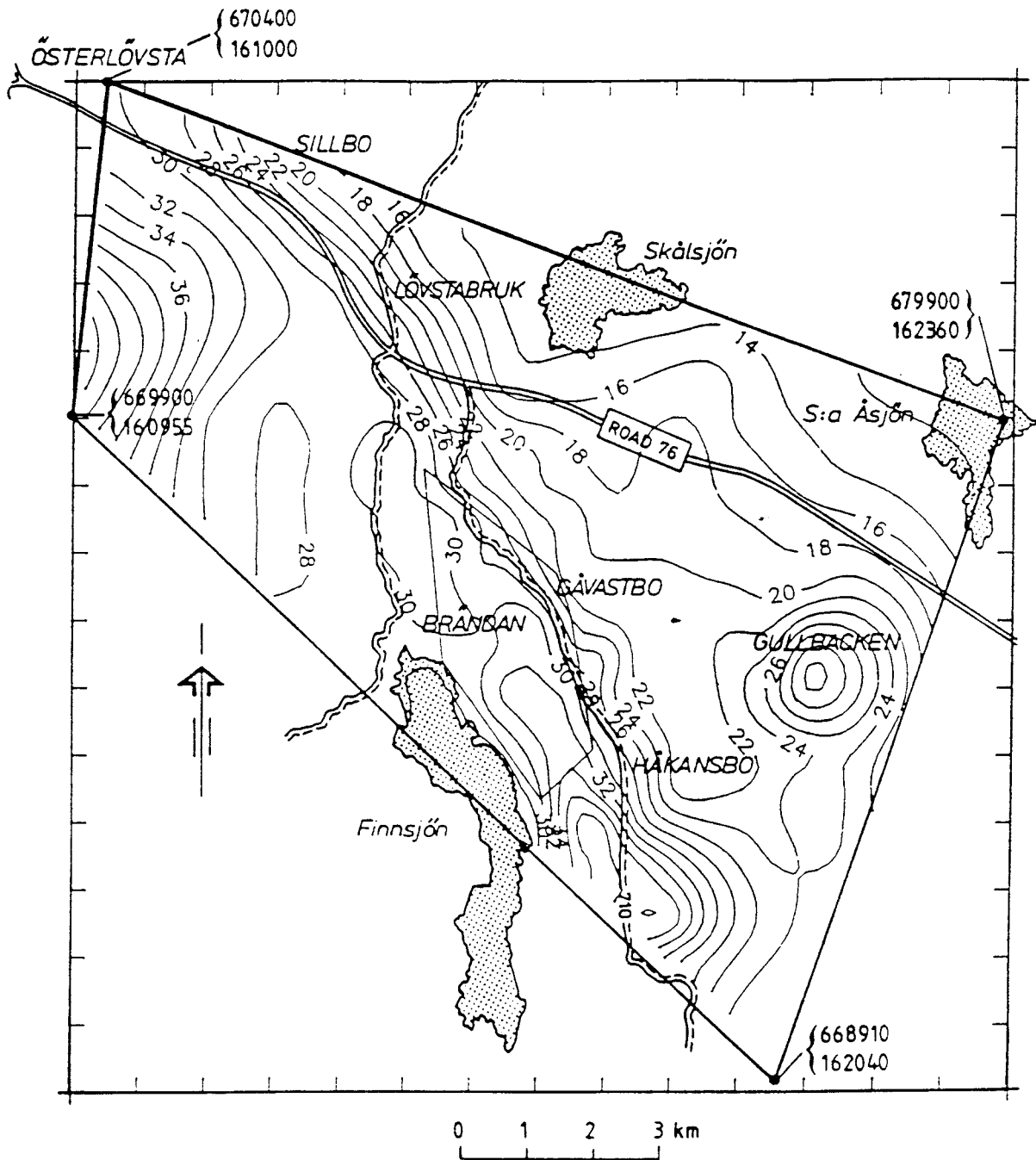


Figure 3.1b Elevation of the groundwater table on the semi-regional scale. (From the Background report.)

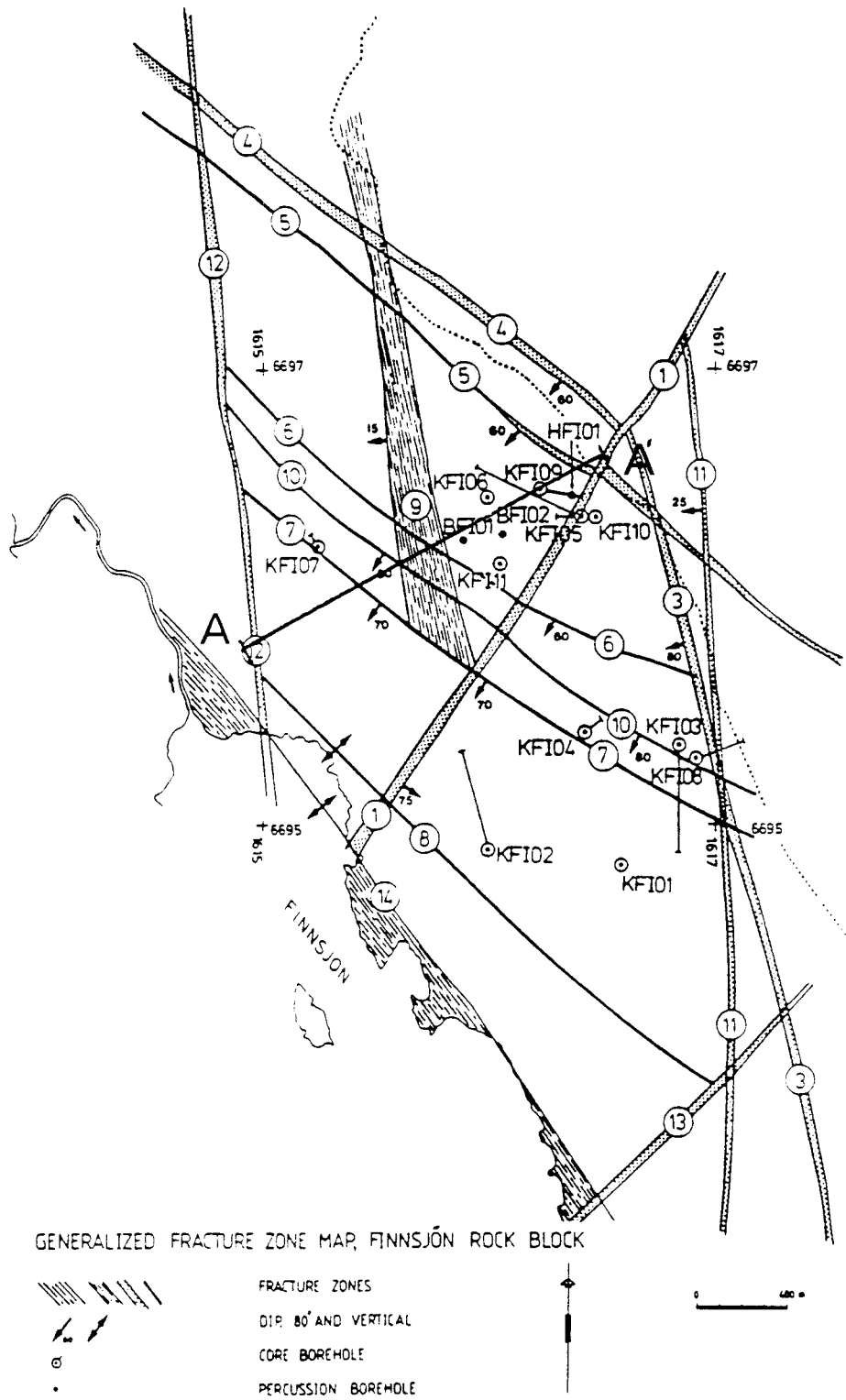


Figure 3.2a

Areal coverage of the local area with the fracture zones indicated. (From the Background report.)

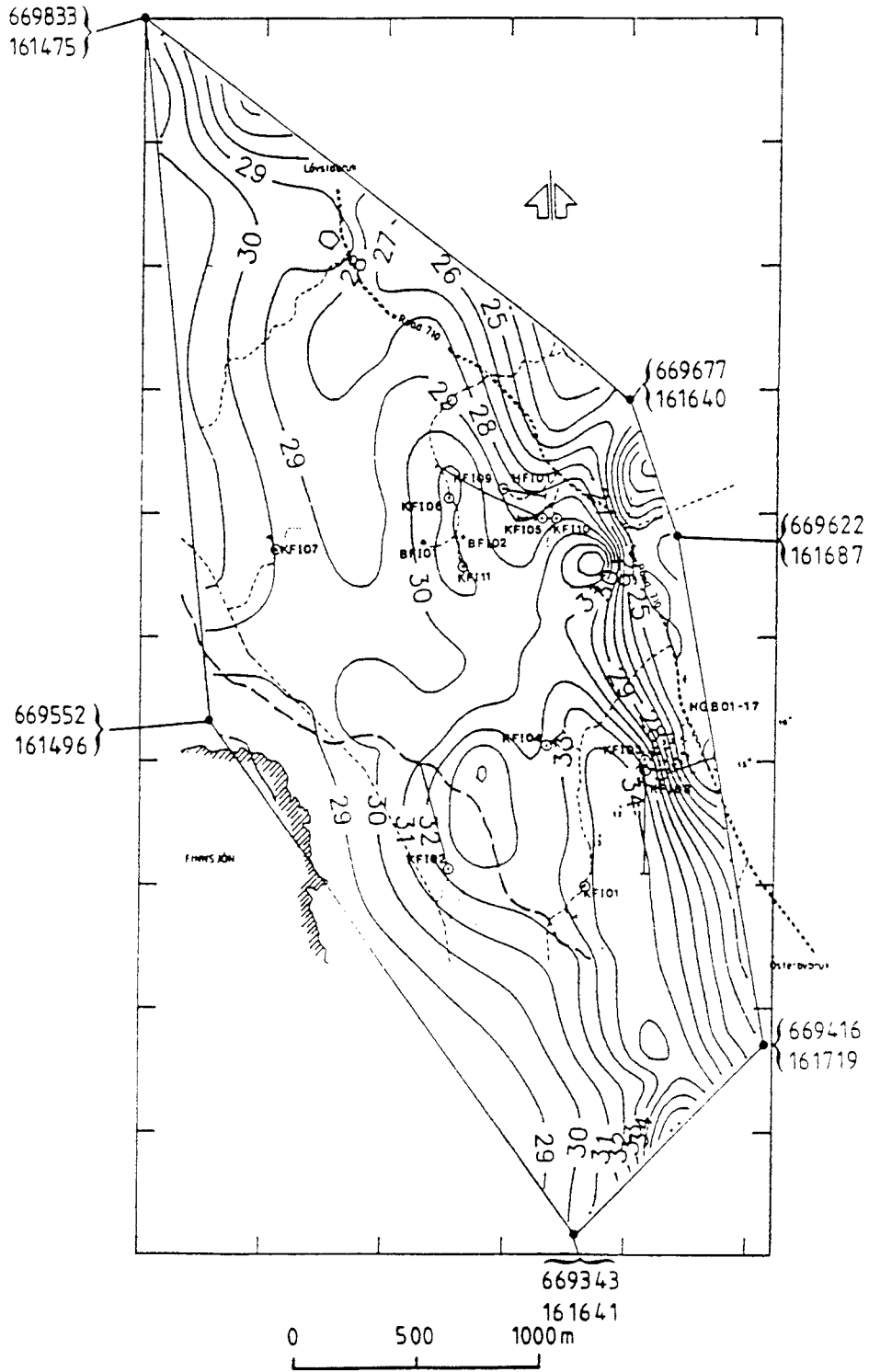


Figure 3.2b Elevation of the groundwater table on the local scale. (From the Background report.)

3.3 Brief Description of the Hydrology

Lake Finnsjön is a long and narrow lake with a maximum depth of about 4 m. Its extension in the north-south direction is about 6.5 km, and it is roughly 1 km wide at its maximum. The catchment area is about 93 km² at the inlet of Lake Finnsjön and about 117 km² at the outlet. Lake Finnsjön is part of the run-off area of the River Forsmarksån.

The Finnsjön area is drained by two separate surface water systems, where the major system drains the central and southern part of the area, while the north-western area is drained by another system. Both systems merge in the north-eastern part of the area at Lake Skålsjön. On a larger scale, the water is primarily drained into the Baltic northwards and into Lake Mälaren in the south.

About 20% of the Finnsjön area is constituted by mires (5 km²), with approximately 3 km² coverage of swamps and about 2 km² coverage of bogs. Bogs are preferably occurring in recharge areas whereas the swamps prevail in low-lying parts of the area where more nutritious groundwater is discharged.

The discharge areas correspond to about 30% of the areal coverage of the Finnsjön area with surroundings. The groundwater recharge rate to the bedrock has been estimated to be in the order of about 10-20 mm/year.

3.4 Hydraulic Properties of the Rock Mass

The determination and classification of the hydraulic properties of the rock mass are based on the field investigations carried out on the local scale. Rather large an effort was put into statistical analyses of the population of data with respect to hydraulic conductivities. A division of the local scale area into a northern and a southern block was found to be feasible. This strategy led to different assumptions and evaluations of the hydraulic properties for the two blocks.

The hydraulic conductivities are assumed to obey a power function, assuming a depth dependent variation of the hydraulic conductivity (K) of the rock mass, which is formulated in a general manner according to Eq 3.1.

$$K = a \cdot z^{-b} . \quad (3.1)$$

The values for the northern block of the local area were evaluated to be:

$$K = 3.90 \cdot 10^{-5} \cdot z^{-1.53} , \quad (3.2)$$

while the corresponding numbers for the southern block are:

$$K = 1.04 \cdot 10^{-6} \cdot z^{-1.10} . \quad (3.3)$$

The modelling of both the semi-regional and the local areas will assume the latter value for the entire rock mass. This assumption is based on the results from personal conversations with one of the authors to the Background Report, since the values of the hydraulic conductivities calculated according to Eq 3.2 may be too biased by the presence of the sub-horizontal zone 2.

3.5 Hydraulic Properties of the Fracture Zones at Finnsjön

The fracture zones comprise both well-expressed major regional lineaments and smaller "local scale" zones. The fracture zones on the semi-regional scale are shown in Figure 3.1a, while the local ones are illustrated in Figure 3.2a. The sub-horizontal zone 2 starts below the surface and is cut off by zones 1, 3, 4, and 12; see Figure 3.4 for a vertical projection of zone 2. In addition to the fracture zones presented in the Background Report, a horizontal zone (called H1) is included in a semi-generic fashion for the modelling of the local scale. It will primarily be modelled as being part of the rock; however, its presence in the finite-element mesh offers a possibility to investigate its importance relative to the other fracture zones on the local scale. The complete set of fracture zones as given in the Background Report is given in Table 3.1.

Table 3.1 Fracture zones in the Finnsjön area as presented in the Background Report. The letter "S" or "L" refers to the fracture being present on the semi-regional scale or the local scale.

Zone	S/L	Penetration depth (m)	Width (m)	Inclination (degrees)	Hydr. cond. (m/s)
1	S&L	55-75 340-360	20	75-70 SE	$5-25 \cdot 10^{-6}$ $5-25 \cdot 10^{-7}$
2	S&L	100-300	100	16 SW	$2-4 \cdot 10^{-5}$
3	S&L	30-120	50-100	80-60 SW	$1-10 \cdot 10^{-6}$
4 ¹	S&L		50-100	60 SW	
5	L	170-180 320-350 550-560	≤10	60 SW	$5-50 \cdot 10^{-6}$ $1-5 \cdot 10^{-6}$ $1-5 \cdot 10^{-7}$
6	L	515-520	≤10	60 SW	$1-10 \cdot 10^{-9}$
7	L	390-480	≤10	70 SW	$1-5 \cdot 10^{-7}$
8 ²	L		≤10	90	
9	L	105-160	50?	15 SW	$5-50 \cdot 10^{-8}$
10	L	80-95 350-380	≤10	80 SW	$1-5 \cdot 10^{-5}$ $5-15 \cdot 10^{-6}$
11	L	50-220 90-145 235-285	50-100	23 SW	$5-20 \cdot 10^{-7}$ $1-10 \cdot 10^{-7}$ $5-20 \cdot 10^{-8}$
12 ³	S&L		50-100	90	
13 ⁴	S&L		50-100	90	
14 ⁵	S&L		50-100	90	
Skogsbo ¹	S		100-200	90	
Giboda ¹	S		100-200	90	
Imundbo ¹	S		100-200	90	
Gräsbo ⁵	S		100-200	90	
Dannemora ⁵	S		100-200	90	
Källviken ⁴	S		100-200	75-90	

¹ Hydraulic properties assumed to be similar to those of Zone 5.

² Hydraulic properties averaged from those of zones 5, 6, 7, and 10.

³ Hydraulic properties assumed to be similar to those of the Singö-fault.

⁴ Hydraulic properties assumed to be similar to those of Zone 1.

⁵ Hydraulic properties assumed to be similar to those of the Singö-fault.

The hydraulic conductivities of the fracture zones are given as interval values in the Background Report corresponding to the depths where the fracture zones have been penetrated by bore holes. The hydraulic conductivities of the fracture zones have been evaluated at these intervals. The initial assumption is that the conductivities of the fracture zones will obey the same depth dependence as the rock mass. In order to fit these point-values to the type-curve expressed in Eq 3.1, the constant "a" has been evaluated backwards. This value expresses the value of the hydraulic conductivity at a depth of 1 m below the ground surface.

Furthermore, the widths and the values of the estimated hydraulic conductivities of the fracture zones are given as range values in the Background Report. The lowest values of the widths were consistently chosen for the present project. When the "a"-constants were back-calculated, the average values of the penetrating depths and the conductivities were consistently chosen. The properties of the fracture zones as interpreted for modelling purposes within the present project are given in Table 3.2.

Table 3.2 Fracture zones in the Finnsjön area as modelled in the present project. The letter "S" or "L" refers to the fracture being present on the semi-regional scale or the local scale. See also Figures 3.1a and 3.2a.

Zone	S/L	Width (m)	Inclination (degrees)	Hydr. Cond (m/s)
1	S&L	20	75 SE	$1.21 \cdot 10^{-3} \cdot z^{-1.10}$
2	S&L	100	16 SW	$1.02 \cdot 10^{-2} \cdot z^{-1.10}$
3	S&L	50	80 SW	$5.77 \cdot 10^{-4} \cdot z^{-1.10}$
4 ¹	S&L	50	60 SW	$3.14 \cdot 10^{-3} \cdot z^{-1.10}$
5	L	10	60 SW	$3.14 \cdot 10^{-3} \cdot z^{-1.10}$
6	L	10	60 SW	$4.86 \cdot 10^{-6} \cdot z^{-1.10}$
7	L	10	70 SW	$2.40 \cdot 10^{-4} \cdot z^{-1.10}$
8 ²	L	10	90	$2.21 \cdot 10^{-3} \cdot z^{-1.10}$
9	L	50	15 SW	$5.29 \cdot 10^{-5} \cdot z^{-1.10}$
10	L	10	80 SW	$5.46 \cdot 10^{-3} \cdot z^{-1.10}$
11	L	50	23 SW	$1.28 \cdot 10^{-4} \cdot z^{-1.10}$
12 ³	S&L	50	90	$3.70 \cdot 10^{-4} \cdot z^{-1.10}$
13 ⁴	S&L	50	90	$1.21 \cdot 10^{-3} \cdot z^{-1.10}$
14 ⁵	S&L	50	90	$3.70 \cdot 10^{-4} \cdot z^{-1.10}$
Zone H1	L	100	0	$1.02 \cdot 10^{-2} \cdot z^{-1.10}$
Skogsbo ¹	S	100	90	$3.14 \cdot 10^{-3} \cdot z^{-1.10}$
Giboda ¹	S	100	90	$3.14 \cdot 10^{-3} \cdot z^{-1.10}$
Imundbo ¹	S	100	90	$3.14 \cdot 10^{-3} \cdot z^{-1.10}$
Gräsbo ⁵	S	100	90	$3.70 \cdot 10^{-4} \cdot z^{-1.10}$
Dannemora ⁵	S	100	90	$3.70 \cdot 10^{-4} \cdot z^{-1.10}$
Källviken ⁴	S	100	90	$1.21 \cdot 10^{-3} \cdot z^{-1.10}$

¹ Hydraulic properties assumed to be similar to those of Zone 5.

² Hydraulic properties averaged from those of zones 5, 6, 7, and 10.

³ Hydraulic properties assumed to be similar to those of the Singö-fault.

⁴ Hydraulic properties assumed to be similar to those of Zone 1.

⁵ Hydraulic properties assumed to be similar to those of the Singö-fault.

The hydraulic conductivities within the present project have been compared with the values used for the KBS 3-study as reported in /Carlsson, L., et al, 1983/. The depth dependence of the conductivities are plotted in Figure 3.3 for rough average values of the conductivities of the rock matrix and the fracture zones for two of the sites investigated within the framework of KBS 3, and for the Finnsjön site. One major difference with the properties of the fracture zones, is that the fractures at Finnsjön have individual values assigned to them (although they were averaged to prepare this very figure), whereas the fracture zones in KBS 3 were treated as one single hydraulic unit, thus having the same hydraulic properties. Although the averaging has been rather crude for the preparation of Figure 3.3, the trend is clearly indicating a much more pervious domain in Finnsjön than the case was for the KBS 3-sites. The fracture zones in the KBS 3-study were regarded as less permeable than the rock matrix at Finnsjön at levels lower than about 450 m below ground surface. However, the curves showing the depth dependent hydraulic conductivities of Finnsjön may be somewhat deceptive because the field measurements carried out were initiated in the late 1970-ties. The measured values may therefore be biased since the detecting-limit of the equipment used by the time, was higher than for the equipment used to evaluate field data used within the KBS 3-study.

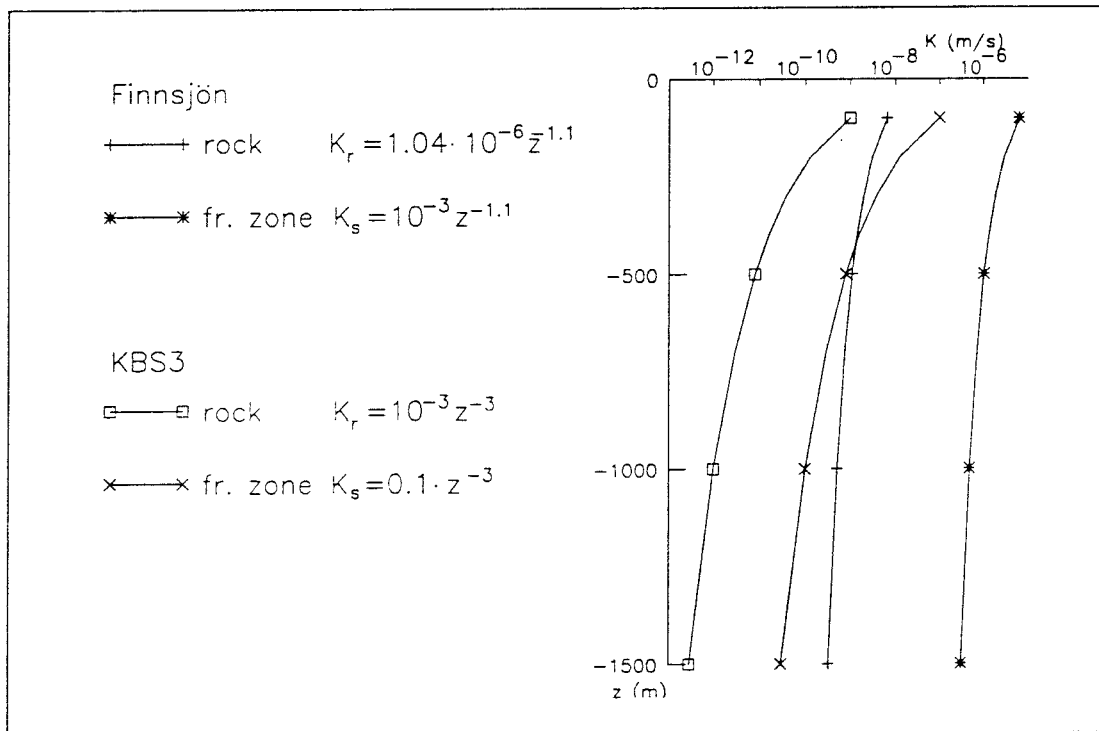


Figure 3.3 Average depth dependent hydraulic conductivities as used within the KBS 3-study compared to the values (averaged) used within the present project.

3.6 Presence of Salt

Saline water has been found below and in Zone 2. The average salt-concentration has been measured to about 5000 ppm. The question as to whether or not the density differences occurring due to the salt content, affect the flow to a measurable limit needs to be elucidated. To this end, a semi-generic model in two dimensions will be carried out. The position of the vertical cut in question is shown in Figure 3.2a as the line indicated with A-A', while Figure 3.4 displays the vertical view of zone 2. The cut will be limited by zones 1 and 12.

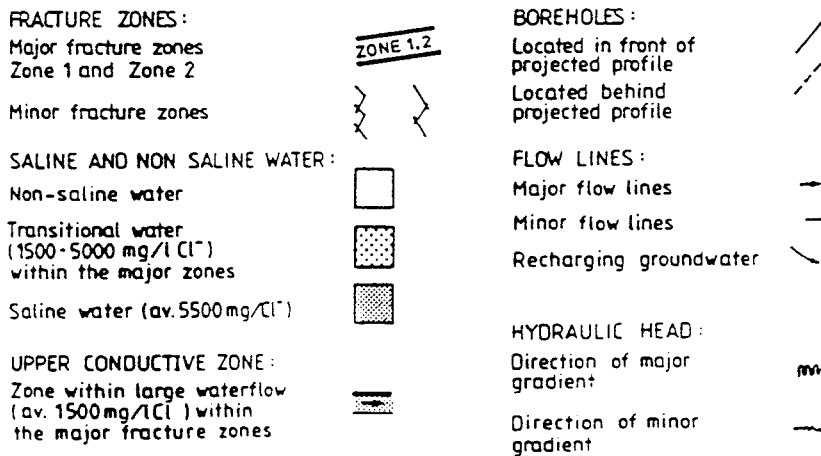
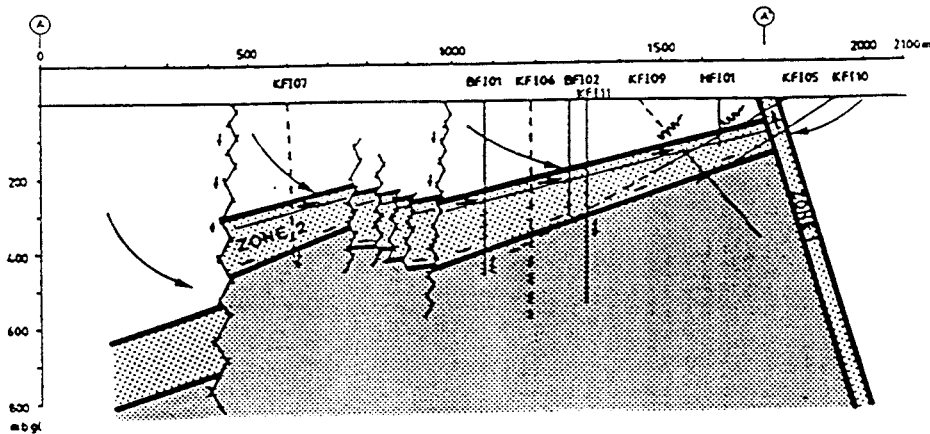


Figure 3.4 Vertical view of zone 2 (From the Background Report).

4. Modelling Strategy

4.1 General

The overall objectives of the present project can be formulated in four steps of different principles:

- Judge the influence of the density gradients occurring due to the presence of saline groundwater below and in Zone 2.
- Analyse the importance of fracture zones in a general sense.
- Investigate the importance and extension of the sub-horizontal Zone 2.
- Calculate flow rates relevant to the safety assessment of a potential site for radioactive waste disposal.

To this end, the modelling with NAMMU is carried out both in two and three dimensions at different scales. The different steps and the associating links between them are described in the following sections.

The main purpose for modelling at different scales, is that the knowledge of the hydraulic properties on the larger scale is limited and that the type of lateral boundary conditions on the smaller scale area is uncertain. Even if the hydraulic properties were known on larger scales, the available computer memory space is prohibitive for modelling larger scales with a well discretised domain. Moreover, by modelling at different scales, a possibility to include the detailed knowledge available on the smaller scale is offered. The strategy within the present project will involve the modelling on a larger scale (the semi-regional scale) with a transfer of the resulting pressure distribution as lateral boundary pressures to the local model. Modelling on both scales are carried out in three dimensions. However, an initial study in two dimensions is required to investigate a possible influence on the groundwater flow due to the presence of salt.

4.2 Modelling of the Presence of Salt in Two Dimensions

Saline water has been encountered below and in Zone 2. Of major importance is therefore to investigate whether or not the salt content causes significant changes compared to pure groundwater flow, to be included also in the three-dimensional models. The salinity will be modelled under steady-state conditions, and only in terms of density gradients occurring, i.e. the transport of salt taking diffusion and/or dispersion into account will not be considered. The strategy chosen will involve comparisons between two situations with different lateral boundary conditions modelled with or without saline water. This will provide means to judge the impact from the density gradients in the domain. Since the transport of salt is neglected, the presence of saline water is given in terms of the increased density of the water as a function of the salt concentration. The hydraulic conductivities of the fracture zones included in the model will be regarded as depth dependent according to the values given in Table 3.2.

4.3 Modelling in Three Dimensions of the Semi-Regional Area

The significance of the fracture zones on the semi-regional scale will be investigated by means of a number of sensitivity analyses including different assumptions with regard to their hydraulic conductivities relative to the surrounding rock mass.

One of the reasons for the large area of the semi-regional model, as originally suggested in the Background Report, was that the estimated flow rate in zone 2 demanded a large enough infiltration area. In particular, the estimated groundwater flow rate in Zone 2 required rather a substantial feed of water. During the course of the project, it has been deemed plausible to assume that a large infiltration area probably is not enough to feed Zone 2 with enough amount of water. Rather, it has been assumed that Zone 2 probably has some hydraulic contact with Lake Finnsjön, either direct or indirect via a connecting fracture zone. Zone 2 will be modelled according to the base case definition intersecting with the position of local fracture zone 7, but as an optional case zone 2 will also be modelled to extend as far south as possible to its intersection with zone 14. The resulting flow distribution from these two extreme situations will be calibrated against the estimated groundwater flow rate in Zone 2 amounting to 5-10 l/s. The case with the most plausible flow rate distribution within zone 2, will be the one considered for a transfer of lateral boundary conditions to the model on the local scale.

The fracture zones considered on the semi-regional scale will be modelled in a traditional manner by explicitly designing the geological features with finite-elements.

4.4 Modelling in Three Dimensions of the Local Area

The evaluation of the modelling on the local scale will be focussed on the sensitivity of the model with regard to different types of boundary conditions. These include for instance a treatment of the lateral boundaries as either being transferred from the semi-regional model or as no-flow boundaries. The upper boundary condition will be described by either the groundwater table on the semi-regional scale or the groundwater table as described on the local scale.

Water balance calculations in zone 2 will also be performed on the local scale. The evaluation and calibration procedure will be along the same lines as for the semi-regional model. This rough calibration will provide hints on which of the cases that could be deemed to best represent the "real" conditions, and by this appoint one of the cases studied as being most suitable for future research within SKB 91.

Furthermore, the rather high permeabilities in Finnsjön may be due to the relatively old measuring equipment used by the time of the field measurements. To analyse a possible effect from more fine-tuned field investigations, the Finnsjön local model will be run with hydraulic properties approximately corresponding to those used in the KBS3-study.

The local fracture zones not included in the semi-regional model, will not be explicitly modelled at the local scale, but will rather be included in the model in an implicit manner. This is achieved by having the fracture zone properties averaged over the finite elements, the locations of which do not necessarily correspond to the location of the fracture zone. To circumvent the evident risk for assigning fracture properties over too large distances, the method as such demands large computer memory space since there is a need for a very fine discretisation. The demand for this fine discretisation has been met by the use of 8-noded brick elements, which allows a discretisation fine enough for the fracture zone widths to be in the same order as the finite elements. The methodology is further described in Appendix D.

5. Two-Dimensional Modelling of the Presence of Salt

5.1 Introduction

The position of the vertical cut which has formed the basis for this part of the modelling, is shown in Figure 3.2a. The conceptual basis for this modelling is shown in Figure 3.4. The cut is about 1800 m long at the top, and the length is roughly 2500 m at its base. It was modelled to a depth of 1500 m. The top boundary coincides with the elevation of the groundwater table according to Figure 3.2b. The bottom boundary was modelled horizontal, whereas the lateral boundaries were sloping according to the inclinations of the bounding lateral fracture zones.

5.2 Discretisation of the Domain

The model was limited by the lateral fracture zones 1 and 12, see Figure 5.1a. The sub-horizontal zone 2 was connected to the lateral zones, crossing the entire domain. The domain apart from fracture zones was regarded as rock mass.

The mesh generated to describe the features mentioned above is shown in Figure 5.1b. It consisted of 1645 elements with eight nodes each, which means that the interpolation scheme between element corners along the element edges is quadratic.

5.3 Case Definitions – Nomenclature, Hydraulic Properties, and Boundary Conditions

Four cases were considered, which differ internally only with respect to the boundary conditions applied and the assumptions of the salt water. The nodal points along the top boundary have been prescribed an atmospheric pressure, i.e. $p=0$ kPa. The lateral boundary conditions included different types, so that either no-flow boundaries or hydro-static pressure boundaries were prescribed. These two types were combined with an increase of the fluid density below zone 2 caused by the salt concentration.

The differences between the cases are illustrated in Table 5.1 below.

Table 5.1 Type of boundary condition for the different cases considered within the two-dimensional modelling of the salt intrusion.

Case no	Lateral boundaries no-flow	Lateral boundaries hydro-static	Density gradient below zone 2
2D1	X		
2D2	X		X
2D3		X	
2D4		X	X

The hydraulic conductivity was assigned to the rock mass according to Eq. 3.3, i.e. $K=1.04 \cdot 10^{-6} \cdot z^{-1.10}$ m/s, where z corresponds to the depth below the ground surface. The conductivities of the fracture zones are shown in Table 5.2.

Table 5.2 Widths, inclinations, and hydraulic conductivities of the fracture zones for the two-dimensional modelling of the salt intrusion.

Zone	Width (m)	Inclination (degrees)	Hydr. Cond (m/s)
1	20	75 (SE)	$1.21 \cdot 10^{-3} \cdot z^{-1.10}$
2	100	16 (SW)	$1.02 \cdot 10^{-2} \cdot z^{-1.10}$
12	50	90	$3.70 \cdot 10^{-4} \cdot z^{-1.10}$

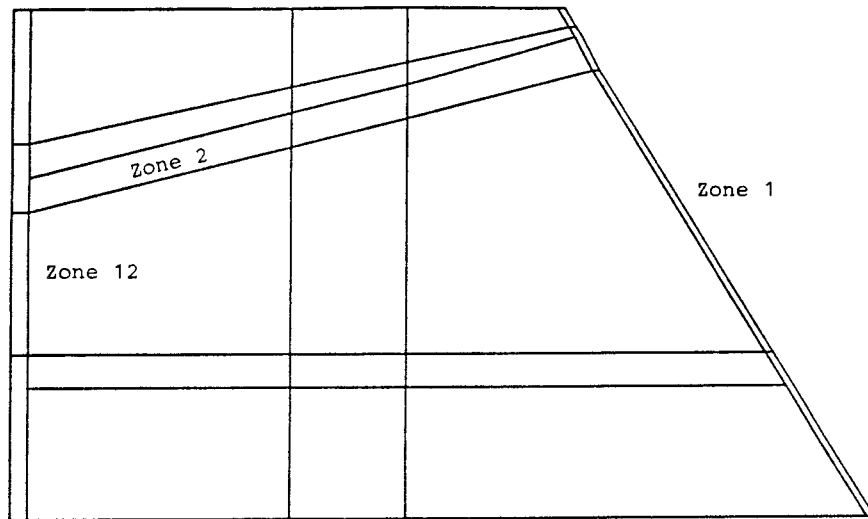


Figure 5.1a The geometry describing the vertical cut and the geological features included in the model.

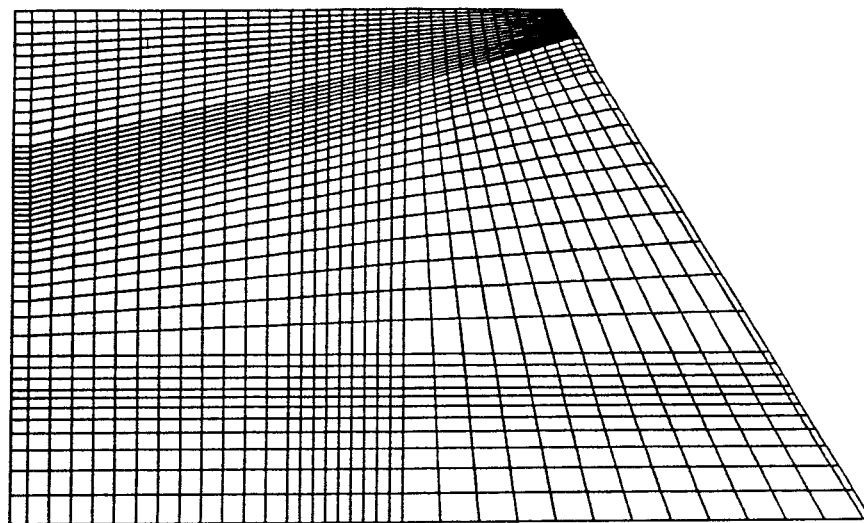


Figure 5.1b The finite-element mesh as generated for the two-dimensional modelling of the salt intrusion.

The salt concentration was prescribed for all the nodal points located in the region beneath zone 2. The density of the saline water was calculated according to Eq. 2.5, i.e.:

$$\rho_i^f = 998.3 + 41.3 \cdot 10^{-3} \cdot C_{\text{NaCl}_i}$$

where C_{NaCl_i} is the concentration of NaCl expressed in mole/m³. The salt concentration has been measured in field to be about 5000 ppm (expressed in Cl⁻) as an average value, which corresponds to a salt content of 155.1 mole/m³ of NaCl. This implies an increase of the density, if compared to fresh water, to $\rho_i^f = 1004.7$ kg/m³, which consequently was prescribed as the fluid density below zone 2.

5.4 Modelling Results

5.4.1 Flux Distribution

Figures 5.2a-5.2d show the flux distribution for the different cases. From the figures, it is evident that the presence of the higher density caused by the salt, lowers the flux above zone 2 to a small extent for both sets of lateral boundary conditions. Below zone 2 the pattern is somewhat different. The two cases with hydrostatic lateral boundaries indicate that the presence of salt below zone 2 does not affect the flow situation to any extent at all, except for the lower left-hand corner. However, the differences in flow at this particular spot is caused by the increased density which forces the flow to have a direction oriented towards the left-hand corner due to the gravity; and here it is contradicted by the hydrostatic boundary condition which acts as an inlet for water.

The differences in flux obtained when the two cases with no-flow lateral boundaries are compared, show somewhat different appearance. The flow below zone 2 is here affected by the increased density of the salt water below zone 2. The fluxes are increased with roughly a factor of ten in this particular area. The differences are even higher close to the intersection between zone 2 and zone 1, but is more or less artificially introduced by the contradictions in terms of the boundary conditions in this area. (The lateral no-flow boundary forces the flow upwards, while the increased density below zone 2 makes the flow strive downwards due to the gravity.) However, one should notice that this is a general pattern of the flow beneath zone 2 when the higher density has been assigned; the flow is in this case oriented in the opposite direction compared to the fresh-water case, i.e. from right to left in the figure. This is further illustrated by the plots showing the particle tracks.

To further illustrate the differences in flux caused by the presence of the increased density below zone 2, the relative difference is plotted in Figures 5.2e and 5.2f. The relative difference was calculated as the flux obtained in the case without salt subtracted by the flux obtained with salt, divided by the flux obtained in the case with salt. The relative differences were calculated for cases 2D1-2D2 and 2D3-2D4, see Figures 5.2e-f. Note, that the contours are labelled with "-"-signs, see the legend.

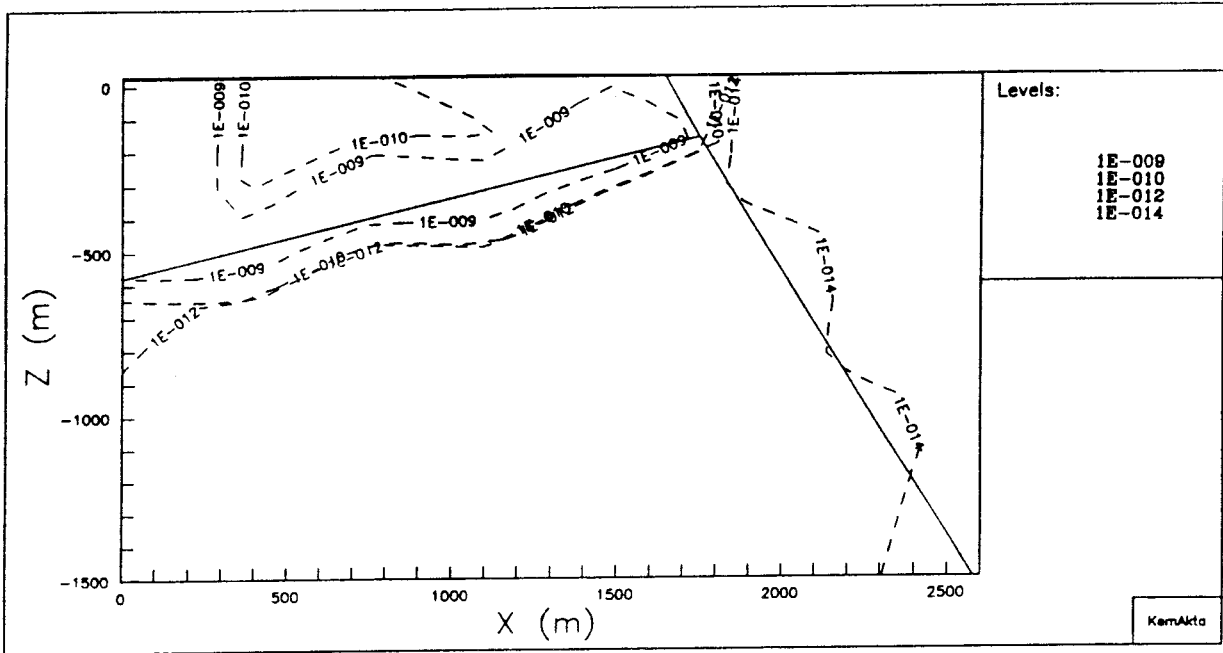


Figure 5.2a Flux distribution for Case 2D1; no-flow lateral boundaries, no salt. Flux values are expressed in $m^3/m^2/s$.

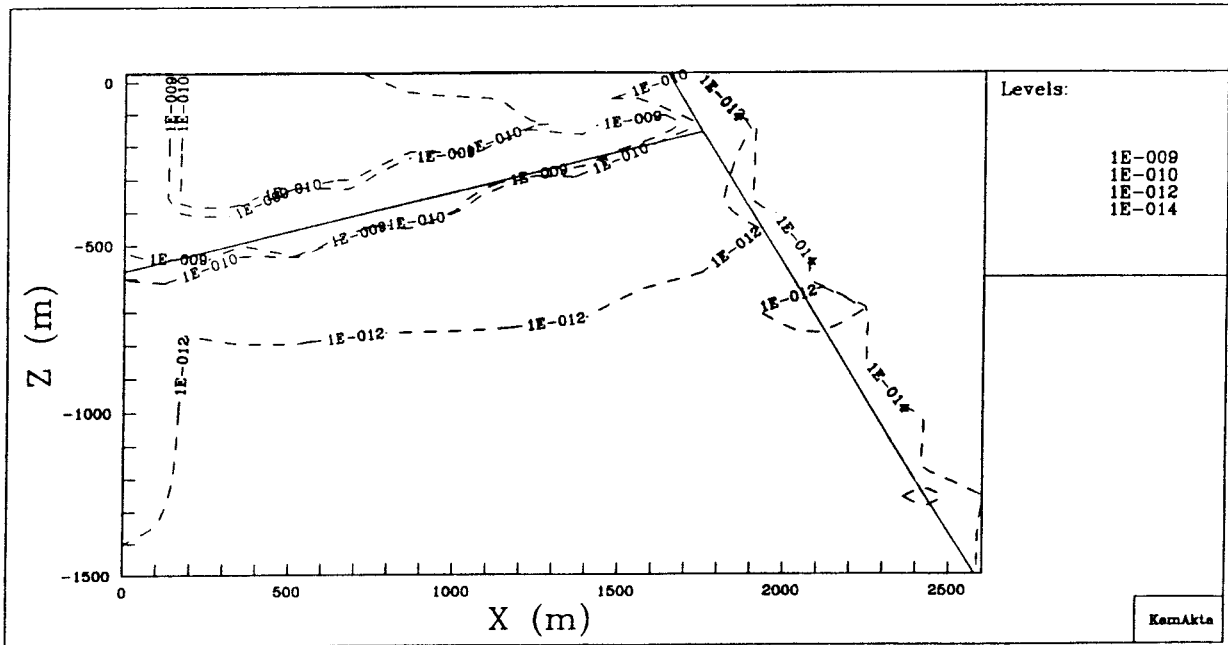


Figure 5.2b Flux distribution for Case 2D2; no-flow lateral boundaries, salt below zone 2. Flux values are expressed in $m^3/m^2/s$.

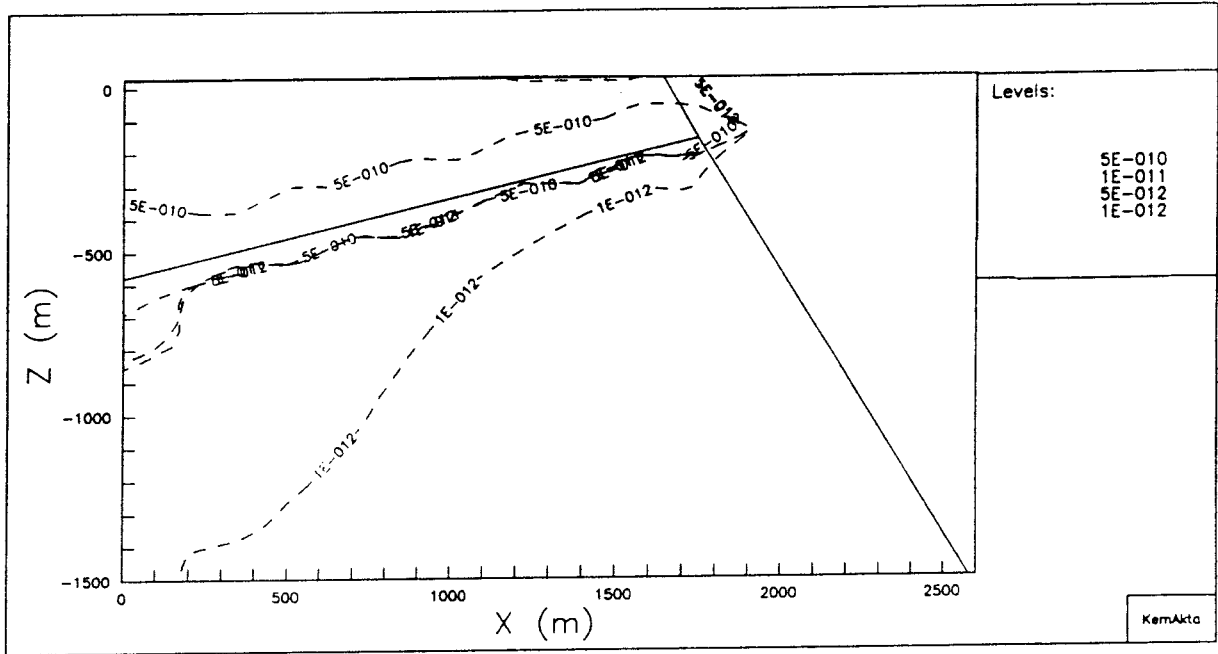


Figure 5.2c Flux distribution for Case 2D3; hydrostatic lateral boundaries, no salt. Flux values are expressed in $m^3/m^2/s$.

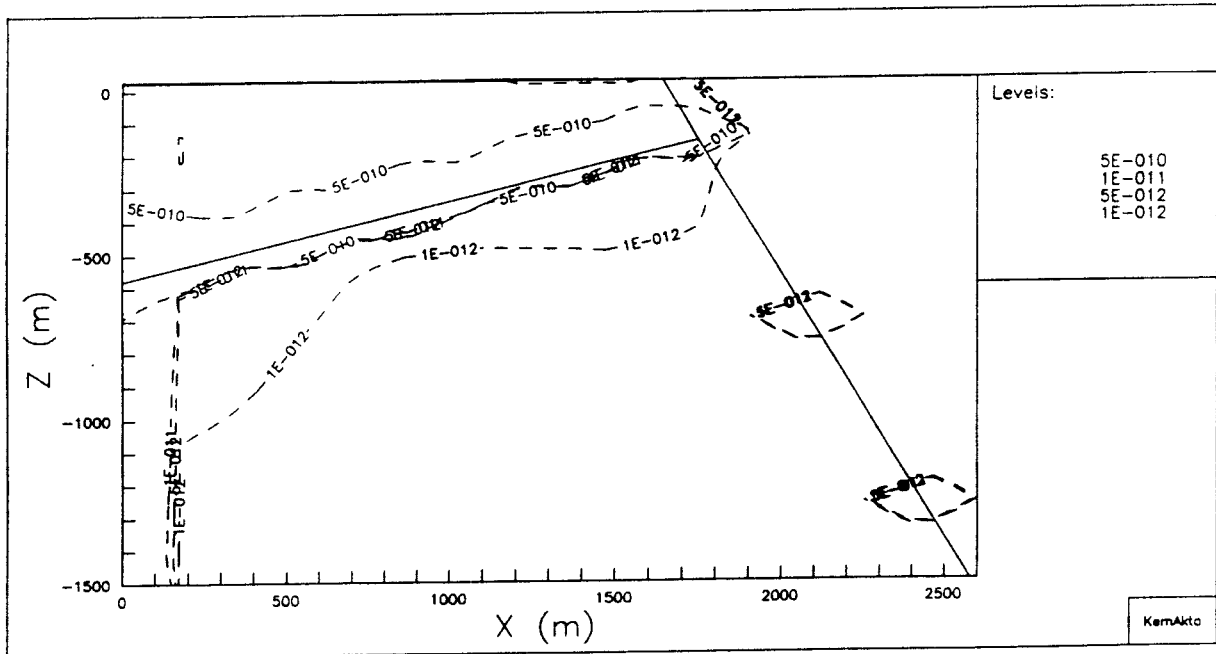


Figure 5.2d Flux distribution for Case 2D4; hydrostatic lateral boundaries, salt below zone 2. Flux values are expressed in $m^3/m^2/s$.

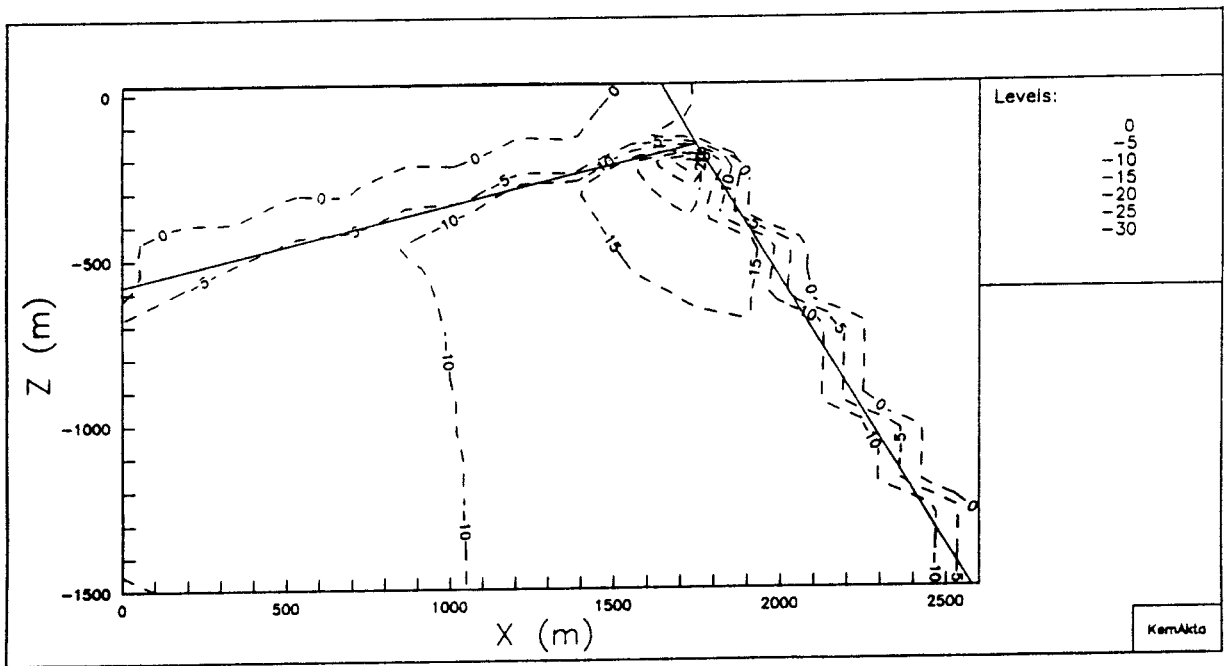


Figure 5.2e Relative difference in flux between Cases 2D1 and 2D2; no-flow lateral boundaries.

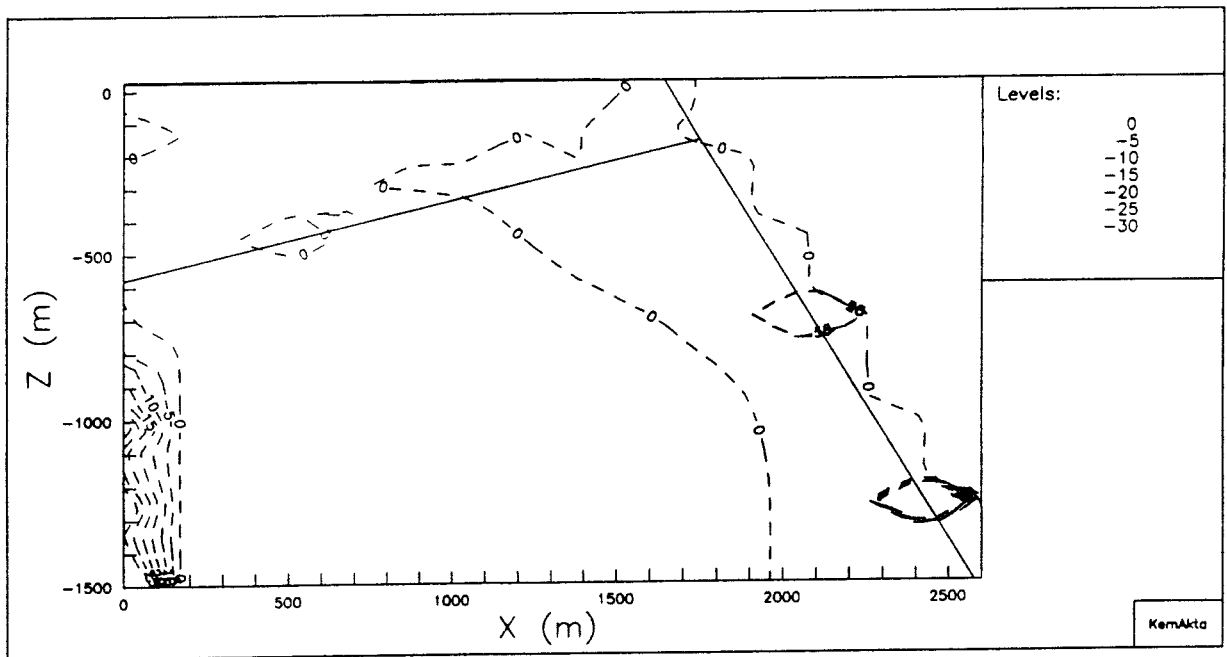


Figure 5.2f Relative difference in flux between Cases 2D3 and 2D4; hydrostatic lateral boundaries.

5.4.2 Particle Tracking

Ten particles were released above and below zone 2. The generated flow paths are indicated in Figures 5.3a-5.3d. These figures show the same flow pattern above zone 2 in all four cases with a downwards directed flow to be drained out to zone 1 via zone 2. This also indicates that the effect from the presence of salt is negligible above zone 2. However, the flow situation below zone 2 seems to be strongly affected by the increased density, at least in terms of flow paths.

The two fresh-water cases (Cases 2D1 and 2D3) show a general flow situation in accordance with the expectations given the boundary conditions. However, the flow for Cases 2D2 and 2D4, i.e. when the increased density has been assigned below zone 2, show results that are somewhat confusing to begin with. Both cases indicate stagnation points just under zone 2 in its low-lying parts. This behaviour is an evidence of the slope of zone 2 and the increased density in combination. The slope of zone 2 creates a triangle located below zone 2 confined by a horizontal line from the intersection between zones 2 and 12, zone 1, and zone 2. This triangle produces an overburden on top of the purely static pressure, and counteracts with the corresponding triangle formed by zone 2, the intersection between zones 1 and 2, and a horizontal line from the latter point to zone 12. This counteraction creates a flow oppositely directed to the case when no salt is present. It is further allowed to take place, since zone 2 is extremely pervious and effectively separates the domain into two flow cells without connection.

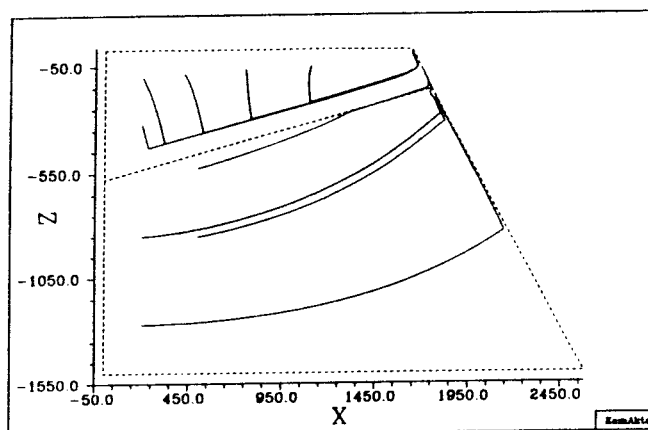


Figure 5.3a Particle tracking Case 2D1; no-flow lateral boundaries, no salt.

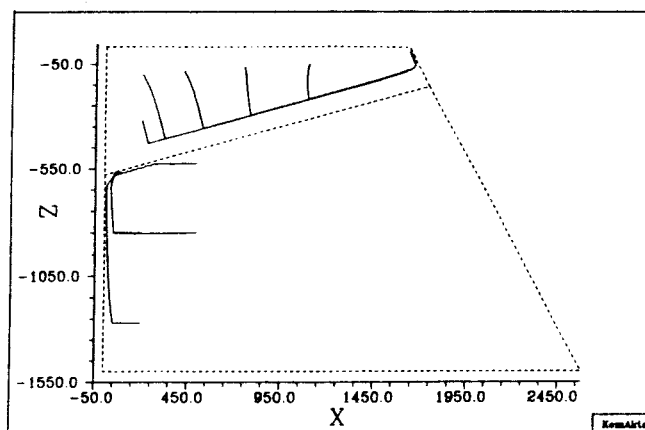


Figure 5.3b Particle tracking Case 2D2; no-flow lateral boundaries, salt below zone 2.

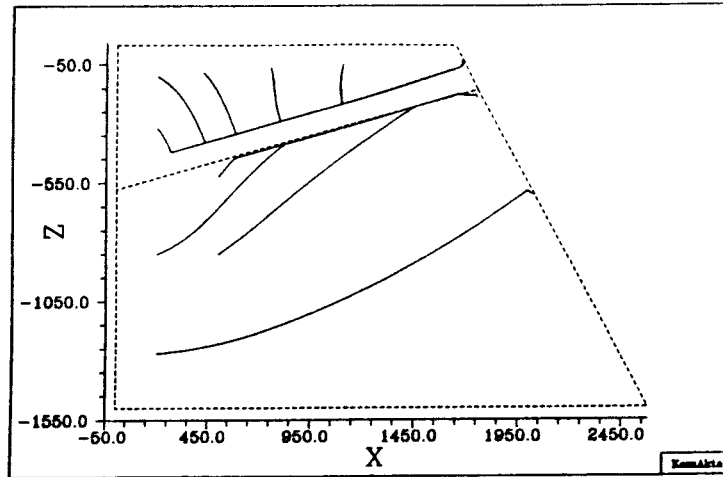


Figure 5.3c Particle tracking Case 2D3; hydrostatic lateral boundaries, no salt.

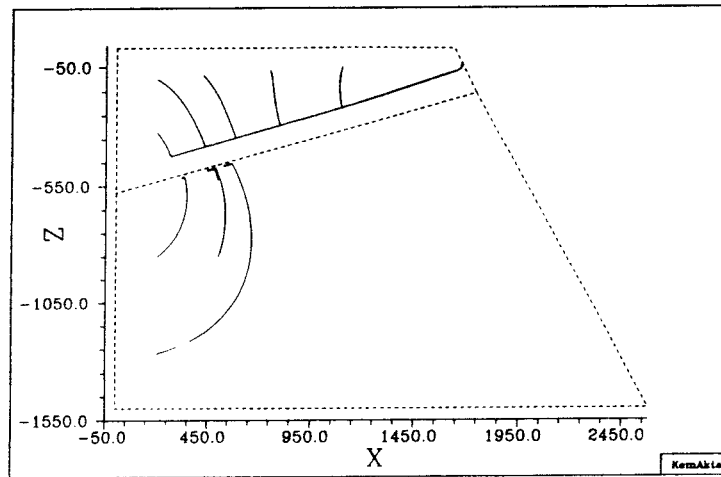


Figure 5.3d Particle tracking Case 2D4; hydrostatic lateral boundaries, salt below zone 2.

The accumulated travel times of the flow paths are all in the order of 100 years for the particles released above zone 2 for all four cases, while the travel times below zone 2 differ substantially and are all subject to large uncertainties since they tend to oscillate for the two cases when salt is present. The flow paths below zone 2 without salt, indicate travel times of roughly 100000 years in the case with no-flow boundaries, and about one order of magnitude faster for the case with hydrostatic boundaries. It should be noted that all these travel times assume a porosity of 1.0.

5.5 Conclusions

Apparently the increased density caused by the presence of salt in combination with the slope of zone 2 affect the flow to a certain degree. The flow above zone 2 does not, however, seem to be affected at all since zone 2 acts as a separating barrier against vertical interaction between the two domains above and below zone 2, respectively. The flow rate below zone 2 has on the other hand increased by the increase in density by roughly a factor of ten in terms of flux values, and also in terms of flow paths. The latter was obvious since oscillating particle tracks were representing stagnation points.

Typical flux values at the level of a potential repository are in the order of 10^{-11} - 10^{-12} $m^3/m^2/s$, which corresponds to about 30-300 $ml/m^2/year$. The fluxes were increased by roughly a factor of ten in the area below zone 2 in the "no-flow cases". However, this increase is favourable in this context since the groundwater is flowing in the opposite direction if compared to the fresh-water case, and would lower the release of radionuclides from a potential repository rather than the opposite. This assumption is based on the resulting stagnation points that were shown. However, if the particles had been released closer to the right hand boundary, their exit points would surely have been located at the right hand boundary; provided that they had been released far enough to the right.

It has to be emphasised though, that the results have to be regarded and evaluated in a qualitative manner since the modelling is performed in a semi-generic fashion with little or no knowledge about the boundary conditions in nature. Particularly the case when hydrostatic lateral boundaries were assumed has to be regarded as rather an unrealistic feature. The cases with no-flow lateral boundaries are probably more realistic.

As mentioned, the results are undoubtedly affected by the salt. Despite this, the possible presence of salt on a three-dimensional scale will not be considered. This decision is based on that the lateral boundary conditions are uncertain, and that the spatial distribution of salt is unknown in the area. This would probably imply that the calculated results would suffer from uncertainties to some extent.

6. Three-Dimensional Modelling on the Semi-Regional Scale

6.1 Introduction

The extension of the semi-regional model is shown in Figure 3.1a. Its areal coverage is roughly 40 km². It has been modelled to a depth of 1500 m. The top boundary coincides with the elevation of the groundwater table according to Figure 3.1b. The bottom boundary is modelled horizontal. The lateral boundaries are vertical, coinciding with the strike and inclination of the bounding fracture zones in east, west, and south, while the northern boundary aligns with the main direction of the gradient prevailing in that area.

6.2 Discretisation of the Domain

The model is limited by the lateral regional lineaments Imundbo (east), Dannemora and Gräsbo (south), and Skogsbo (west). The northern boundary aligns with the main gradient in that particular area; see further Figure 3.1a for the positions of the boundaries. Apart from the bounding regional lineaments, a number of well expressed zones are included, which are referred to as semi-regional fracture zones. These are numbered 1, 3, 4, 12, 13, and 14. Moreover, zone 2 was also included because of its hydraulic significance.

A horizontal view of the geometry of the domain and the finite element mesh describing the semi-regional model are shown in Figure 6.1; compare with Figure 3.1a. The geometry shows how the fracture zones are defined. The discretisation of the domain into finite elements is shown in the right-most figure. The division of the area between zones 1, 4, 12, and 14 is intended for a possible step-wise increasing extension of zone 2. Note that the figures show a horizontal view, implying that zone 2 is not explicitly visible since it is located below the ground surface. The mesh consists of roughly 35000 8-noded brick elements evenly distributed in 24 layers. The element widths are in the order of 50-60 m.

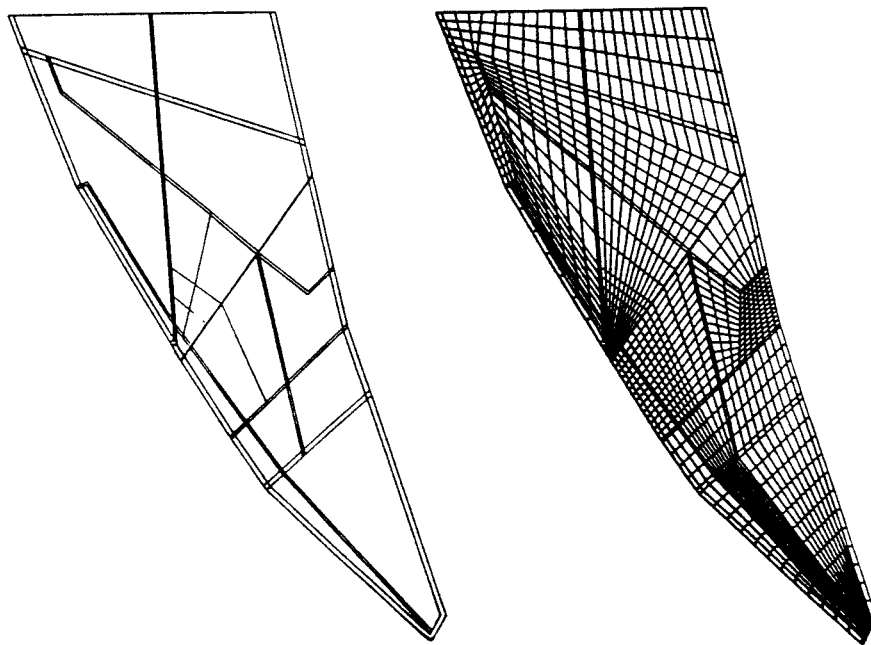


Figure 6.1 Horizontal view of the top boundary of the geometry of the domain intended to describe the geological features (left), and the finite element mesh (right); see also Figure 3.1a

6.3 Case Definitions – Nomenclature, Hydraulic Properties, and Boundary Conditions

The hydraulic data provided in the Background Report, are given with uncertainty ranges. For instance, the power function determining the hydraulic conductivity variation with depth for the rock mass has been reported as a 95% confidence interval. Furthermore, it is stated that the evaluation of the conductivities of the fracture zones is uncertain, since some of the zones have not been penetrated by boreholes meaning that no field measurements have been performed in these zones. Another issue of importance is the extension of the sub-horizontal zone 2. Its areal coverage is not known in detail, and the estimated groundwater flow in it, is high enough to suspect that the zone has direct or indirect connection with a water source, which is assumed to be Lake Finnsjön.

These uncertainties, suggest that the flow analysis on the semi-regional scale should include a sensitivity analysis with respect to the assumed hydraulic conductivities of the rock mass and the fracture zones, and with respect to the extension of zone 2 towards Lake Finnsjön. To this end, three different set-ups (apart from the Base Case) have been formulated. They include analyses concerning i) the limit values of the conductivity of the rock mass according to the specified confidence interval of the power function describing the depth dependence, ii) fracture zones having the same properties as the rock mass, iii) extension of zone 2 towards Lake Finnsjön. Following cases were considered within the study (the model set-ups are also shown in Table 6.1):

- Base Case, from now on called Case 3DSB: Hydraulic properties in accordance with the reference values given in Sections 3.4 and 3.5.
- Variation 1 (intends to illustrate the model’s sensitivity to uncertainties in the conductivities of the rock mass): Hydraulic conductivities of the fracture zones are the same as for the Base Case. The hydraulic conductivity of the rock mass is assumed to be depth dependent according to the upper and lower limit for the 95% confidence interval of the power function describing the depth dependence. This implies two cases, from now on called Case 3DS1A (upper limit) and 3DS1B (lower limit), respectively.
- Variation 2 (intends to illustrate the model’s sensitivity to the presence of fracture zones): Hydraulic conductivities of the fracture zones are equal to those of the rock mass, i.e. the fracture zones are neglected. This case is from now on called case 3DS2.
- Variation 3 (intends to analyse the extension of zone 2 towards Lake Finnsjön): Zone 2 is modelled to intersect with zone 14. The results from this variation will be focussed on flow calculations in and to zone 2, in order to have the model calibrated against the estimated natural groundwater flow rate in zone 2. The conductivities of the fracture zones and the rock mass are the same as for the Base Case (apart from the indirect change the elongated zone 2 implies). This variation is from now on called case 3DS3.

Table 6.1 Model set-ups for the cases considered for the semi-regional model.

Case	Rock Mass		Fracture Zones	
	ref. value	Upper limit ¹	Lower limit ¹	ref. value rock mass
3DSB	X			X
3DS1A		X		X
3DS1B			X	X
3DS2	X			X
3DS3 ²	X			X

¹ refers to the limits of the 95% confidence interval.

² zone 2 modelled to extend to intersect with zone 14.

The hydraulic conductivities for the different cases are shown in Table 6.2, and the fracture zone conductivities corresponding to the reference values are shown below in Table 6.3.

Table 6.2 Hydraulic conductivities (m/s) for the cases on the semi-regional model.

Case	Rock mass	Fracture zones
3DSB	$1.04 \cdot 10^{-6} \cdot z^{-1.10}$	Ref. values
3DS1A	$1.04 \cdot 10^{-6} \cdot z^{-0.82}$	Ref. values
3DS1B	$1.04 \cdot 10^{-6} \cdot z^{-1.37}$	Ref. values
3DS2	$1.04 \cdot 10^{-6} \cdot z^{-1.10}$	$1.04 \cdot 10^{-6} \cdot z^{-1.10}$
3DS3	$1.04 \cdot 10^{-6} \cdot z^{-1.10}$	Ref. values

Table 6.3 Reference values of the hydraulic conductivities (m/s) for the fracture zones.

Zone	Width (m)	Inclination (degrees)	Hydr. Cond (m/s)
1	20	75 SE	$1.21 \cdot 10^{-3} \cdot z^{-1.10}$
2	100	16 SW	$1.02 \cdot 10^{-2} \cdot z^{-1.10}$
3	50	80 SW	$5.77 \cdot 10^{-4} \cdot z^{-1.10}$
4	50	60 SW	$3.14 \cdot 10^{-3} \cdot z^{-1.10}$
12	50	90	$3.70 \cdot 10^{-4} \cdot z^{-1.10}$
13	50	90	$1.21 \cdot 10^{-3} \cdot z^{-1.10}$
14	50	90	$3.70 \cdot 10^{-4} \cdot z^{-1.10}$
Skogsbo	100	90	$3.14 \cdot 10^{-3} \cdot z^{-1.10}$
Giboda	100	90	$3.14 \cdot 10^{-3} \cdot z^{-1.10}$
Imundbo	100	90	$3.14 \cdot 10^{-3} \cdot z^{-1.10}$
Gräsbo	100	90	$3.70 \cdot 10^{-4} \cdot z^{-1.10}$
Dannemora	100	90	$3.70 \cdot 10^{-4} \cdot z^{-1.10}$
Källviken	100	90	$1.21 \cdot 10^{-3} \cdot z^{-1.10}$

The boundary conditions applied are of no-flow type along the bottom boundary and the lateral boundaries. The nodal points located at the top boundary coincide with the elevation of the groundwater table, and an atmospheric pressure $p=0$ kPa has been prescribed to these nodes.

6.4 Modelling Results

6.4.1 General

The evaluation of the modelling results has comprised pressure distribution calculations in four horizontal and four vertical cross-sections, particle tracking, and flux calculations for all cases studied, except for Case 3DS3. The evaluation of Case 3DS3 is oriented towards mass balance and flow calculations in order to analyse the flow into and out of zone 2 for calibration purposes, rather than a presentation of the results in a traditional way.

The amount of figures to present is rather substantial. In order to reduce the volume of the report to some extent, a representative selection of figures will be shown in the report in the running text for those cases that are commented upon. The evaluation of Cases 3DS1A and 3DS1B showed that the model results were affected only to a limited degree by the variation of the hydraulic conductivities in these cases; only by a scaling factor consistent with the change of conductivity. No major impact on the flow system in a general sense was visible for these cases. Thus, in order to reduce the volume of the report, these cases will not be commented upon in the running text. However, the complete set of figures associated with the evaluation of the results are shown in Appendix A for all the cases.

6.4.2 Pressure Distribution

Horizontal cross-sections

The pressure distribution was evaluated at following levels:

- At 200 m below the ground surface (located between zone 2 and the top surface),
- At 500 m below the ground surface, corresponding to the depth of a potential repository,
- At 800 m below ground surface, (roughly 200-500 m below zone 2), and
- At 1300 m below the ground surface to illustrate the flow situation at great depths.

The positions for these cuts will be maintained for the complete analysis on the semi-regional scale, and furthermore, they will also be considered for the evaluation of the results on the local scale described in Chapter 7. The general impression is that the vertical pressure drop is limited to be only in the order of 1-2 m in hydraulic head from a level at $z=-200$ m below ground surface down to a level at -1300 m below ground surface for all cases. The reason for this is that the fracture zones act as transmitters for the pressure at the top boundary since they are very pervious if compared to the rock matrix (roughly three orders of magnitude as an average). To illustrate this, the pressure in a cut at 200 m below ground surface is compared with the pressure in a cut at -1300 m for Case 3DSB, see Figures 6.2a-b.

Another main feature is that the cases do not differ internally to a very large extent. If the plots showing the pressure distribution at a certain level are superimposed, they align almost perfectly. The lack of difference between the cases could be seen as an evidence of that the flow is governed by the topography for all cases. The small differences obtained between the cases are shown in Figures 6.3a-6.3b, where the pressure distribution is shown for Cases 3DSB and 3DS2 at the level $z=-500$ m below ground surface.

Vertical cross-sections

The pressure distribution in four vertical cuts has been evaluated. The locations of these are shown in the legends of the figures. The intention has been to show the overall pressure distribution vertically and to illustrate the importance of the fracture zones within the local area. The locations of the vertical cuts will be maintained for all the cases analysed within the modelling of the semi-regional area.

One out of four vertical cross-sections has been chosen for presentation. This cut crosses the entire domain from south-west to north-east. It was selected to illustrate the hydraulic importance of zone 2 which is strongly emphasised here, see Figures 6.4a and 6.4b. The curvature of the isopotentials are approximately aligning with the slope of zone 2 for Case 3DSB as opposed to the situation for Case 3DS2. Conclusively, the distribution of pressure differs only in the case when the fracture zones were regarded as rock mass (Case 3DS2).

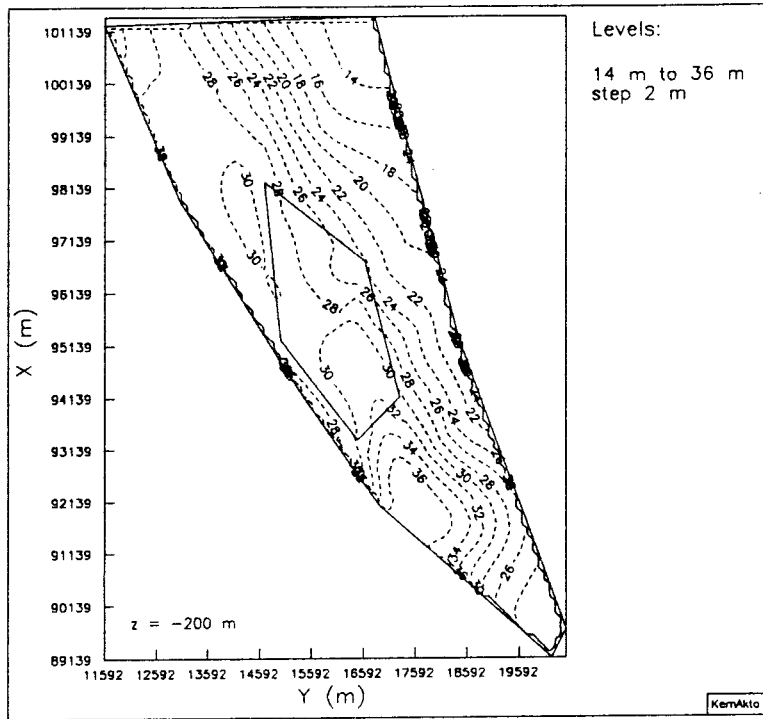


Figure 6.2a Pressure distribution at a level of $z=-200$ m; Case 3DSB, the Base Case.

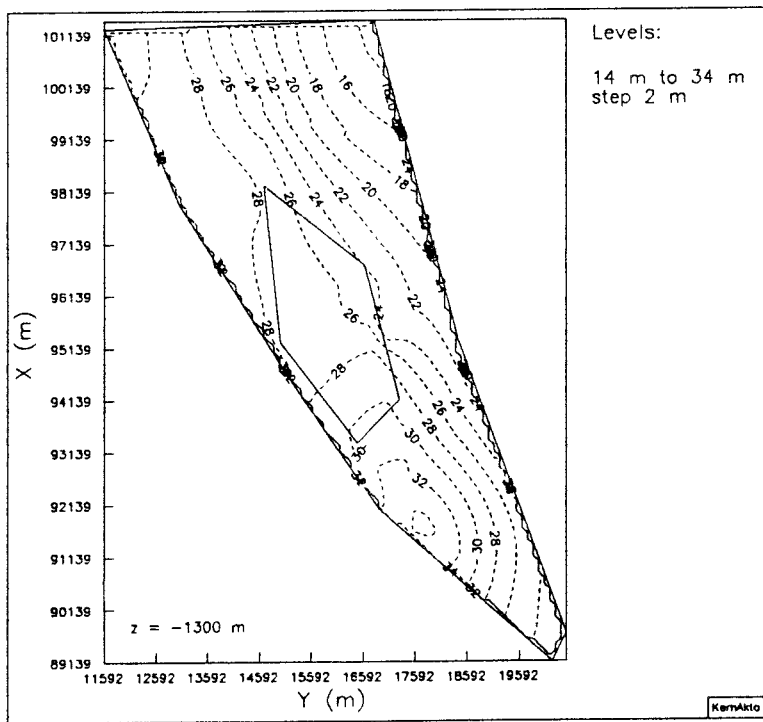


Figure 6.2b Pressure distribution at a level of $z=-1300$ m; Case 3DSB, the Base Case.

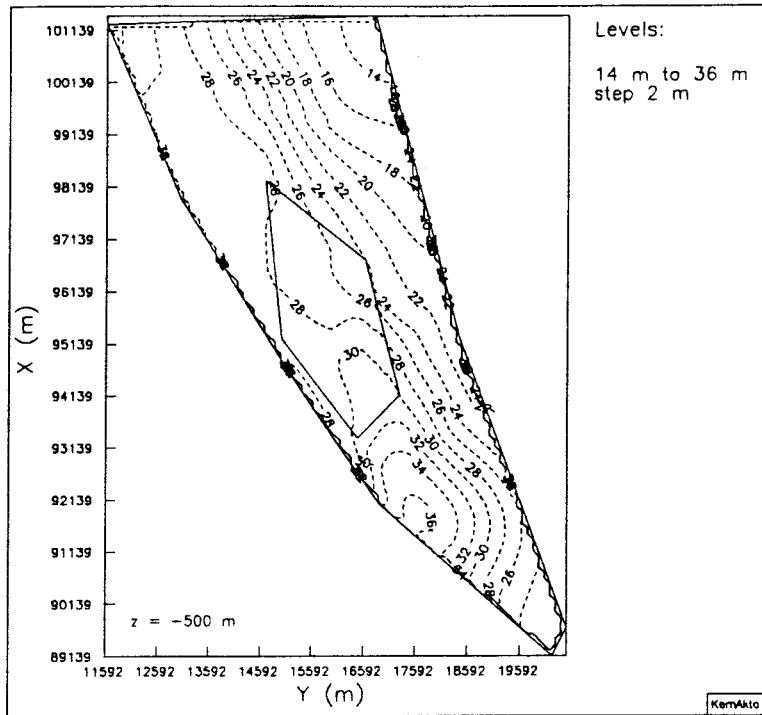


Figure 6.3a Pressure distribution at a level of $z = -500$ m; Case 3DSB, the Base Case.

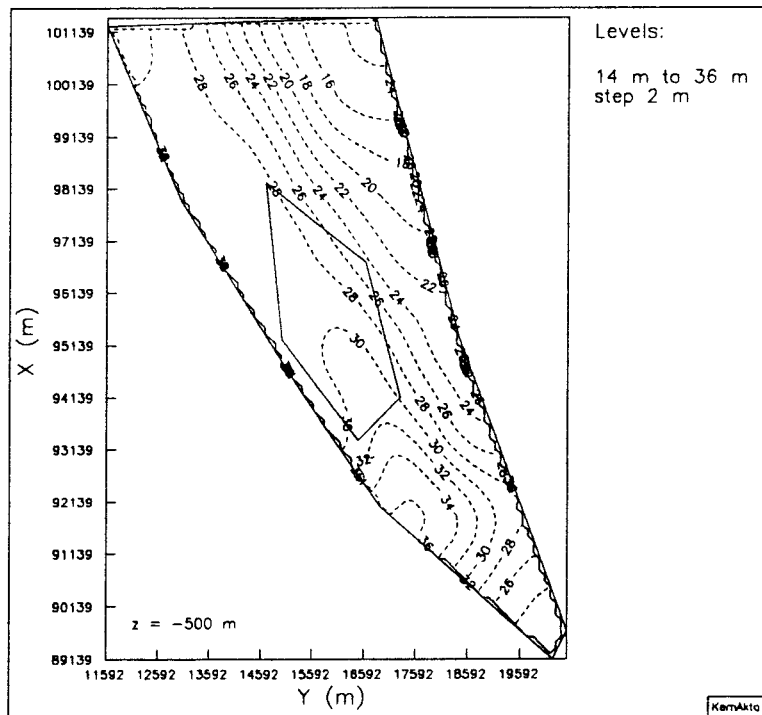


Figure 6.3b Pressure distribution at a level of $z = -500$ m; Case 3DS2, homogeneous rock mass properties.

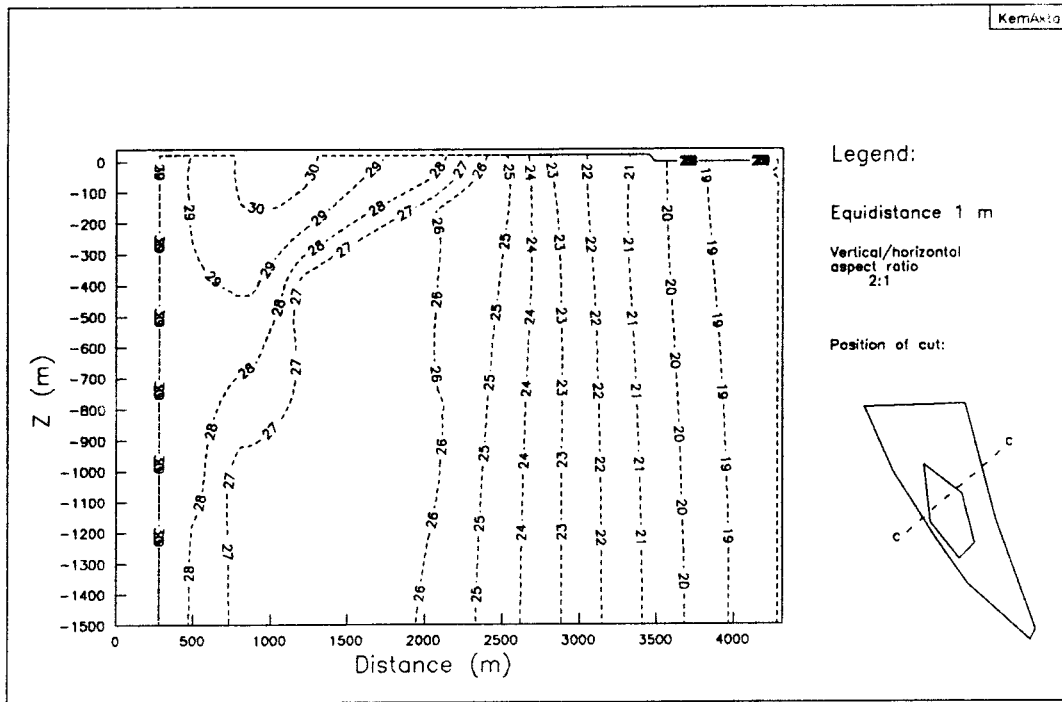


Figure 6.4a Pressure distribution in vertical cut 3; Case 3DSB, the Base Case.

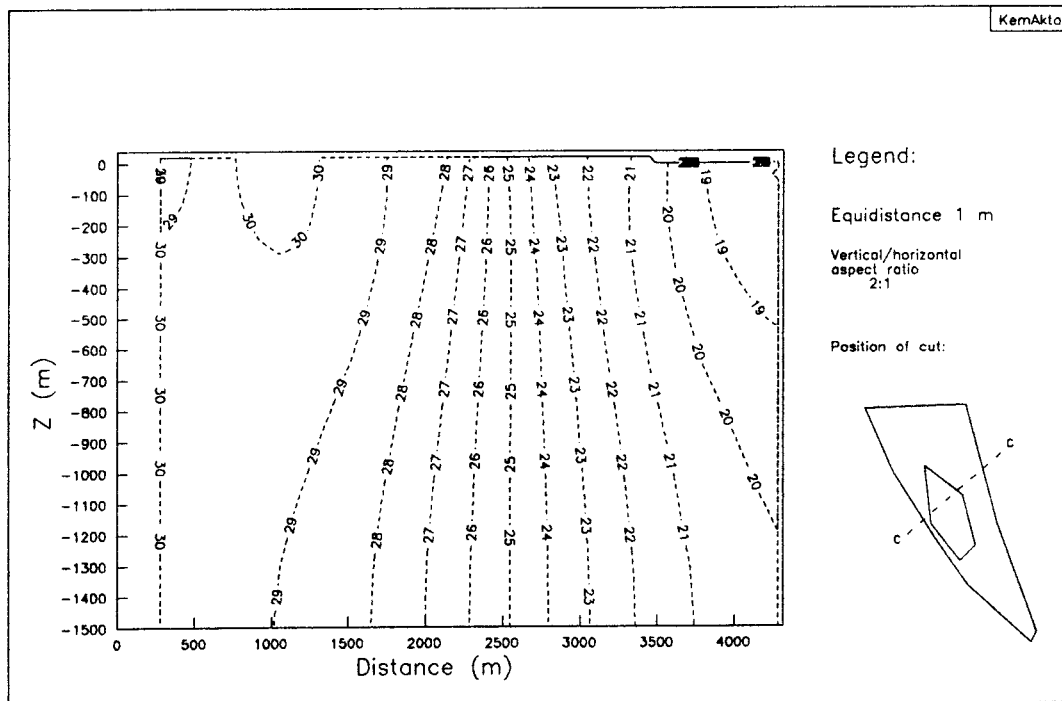


Figure 6.4b Pressure distribution in vertical cut 3; Case 3DS2, homogeneous rock mass properties.

6.4.3 Particle Tracking

Eight particles were released within an area corresponding to the potential repository. All of them were released at the level of the repository, i.e. at 500 m below ground surface. See Figure 6.5 for the positions and coordinates of the release points in a horizontal projection. The resulting flow paths are presented graphically in one horizontal projection and two vertical projections, and as tabulated values on accumulated time and length of the flow paths. It should be noted that the release points for water particles will be the same for the local modelling, which will provide a means for a check of the consistency in the calculated results on the two scales. The complete set of figures showing the pathlines on the semi-regional scale is shown in Appendix A.

The horizontal projections of the pathlines intend to illustrate the importance of fracture zones by comparing Case 3DSB with Case 3DS2, and to show the rough regional flow pattern in the area of concern as illustrated in Case 3DS2. These plots are displayed in Figure 6.6. The figure illustrates the important role played by the fracture zones, since the discharge is not specifically directed to a particular point for Case 3DS2, but rather to the top boundary in general. The discharge point for Case 3DSB is concentrated to the intersection between zones 1 and 4 for further discharge at the top boundary at a location a distance north-east of this intersection. The water is preferentially flowing in zone 2 on its way to the intersection between zones 1 and 4.

The flow paths in the vertical cut for Cases 3DSB and 3DS2 illustrate that the flow paths are strongly affected vertically by the presence of fracture zones, see Figures 6.7a-b. In particular, the draining effect of zone 2 is visible in Figure 6.7a. The differences between the cases are further illustrated in Table 6.4, where the accumulated travel times and travel lengths are summarised. A porosity of $1 \cdot 10^{-4}$ has been assumed for the calculation of travel times.

Table 6.4 *Accumulated travel time (ACT) in years and accumulated travel length (ACL) in metres for Cases 3DSB and 3DS2.*

Case:	3DSB		3DS2	
Path no	ACT	ACL	ACT	ACL
1	1712	2628	2378	3582
2	539	2178	1427	2412
3	1649	2286	951	1926
4	3108	2664	2917	3204
5	1903	2394	2347	2844
6	1649	2286	1998	2592
7	32	1584	6405	4032
8	95	1584	5708	3762

The results in Table 6.4 indicate that the resulting flow paths are consistent in terms of travel times and travel lengths given the conductivities assigned for the two cases. The travel lengths are consistently higher for Case 3DS2 (with one exception), which also is in agreement with the expectations.

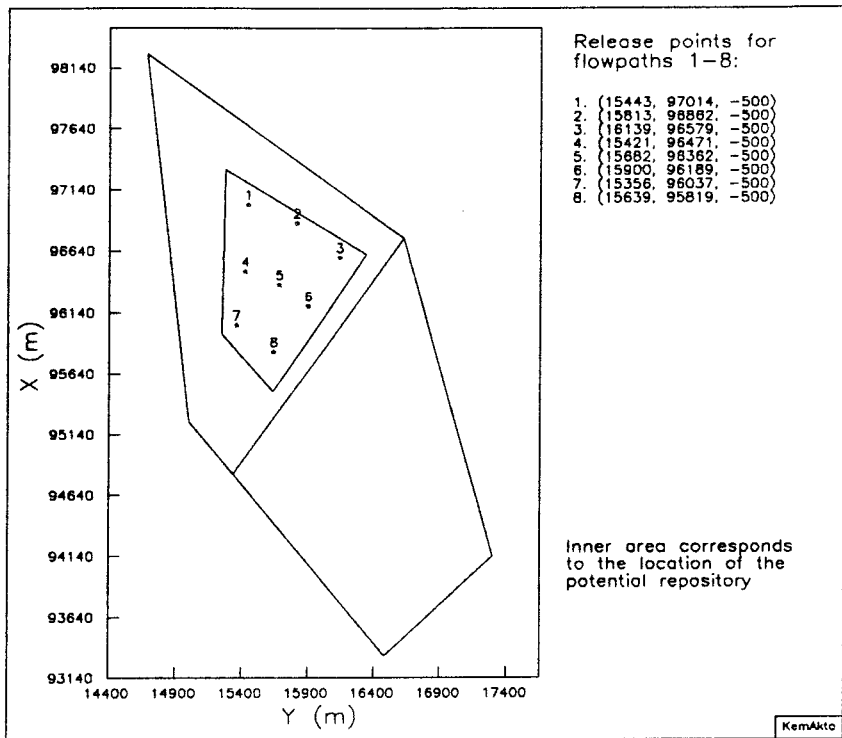


Figure 6.5 Horizontal view of release points for water particles. The potential repository is located within the inner marked area.

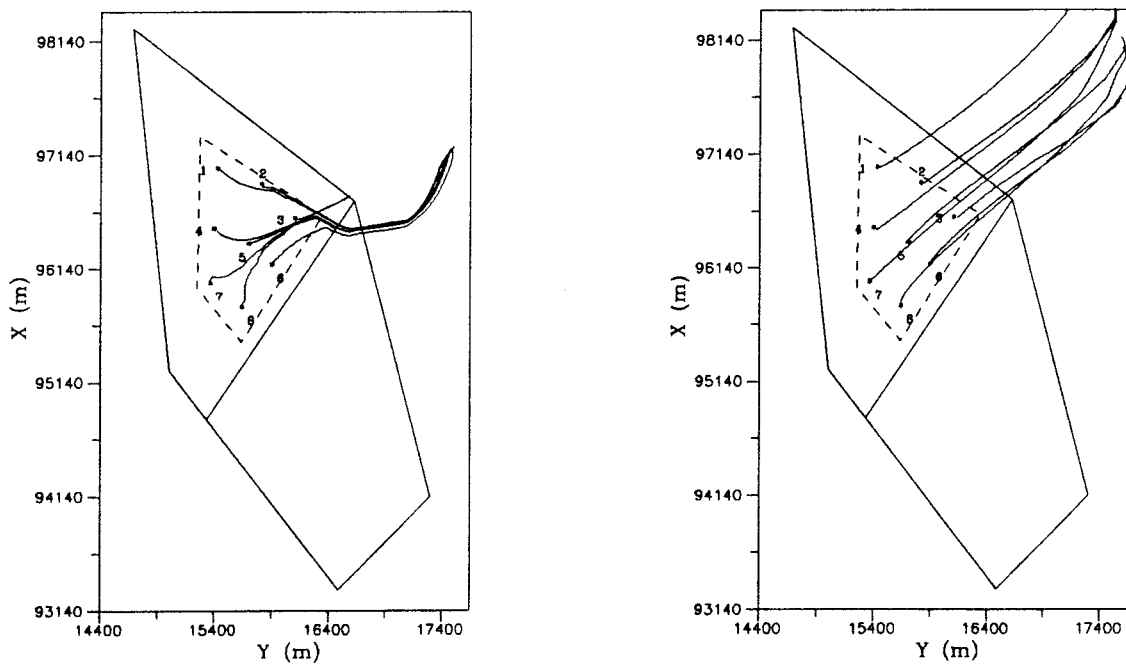


Figure 6.6 Horizontal projection of pathlines for Cases 3DSB (left) and 3DS2 (right).

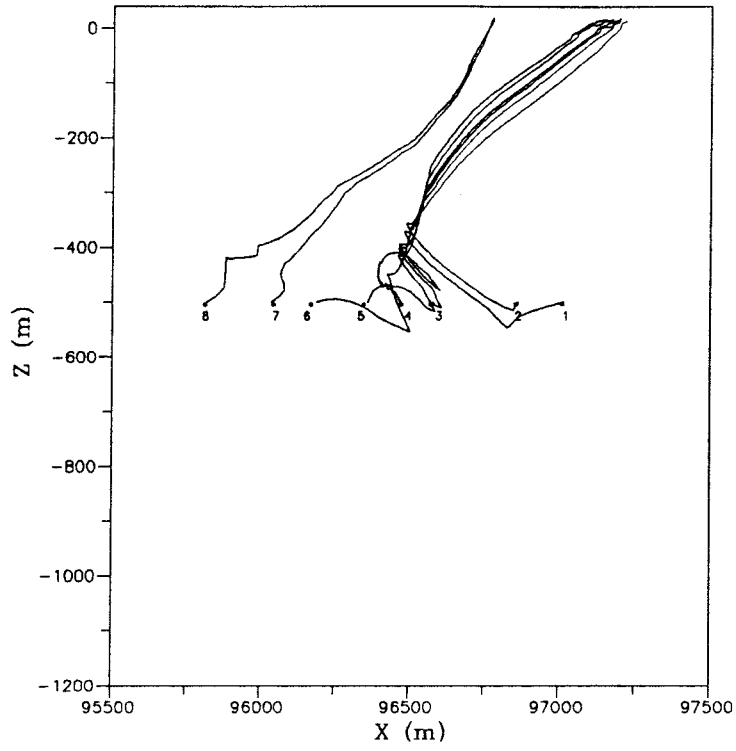


Figure 6.7a Vertical projection (xz-plane) of pathlines; Case 3DSB, the Base Case.

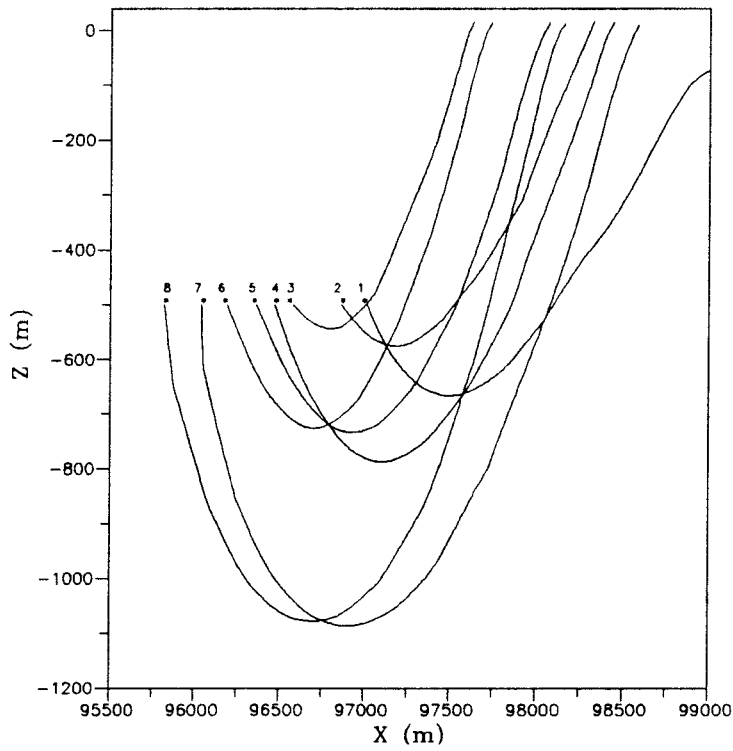


Figure 6.7b Vertical projection (xz-plane) of pathlines; Case 3DS2, homogeneous rock mass properties.

6.4.4 Flux Distribution in the Potential Repository

The flux distribution in a horizontal cut covering the potential repository is evaluated for each of the cases (except for Case 3DS3), again for reasons of possibilities for comparisons between the different cases. Furthermore, the flux distribution when evaluated within the modelling of the local area, is calculated at exactly the same positions, which again will provide means for judging the consistency of the results on the semi-regional and the local scale. This may give hints on the significance of the grid resolution and the future transfer of boundary conditions from the semi-regional to the local scale model.

The flux values given in the figures to follow correspond to the volumetric flux ("Darcy velocity") calculated as the sum of absolute values in the x-, y-, and z-directions, discarding the direction of the flow, which should be interpreted as the flux value at a given point in space regardless of the direction of the flow. This is calculated as follows:

$$|q| = \sqrt{q_x^2 + q_y^2 + q_z^2}$$

The resulting fluxes are displayed in figures 6.8a-6.8b for Cases 3DSB and 3DS2. It cannot be strongly enough emphasised that the figures only intend to illustrate typical flux values, and therefore a number of contour levels are omitted. In order for the reader to show some caution when these plots are studied, the plotted levels and the highest and lowest values are indicated in the legend of these figures.

The fluxes in the fracture zones by far exceed the values in the interlying rock matrix; sometimes by several orders of magnitude. Case 3DSB show typical flux values of about 100 ml/m²/year in the area between zones 1, 4, and 12. The major portion of the flow takes place in the fracture zones. The evidence for this is that the location of the contours with high values roughly coincide with the strikes of the fracture zones. The opposite pattern is naturally at hand in Figure 6.8b for Case 3DS2, where the fluxes show values somewhere between 50 and 200 ml/m²/year unevenly distributed over the whole area. The latter figure merely shows the flux values, had the rock been intact with no disturbances in terms of fracture zones.

The flux values obtained at Finnsjön are roughly the same as those reported in the KBS 3-project. This may seem a bit surprising, since the hydraulic conductivities of both the rock matrix and the fracture zones in Finnsjön are substantially higher than those used in the KBS 3-project, which ought to lead to higher flux values. This apparently is not the case as shown in Figures 6.8a-6.8b. It could probably be explained by the relatively higher hydraulic conductivities assigned to the fracture zones in Finnsjön than in the KBS 3-study, which leads to the conclusion that the major portion of water flow takes place in the fractures. However, the main reason for this, is probably the fact that zone 2 unloads the system hydraulically and divides the domain into two flow regimes located above zone 2 (relatively high fluxes) and below it (relatively low fluxes). It may be worth noticing that the repository is located below zone 2 in the present study.

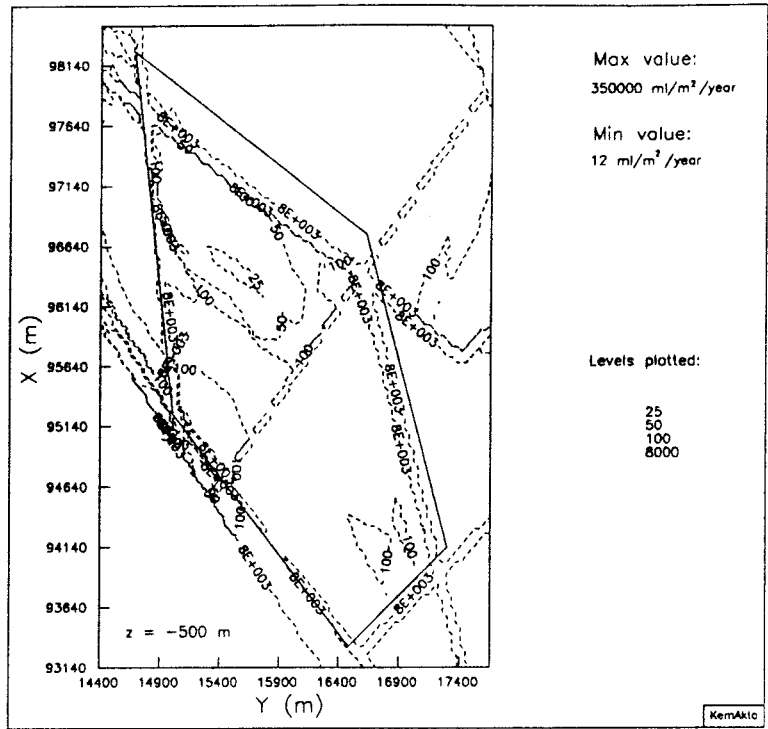


Figure 6.8a Flux distribution at a level of $z=-500$ m; Case 3DSB, the Base Case.

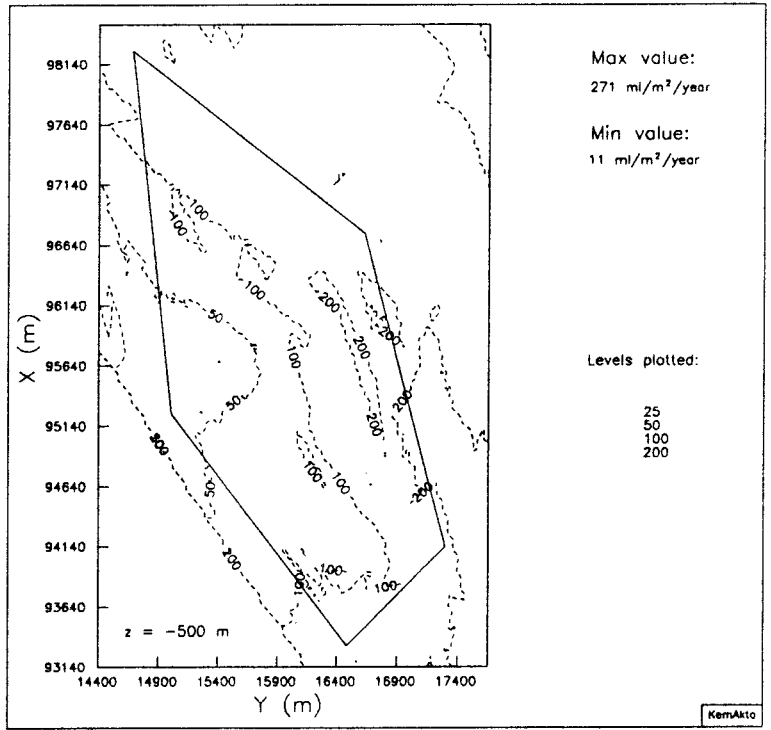


Figure 6.8b Flux distribution at a level of $z=-500$ m; Case 3DS2, homogeneous rock mass properties.

6.4.5 Evaluation of the Extension of Zone 2 Towards Lake Finnsjön

The position of the south-most confinement of zone 2 is somewhat uncertain. According to the initial understanding, zone 2 was intersected by zone 7 (which is a local fracture zone and not modelled on this scale). This intersection coincides with the south-most edge of zone 2 in Case 3DSB. However, there was reason to believe that zone 2 had either direct or indirect connection with a water source with enough storage to feed zone 2 with the amount of water estimated as the natural groundwater flow. The water source in this context is of course Lake Finnsjön. The flow rate in zone 2 has, according to the Background Report, been evaluated from field investigations and has been estimated to be roughly 5-10 l/s or 150000-300000 m³/year. The present analysis is oriented towards a calibration of the model against this flow rate. This of course has to be judged as rather a rough calibration measure, but it could give hints on the quality of the behaviour of the model. The flow was estimated in a vertical cut, the position of which is shown in Figure 6.9.

To investigate if the model was sensitive to alternative locations of the south-most edge of zone 2 with regard to the flow rates in zone 2, the latter was in Case 3DS3 modelled to intersect with zone 14 in south. The intention was to investigate whether or not Lake Finnsjön could feed zone 2 with water, either directly or via zones 1 and/or 12. Cases 3DSB and 3DS3 are compared to each other in this context.

To this end, water balance calculations were performed. The flow rates have been calculated both globally, and in a local sense by calculating the flow through individual element faces at particular points.

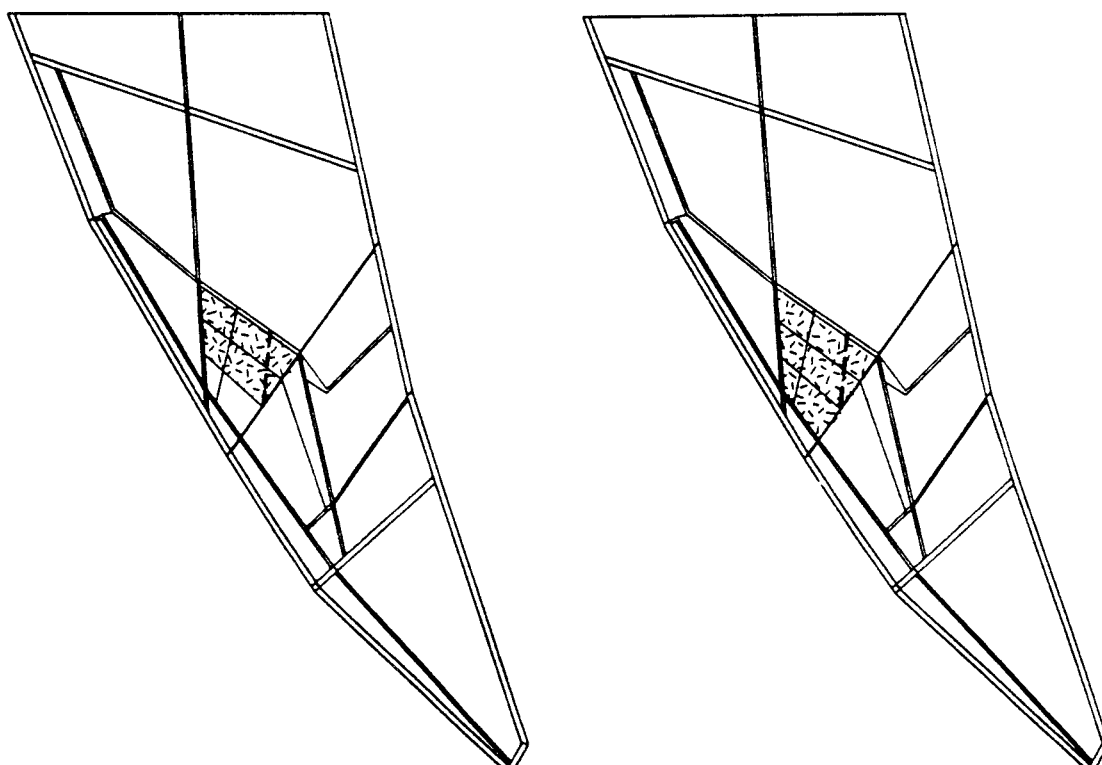


Figure 6.9 Horizontal view of the top boundary indicating the areal coverage of zone 2 (screened area) in Case 3DSB (left), and Case 3DS3 (right), as modelled on the semi-regional scale. The dashed line corresponds to the position of the cut through which the natural groundwater flow was estimated.

The results from the water balance calculations are tabulated with the use of some abbreviations. The calculation procedures and the abbreviations used in Tables 6.5a and 6.5b are explained below:

- TSA: flow through the top surface above zone 2,
- TS12: flow through the top surface of zone 12 between zone 4 and the location corresponding to zone 7 (Case 3DSB), or between zones 4 and 14 (Case 3DS3),
- TS1: flow through the top surface of zone 1 between zone 4 and the location corresponding to zone 7 (Case 3DSB), or between zones 4 and 14 (Case 3DS3),
- TS4: flow through the top surface of zone 4,
- TS14: flow through the top surface of zone 14,
- TC2: flow through top confinement of zone 2,
- BC2: flow through bottom confinement of zone 2,
- LC21: flow through lateral confinement of zone 2, facing zone 1,
- LC24: flow through lateral confinement of zone 2, facing zone 4,
- LC212: flow through lateral confinement of zone 2, facing zone 12,
- LC2S: flow through south-most lateral confinement of zone 2,

The flow through the top surface of the whole area was calculated to be $1.99 \cdot 10^6$ m³/year, which corresponds to an infiltration rate of roughly 46 mm/year as an average value distributed over the whole area of about 43 km². Corresponding calculations were performed for the case when only the fracture zones were considered. It turned out that $1.97 \cdot 10^6$ m³/year infiltrated through the fracture zones, which corresponds to about 370 mm/year over the fracture zones only, or 99% of the infiltrated water. This implies that the recharge rate through the rock matrix would be about 0.5 mm/year, with the fracture zones excluded.

Table 6.5a The flow (m³/year) into and out of zone 2 through its confining features for Cases 3DSB and 3DS3.

Feature	3DSB		3DS3	
	in	out	in	out
TC2	109000	45800	121000	51000
BC2	10100	41900	8750	46100
LC21	49500	14000	57300	15900
LC24	11100	135000	8630	148000
LC212	27600	0	32700	0
LC2S	14600	564	3790	0
	221900	237264	232170	261000
Deviation:	-15364 (6.7%)		-28330 (11.5%)	

The outflow is larger than the inflow for both cases, indicated by the "Deviation" in Table 6.5a. The mass balance deviation is thus calculated to be roughly 5% in Case 3DSB, and about 10% in Case 3DS3. Both values are considered relatively low, which has been possible to achieve due to the dense discretisation of the domain.

To further complement the flow values given in Table 6.5a, the flow through the top surface above zone 2 and the flow through the top surfaces of the fracture zones confining zone 2 were calculated. These flow rates are shown in Table 6.5b.

Table 6.5b The net flow (m³/year) through the top surfaces of fracture zones confining zone 2, and the rock matrix above zone 2.

Feature	3DSB	3DS3
TSA2	4770	5110
TS1	107000	126000
TS4	291900	279300
TS12	34500	29100
TS14	-	18100

The vertically directed flow from the top surface above zone 2, does obviously not contribute to the recharge of water to zone 2 vertically; compare features TSA2 and TC2 in the tables above. The main portion of water infiltrating through the top confinement of zone 2 rather emerges from the water from the bounding fracture zones; in particular from zone 12 and zone 1. A substantial amount of the water in these zones infiltrates laterally into the rock matrix above zone 2 for further vertical transport into zone 2. The remaining feed of water from the confining fracture zones to zone 2 are recharged through the lateral faces between zone 2 and the confining fracture zones.

The recharge rates shown in Table 6.5b indicate the pure vertical transport of water through the top boundaries of the fracture zones. This transport of water is not only directed to zone 2. This is particularly the case for the recharge to zone 4, which has the main part of the water discharged through elements not facing zone 2. The major discharge point in the area is the intersection between zones 1 and 4. About 80% of the water entering zone 12 is discharged to zone 2 at the element faces of zone 2, while corresponding values for zone 1 is about 33%. Moreover, zone 4 is recharged vertically from the top surface with 291900 m³/year, and is also recharged from zone 2 with about 124000 m³/year, which also indicates that the intersection between zones 1 and 4 is the main discharge point in the area of concern. These values all refer to Case 3DSB, with rather small differences if compared to Case 3DS3.

To further illustrate that the discharge point is located at the intersection between zone 1 and zone 4, the distribution of the recharge as a function of the distance along the element faces between zone 2 and zones 1 and 4, are shown in Figures 6.10a-6.10b for Cases 3DSB and 3DS3. From these figures it is obvious that zone 1 feeds zone 2 with water in the south-most part of their intersection, while the discharge is taking place in the northern part of zone 1 at its intersection with zone 4. The recharge to zone 2 from zone 4 is concentrated to the north-western corner and is very small if compared to the discharge which takes place along almost the whole intersection between the zones. The discharge from zone 2 into zone 4 increases rapidly towards the intersection between zones 4 and zone 1.

These figures indicate that the discharge is taking place by the intersection between zones 1 and 4, which is in good agreement with the position where the natural groundwater flow was estimated. This leads to the conclusion that the calculated flow rates also are in very good agreement with the ones measured in field; roughly 150000 m³/year for Case 3DSB.

What may seem surprising, is that the differences between the two cases 3DSB and 3DS3 are small. There was reason to believe that the flow in zone 2 in Case 3DS3 would be much higher than in Case 3DSB, since the elongation of zone 2 towards Lake Finnsjön would provide a means for a feed of water from the lake. However, the area of the intersection between zone 2 and zone 14 is rather small and is not significant in this context. In combination with a relatively low hydraulic conductivity of zone 2 at this

intersection, it made the elongation towards Lake Finnsjön less hydraulically important than initially anticipated. Furthermore, the boundary condition at the outer face of zone 14 is a no-flow boundary, which prevents water from entering zone 2 via zone 14. One possibility to increase the amount of water this way, had been to prescribe hydrostatic pressure to the nodes corresponding to the bottom of the lake, but since the maximum depth of Lake Finnsjön is only 4 m, this measure would certainly not have been enough to affect the results significantly.

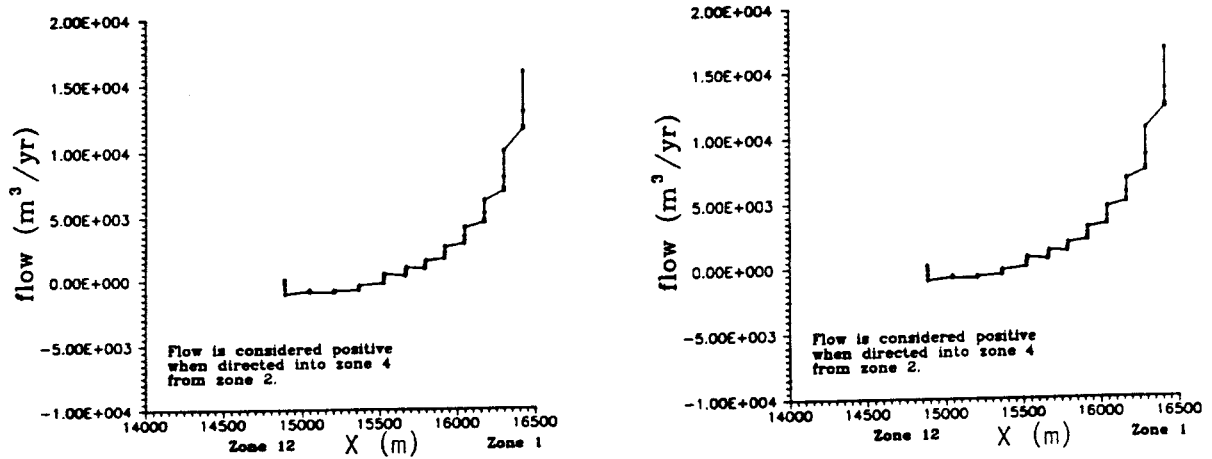


Figure 6.10a Flow distribution between zones 2 and 4 along the connecting element faces. Case 3DSB, the Base Case (left); Case 3DS3, zone 2 extended (right).

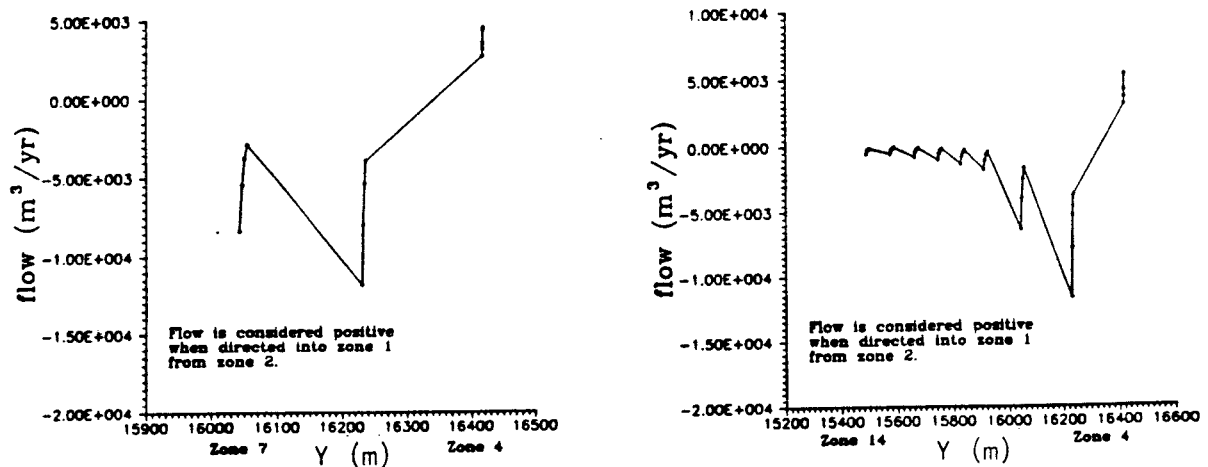


Figure 6.10b Flow distribution between zones 2 and 1 along the connecting element faces. Case 3DSB, the Base Case, (left); Case 3DS3, zone 2 extended (right).

6.5 Summing up

The general impression from the modelling on the semi-regional scale, is that the results obtained with the different cases are consistent with the expectations, which naturally depends on that the changes introduced from one case to another were rather modest.

The pressure distribution in both horizontal and vertical cuts showed that the vertical pressure drop is modest for all cases, which depends on that the fracture zones act as "transmitters" for the hydraulic head from the top surface down to the deeper parts of the domain. The relatively small differences between the cases when fracture zones were modelled are due to the rather small changes in hydraulic conductivities introduced.

It has also been shown that the fracture zones are important for the flow on the semi-regional scale. This was particularly indicated by the generated particle tracks for the case when the entire domain was treated as rock, when compared to the remaining cases. Moreover, this was supported when the infiltration rates were calculated over the top surface of the model, which showed that about 99% of the infiltrating water entered the model through the top surfaces of the fracture zones. The presence of fracture zones of course also affects the flow rates at the potential repository. These were calculated to be roughly 50-100 ml/m²/year for the Base Case in the inner part of the domain with substantially higher values in the fracture zones; sometimes with several orders of magnitude.

The water balance calculations performed for Cases 3DSB and 3DS3 indicated that the initial extension of zone 2 according to the formulation in Case 3DSB, had sufficient connection with the fracture zones to feed zone 2 with water enough to be able to judge the model set-up as calibrated in terms of groundwater flow through zone 2. The estimate of the natural groundwater flow was based on two independent measurement methods and considerations in general with regard to infiltration capacities and precipitation. This indicates that the estimate at least to some extent is based on firm grounds, despite that the estimated groundwater flow in zone 2 was reported in rather a wide span. Conclusively, the model set-up for Case 3DSB is considered calibrated, since the calculated amount of flow through zone 2 was within the span for this case. This is particularly valid since it has been reported orally by the authors to the Background report that the lower limit was more realistic than the upper.

Further, the extension of zone 2 aligning with the position of local fracture zone 7 was considered to be more likely than a position of the south-most edge of zone 2 intersecting with zone 14; especially since the differences in terms of flow through zone 2 between the two cases compared were rather limited. A feasible conclusion thus seems to be that the model to be used for a transfer of lateral boundary conditions to the local model, must be Case 3DSB. However, if a water balance calculation like the one presented in Section 6.4.5 will be carried out on the local scale, Case 3DS3 has to be used for a transfer of the lateral boundary conditions.

7. Three-Dimensional Modelling on the Local Scale

7.1 Introduction

The original intention of the modelling procedure of the present project, was to apply the semi-regional topography (i.e. the topography of the groundwater table) on the top of the semi-regional mesh. Correspondingly, the local topography would be applied on the top of the local mesh. The lateral boundary conditions on the local model would be transferred from a base case on the semi-regional scale. However, it is a well-known fact that it is a difficult task to produce topographic maps on different scales (in surveying in general), the contours of which can show a perfect fit at the different scales. The deviations from a perfect fit on the semi-regional and the local topography in this particular case, are illustrated in Figures 7.1a and 7.1b showing the semi-regional topography covering the area of the local scale compared to the local topography. As can be seen, there are rather large deviations, in particular along fracture zone 4, the northern boundary on the local scale.

When the initial calculations were performed on the local scale with transferred boundary conditions and a local scale topography, the model turned out to be extremely sensitive to the discrepancies in the description of the topography. In fact, the deviations appeared to be devastating to the model results on the local scale, when the local lateral boundary conditions were transferred from the semi-regional model. The reason for this is that the local topography is applied on the top of the local mesh, while the transferred boundary conditions originally stem from the semi-regional model. This implies that the nodal points one element row downwards from the top nodes located at the lateral boundaries of the local model, have pressure values roughly corresponding to those of the topography on the semi-regional model. This causes erroneously introduced gradients along the boundaries. These artificial gradients were calculated to be roughly 10-20% vertically directed in the initial calculations on the local scale.

Since the initial calculations on the local scale from the reasons mentioned above suffered severely from the lack of fit in the representation of the topography, the initial modelling strategy therefore had to be changed. It was decided that the local scale calculations would be performed with either the semi-regional or the local topography applied on the top of the local mesh. Furthermore, it was decided to study the impact of the type of lateral boundary condition by not only having the lateral boundary conditions transferred from the semi-regional base case, but also by simulating no-flow lateral boundaries for one of the cases. The TBC-code within the HYPAC-package was used for the calculation of the transfer of boundary conditions. This code is designed for the user to specify a tolerance width when interpolating nodal head values from the semi-regional scale to the local scale. This tolerance was set to 0.5 m in the present project. It could be chosen to a lower value, but by the cost of an increased computing time. The reader is advised to see in reference /Grundfelt, B., et al, 1989/ for further details on this parameter.

The major differences between the modelling on the semi-regional and the local scale concerning the description of the flow on the local scale, are a) the presence of local fracture zones, and b) the increased grid resolution.

The extension of the local model is shown in Figure 3.2a with an areal coverage of 6.6 km². It has been modelled to a depth of 1500 m with a horizontal bottom confinement. The lateral boundaries are coinciding with the strikes and inclinations of the bounding fracture zones in all directions.

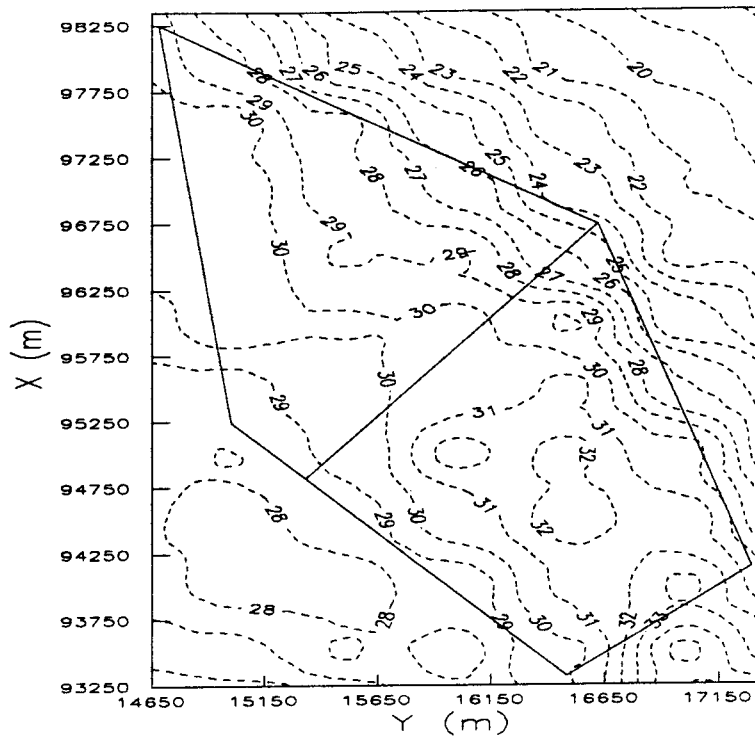


Figure 7.1a Topography on the local area as represented on the semi-regional scale. Note, that the aspect ratio is not 1 to 1.

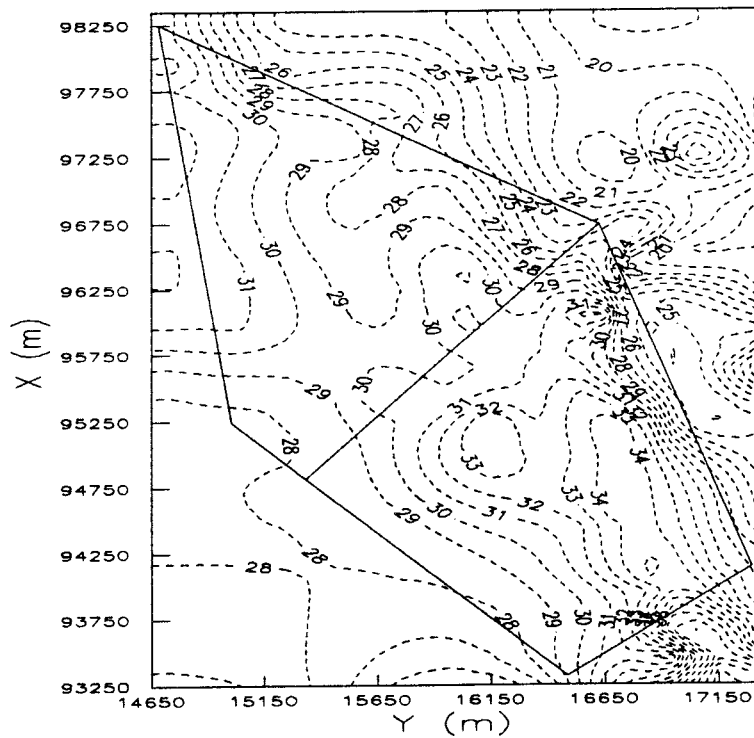


Figure 7.1b Topography on the local area as represented on the local scale. Note, that the aspect ratio is not 1 to 1.

7.2 Discretisation of the Domain

- Fracture Zones Included

The model is limited by fracture zones 3 (east), 4 (north), 12 (west), 13 (east), and 14 (south); see further Figure 3.2a for the positions of the boundaries. Apart from the bounding fracture zones, the sloping fracture zone 1, the subhorizontal zone 2, and the semi-generic fracture zone H1, are explicitly modelled. The remainder of local fracture zones have been modelled implicitly according to the strategy described in Appendix D. The latter zones of concern are numbered 5, 6, 7, 8, 9, 10, and 11.

- The Finite-Element Mesh

The geometry of the domain describing the fracture zones is shown in Figure 7.2 (apart from the local zones) in a horizontal view of the top boundary (left) and the bottom boundary (middle). These two figures intend to show the change in areal coverage with increasing depth caused by the slanting bounding fracture zones; compare also with Figure 3.2a. The division of the area between zones 1, 4, 12, and 14 is intended for a possible step-wise increasing modelling of the areal coverage of zone 2. Zone 2 is located below the ground surface and is therefore not explicitly visible in the figure. A horizontal view of the top boundary of the finite-element mesh describing the discretisation of the domain is shown in the right-most figure below. The mesh consists of about 36000 8-noded brick elements, divided into 24 layers. The element widths are in the order of 50 m.

Figure 7.3 shows a perspective view of the implementation of zone 2 and zone H1. Note that the local semi-generically modelled horizontal zone H1 has been included in the mesh, which was not the case for the semi-regional model. This zone will however not be considered in the present project, but was included in the mesh to provide possibilities for future sensitivity analyses with regard to deeply located horizontal fracture zones.

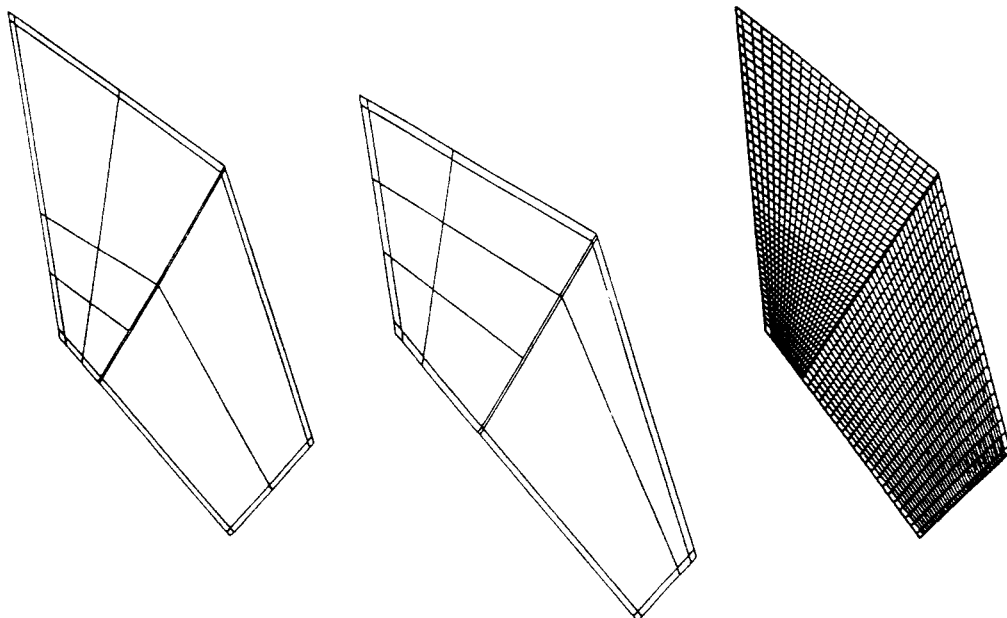


Figure 7.2 Horizontal view of the top boundary (left) and the bottom boundary (middle) of the geometry of the bounding fracture zones; horizontal view of the top boundary of the finite element mesh (right); compare Figure 3.2a.

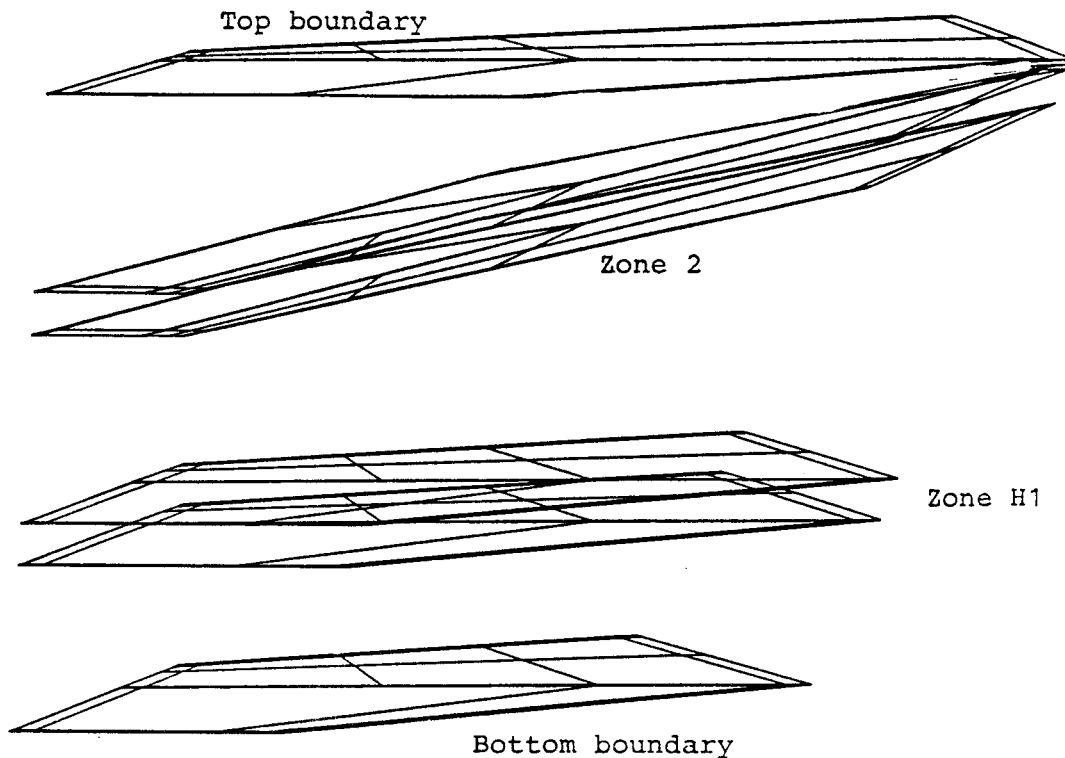


Figure 7.3 Perspective view of the implementation of zone 2 and zone H1.

7.3 Case Definitions – Nomenclature, Hydraulic Properties, and Boundary Conditions

The model sensitivity to different assumptions of the hydraulic conductivities were rather thoroughly investigated on the semi-regional scale. The analysis on the local scale will rather be oriented towards the model's sensitivity to different types of boundary conditions. To this end, a number of cases will be run through with different approaches with regard to the boundary conditions applied. Furthermore, a case will be studied with hydraulic conductivity values approximately corresponding to those used in the KBS3-study.

The different cases to be studied on the local scale are listed below:

- Case 3DLSR, a reference case. Lateral boundary conditions transferred from semi-regional Case 3DSB. No local fracture zones are modelled; semi-regional topography applied on the top of the mesh. This case intends to illustrate the consistency in the results obtained at the semi-regional scale and the local scale. No purely conceptual differences between Case 3DSB on the semi-regional scale and this case exist, which means that the case provide means to check the consistency of the results and to analyse the effect of the grid resolution and the transferred boundary conditions. This case is primarily to be compared to the Base Case below, but also to Case 3DSB on the semi-regional scale.
- Case 3DLSB, a Base Case. Lateral boundary conditions transferred from semi-regional Case 3DSB. Local fracture zones are modelled; semi-regional topography applied on the top of the mesh. This case will act as a base case on the local scale. The only difference between this case and Case 3DLSR above, is the presence of the local fracture zones in this case.

- Case 3DLS1. This case intends to illustrate the model sensitivity to the lateral boundary conditions. The case is identical to Case 3DLSB, apart from the lateral boundary conditions, which in this case are treated as no-flow boundaries.
- Case 3DL1. This case is identical to Case 3DLS1, with the exception that the local topography has been assigned to the top of the mesh in this case. The case therefore intends to illustrate possible effects on the flow system caused by differences in the representation of the topography.
- Case 3DL2. This case intends to show the effect of a possible bias towards too high conductivities in the evaluation of the field investigations at the Finnsjön site. Hydraulic conductivities approximately corresponding to those used in the KBS3-study will be assigned to the model, and the results will primarily be compared to Case 3DL1. No-flow lateral boundary conditions and local topography are prescribed.

The local fracture zones were included according to Figure 3.2a for all cases except for Case 3DLSR. They were modelled implicitly.

The bottom confinement is treated as a no-flow boundary. The nodal points at the top surface coincide with the elevation of the groundwater table, and an atmospheric pressure $p=0$ kPa has been prescribed to these nodes. The boundary conditions at the lateral boundaries and at the top surface differ from case to case according to the information given in Table 7.1 below.

Table 7.1 *Boundary conditions for the different cases on the local scale.*

Case	Lateral boundaries	Top boundary
3DLSR*	Transferred	Semi-regional topography
3DLSB	Transferred	Semi-regional topography
3DLS1	No flow	Semi-regional topography
3DL1	No flow	Local topography
3DL2	No flow	Local topography

* No local fracture zones

The hydraulic conductivities are the same for all cases except for Case 3DL2, where KBS3-like values were assigned to the model. The conductivities for Case 3DL2 were $K=10^{-3} \cdot z^{-3}$ m/s for the rock mass, and $K=0.1 \cdot z^{-3}$ for the fracture zones. The remainder of the cases on the local scale have been assigned a value of $K=1.04 \cdot 10^{-6} \cdot z^{-1.10}$ for the rock mass, and values according to Table 7.2 for the fracture zones. However, note that no local fracture zones (zones 5, 6, 7, 8, 9, 10, and 11) were included in the model for Case 3DLSR, as opposed to the rest of the cases.

Table 7.2 Reference values of the hydraulic conductivities (m/s) for the fracture zones as modelled on the local scale.

Zone	Width (m)	Inclination (degrees)	Hydr. Cond (m/s)
1	20	75 SE	$1.21 \cdot 10^{-3} \cdot z^{-1.10}$
2	100	16 SW	$1.02 \cdot 10^{-2} \cdot z^{-1.10}$
3	50	80 SW	$5.77 \cdot 10^{-4} \cdot z^{-1.10}$
4	50	60 SW	$3.14 \cdot 10^{-3} \cdot z^{-1.10}$
5 ¹	10	60 SW	$3.14 \cdot 10^{-3} \cdot z^{-1.10}$
6 ¹	10	60 SW	$4.86 \cdot 10^{-6} \cdot z^{-1.10}$
7 ¹	10	70 SW	$2.40 \cdot 10^{-4} \cdot z^{-1.10}$
8 ¹	10	90	$2.21 \cdot 10^{-3} \cdot z^{-1.10}$
9 ¹	50	15 SW	$5.29 \cdot 10^{-5} \cdot z^{-1.10}$
10 ¹	10	80 SW	$5.46 \cdot 10^{-3} \cdot z^{-1.10}$
11 ¹	50	23 SW	$1.28 \cdot 10^{-4} \cdot z^{-1.10}$
12	50	90	$3.70 \cdot 10^{-4} \cdot z^{-1.10}$
13	50	90	$1.21 \cdot 10^{-3} \cdot z^{-1.10}$
14	50	90	$3.70 \cdot 10^{-4} \cdot z^{-1.10}$

¹ The fracture zone has been implicitly modelled. Implicitly modelled fracture zones are not included in Case 3DLSR.

7.4 Modelling Results

7.4.1 General

The evaluation of the modelling on the local scale is focussed on the same issues as on the semi-regional scale. It consists of different parts including evaluation of the pressure distribution, particle tracking, and flux distribution within a potential repository. In addition, the flow into and out of zone 2 is evaluated. The main part of the evaluation of the modelling results is focussed on comparisons between the cases within the modelling on the local scale. To this end, positions of horizontal and vertical cuts in which the pressure distribution is evaluated is maintained for all cases, release points for water particles to be tracked are the same for all cases, etc. Furthermore, in order to judge the consistency of the results obtained on the local and the semi-regional scale, positions for release points, levels of the horizontal cuts etc, are the same as for the evaluation of the results on the semi-regional scale.

A selection of representative figures will be displayed in the following sections. The complete set of evaluation figures is shown in Appendix B for all the cases considered on the local scale. However, the evaluation was reduced for Case 3DLSR.

7.4.2 Pressure Distribution

Horizontal cross-sections

The pressure distribution was evaluated at following levels:

- At 200 m below the ground surface (located between zone 2 and the top surface),
- At 500 m below the ground surface, corresponding to the depth of a potential repository,
- At 800 m below ground surface (roughly 200-500 m below zone 2), and
- At 1300 m below the ground surface to illustrate the flow situation at great depths.

The pressure distribution in a horizontal cut at $z=-200$ m will be studied for Cases 3DLSR and 3DLSB to be compared to Case 3DSB; i.e. the Base Case on the semi-regional scale. The differences between the three cases at $z=-200$ m are rather small, see Figures 7.4a-7.4c. The deviations in terms of pressure between Case 3DLSR and Case 3DSB are almost non-existing. The figure showing the pressure distribution for Case 3DSB is a blow-up of Figure 6.2a. The small deviations between Cases 3DLSR and 3DLSB are subject to the presence of the local fracture zones in the latter case; the contours show somewhat sharper curvature due to the local fracture zones. In particular this is visible for the 29m-contour in the middle of the western part of the domain. This corresponds to the position of local fracture zone 7. Also the contours north of this spot show the same tendency to be sharper for Case 3DLSB than in Case 3DLSR.



Figure 7.4a Blow-up of the pressure distribution at a level of $z=-200$ m; Case 3DSB, the Base Case on the semi-regional scale.

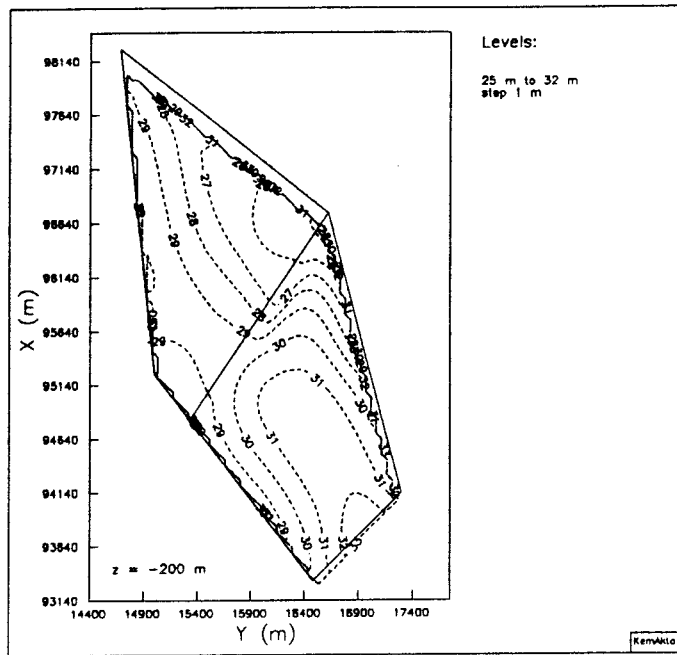


Figure 7.4b Pressure distribution at $z=-200$ m; Case 3DLSR, transferred lateral boundary conditions, semi-regional topography, no local fracture zones.

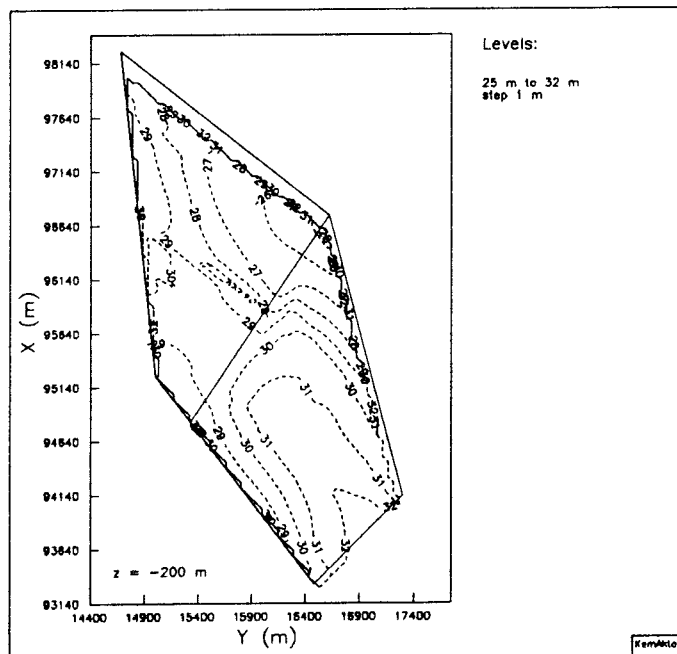


Figure 7.4c Pressure distribution at $z=-200$ m; Case 3DLSB, transferred lateral boundary conditions, semi-regional topography, local fracture zones.

The head distribution shown in Figures 7.5a-7.5d corresponds to the horizontal cross section at $z=-500$ m for all the cases considered on the local scale. The same type of conclusion regarding the importance of the local fracture zones can be drawn here. It is also interesting to note that the differences in this cross section between Case 3DLSB and Case 3DLS1 are rather small. However, there are some minor deviations between the two cases in the middle of the western part of the domain, where the contours differ a bit. This could possibly be seen as an evidence of the transferred boundary conditions in Case 3DLSB as opposed to Case 3DLS1. In the latter case, no-flow conditions are assumed along the lateral edges, which means that the 28m-contour and the 29m-contour running parallel are doing so because zone 7 is located at this spot, and the flow is not subject to any suction from lateral boundary pressures. There are also some small differences between Cases 3DLS1 and 3DL1. The 29m-contour running from west to east in the former case, has been divided into two contours in Case 3DL1, see Figures 7.5b and 7.5c. Apparently, the model was able to sense a dividing point in Case 3DL1 caused by the local topography, which was not present in Case 3DLS1.

Apart from these minor deviations, the results are rather alike for all the cases except for Case 3DL2, a case in which the hydraulic properties differ substantially from the other cases. In this case, the vertical pressure drop is less than for the other cases, and furthermore, the local fracture zones do not seem to affect the results to the same degree as for the rest of the cases.

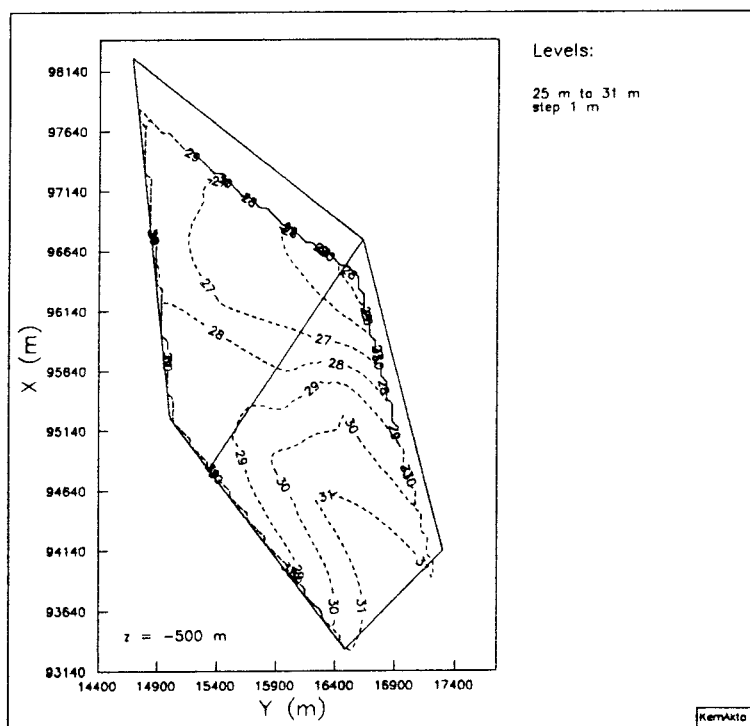


Figure 7.5a Pressure distribution at $z=-500$ m; Case 3DLSB, transferred lateral boundary conditions, semi-regional topography, local fracture zones.

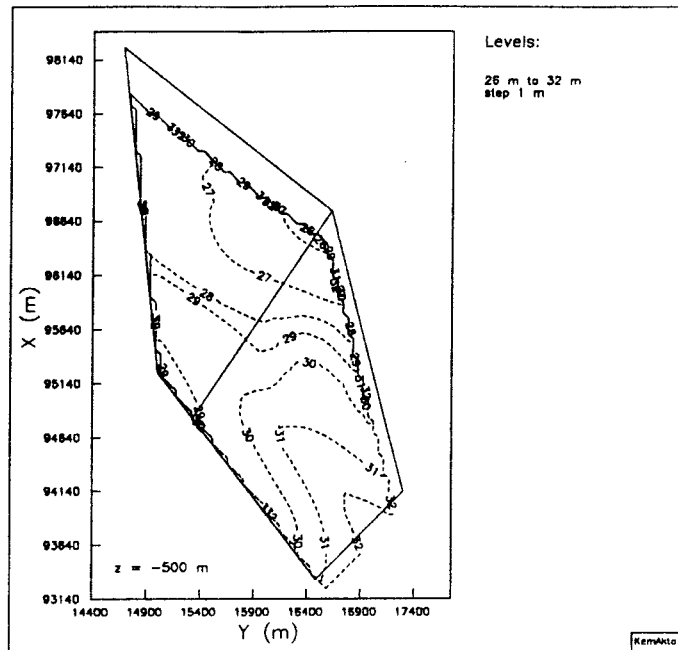


Figure 7.5b Pressure distribution at $z=-500$ m; Case 3DLS1, no-flow lateral boundaries, semi-regional topography, local fracture zones.

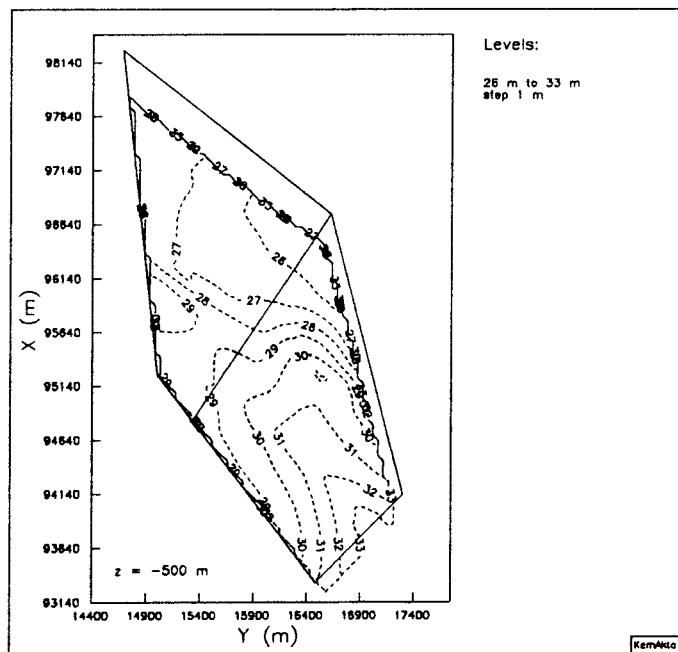


Figure 7.5c Pressure distribution at $z=-500$ m; Case 3DL1, no-flow lateral boundaries, local topography, local fracture zones.

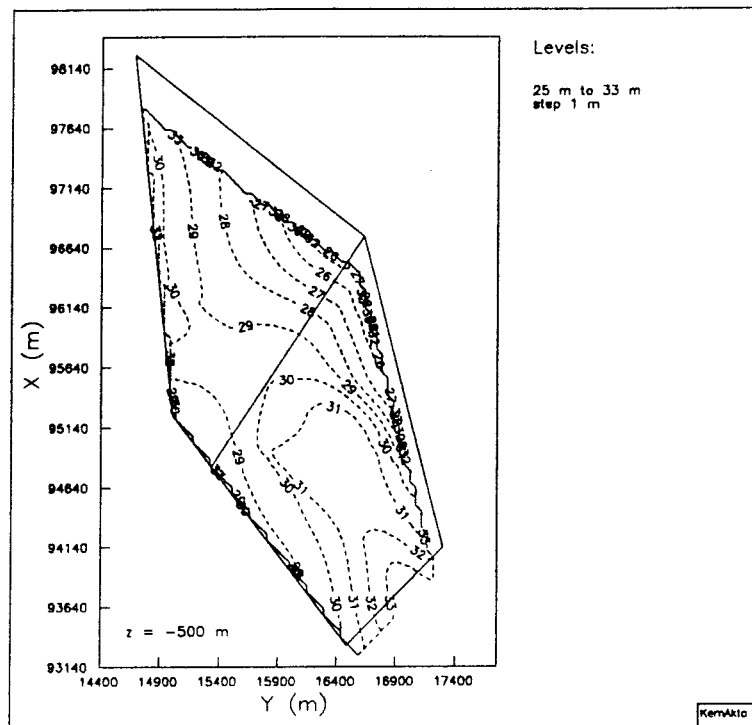


Figure 7.5d Pressure distribution at $z=-500$ m; Case 3DL2, no-flow lateral boundaries, local topography, local fracture zones, KBS3-like conductivities.

Vertical cross-sections

The pressure distribution has been evaluated in three vertical cuts. The locations of these cuts are shown in the legends of the figures showing the pressure distribution in question. The intention has been to show the overall pressure distribution vertically and at the lateral boundaries in particular, and furthermore to illustrate the importance of the fracture zones within the local area.

The pressure distribution in the vertical cut chosen for presentation, see Figure 7.6a-d, reveals that the largest vertical pressure drop is found in Case 3DLSB, which is a consequence of the transferred lateral boundary conditions. The two cases 3DLS1 and 3DL1, which differ only by their upper boundary condition, show very similar contour patterns. The deviations occur only in the uppermost part, which of course is due to the discrepancies in the representation of the topography for the two cases. Case 3DL2 again shows that the low permeability combined with the no-flow boundaries, make the contours persist vertically through the domain, far more than the other cases. This implies that the magnitude of the gradients at deeper depths are larger in this case, than in the other.

Furthermore, the position of zone 2 is clearly illustrated in Figures 7.6a-c. It is visible by the 27m-contour which follows the inclination of zone 2. It is also worth noticing that the less pronounced evidence of zone 2 is seen in Case 3DL2. This depends on that all fracture zones in this case are assumed to have the same hydraulic properties, whereas the fracture zones for the rest of the cases have been assigned individual values. This is particularly the case for zone 2, since this is thought to be the most permeable feature at the site.

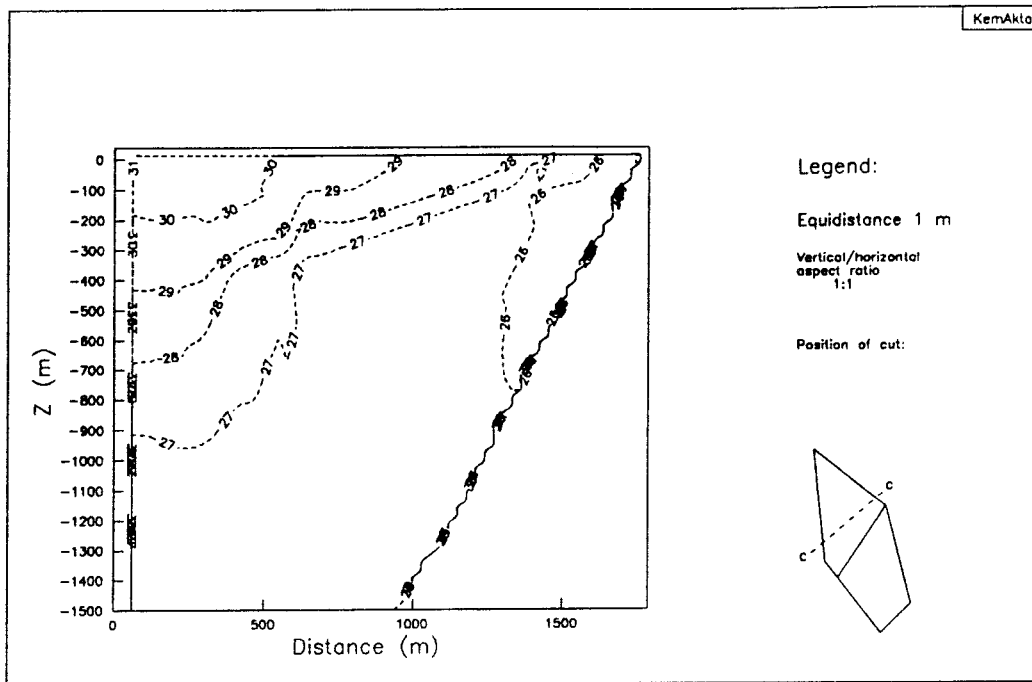


Figure 7.6a Pressure distribution in vertical cut 2; Case 3DLSB, transferred lateral boundary conditions, semi-regional topography, local fracture zones.

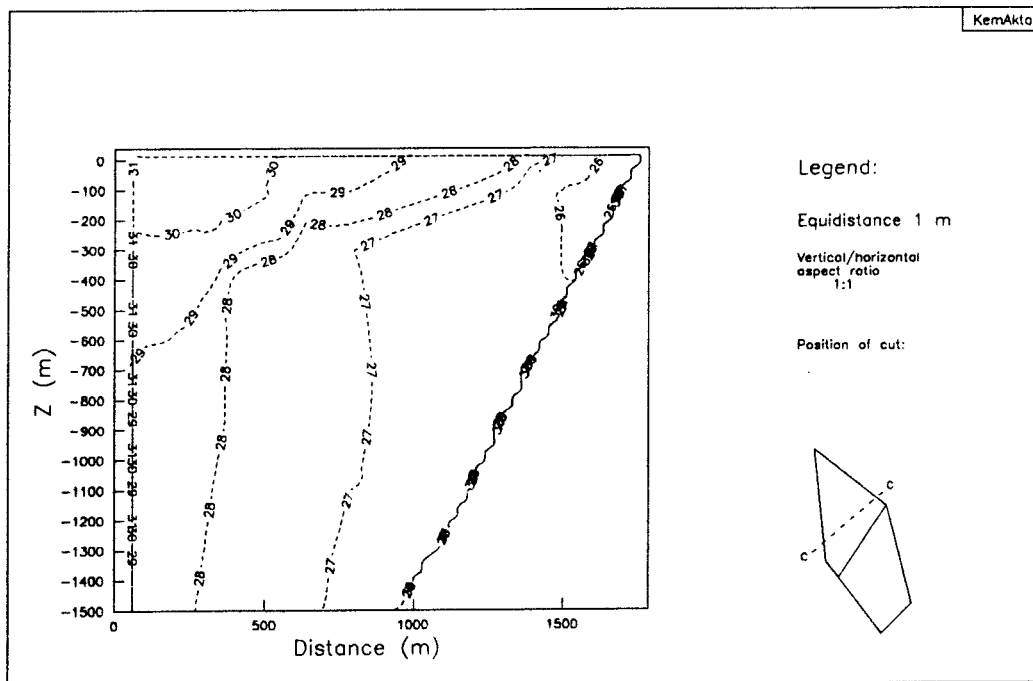


Figure 7.6b Pressure distribution in vertical cut 2; Case 3DLS1, no-flow lateral boundaries, semi-regional topography, local fracture zones.

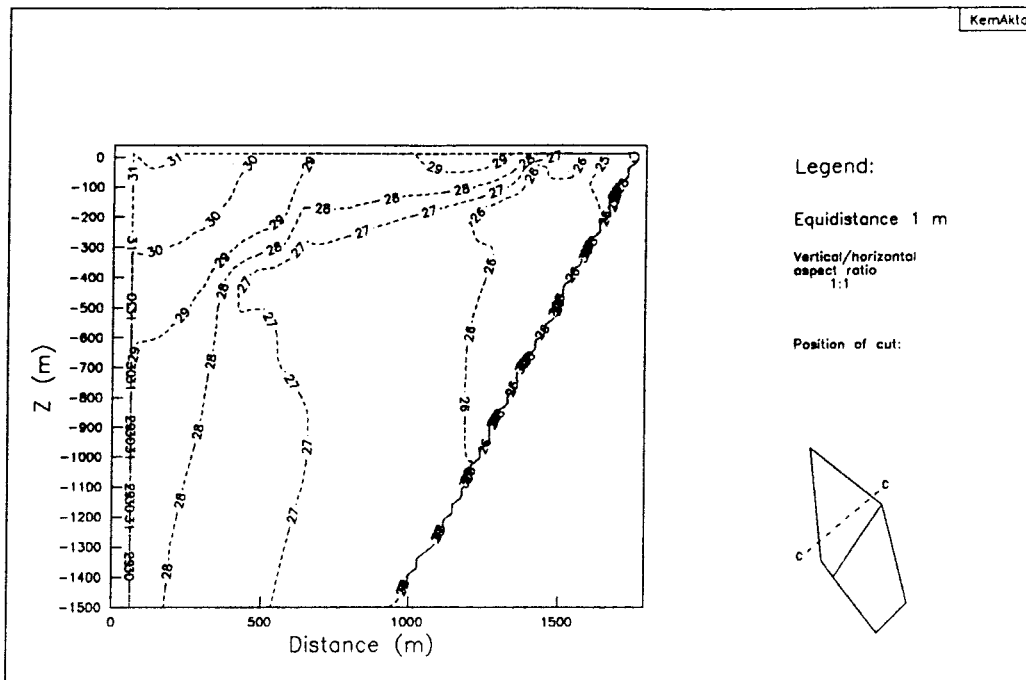


Figure 7.6c Pressure distribution in vertical cut 2; Case 3DL1, no-flow lateral boundaries, local topography, local fracture zones.

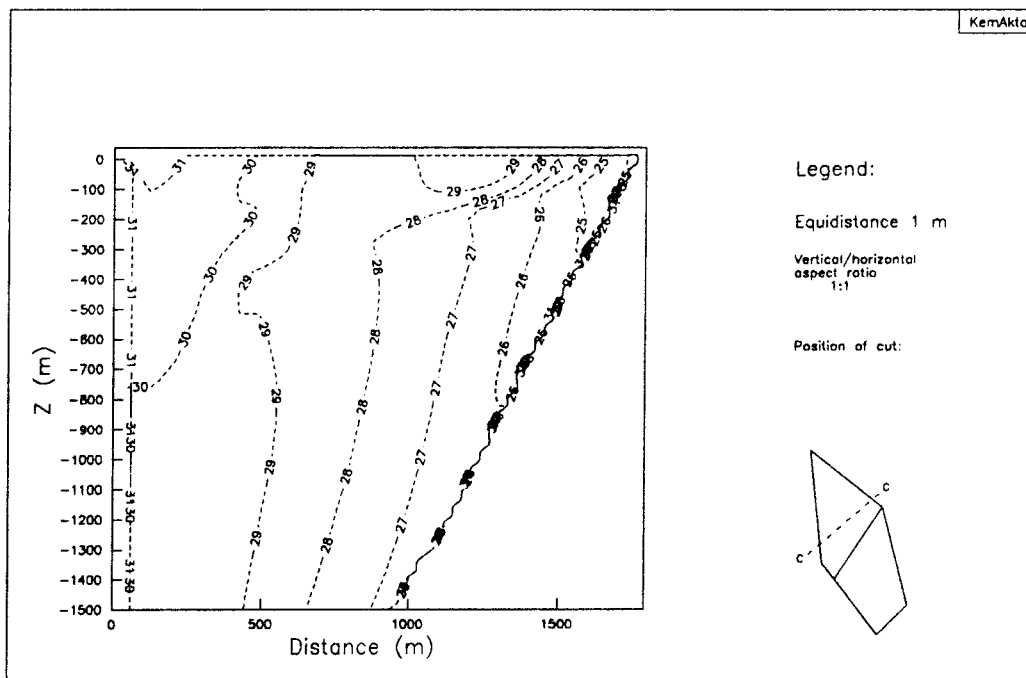


Figure 7.6d Pressure distribution in vertical cut 2; Case 3DL2, no-flow lateral boundaries, local topography, local fracture zones, KBS3-like conductivities.

7.4.3 Particle Tracking

Eight particles were released for all the cases on the local scale. The release points are shown in Figure 6.5. The resulting flowpaths have been plotted and projected onto the three cartesian coordinate planes. In the following, a selection of these plots are shown. The horizontal and one vertical projection of the pathlines for Cases 3DSB, 3DLSR, 3DLSB, 3DLS1, and 3DL1 will be shown. (The results from Case 3DL2 will not be presented here, but are shown in Appendix B.) The reason for showing the horizontal projection is to illustrate that the flow pattern remains the same on the local scale modelling as on the semi-regional modelling; i.e. further evidence on that the transfer of boundary conditions was reliable, and also to elucidate the presence of local fracture zones in Case 3DLSB compared to Case 3DLSR. Furthermore, the vertical projection is intended to illustrate that the cases with transferred boundary conditions show pathlines that exit the domain at locations corresponding to the exit-points in the semi-regional modelling. Moreover, by comparing these four cases, the intention is to illustrate that the flowpaths are oriented in very much the same direction regardless of the type of boundary condition (in particular Case 3DLSB and 3DL1 are of concern). The latter does not hold for the vertical projections, since the flowpaths for Case 3DLSB are forced to exit the domain through a lateral boundary, whereas the flowpaths for Case 3DL1 for the same reason are forced to exit the domain at the upper boundary.

Horizontal projections of the pathlines are shown in Figures 7.7a-c for Cases 3DSB, 3DLSR, 3DLSB, 3DLS1, and 3DL1, respectively. When Cases 3DSB and 3DLSR are compared, it appears as if the flow pattern is identical for the two cases; the point of outlet seems to be in perfect agreement. The corresponding pathlines for Case 3DLSB are almost aligning with those of the two former cases. There are however some minor deviations in the vicinity of the discharge point. At this point, two of the pathlines for Case 3DLSB (number 5 and 8) are closer connected to the rest of the pathlines, clustering at the discharge point, than is the case for Cases 3DSB and 3DLSR. This difference is caused by the presence of the local fracture zone 5 in Case 3DLSB, which is not present in the other two cases.

When the pathlines for Cases 3DLS1 and 3DL1 are studied, the point of discharge is almost the same as for the rest of the cases. It is however, moved a little bit towards north-west in this horizontal projection. This is due to the no-flow lateral boundary condition, which in these cases forces the water particles upwards rather than to a lateral boundary which was the case for the three former cases. It is worth noticing that Cases 3DLS1 and 3DL1 seem not to differ at all, despite the differences in the upper boundary condition.

The vertical projection (onto the yz-plane) of the calculated flowpaths is shown in Figures 7.8a-b for Cases 3DLSR, 3DLSB, 3DLS1, and 3DL1. Since it is difficult to compare the vertical projections on different scales, the corresponding flowpaths for Case 3DSB were omitted here. Figure 7.8a (Case 3DLSR) shows that six of the eight particles exit the domain at the lateral boundary subject to a suction from the transferred boundary condition. The two pathlines that do not have the same exit point are number 5 and 7, which travel to the top boundary seemingly unaffected by the lateral boundary condition. However, pathlines 5 and 7 are affected by the presence of fracture zone 5 in Case 3DLSB as opposed to the situation in Case 3DLSR. Apart from this slight difference, these two cases are similar to each other. The vertical projections for Cases 3DLS1 and 3DL1 show very similar travel paths (Figure 7.8b). As mentioned earlier, they are forced upwards by the no-flow lateral boundaries. The only visible difference between these two cases is a small kink on one of the left-most flowpaths for one of the cases. Apart from this, they are almost identical to each other.

The pathline data are collected in Table 7.3 below, in which the impact from the different types of boundary conditions are illustrated. Note, that the pathlines for Case 3DSB have been omitted also here, since it is no use in comparing travel lengths etc on the different scales. A porosity of 0.0001 was assumed when the travel times were calculated.

Table 7.3 Accumulated travel times (ACT) in years and accumulated travel lengths (ACL) in metres for the cases considered on the local scale.

Case:	3DLSR		3DLSB		3DLS1		3DL1	
Path no	ACT	ACL	ACT	ACL	ACT	ACL	ACT	ACL
1	1525	1320	1705	1376	2245	1264	2109	1856
2	233	904	156	896	375	856	859	840
3	130	512	102	520	195	616	537	592
4	2087	1296	1754	1336	2286	1080	2281	1536
5	1339	1016	1003	1088	1404	768	917	696
6	1037	848	761	912	1514	1128	1139	1088
7	14	1584	2121	1624	10	1512	4600	1560
8	47	1536	1627	1832	1042	1680	3435	1624

When the travel times and travel lengths are studied, it appears as if pathlines 5, 7, and 8 are rather sensitive to the changes in boundary conditions between the cases, and also to the presence of local fracture zones in some instances. All the pathlines exit the domain according to the prescribed boundary condition in Case 3DLSR, see Figure 7.8a. However, when the local fracture zones are included in the model (Case 3DLSB), all the pathlines move vertically a certain distance; even pathlines 5 and 7. The pathlines are then continuing to the lateral boundary according to the lateral boundary condition.

Moreover, pathlines 5 and 7 are running in or close to zone 2 for the rest of the cases. When they are travelling in zone 2, it is visible as an extremely short travel time (14 and 10 years for Cases 3DLSR and 3DLS1, respectively). On the other hand, the same pathlines appear to travel just near zone 2 in Cases 3DLSB and 3DL1; probably prevented to enter the zone because of numerical disturbances at the element boarder of zone 2 and the rock mass.

The general impression, is that the travel times and travel lengths are roughly the same for the individual pathlines for all cases apart from number 5, 7, and 8. This indicates in some sense that the model is rather insensitive to the differences between the cases studied; both in terms of the upper and the lateral boundary conditions.

The local fracture zones seem, however, to have some influence but it is restricted to be located near the zone in question. This is shown in Figure 7.7c, in which pathline 1 enters one of the local fracture zones and runs in it all the way to the exit point. The same zone is present in Case 3DLSB, but the suction from the lateral boundary condition is in this case stronger than the impact from the fracture zone as opposed to the situation in the former two cases.

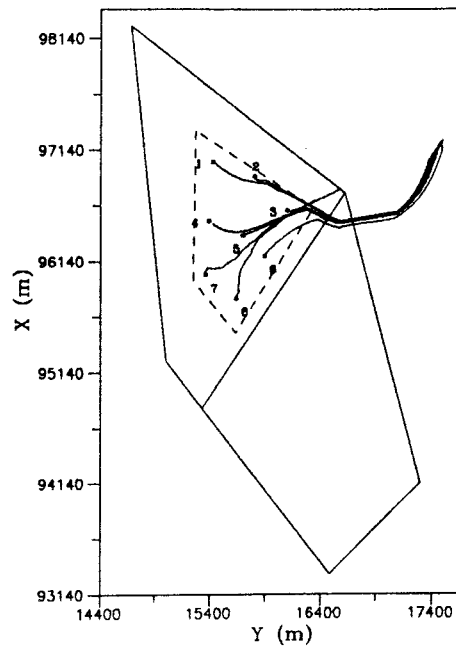


Figure 7.7a Horizontal projection of pathlines; Case 3DSB, the Base Case on the semi-regional scale.

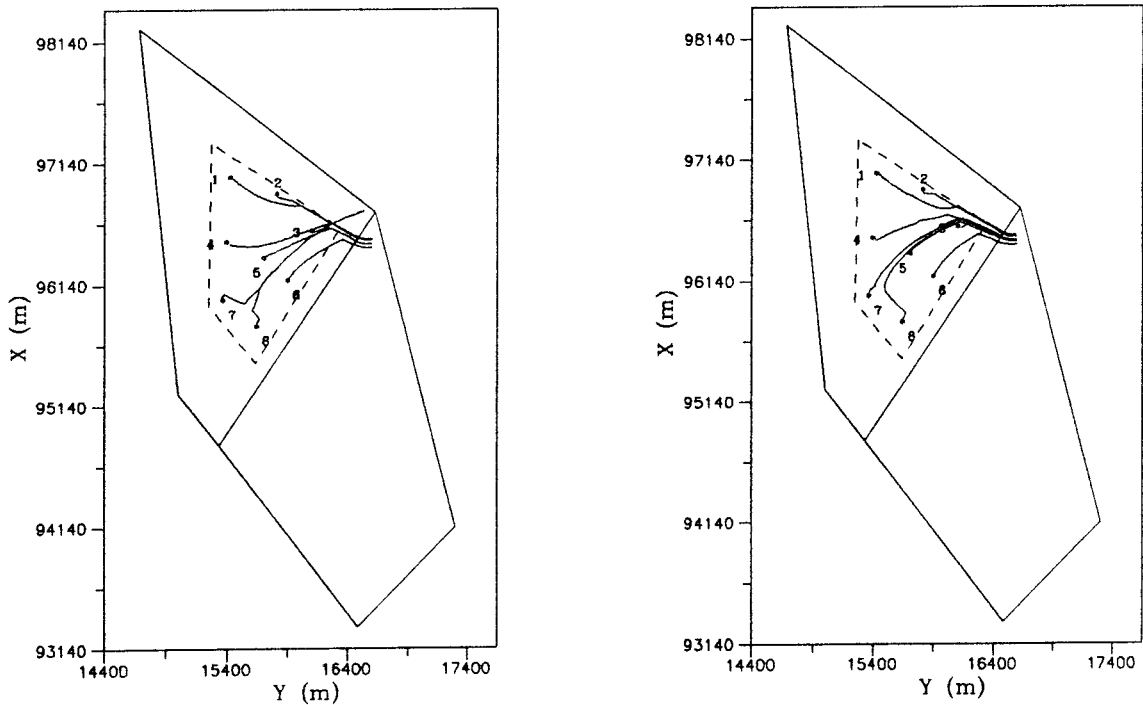


Figure 7.7b Horizontal projection: Case 3DLSR, transferred boundaries, semi-regional topography, no local fracture zones (left); Case 3DLSB, transferred boundaries, semi-regional topography, local fracture zones (right).

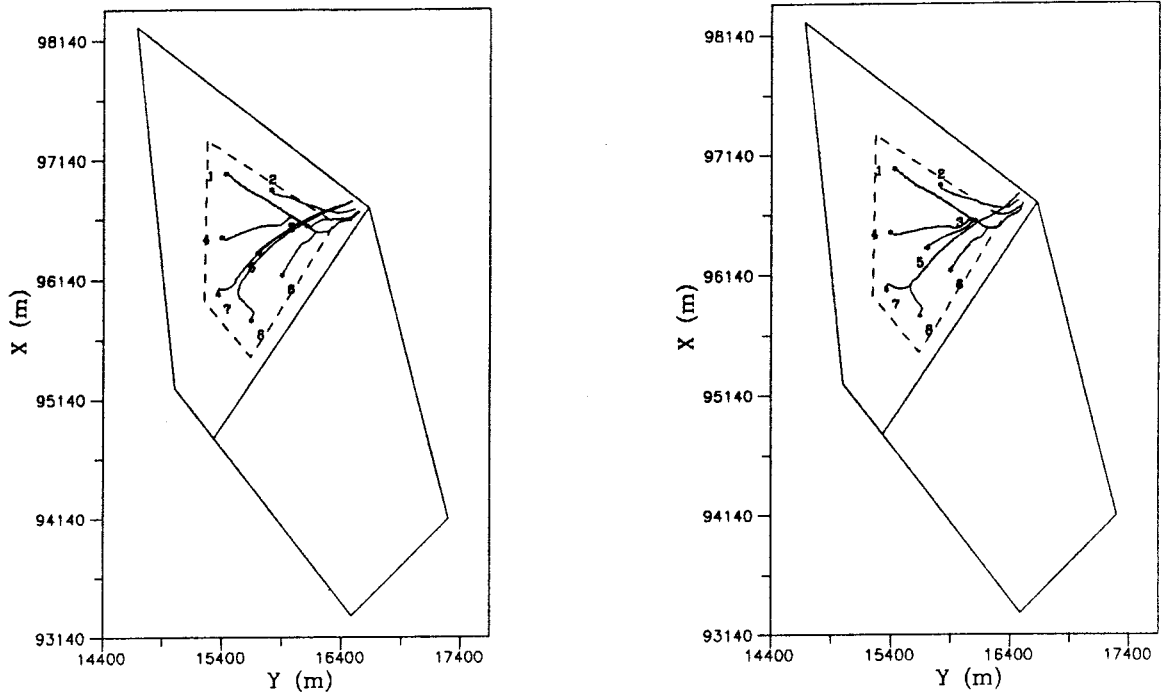


Figure 7.7c Horizontal projection: Case 3DLS1, no-flow boundaries, semi-regional topography, local fracture zones (left); Case 3DL1, no-flow boundaries, local topography, local fracture zones (right).

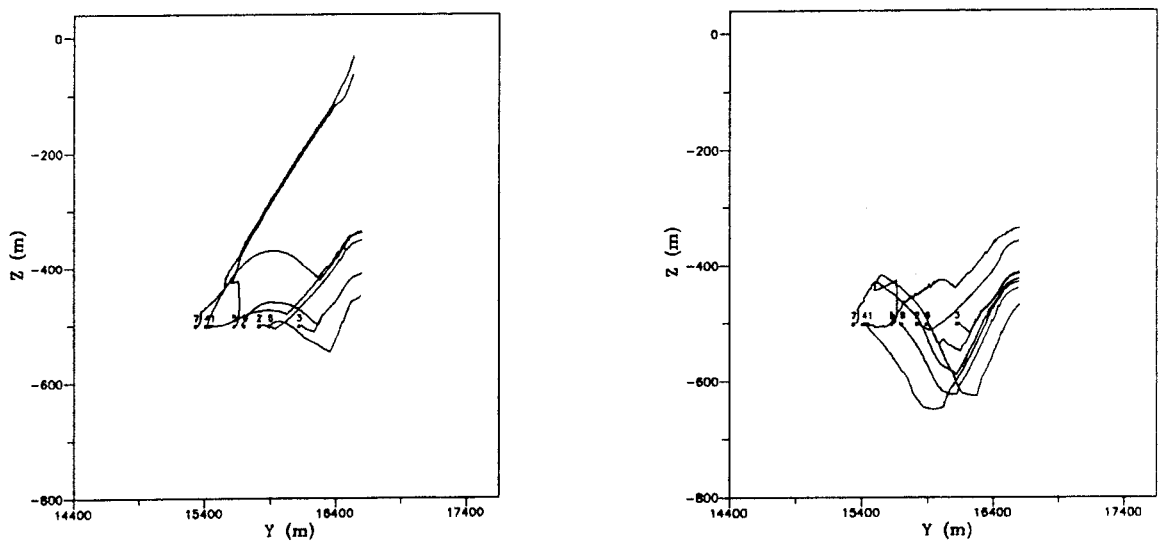


Figure 7.8a Vertical projection. Case 3DLSR, transferred boundaries, semi-regional topography, no local fracture zones (left); Case 3DLSB, transferred boundaries, semi-regional topography, local fracture zones (right).

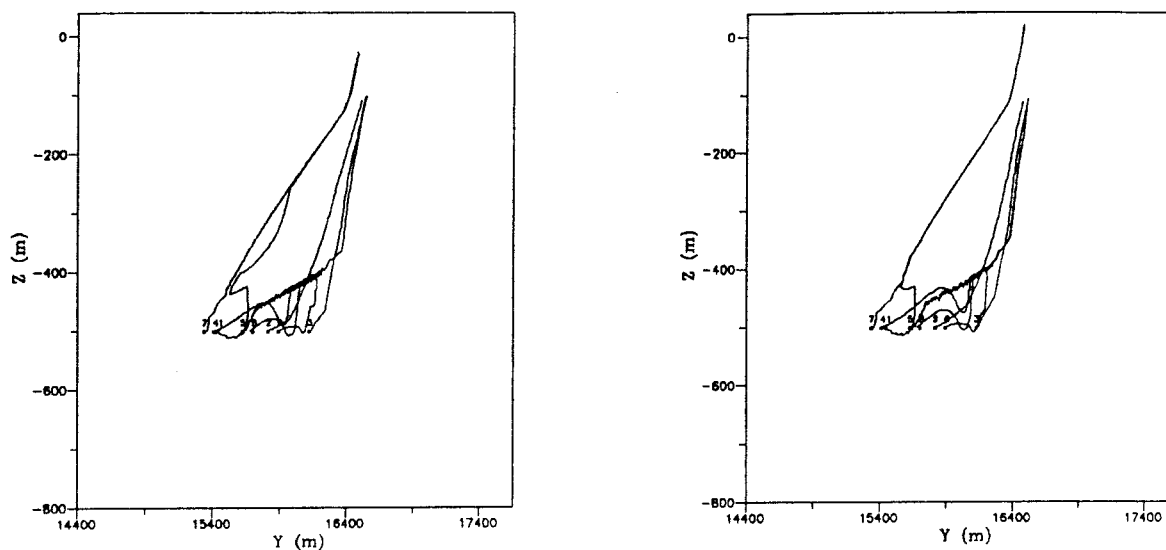


Figure 7.8b Vertical projection. Case 3DLS1, no-flow lateral boundaries, semi-regional topography, local fracture zones (left); Case 3DL1, no-flow lateral boundaries, local topography, local fracture zones (right).

7.4.4 Flux Distribution in the Potential Repository

The flux distribution was evaluated over the entire domain in a horizontal cut at the level of the potential repository (at $z=-500$ m) for all the cases considered. The resulting fluxes are shown in Figures 7.9a-7.9f. Note, that the figures of concern intend to illustrate typical flux values rather than absolute values at every single location in the area. Furthermore, a number of contour levels are omitted. The plotted levels and the highest and lowest values are indicated in the legend of these figures.

The flux values given in the figures correspond to the volumetric flux ("Darcy velocity") calculated as the sum of absolute values in the three cartesian directions, which should be interpreted as the flux value at a given point in space regardless of the direction of the flow - this is further described in Section 6.4.4.

The flux distribution in Case 3DSB is shown in Figure 7.9a for direct comparison with Case 3DLSR in Figure 7.9b. It is evident that the distribution of fluxes is next to identical for the two cases - again implying that the transfer of boundary conditions seems to have worked. The inclusion of the local fracture zones in Case 3DLSB to be compared to Case 3DLSR indicates that the fluxes have been increased due to the high conductivities in the local fracture zones. However, the affected area at this level seems to be restricted to the absolute neighbourhood of the fracture zone in question. The contours with increased flux values, corresponding to the locations of zones 5, 6, 7, 8, and 10 are running more or less parallel to the northern boundary (zone 4), see also Figure 3.2a. The presence of these zones is visible in Figure 7.9c as contours indicating the 500 ml-level. Typical flux values in this plot are roughly 50-100 ml/m²/year for the bedrock interlying the fracture zones, and roughly 10 times higher values in the vicinity of the fracture zones. However, there are flux values higher than those indicated in the figures.

Figures 7.9d-f display the flux distribution for Cases 3DLS1, 3DL1, and 3DL2, i.e. for the cases with no-flow lateral boundaries. The flux distribution is almost identical to the distribution in Case 3DLSB for Cases 3DLS1 and 3DL1 with only some minor deviations that are possible to distinguish. In a few spots, the fluxes are a little bit lower in the latter cases. However, the differences are too small to be significant. This indicates that the flux values are independent of the assigned boundary conditions in relative terms.

Case 3DL2 show flux values that are roughly two or three orders of magnitude lower than for the remainder of the cases. This is however by no means surprising, since the hydraulic conductivities in this case are roughly two to three orders of magnitude lower than for the remaining cases. The fluxes would probably have been even lower, had zone 2 been modelled more permeable; i.e. more according to the field data at the Finnsjön site. This would surely have implied that zone 2 had acted more like a barrier, separating the flow in one flow regime above and one flow regime below the zone. Typical flux values are in the order of 2-5 ml/m²/year for the rock mass, and roughly ten times higher in the fracture zones. The presence of the local fracture zones is visible according to the same discussion as above.

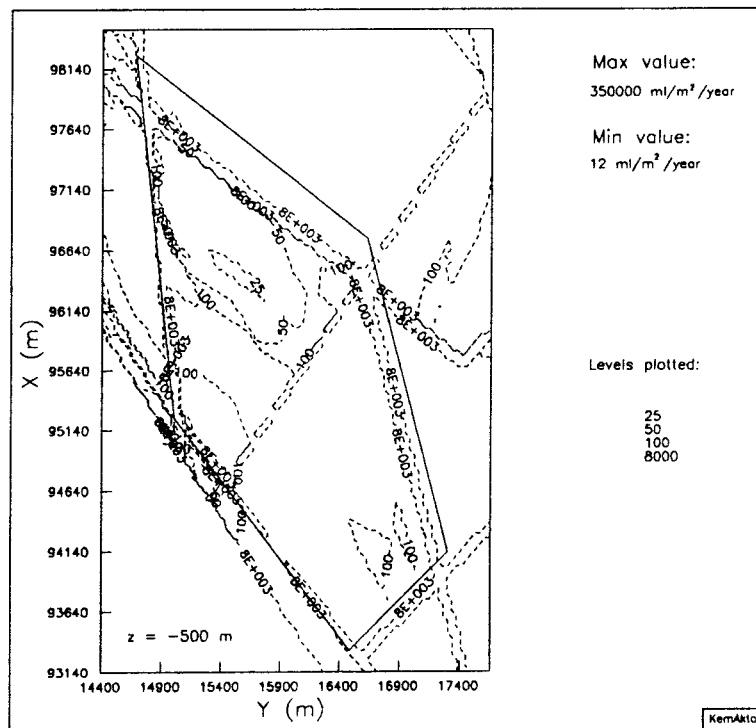


Figure 7.9a Flux distribution at z=-500 m; Case 3DSB, The Base Case on the semi-regional scale.

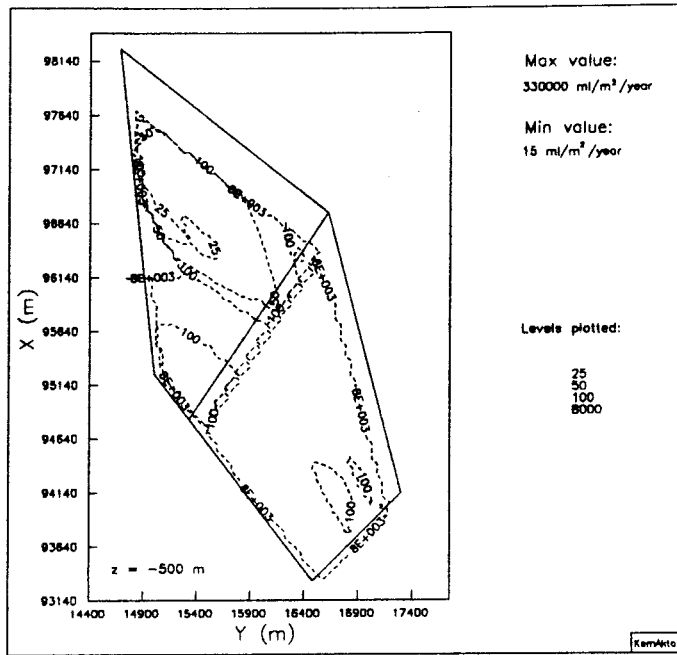


Figure 7.9b Flux distribution at $z=-500$ m; Case 3DLSR, transferred lateral boundaries, semi-regional topography, no local fracture zones.

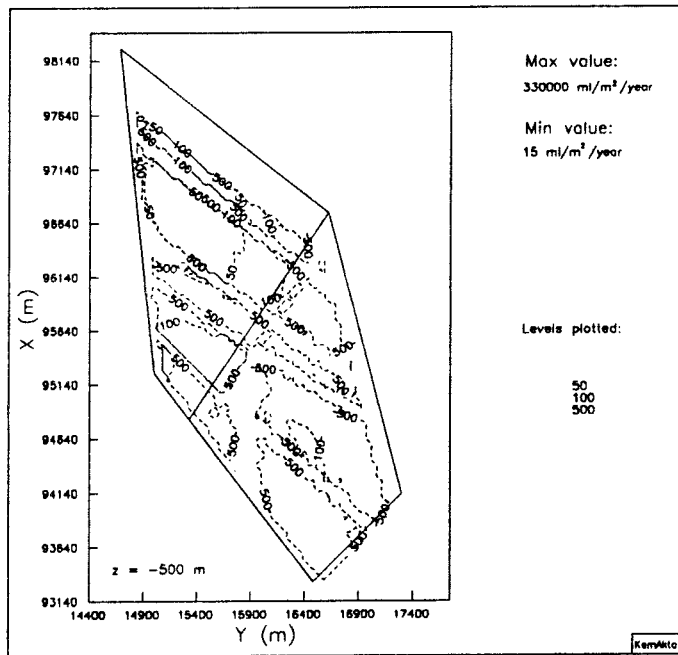


Figure 7.9c Flux distribution at $z=-500$ m; Case 3DLSB, transferred lateral boundaries, semi-regional topography, local fracture zones.

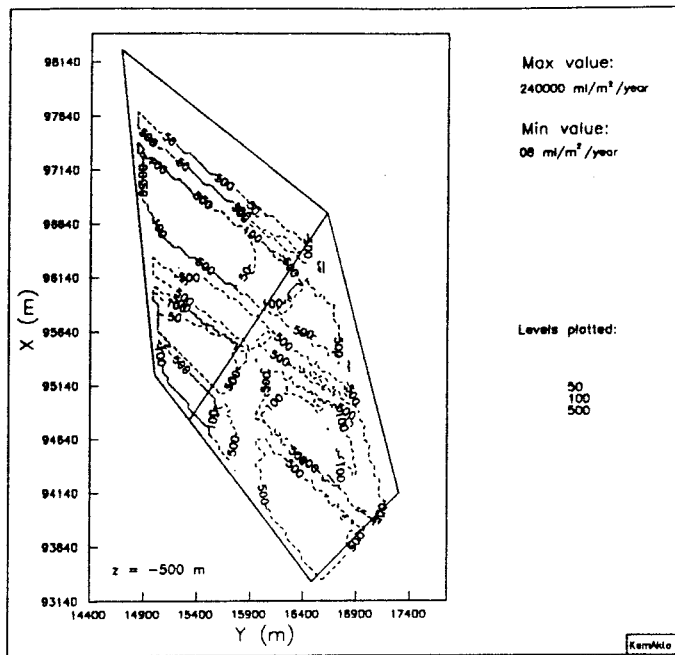


Figure 7.9d Flux distribution at $z=-500$ m; Case 3DLS1, no-flow lateral boundaries, semi-regional topography, local fracture zones.

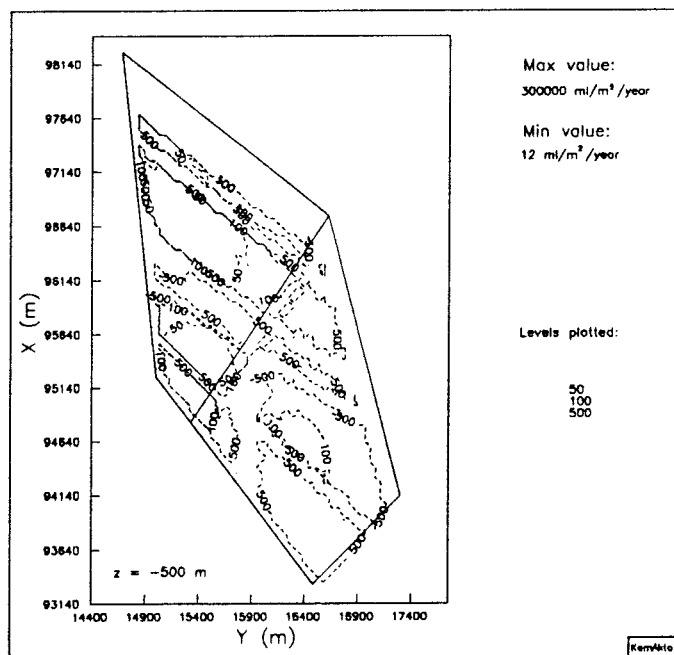


Figure 7.9e Flux distribution at $z=-500$ m; Case 3DL1, no-flow lateral boundaries, local topography, local fracture zones.

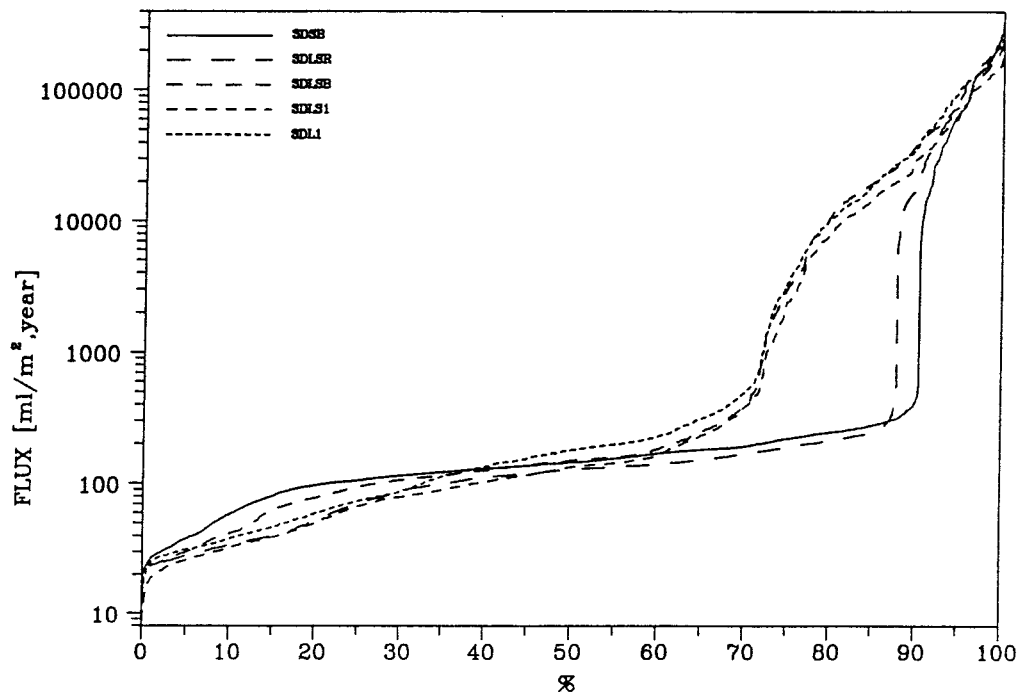


Figure 7.10 Frequency diagram of the flux distribution for Cases 3DSB (base case on semi-regional scale), 3DLSR (reference case with transferred lateral boundary conditions and semi-regional topography), 3DLSB (base case on the local scale with transferred lateral boundary conditions, semi-regional topography and local fracture zones), 3DSL1 (no-flow lateral boundaries, semi-regional topography and local fracture zones), and 3DL1 (no-flow lateral boundaries, local topography and local fracture zones). The diagram has been plotted with the use of the same point values that were used for the calculation of the contoured levels in Figures 7.9a-f. Note, that the scaling of the flux is logarithmic.

7.4.5 Mass Balance Calculation Around Zone 2

The mass balance calculations performed on the semi-regional scale as described in Section 6.4.5, indicated that the model was rather insensitive to the different assumptions regarding the extension of zone 2. The calculations on the local scale will therefore be focussed on the model's sensitivity of the flow rates into and out of zone 2 to the different boundary conditions considered on the local scale.

The natural flow through zone 2 was estimated in a vertical cut, the position of which is shown in Figure 7.5, and was amounting to about 5-10 l/s or 150000-300000 m³/year.

The results from the water balance calculations are presented as tabulated values. As on the semi-regional scale, some abbreviations were used to denote different features through which the water flow was studied. These abbreviations are mainly the same as those used on the semi-regional scale, see Section 6.4.5. The denotations used are listed below:

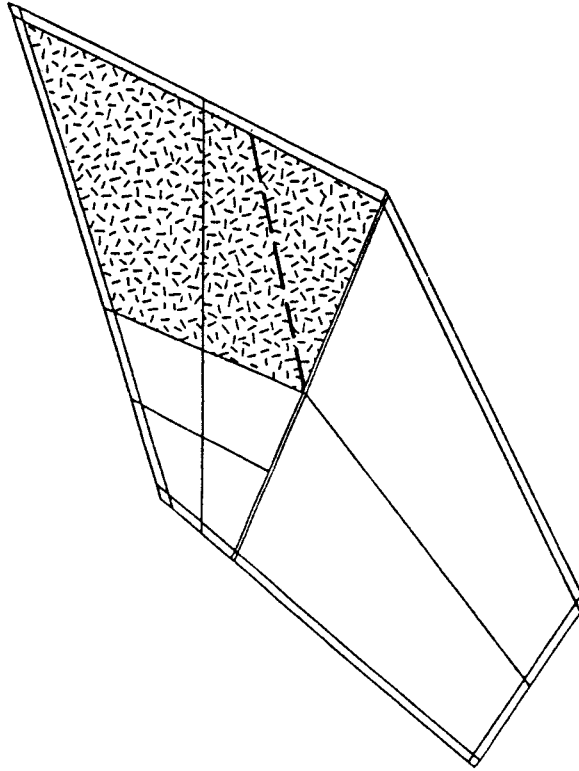


Figure 7.11 Horizontal view of the top boundary indicating the areal coverage of zone 2 (screened area). The dashed line corresponds to the position of the vertical cut through which the natural groundwater flow was estimated according to the Background Report.

- TSA2: flow through the top surface above zone 2,
- TS12: flow through the top surface of zone 12,
- TS1: flow through the top surface of zone 1,
- TS4: flow through the top surface of zone 4,
- TS14: flow through the top surface of zone 14,
- TC2: flow through top confinement of zone 2,
- BC2: flow through bottom confinement of zone 2,
- LC21: flow through lateral confinement of zone 2, facing zone 1,
- LC24: flow through lateral confinement of zone 2, facing zone 4,
- LC212: flow through lateral confinement of zone 2, facing zone 12,
- LC27: flow through south-most lateral confinement of zone 2, facing zone 7.

The calculated flow rates through zone 2 are listed below in Tables 7.4a-b for the different cases considered on the local scale. To complement these values, the infiltration through the top surfaces of the confining features are shown in Tables 7.5a-b.

Table 7.4a The flow ($m^3/year$) into and out of zone 2 through its confining features for Case 3DSB (from the semi-regional scale) and the cases with transferred boundary conditions on the local scale; Cases 3DLSR and 3DLSB.

Case: Feature	3DSB		3DLSR		3DLSB	
	in	out	in	out	in	out
TC2	109000	45800	99400	39500	165000	38500
BC2	10100	41900	7160	31000	2800	52200
LC21	49500	14000	64900	18300	65500	21100
LC24	11100	135000	23700	147000	3130	212000
LC212	27600	0	27400	0	18400	210
LC27	14600	564	6390	0	4810	30
	<hr/>	<hr/>	<hr/>	<hr/>	<hr/>	<hr/>
	221900	237264	228950	235800	259640	324040
Deviation:	-15364		-6850		-64400	

Table 7.4b The flow ($m^3/year$) into and out of zone 2 through its confining features for the cases with no-flow boundaries on the local scale; Cases 3DLS1, 3DL1 and 3DL2.

Case: Feature	3DLS1		3DL1		3DL2	
	in	out	in	out	in	out
TC2	146000	54700	128000	60200	500	66
BC2	6590	25300	14100	34800	3	72
LC21	61800	20100	96700	0	421	0
LC24	2120	156000	7260	204000	0	788
LC212	23400	0	30900	0	34	0
LC27	5910	0	6670	0	2	0
	<hr/>	<hr/>	<hr/>	<hr/>	<hr/>	<hr/>
	245820	256100	283630	299000	960	926
Deviation:	-10280		-15370		34	

Table 7.5a The net flow ($m^3/year$) through the top surfaces of fracture zones confining zone 2, and the rock matrix above zone 2 for Case 3DSB (from the semi-regional scale), and the cases with transferred boundary conditions on the local scale; Cases 3DLSR and 3DLSB.

Case: Feature	3DSB	3DLSR	3DLSB
TSA2	4770	4340	86190
TS1	107000	97650	90550
TS4	291900	1190000	1150000
TS12	34500	15700	16850

Table 7.5b The net flow (m³/year) through the top surfaces of fracture zones confining zone 2, and the rock matrix above zone 2 for the cases with no-flow boundaries on the local scale; Cases 3DLS1, 3DL1 and 3DL2.

Case: Feature	3DLS1	3DL1	3DL2
TSA2	79200	67800	900
TS1	80280	103390	2800
TS4	185000	177000	16880
TS12	30100	57580	3430

The general impression is that the mass balances are very good with regard to the flow into and out of zone 2 as shown in Tables 7.4a-b, except for Case 3DLSB. The deviation is roughly 5-10% for the remainder of the cases, while the deviation for this case is about 25%, which has to be considered as a high value. The explanation to this is that the model is sensitive to the transferred boundary conditions in combination with the implicitly modelled fracture zones; this will be further discussed in Section 7.5.6. The mass balances for the cases with no-flow boundaries (Cases 3DLS1 and 3DL1 in particular) all show better agreement between inflow and outflow than Case 3DLSB. In fact, Cases 3DLS1 and 3DL1 show very good internal agreement, which would indicate that the upper boundary condition is of less importance than the transferred boundary pressures.

The vertically directed flow from the top surface above zone 2, contributes to the recharge of water to zone 2 more than it did on the semi-regional scale. This is illustrated by the increased value in Tables 7.5a-b with an increased infiltration through the top surface above zone 2 (feature TSA2) for all the cases compared to Cases 3DSB and 3DLSR. This is a further evidence of the presence of the implicitly modelled local fracture zones which were not present in the latter two cases. The main impression is still that a certain amount of water enters zone 2 from its top confinement, stemming from the bounding fracture zones. Part of the water in these zones infiltrates laterally into the rock matrix above zone 2 for further vertical transport into zone 2; although not to the same degree as on the semi-regional scale.

As well as on the semi-regional scale, the major portion of infiltration takes part through the fracture zones. The flow through the top surfaces of the fractures zones bounding the local model was calculated to be about $1.48 \cdot 10^6$ m³/year, corresponding to roughly 2250 mm/year. These values are about 98% of the total amount of water infiltrating through the model. This implies that the infiltration through the rock matrix amounts to about 200 mm/year; fracture zones excluded. However, the implicitly modelled fracture zones are regarded as part of the rock matrix in this context, and are not possible to separate from the rock mass, which means that the infiltration rate by the presence of the implicit local fracture zones is higher than corresponding values on the semi-regional scale. This is also illustrated in Table 7.5a as an increased infiltration through the top surface above zone 2. The values mentioned above are valid for Case 3DLSB and are roughly the same for Case 3DLSR. The model is insensitive to the errors introduced when the boundary conditions are transferred from the semi-regional model, since the infiltration values for Case 3DLS1 are in the order of one third lower than for the cases mentioned above.

Further suspicions that the interpolation errors introduced by the transfer of boundary conditions may affect the results, are shown in Table 7.5a, where it is evident that the most sensitive part of the model appears to be zone 4. The flow through the top surface of zone 4 is about 4 times higher in Cases 3DLSR and 3DLSB than for the corresponding simulation on the semi-regional scale. The amount of infiltrated water was about $1.65 \cdot 10^6$ m³/year for the whole model, with roughly $1.2 \cdot 10^6$ m³/year infiltrating through zone 4; i.e. about 80 % of the infiltrated water enters zone 4 (Case 3DLSB).

With regard to Case 3DL2, it has to be stated that this is more or less an artificial set-up, since the hydraulic conductivities assigned to this case are evaluated at a different location than the Finnsjön site. However, it may be worth noticing that the flow in zone 2 is lowered by a factor of roughly 300 compared to Case 3DL1. However, since the model with Finnsjö-data was able to reproduce flow values that were in agreement with the estimated ones, a certain degree of confidence has to be put into the evaluation of the hydraulic conductivities as applied to the model with Finnsjö-data. The case with KBS3-like conductivities has to be regarded as a "what-if"-case rather than as an evidence for lower flow rates with an up-to date field measuring equipment.

Finally, apart from the bad mass conservation in Case 3DLSB, it can generally be claimed that the results on the local scale are in good agreement in terms of the flow rates through zone 2. It appears as if the model is sensitive to the errors introduced by the transfer of boundary conditions from the semi-regional scale - in particular zone 4 is of concern. On the other hand, the model seems to be less influenced by the type of upper boundary condition applied than perhaps anticipated. This is shown by the relative conformity shown between Cases 3DLS1 and 3DL1. These two cases are further in reasonably good agreement with Case 3DLSR. The flow has increased in Case 3DLS1 compared to Case 3DLSR, which of course is an effect of the local fracture zones in the former case. The flow has increased further in Case 3DL1 compared to Case 3DLS1. This is caused by the local topography in Case 3DL1, in which local gradients can have a certain impact on the results. This is particularly clear if the flow through feature LC21 (the face between zones 1 and 2) is studied. Case 3DL1 shows a zero-flow out of this face - as opposed to the situation in Case 3DLS1. This is probably caused by a local "hill" just east of the intersection between zones 1 and 4, see Figures 7.1a-b. This hill prevents the water to discharge from zone 2 to zone 1 at the point of discharge for Case 3DLS1, and the outlet point is hereby moved a little bit west-wards.

7.4.6 Investigation of Transferred Lateral Boundary Conditions

When a pressure value is to be transferred from the semi-regional scale to the local scale, the coordinate of a nodal point on the local scale is sought for in the semi-regional mesh. Once a suitable element on the semi-regional scale has been found, a stepping algorithm is used to find a point in the element of concern that matches the nodal point on the local scale. When a point from the local scale mesh has been accepted in the element from the semi-regional scale, the pressure values of all the nodal points in the element on the semi-regional scale are used to interpolate a pressure value to be prescribed to the nodal point on the local scale mesh.

The large amounts of water that were found to infiltrate through the top surface of zone 4 in Cases 3DLSR and 3DLSB depended on that the area north of zone 4 in the semi-regional model was located in a rather strong discharge area. The nodal points along zone 4 in the semi-regional model that were located outside the local scale mesh were situated in this discharge area. The nodal points in the local area that were located at the boundary were therefore subject to an artificial suction from the nodal points located outside the domain, which in turn led to the large amount of infiltrated water through the top surface of zone 4. The procedure with the calculation of boundary pressures continued vertically,

and hence the infiltrating water through the top surface of zone 4 was discharged through the lateral boundary aligning with the outer edge of zone 4. It had therefore little or no influence on the flow of the rest of the domain.

When it comes to the bad mass conservation in zone 2 that was observed for Case 3DLSB (as opposed to Case 3DLSR), it was found to depend on that local fracture zone 5 was included in the former case but not in the latter. The intersection between zones 2 and 5 is located just in the shallow part of zone 2 by its intersection with zone 4. The flow situation was difficult to handle numerically by the code, since this is the place where zone 2 is recharged from zone 5 and the rest of the fracture zones, and discharged into zone 4, at the same time as zone 4 is recharged by infiltration.

7.4.7 Global Mass Balance

Apart from the mass balance calculation that was discussed in the previous section, the global mass conservation was calculated. A deviation from a perfect mass conservation is expressed as a percentage deviation, i.e. it varies between 0 and 100%. The mass balance is calculated as the sum of flow through element faces (taking the direction of the flow into account), divided by the sum of flow through the same element faces (absolute values). This is repeated for each element in the model. The elements in the model are grouped according to the deviations in Table 7.6. The values from the semi-regional scale are shown as a comparison together with the results of Cases 3DLSB and 3DLS1.

Table 7.6 Mass conservation deviation for Cases 3DSB, 3DLSB and 3DLS1.

Deviation	Number of elements for Case:		
	3DSB	3DLSB	3DLS1
0-1 %	14045	8198	8938
1.01-10 %	16574	19391	19644
10.01-20 %	2313	4276	3623
20.01-100 %	1532	3703	3363
Σ elements	34464	35568	35568

As shown in Table 7.6, the global mass conservation is extremely good for all three cases; 80-90 % of the elements have deviations less than 10 %. By experience, this is judged to be far better than has been possible to achieve with computers with limited memory space. The areas with less good mass conservation are located in the bounding local fracture zones; in particular zone 4 and the intersection between zones 14 and 12 are of concern. Surprisingly enough the mass conservation in Case 3DLS1 is even a bit improved compared to Case 3DLSB – the no-flow boundaries in the former case do not seem to have affected the results in a negative direction, which usually is the case.

7.5 Summing up

The flow on the local scale is governed by the topography, and the major flow pattern is directed towards the intersection between zones 1, 4, and 3. This is particularly the case for the northern block. The south-most part of the southern block is discharged at the south-east boundary, while the remaining part of the southern block is discharged in a north-west direction.

The main impression from the modelling on the local scale, is that the model is rather insensitive to the boundary condition applied along the top surface, and along the lateral boundaries. The sensitivity to the transfer of boundary conditions is caused by the way in which the transferred boundary conditions were calculated, but this effect was shown to appear only locally around zone 4. This was shown for example as an increase of the water entering the top of zone 4 in one of the cases. However, in general the results from the cases with transferred boundary pressures seemed to be reliable. The only exception from this was the bad mass conservation for one of the cases when the water balance in zone 2 was studied.

The pressure distribution in horizontal and vertical cross sections revealed that the transfer of boundary conditions was reliable, although the distribution of pressure is known not to be a fine-tuned enough measure for sensitivity analyses.

The particle tracks indicated that the flow pattern is very much the same on the local scale as on the semi-regional scale; a strong clustering of flow paths at the intersection between zones 1 and 4 was demonstrated also on this scale. The transfer of boundary pressure seemed to yield pathlines that had exit points that corresponded to those on the semi-regional scale; i.e. through the lateral boundaries for the cases of concern.

The flux distribution that was calculated for the different cases indicated that the fluxes were increased in the area due to the presence of the local fracture zones. Typical flux values in the rock mass were roughly 300 ml/m²/year at z=-500 m for all cases. A frequency diagram of the fluxes at repository level indicated that about 90 % of the area had flux values lower than 300 ml/m²/year when the local fracture zones were omitted. Typical values when the local fracture zones were modelled were that 70 % of the area had lower fluxes than 300 ml/m²/year. Flux values in the fracture zones exceeded by far this value for all the cases. The pattern of the flux contours was similar, if not identical, for all cases with local fracture zones which would indicate that the type of lateral boundary conditions are less important than the local fracture zones themselves. The increased flux values occur preferably in the vicinity of the fracture zones in a local sense. This was also confirmed by the frequency diagram mentioned above.

The water balance calculations in zone 2 showed that regardless of which case that was studied, the calculated flow rate was within the range that was specified as the natural groundwater flow through zone 2. Bad mass conservation was obtained for Case 3DLSB, but extremely good mass balances were on the other hand obtained for the remainder of the cases.

The errors associated with the transferred boundary conditions were found to depend on that all corner nodes in an element on the semi-regional scale took part in the interpolation procedure when pressures from the semi-regional model were transferred to the local scale model. Unfortunately enough, the boundary of the local model was located along a fracture zone, which made the model extremely sensitive to the errors introduced. These errors made extremely large amounts of water to infiltrate through the top of zone 4 in particular. The amount of infiltrated water was about $1.65 \cdot 10^6$ m³/year for the whole model, with roughly $1.2 \cdot 10^6$ m³/year infiltrating through zone 4; i.e. about 80 % of the infiltrated water enters zone 4 (these values are for Case 3DLSB). The fact that this large amount of water is entering zone 4 at the same time as it acts as the major discharge point for water from zone 2 gave rise to the bad mass conservation earlier discussed for Case 3DLSB. The fortunate circumstance was however that the area of concern (the vicinity of zone 4) was located in a discharge area, which implied that the large amount of water that infiltrated through the top surface of this zone was discharged through the lateral boundary describing the outer edge of the zone. This made the infiltrated water less important for the overall flow system than if the boundary would have been located in a strong recharge area. This would surely have implied that large amounts of water would have entered the system.

One way of reducing the effect of this would have been to locate the boundaries of the local model so that it would cover a larger part of the semi-regional model.

Finally, the frequency diagram of the flux distribution mentioned above, revealed some interesting features and conclusions. The flux distribution for Case 3DSB and Case 3DLR are in good agreement; they should under ideal conditions align. This means that the transfer of boundary conditions seems to have yielded reliable pressure distribution for the local model boundaries. Furthermore, the three cases 3DLSB, 3DLS1, and 3DL1 are almost aligning perfectly. This would imply that neither the type of lateral boundary (transferred or no-flow), nor the type of upper boundary (semi-regional topography or local topography) is as important as the local fracture zones for this study. This implies that, as far as fluxes are concerned, the local scale model may be described by transferred lateral boundaries and a semi-regional topography (Case 3DLSB), as well as by a case with no-flow boundaries and a local topography (Case 3DL1).

8. Summing Up of Technical Aspects

Conductivities - Recharge

The hydraulic conductivities of the fracture zones were reported as range values (in the Background Report) at specific points, corresponding to the positions where the fracture zone in question was penetrated by a borehole. The average value from the reported span was chosen as the value to be assigned to the finite element model. Furthermore, the power function representing the hydraulic conductivity variation with depth was matched from these average values, thus to some extent suffering from uncertainties. Since it has been shown that about 99% of the infiltrating water enters the domain through the fracture zones, the model is most likely sensitive to different assumptions with regard to the conductivities of the fracture zones. A decrease by one order of magnitude for all fracture zones would thus reduce the amount of infiltrated water through the top surfaces of the fracture zones by one order of magnitude, which probably would affect the flow in general, and in zone 2 in particular to a large extent. However, since the calculations indicated that the model was able to reproduce flow values that were in agreement with those estimated in field, the conductivities applied were probably realistic. The statements above should therefore be regarded as a warning towards the sensitivities in model results in general to assumptions with regard to hydraulic conductivities, which often are subject to large uncertainties and usually are reported as range values.

The large volumes of infiltrating water should rather be seen as a consequence of the upper boundary condition – this amount of water is required to maintain the groundwater table at its position. The recharge rates depend linearly on the hydraulic conductivities in the upper-most layers of the domain. The model should according to this be extremely sensitive to different assumptions with regard to the conductivities of the fracture zones.

One effect that could possibly reinforce the infiltration rates, is that when the upper part of the mesh is adjusted vertically to coincide with the elevation of the groundwater table, also the nodes located in the fracture zones are elevated. This could seem a bit artificial, since fracture zones in nature often are located in valleys, which are relatively flat. By adjusting the nodes in the fracture zones vertically, a gradient is prescribed along the fracture zone, which according to Darcy's law implies that water is infiltrated through the top surface of the fracture zone. However, a procedure involving a special treatment of the topography of the fracture zones is prevented due to the limited knowledge on the detailed scale that this would require.

A more strict approach could be to prescribe a recharge rate which is considered reasonable, and to calibrate the hydraulic conductivities to match the groundwater table. This approach is in itself a matching procedure in a number of steps, which is prevented by the heavy consumption of computer time and man power involved.

Upper boundary condition

The original intention of the modelling procedure of the present project, was to apply the semi-regional topography of the groundwater table on the top of the semi-regional mesh. Correspondingly, the local topography would be applied on the top of the local mesh. The lateral boundary conditions on the local model would be transferred from a base case on the semi-regional scale. However, it is a difficult task to produce topographic maps on different scales, the contours of which can show a perfect fit at the different scales. It was shown that the results from the initial calculations (not reported here) suffered severely from the lack of consistency in the representation of the groundwater tables at the different scales. This was particularly the case for the bounding fracture zones.

Lateral Boundary Condition

It has been shown specific to this project, that the local model was sensitive to the errors occurring when the pressures were transferred from the semi-regional scale, particularly along one of the bounding fracture zones (zone 4). The errors associated with the transferred boundary conditions were found to depend on that all corner nodes in an element on the semi-regional scale took part in the interpolation procedure when pressures from the semi-regional model were transferred to the local scale model. The local model in this particular project was certainly more sensitive than anticipated. One fortunate circumstance was however that the area of concern (the vicinity of zone 4) was located in a discharge area, which implied that the large amount of water that infiltrated through the top surface of this zone was discharged through the lateral boundary describing the outer edge of the zone. This made the infiltrated water less important for the overall flow system than if the boundary would have been located in a strong recharge area. This would surely have implied that large amounts of water would have entered the system in an incorrect way. An approach to reduce the sensitivity in the present project, would have been to move the boundaries of the local model laterally not to coincide with the fracture zones.

Future Research

It has been shown in the present study that there are a few sources of uncertainties which can be referred to either as site-specific or as model-specific. The three main sources are:

- The hydraulic conductivities of the fracture zones in general, and for zone 2 in particular. The hydraulic significance of zone 2 is indisputable, but there is a need for further investigations as to whether or not an alternative interpretation of the conductivities of zone 2 affects the results to a significant degree. It is still uncertain if the conductivity of zone 2 is depth dependent or not.
- The upper boundary condition. This was represented differently on the two scales. To what degree did the semi-regional topography affect the results on the local scale when applied at the top of the local mesh ?
- The lateral boundary conditions. As discussed in the previous sections, the results suffer from uncertainties to some extent by the use of transferred lateral boundary conditions. It was shown within this study that these uncertainties affect the flow situation in a local sense just by the boundaries. However, a quantitative statement in this context would be of utmost use; not only for this project but also for future studies involving modelling at different scales with a transfer of boundary conditions.

The three main sources of uncertainty mentioned above all have an impact on the flow situation within the present study. If sensitivity analyses are to be performed for the results presented here, it would be useful if these could be oriented towards investigations of the impact on the fluxes at repository level, and towards the calculated groundwater flow in zone 2 against which the model results were calibrated in a rough sense.

9. Conclusions

Presence of Salt

The results from the two-dimensional modelling of the saline water have to be regarded and evaluated in a qualitative manner since the modelling is performed in a semi-generic fashion with little or no knowledge about the boundary conditions in nature. This is particularly the case when hydrostatic lateral boundaries were assumed. The no-flow lateral boundaries are probably more realistic.

The increased density caused by the presence of salt together with the inclination of zone 2, create a density-dependent flow below zone 2, whereas the flow above the zone is seemingly unaffected by the higher density below zone 2. This depends on that zone 2 acts as a separating barrier against vertical interaction between the two domains above and below zone 2. The flow below zone 2 thus mainly depends on the salinity of the groundwater and the inclination of zone 2. This implies that the groundwater would have been stagnant below zone 2, had the zone been horizontal. The fluxes below zone 2 are increased with roughly a factor of ten when saline water is considered. Typical flux values were in the order of 30-300 ml/m²/year at z=-500 m in the middle of the domain. The density-dependent flow is not yet fully understood, since the lateral boundary conditions are uncertain and the spatial distribution of salt is unknown in the area. The presence of salt was therefore not considered for the following three-dimensional calculations.

To compare the calculational results in a rough manner on the 2D scale and the local 3D scale, the fluxes could be studied. The 2D case with no-flow lateral boundaries without salt could be compared to the 3D Base Case on the local scale. It turns out that the 2D model is too crude in the vicinity of this particular level, since the flux contours in the figures that were used to evaluate the fluxes, are difficult to distinguish from each other. This depends on that the sub-horizontal zone in the 2D cross-section unloads the system hydraulically, and large differences in fluxes are therefore observed just below this zone. However, possible flux values of about 30-300 ml/m²/year in the rock mass could be deemed as representative values for the 2D model, which covers the span for the rock mass in the 3D local model. It should be noticed though, that these figures are subject to large uncertainties due to the lack of legibility of the figures. Therefore, it cannot be stated clearly that the 2D results are in good agreement with those obtained at the 3D local scale.

Semi-regional Scale Modelling

The general flow was directed from south-west to north-east with rather gentle fluctuations in the topographic gradient. The model appeared to be rather insensitive to the different assumptions with regard to the hydraulic conductivities. The results obtained with the different cases are consistent with the expectations, which naturally depends on that the changes introduced from one case to another were rather modest.

It was shown that the fracture zones are important for the flow on the semi-regional scale. This was particularly indicated by the generated particle tracks for the case when the entire domain was treated as rock, when compared to the remaining cases. Moreover, this was supported when the infiltration rates were calculated over the top surface of the model, which showed that about 99% of the infiltrating water entered the model through the top surfaces of the fracture zones.

The calculated flowpaths indicated a strong clustering at the intersection between zones 1 and 4 for all cases, except for the case when a homogeneous rock mass was assumed. Furthermore, the flux distribution in the rock mass within the potential repository indicated that values of about 100 ml/m²/year were representative for the base case formulation. The cases differ internally more or less only by a scaling factor corresponding to the changes introduced in terms of hydraulic conductivities for the rock mass.

The water balance calculations performed for the flow into and out of zone 2 indicated that its position according to the Base Case formulation had sufficient connection with the fracture zones to feed zone 2 with water. The model set-up for the Base Case was therefore considered calibrated, since the amount of water estimated as the natural flow through zone 2 was achieved with this case. Further, the extension of zone 2 aligning with the position of local fracture zone 7 was considered to be more likely than a position of the south-most edge of zone 2 intersecting with zone 14; especially since the differences in terms of flow through zone 2 between the two cases were rather limited. A feasible conclusion thus seems to be that the model to be used for a transfer of lateral boundary conditions to the local model, must be the Base Case.

Local Scale Modelling

The flow on the local scale was governed by the topography, and the major flow pattern is directed towards the intersection between three fracture zones in the upper north-east corner. This is particularly the case for the northern block. The south-most part of the southern block is discharged at the south-east boundary, while the flow in the remaining part of the southern block is discharged in a north-west direction.

The model on the local scale is rather insensitive to the boundary condition applied along the top surface assuming no-flow lateral boundaries, although it appeared to be extremely sensitive to the errors stemming from the transfer of lateral boundary pressures from the semi-regional model. However, this effect was restricted to the vicinity of zone 4, and the results in general did not seem to be affected by this.

The particle tracks indicated that the overall flow pattern is roughly the same as on the semi-regional scale. The flowpaths had exit points at the intersection between zone 1 and zone 4, see Figure 8.1.

The transfer of boundary pressure seemed to yield pathlines that had exit points that corresponded to those on the semi-regional scale; i.e. through the lateral boundaries for the cases of concern. The flowpaths for the cases with no-flow boundaries had, due to the boundary condition itself, their exit points at the top surface or close to it.

The travel times for the particles that were released at repository level were in the order of 1000 to 1500 years assuming a porosity of 0.0001. These values are valid for the cases with transferred lateral boundary pressures, with longer travel times for the cases with no-flow lateral boundaries. The latter depends on that the travel path to the exit point is longer for these cases since the exit point is located at the upper boundary. The exit points for the cases with transferred lateral boundaries are located at the lateral boundaries according to the pressure that was prescribed from the transfer of the boundary pressures, see also Figure 8.1 (right).

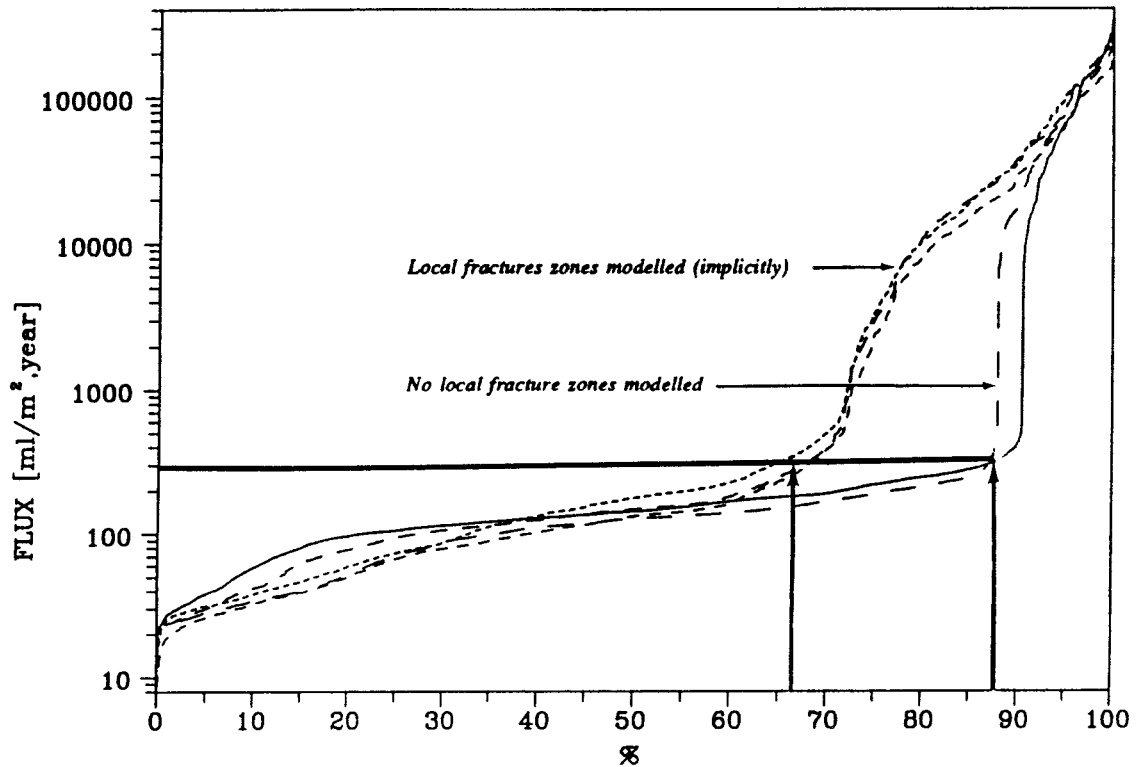


Figure 8.2 *Frequency diagram of the flux distribution for the cases considered on the local scale and the base case on the semi-regional scale. The solid line corresponds to the base case on the semi-regional scale; the curve almost coinciding with it corresponds to a case on the local scale with transferred lateral boundary conditions but with the local fracture zones discarded. The three remaining curves are cases on the local scale with local fracture zones modelled. Transferred or no-flow lateral boundary conditions were modelled for the latter cases with either the semi-regional or the local topography applied at the top surface.*

The water balance calculations in zone 2 showed that regardless of which case that was studied, the calculated flow rate was within the range that was specified as the natural groundwater flow through zone 2. Virtually all the flow that entered zone 2 was recharged at the intersection between zones 1 and 4. The estimated natural flow through zone 2 was in the range of 150000-300000 m³/year. The calculated flow amounted to about 250000 m³/year as an average for all the cases on the local scale. Zone 2 was recharged from its top confinement with 165000 m³/year (corresponding to about 40 mm/year), and by roughly 80000 m³/year from its confining fracture zones. Extremely low mass conservation deviations were obtained for all the cases, with somewhat higher values for the Base Case. These higher values were found to depend on numerical difficulties in the vicinity of an intersection between three local fracture zones, where zone 2 is recharged from one of these zones and discharged into another, at the same time as the latter zone was recharged by infiltration.

Conclusively, it was shown that the cases differ internally to a limited extent in terms of flux values at repository level. It was illustrated by frequency diagrams of the flux distribution that the local scale model well may be described by a model with transferred lateral boundary conditions and a semi-regional topography *or* by a model with no-flow lateral boundaries and a local topography, since they seem to yield results that are in good agreement with one another. For possible future research efforts within the SKB 91-project, the latter case is however appointed as the best suitable, since this case offers the opportunity to include as much detailed knowledge as possible.

The field investigations at the Finnsjön site were carried out with equipment that was older than those used for the investigations within the KBS 3-study. Whether or not this would affect the results within the present study was investigated. This is more or less an artificial set-up, since the hydraulic conductivities assigned to this case are evaluated at a different location than the Finnsjön site. However, it may be worth noticing that the flow in zone 2 is lowered by a factor of roughly 300 when KBS 3-data were used, compared to the other cases on the local scale. Furthermore, the fluxes were in the order of 2-5 ml/m²/year in the rock mass at repository level, to be compared to about 100 ml/m²/year obtained with Finnsjö-data. However, the calculated flow with Finnsjö-data was within the span that was reported as natural flow in zone 2, which means that a certain degree of confidence has to be put into the evaluation of the hydraulic conductivities as applied to the model with Finnsjö-data. The case with KBS 3-like conductivities has to be regarded as a "what-if"-case rather than as an evidence for that lower flow rates would have been obtained with an up-to date field measuring equipment.

References

Background Report:

- Andersson J-E, R. Nordqvist, G. Nyberg, J. Smellie, S. Tirén, 1989,
"Hydrogeological Conditions in the Finnsjön Area; Compilation of Data and Conceptual Model", SKB Working Report 89-24, Swedish Nuclear Fuel and Waste Management Co., Stockholm, Sweden.
- Ahlbom, K., S. Tirén, 1989,
"Overview of geologic and hydrogeologic character of the Finnsjön site and its surroundings", SKB Working Report 89-08, Swedish Nuclear Fuel and Waste Management Co., Stockholm, Sweden.
- Atkinson R., A.W. Herbert, C.P. Jackson, P.C. Robinson, 1985,
"NAMMU User Guide", Report AERE R-11364, U.K. Atomic Energy Research Establishment, Harwell Laboratory, United Kingdom.
- Carlsson, L., A. Winberg, B. Grundfelt, 1983
"Model Calculations of the Groundwater Flow at Finnsjön, Fjällveden, Gideå, and Kamlunge", Technical Report KBS TR 83-45, Swedish Nuclear Fuel and Waste Management Co., Stockholm, Sweden.
- FEMPROG AB, 1987,
"FEMGEN User Manual, version 8.6", FEMPROG AB (Studentlitteratur), Lund, Sweden.
- Golden Software Incorporated,
"Grapher & Surfer Reference Manuals", Golden Software Incorporated, 807 14th Street, P.O. Box 281, Golden, Colorado 80402, U.S.A.
- Grundfelt, Bertil, 1983,
"GWHRT - A Finite Element Solution to the Coupled Ground Water Flow and Heat Transport Problems in Three Dimensions", Technical Report KBS TR 83-51, Swedish Nuclear Fuel and Waste Management Company, Stockholm, Sweden.
- Grundfelt, B., A. Boghammar, H. Lindberg, 1989
"HYPAC User's Guide", Working Report 89-22, Swedish Nuclear Fuel and Waste Management Company, Stockholm, Sweden.
- Rae J., P.C. Robinson, 1979,
"NAMMU: Finite-Element program for coupled heat and groundwater flow problems", Report AERE R-9610, U.K. Atomic Energy Research Establishment, Harwell Laboratory, United Kingdom.
- Thunvik, R., C. Braester, 1980,
"Hydrothermal Conditions Around a Radioactive Waste Repository", Technical Report KBS TR 80-19, Swedish Nuclear Fuel and Waste Management Company (SKB), Stockholm, Sweden.
- Thunvik, R., C. Braester, 1988,
"GWHRT - A flow model for coupled groundwater and heat flow", Technical Report SKB TR 88-10, Swedish Nuclear Fuel and Waste Management Company (SKB), Stockholm, Sweden.
- Lindbom, B., A. Boghammar, H. Lindberg, J. Bjelkås, 1990,
"Numerical Groundwater Flow Calculations at the Finnsjön Site", Working Report SKB 90-16, Swedish Nuclear Fuel and Waste Management Company (SKB), Stockholm, Sweden.

List of Symbols

C	Salt concentration	(mg/l)
H	Heat source strength	(W/m ²)
K	hydraulic conductivity	(m/s)
T	common rock/fluid temperature	(K)
c	compressibility	(Pa ⁻¹)
c ^f	compressibility of fluid	(Pa ⁻¹)
c ^r	compressibility of rock	(Pa ⁻¹)
c _p	specific heat	(J/K/kg)
c _p ^f	fluid specific heat	(J/K/kg)
c _p ^r	rock specific heat	(J/K/kg)
g	gravity acceleration	(m/s ²)
h	groundwater (piezometric) level	(m)
k	permeability (intrinsic)	(m ²)
p	(total) fluid pressure	(Pa)
p _d	dynamic fluid pressure	(Pa)
q	(Volumetric) flux, Darcy velocity	(m ³ /m ² /s), (m/s)
x,y,z	cartesian coordinates	(m)
Γ _a	averaged dispersion constant	(m ² /s)
ε	rock porosity	(-)
η	dynamic viscosity of the fluid	(Pa·s)
φ	potential (piezometric level)	(m)
ρ _a ^f	average fluid density	(kg/m ³)
ρ ^f	density of fluid	(kg/m ³)
ρ _a ^f	fluid density of saline water	(kg/m ³)
ρ ^r	density of rock matrix	(kg/m ³)
(ρ _p) _a	average heat capacity of rock and fluid	(J/K/kg)
∇	nabla operator	

Superscripts

f fluid

r rock

Subscripts

a average value

d dynamic

s related to salt

Overlying horizontal bar indicates vectorial unit.

APPENDIX A

The figures presented in this appendix are organised so that the different cases considered on the semi-regional are presented consecutively, starting with pressure distribution in horizontal cuts for Case 3DSB, pressure distribution in vertical cuts for Case 3DSB, particle tracking for Case 3DSB, and flux distribution for Case 3DSB. This suite of figures is repeated for Cases 3DS1A, 3DS1B, and 3DS2 respectively.

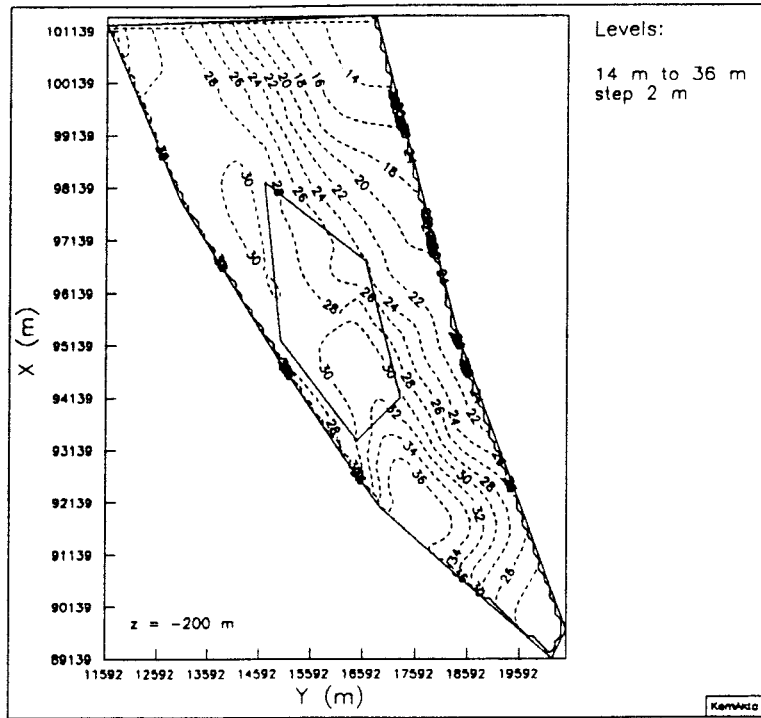


Figure A1 Pressure distribution at $z=-200$ m; Case 3DSB.

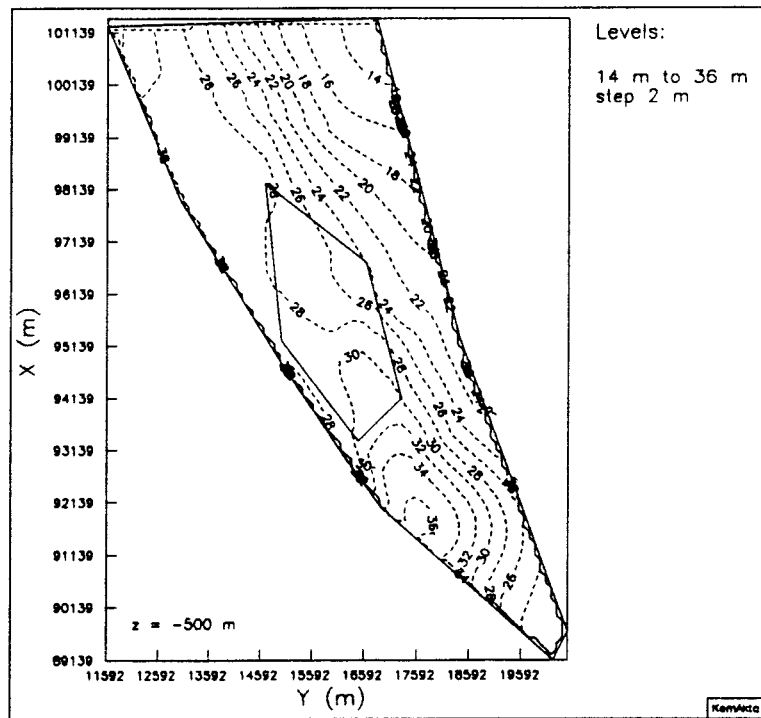


Figure A2 Pressure distribution at $z=-500$ m; Case 3DSB.

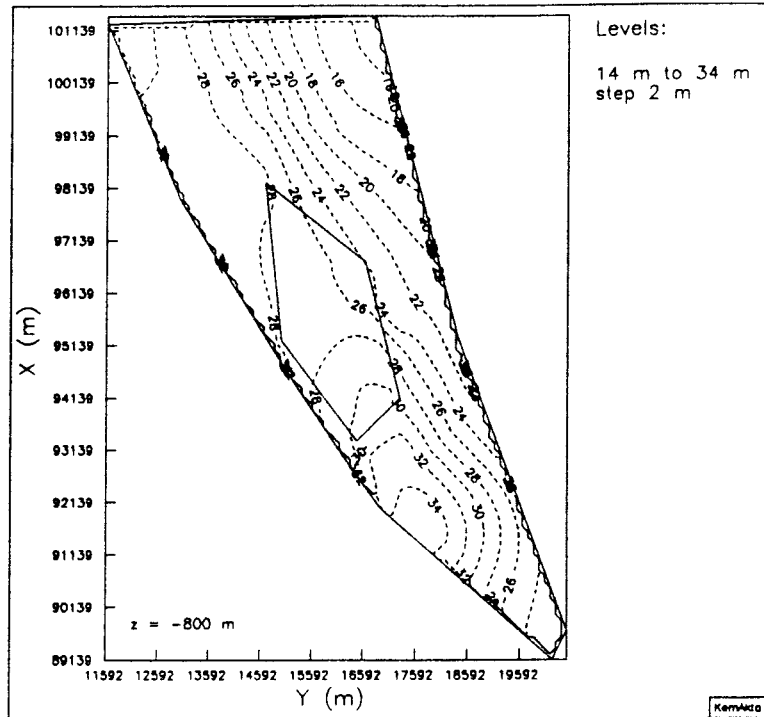


Figure A3 Pressure distribution at $z=-800$ m; Case 3DSB.

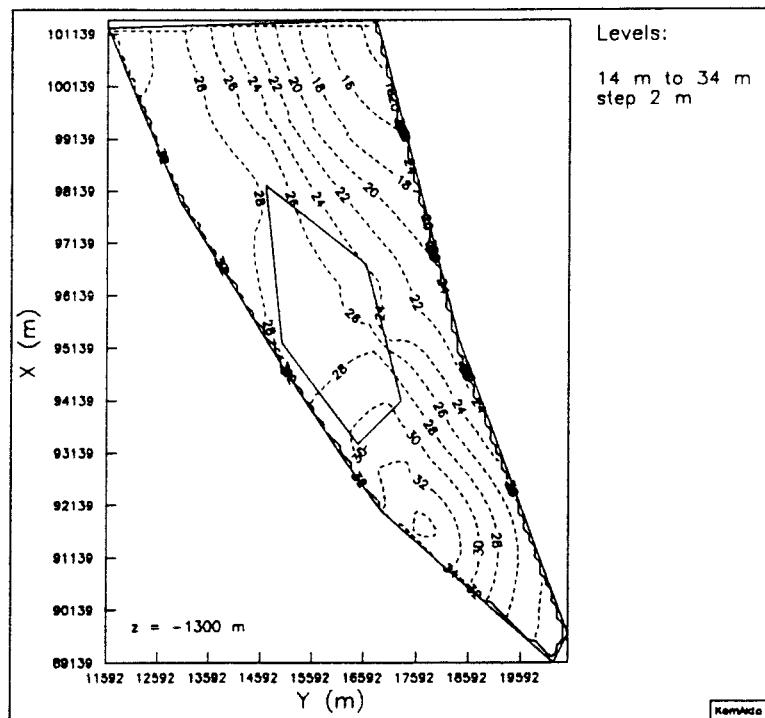


Figure A4 Pressure distribution at $z=-1300$ m; Case 3DSB.

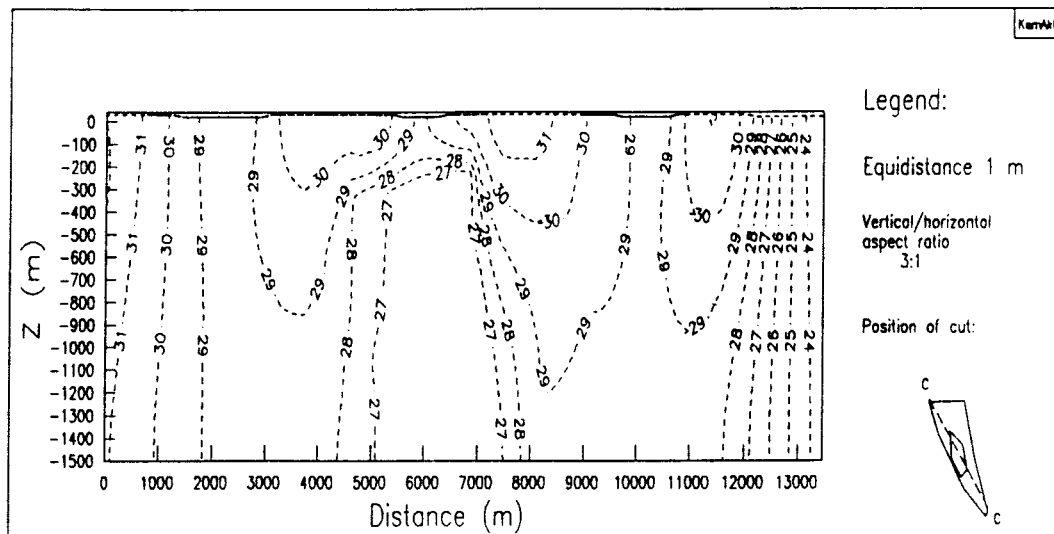


Figure A5 Pressure distribution in vertical cut 1; Case 3DSB.

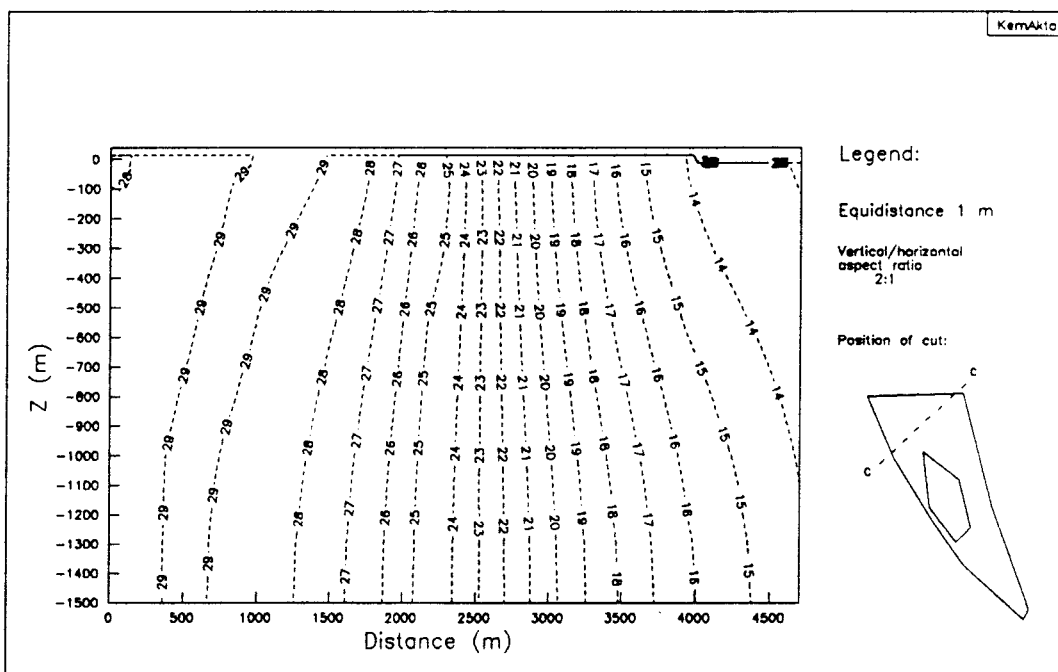


Figure A6 Pressure distribution in vertical cut 2; Case 3DSB.

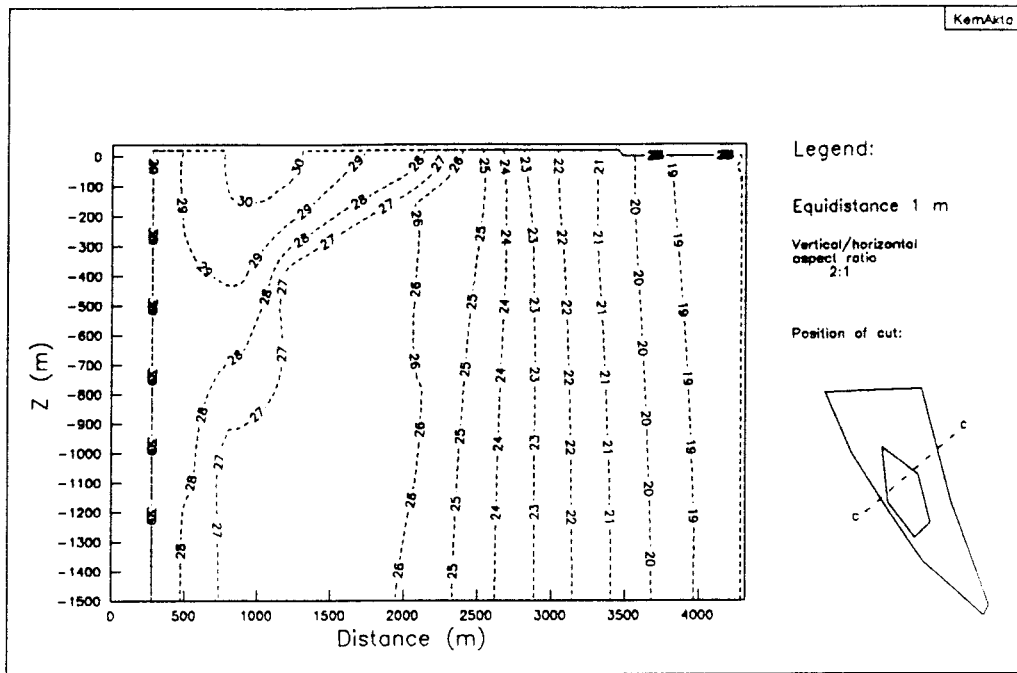


Figure A7 Pressure distribution in vertical cut 3; Case 3DSB.

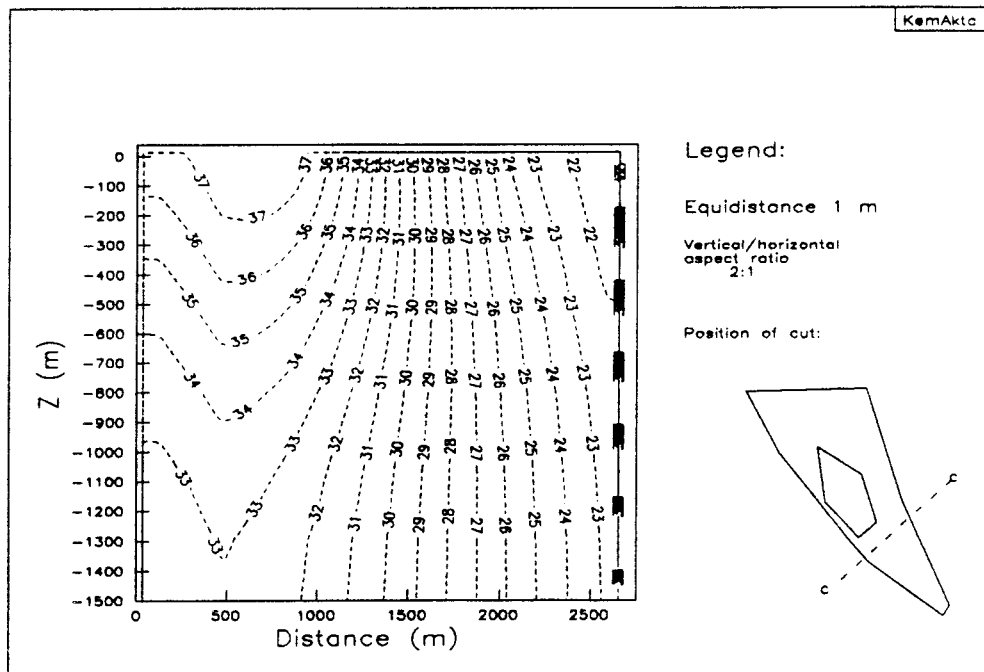


Figure A8 Pressure distribution in vertical cut 4; Case 3DSB.

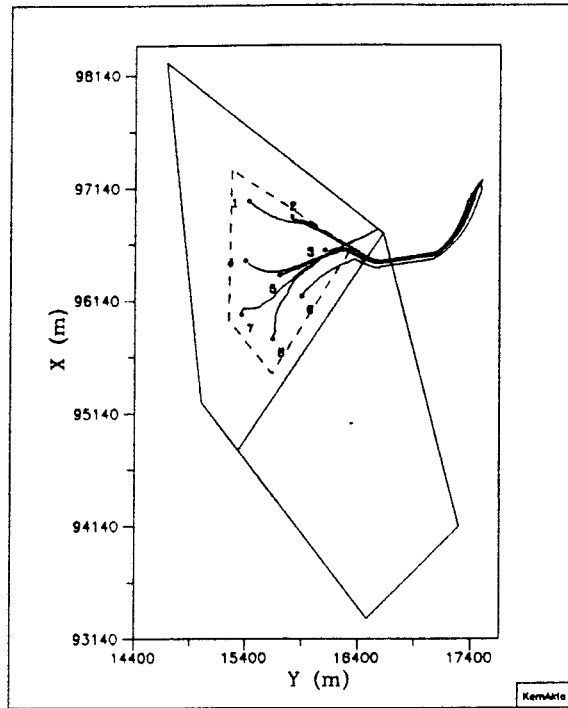


Figure A9 Horizontal projection of pathlines; Case 3DSB.

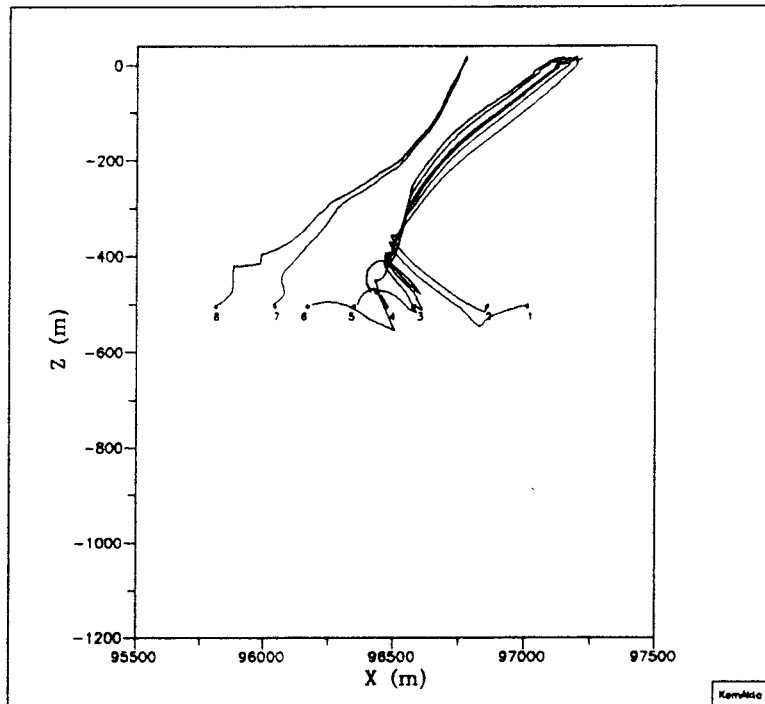


Figure A10 Vertical projection (xz-plane) of pathlines; Case 3DSB.

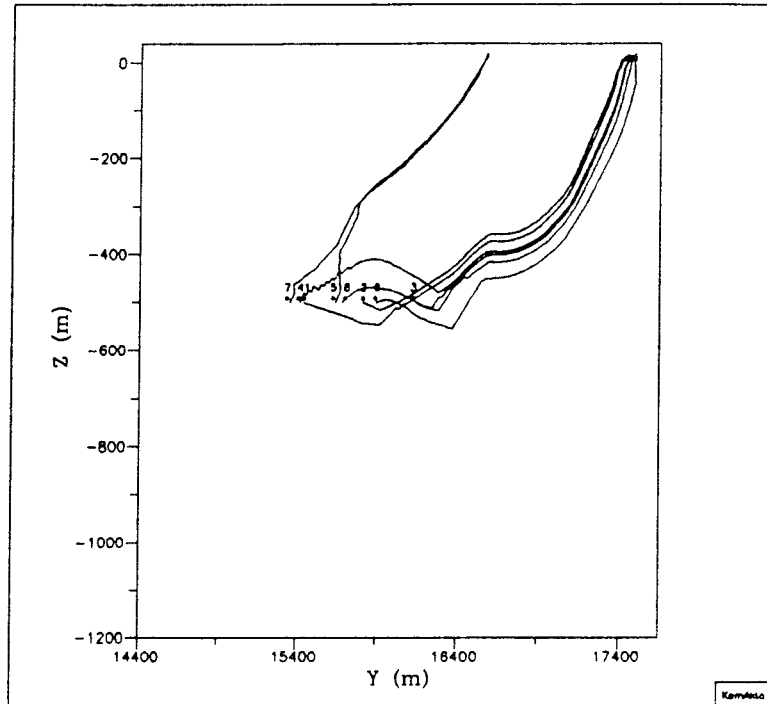


Figure A11 Vertical projection (yz-plane) of pathlines; Case 3DSB.

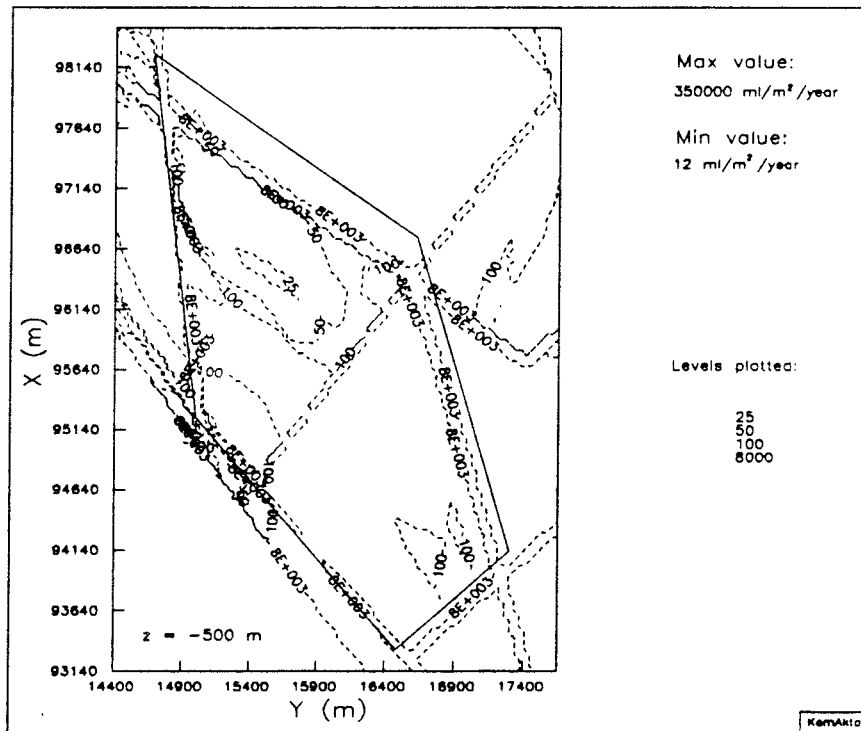


Figure A12 Flux distribution at z=-500 m; Case 3DSB.

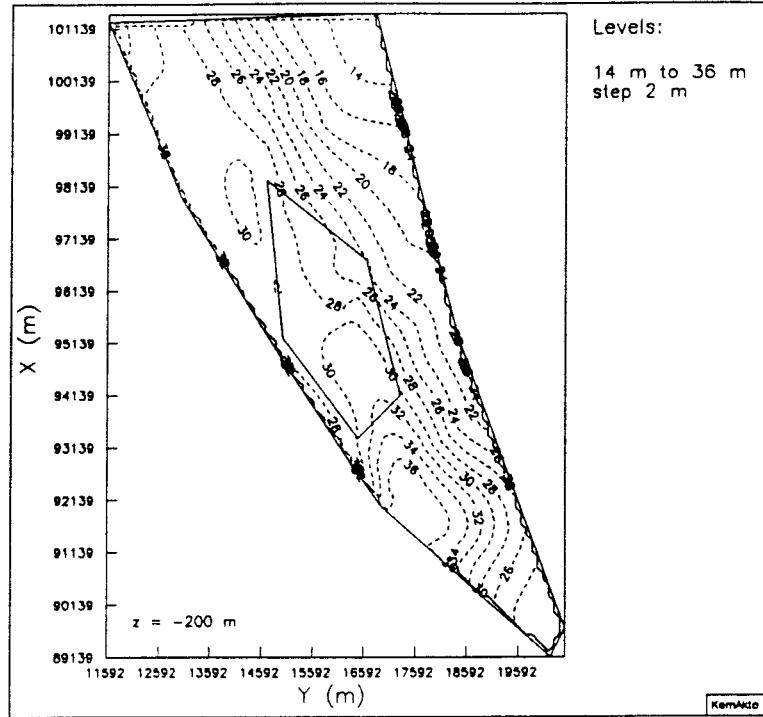


Figure A13 Pressure distribution at $z=-200$ m; Case 3DS1A.

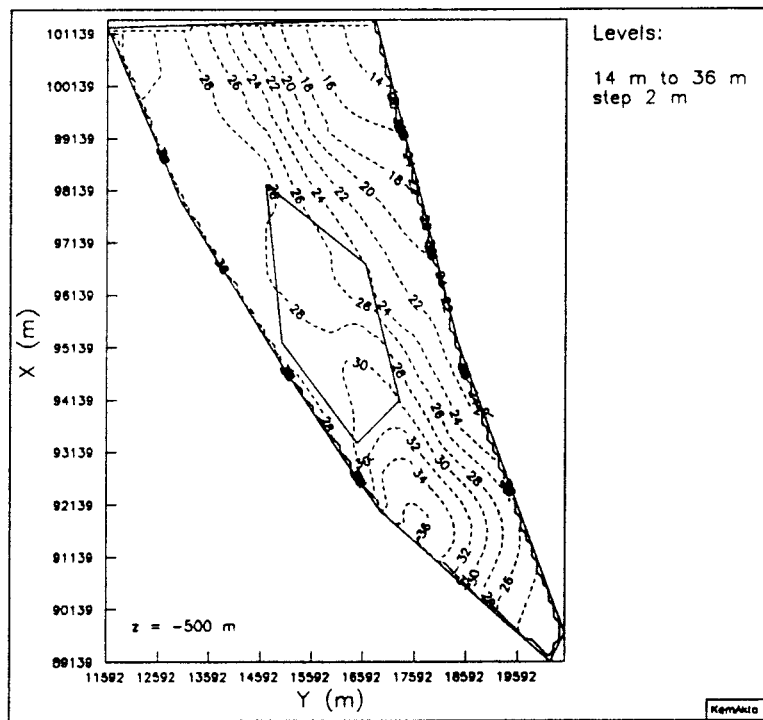


Figure A14 Pressure distribution at $z=-500$ m; Case 3DS1A.

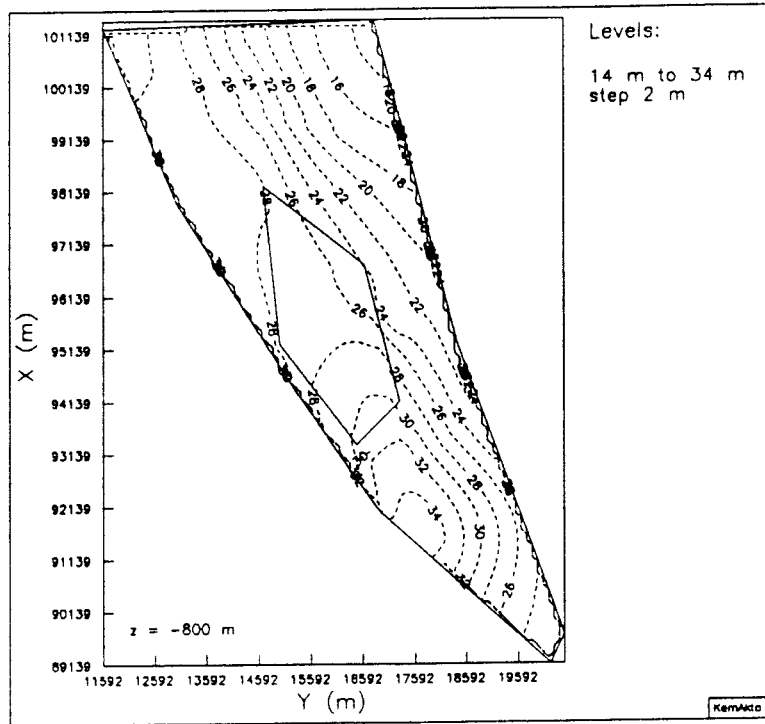


Figure A15 Pressure distribution at $z=-800$ m; Case 3DS1A.

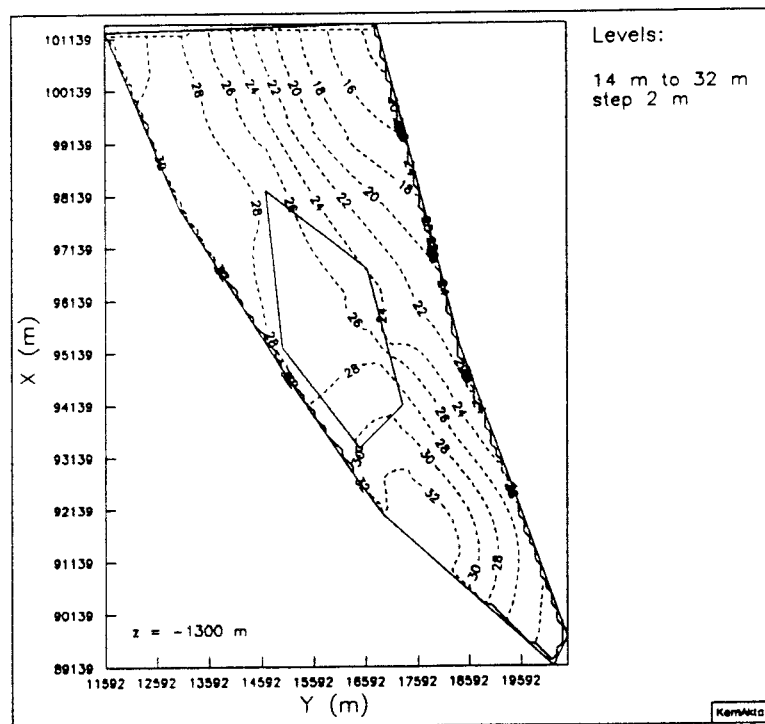


Figure A16 Pressure distribution at $z=-1300$ m; Case 3DS1A.

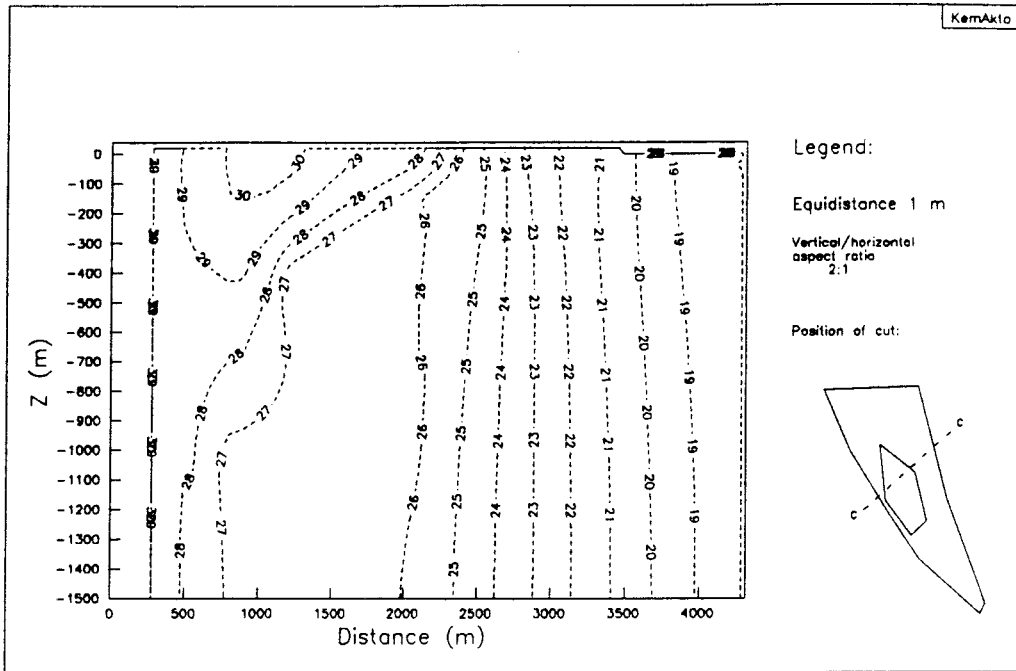


Figure A19 Pressure distribution in vertical cut 3; Case 3DS1A.

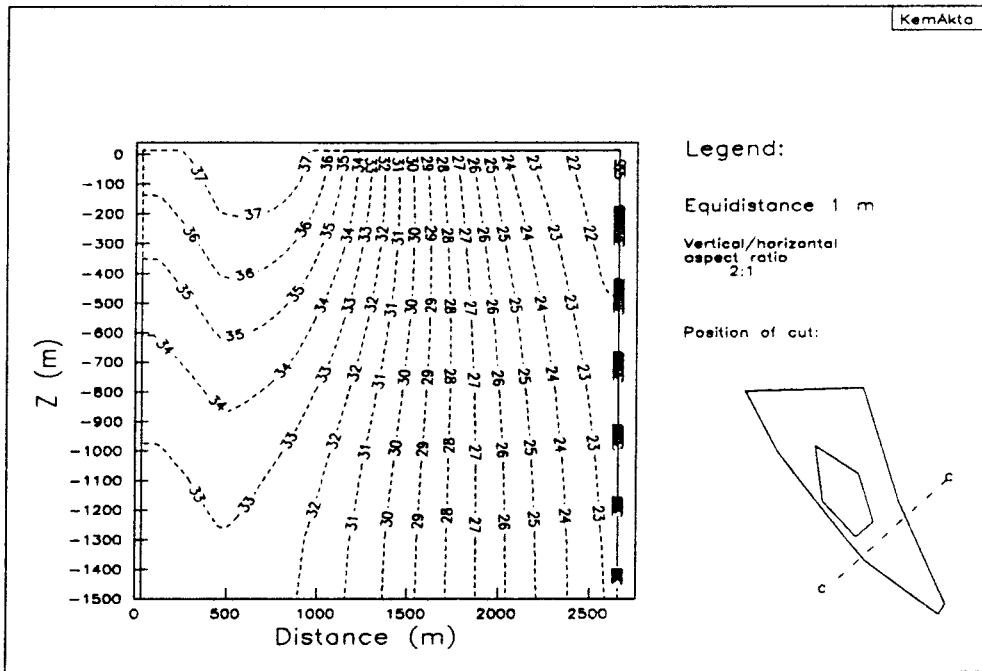


Figure A20 Pressure distribution in vertical cut 4; Case 3DS1A.

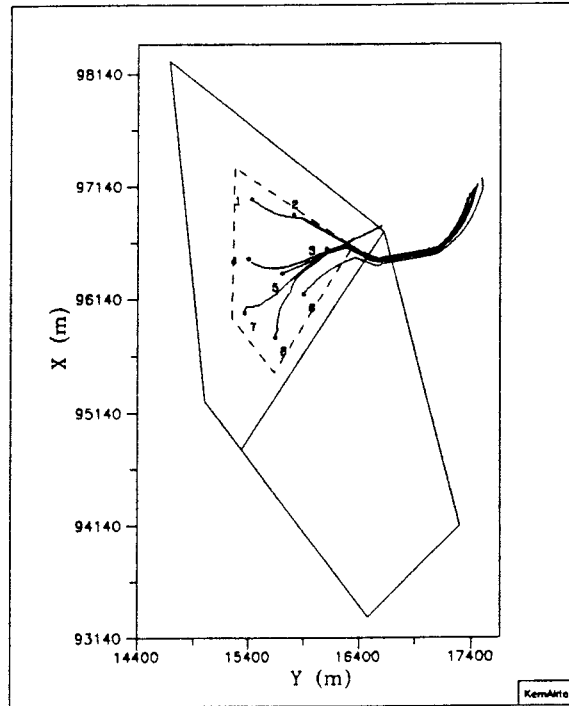


Figure A21 Horizontal projection of pathlines; Case 3DS1A.

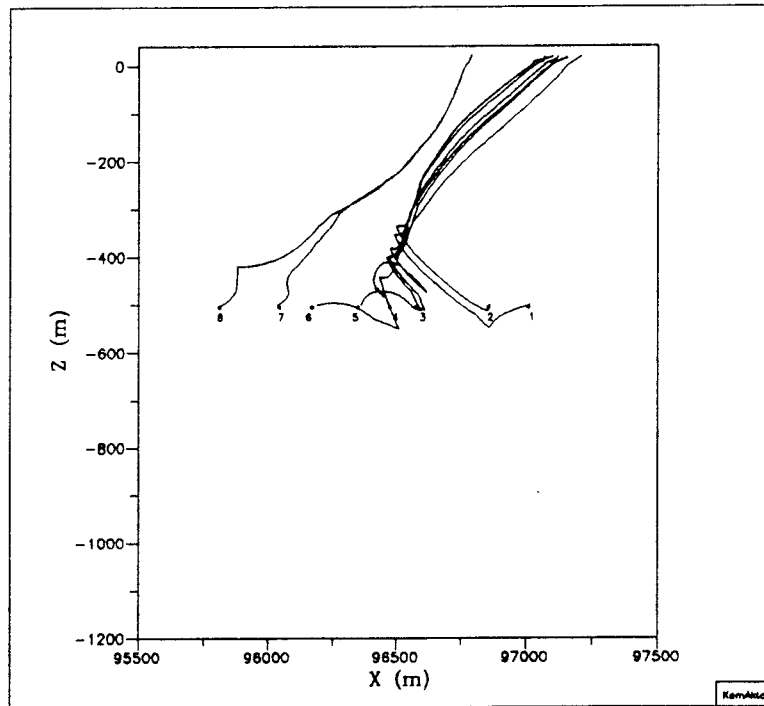


Figure A22 Vertical projection (xz-plane) of pathlines; Case 3DS1A.

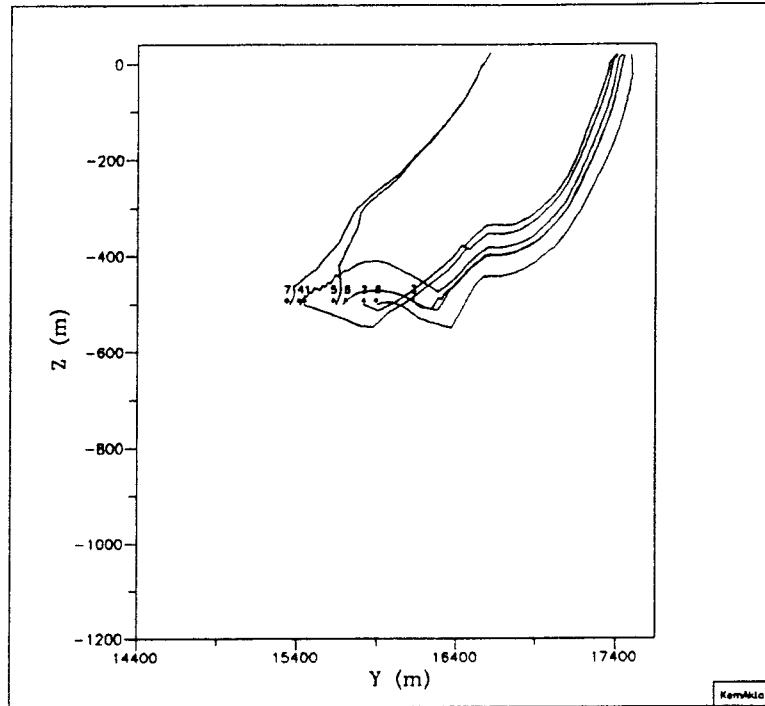


Figure A23 Vertical projection (yz-plane) of pathlines: Case 3DS1A.

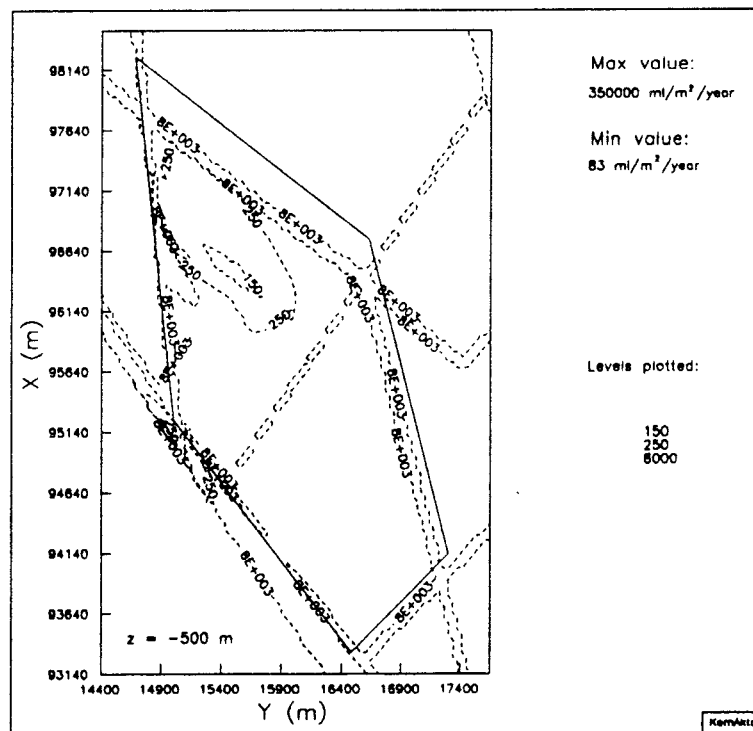


Figure A24 Flux distribution at z=-500 m; Case 3DS1A.

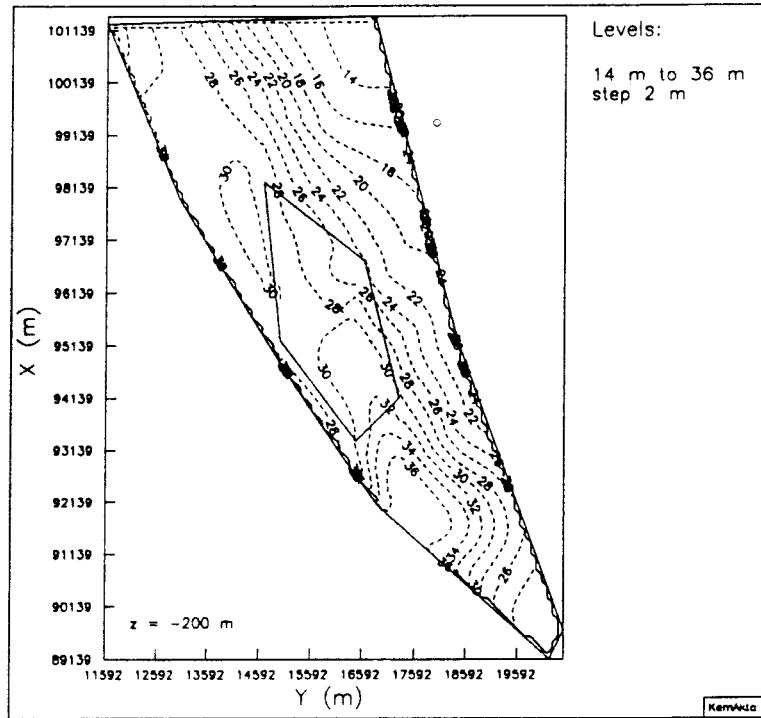


Figure A25 Pressure distribution at $z=-200$ m; Case 3DS1B.

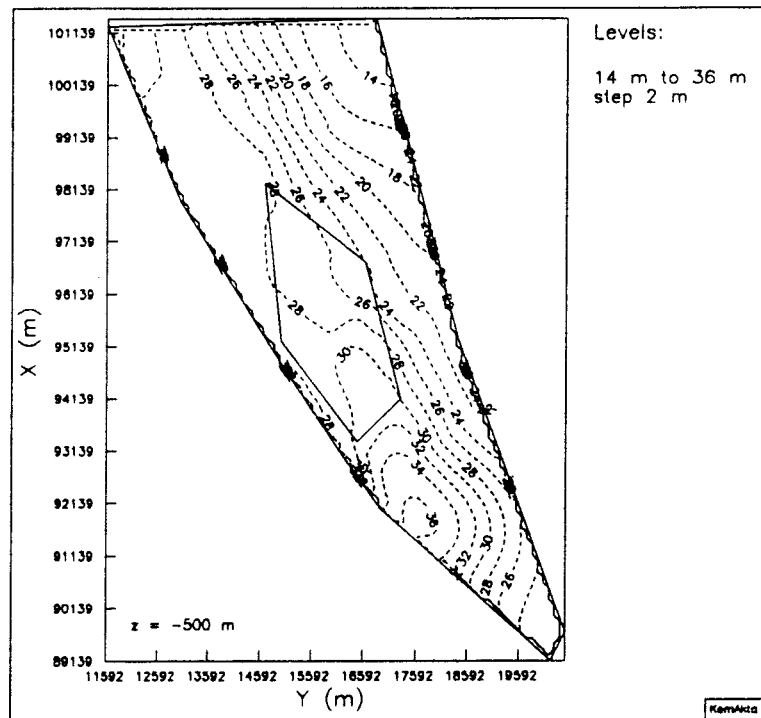


Figure A26 Pressure distribution at $z=-500$ m; Case 3DS1B.

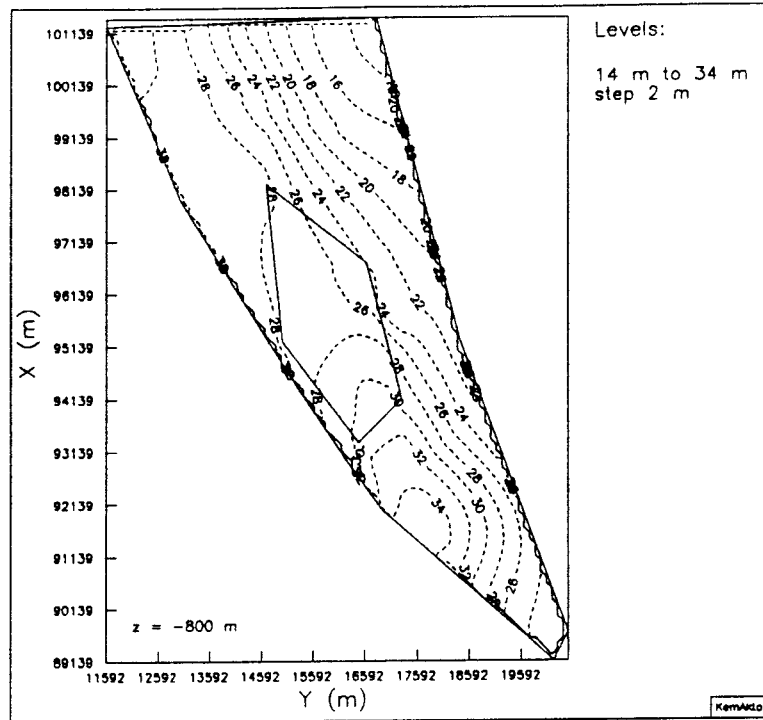


Figure A27 Pressure distribution at $z=-800$ m; Case 3DS1B.

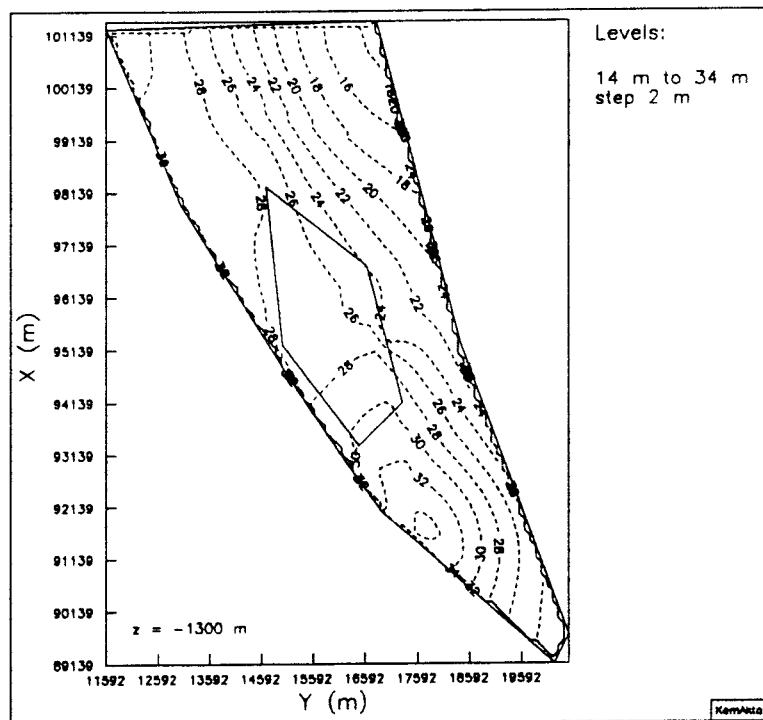


Figure A28 Pressure distribution at $z=-1300$ m; Case 3DS1B.

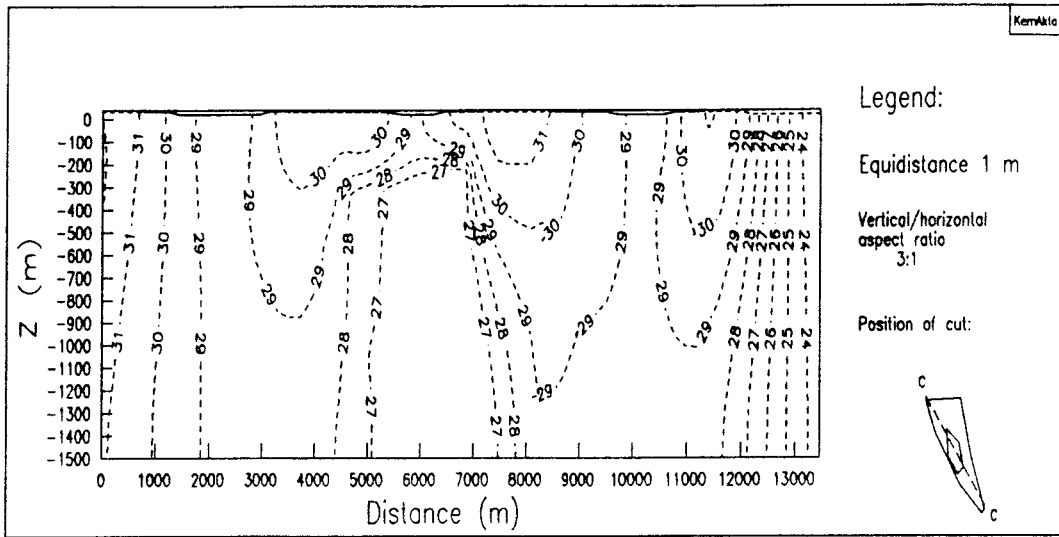


Figure A29 Pressure distribution in vertical cut 1; Case 3DS1B.

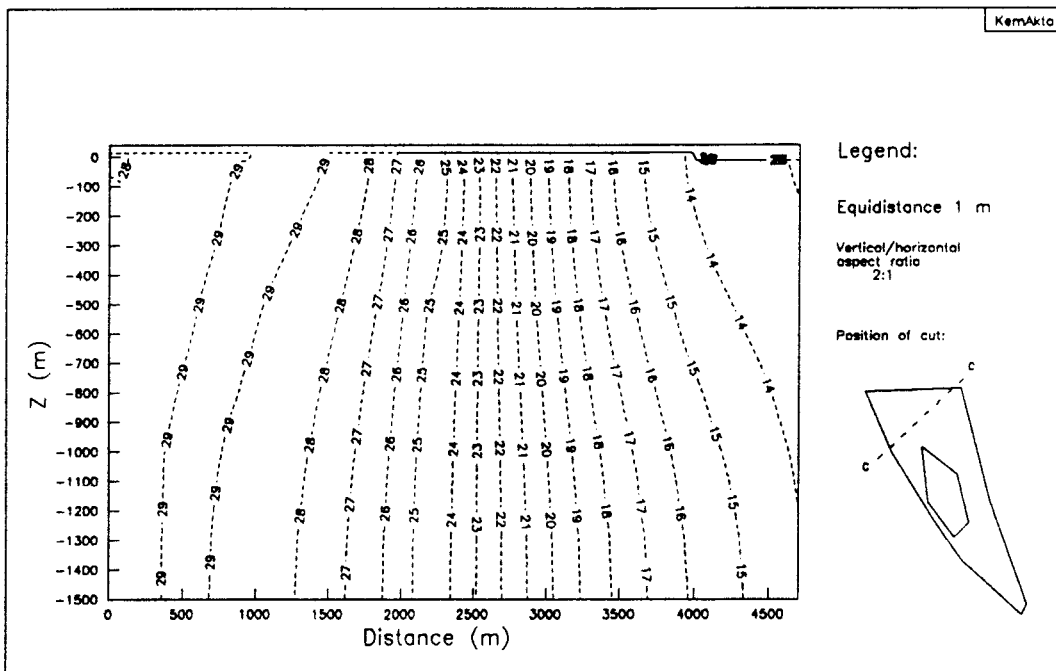


Figure A30 Pressure distribution in vertical cut 2; Case 3DS1B.

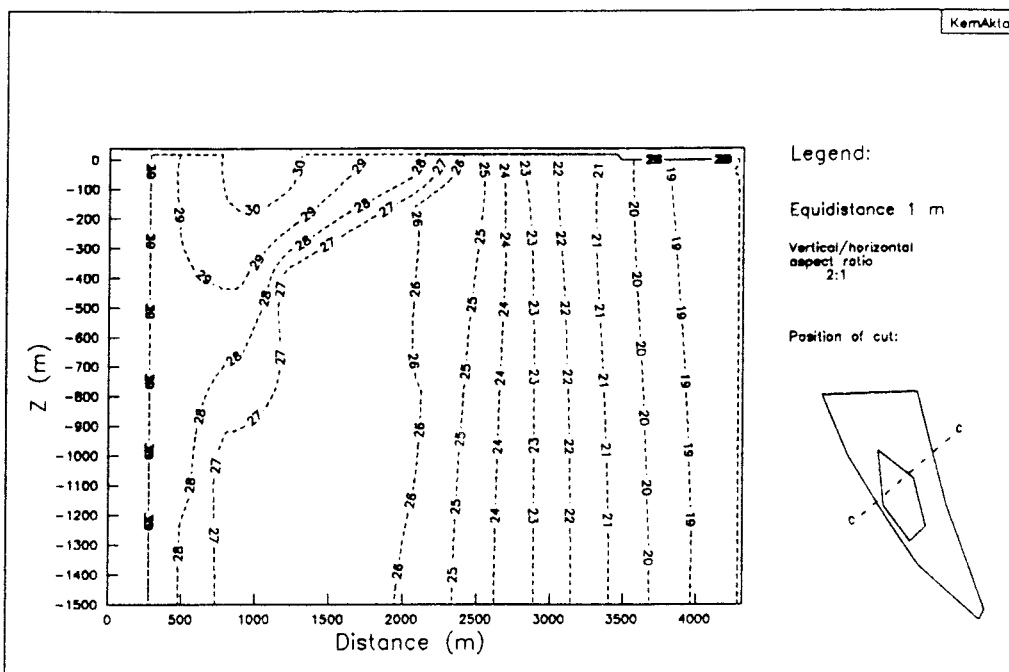


Figure A31 Pressure distribution in vertical cut 3; Case 3DS1B.

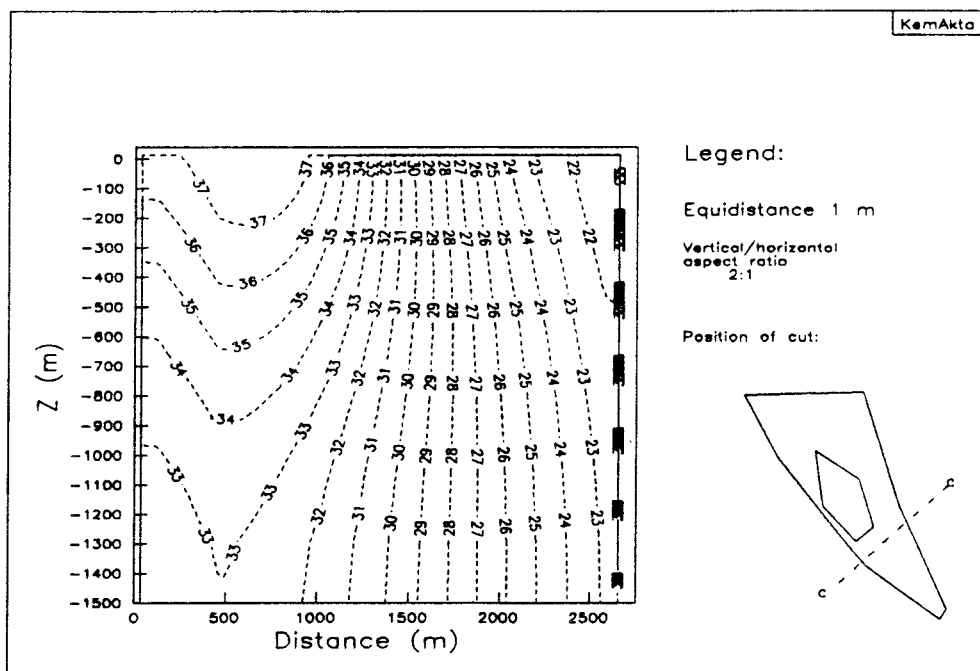


Figure A32 Pressure distribution in vertical cut 4; Case 3DS1B.

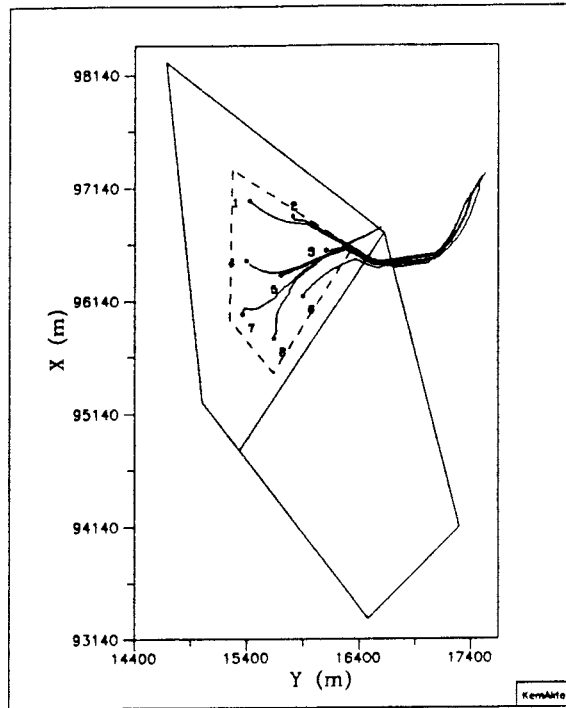


Figure A33 Horizontal projection of pathlines; Case 3DS1B.

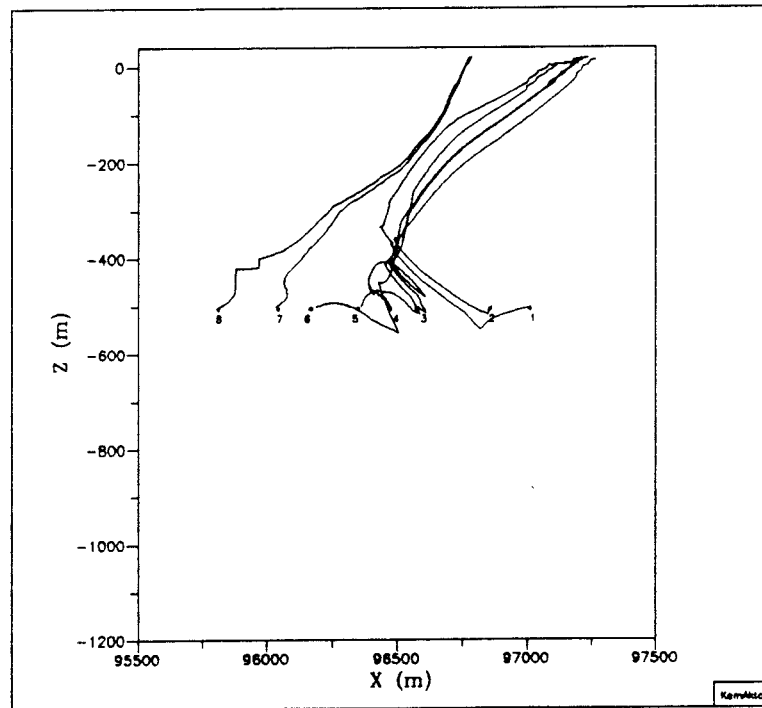


Figure A34 Vertical projection (xz-plane) of pathlines; Case 3DS1B.

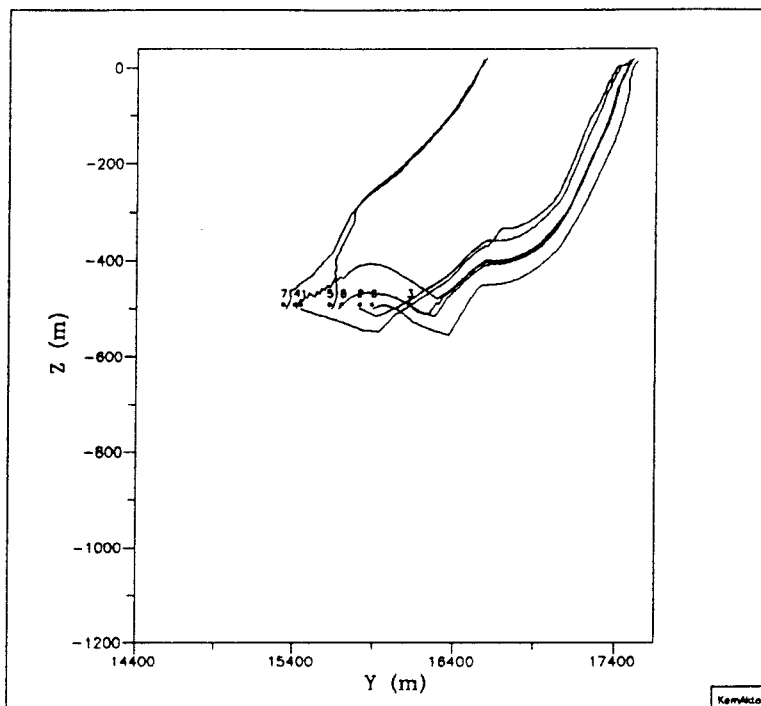


Figure A35 Vertical projection (yz-plane) of pathlines; Case 3DS1B.

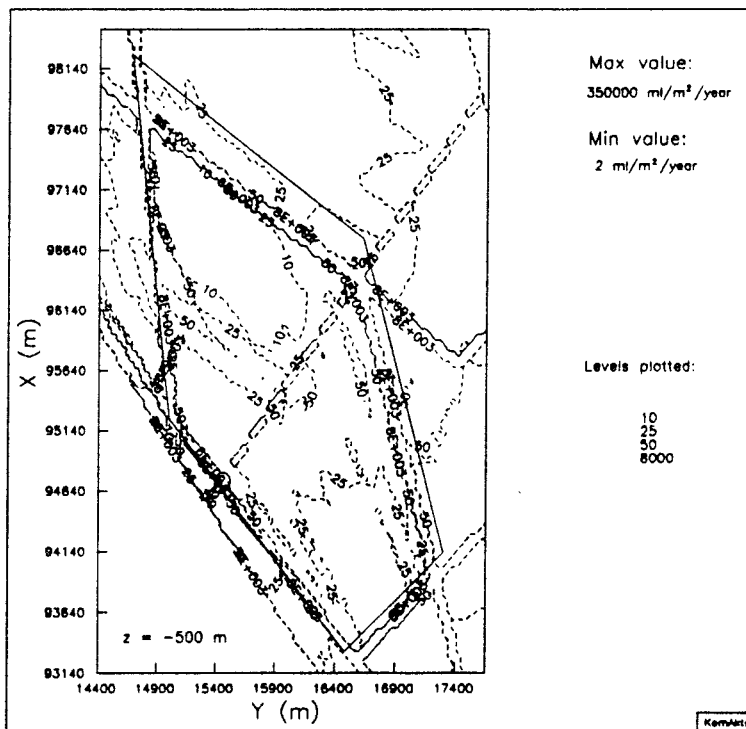


Figure A36 Flux distribution at $z=-500$ m; Case 3DS1B

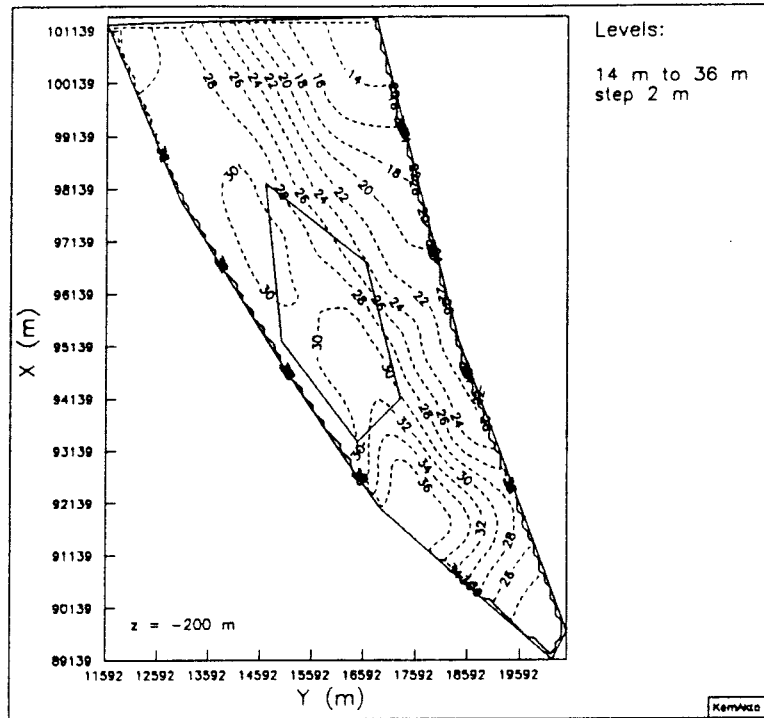


Figure A37 Pressure distribution at $z=-200$ m; Case 3DS2.

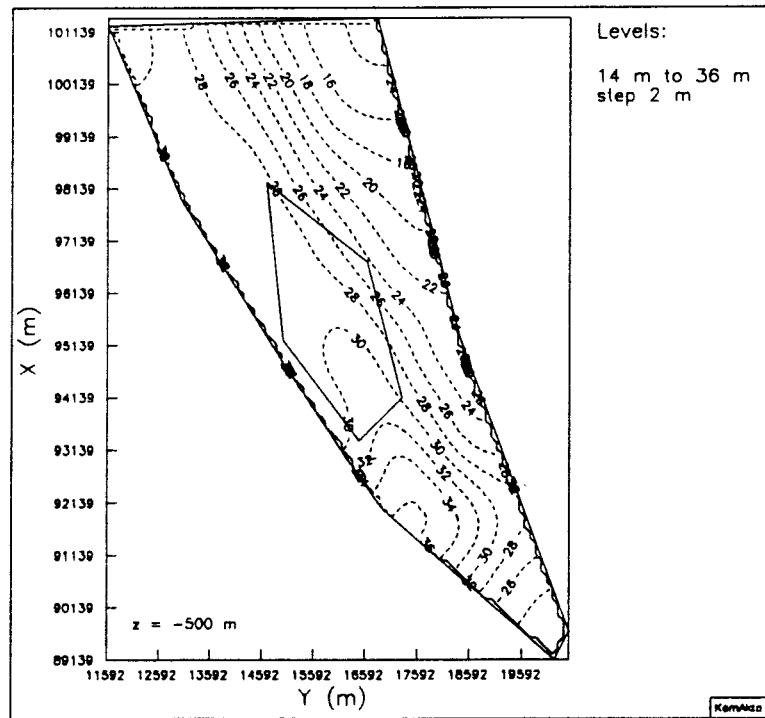


Figure A38 Pressure distribution at $z=-500$ m; Case 3DS2.

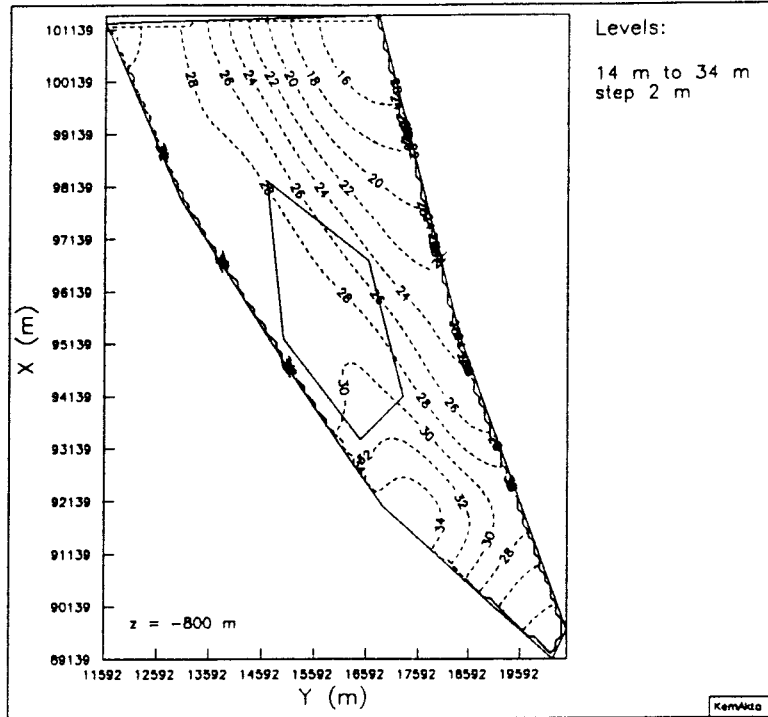


Figure A39 Pressure distribution at $z=-800$ m; Case 3DS2.

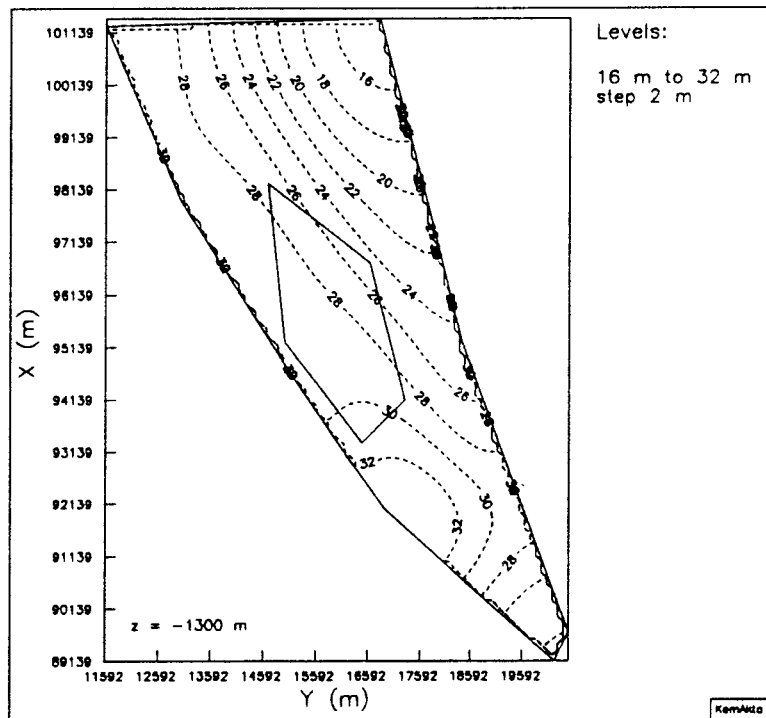


Figure A40 Pressure distribution at $z=-1300$ m; Case 3DS2.

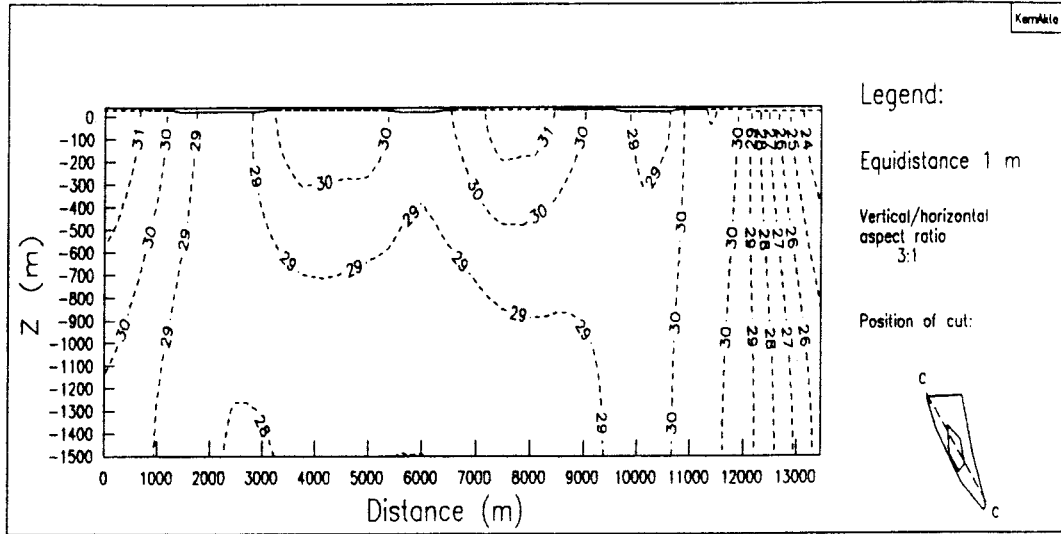


Figure A41 Pressure distribution in vertical cut 1; Case 3DS2.

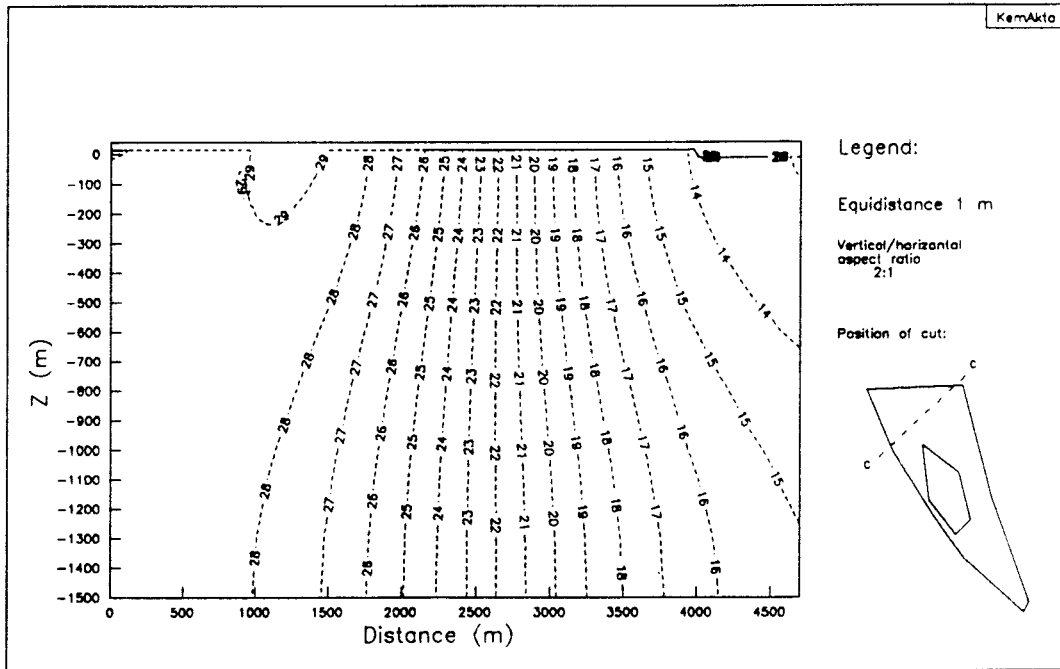


Figure A42 Pressure distribution in vertical cut 2; Case 3DS2.

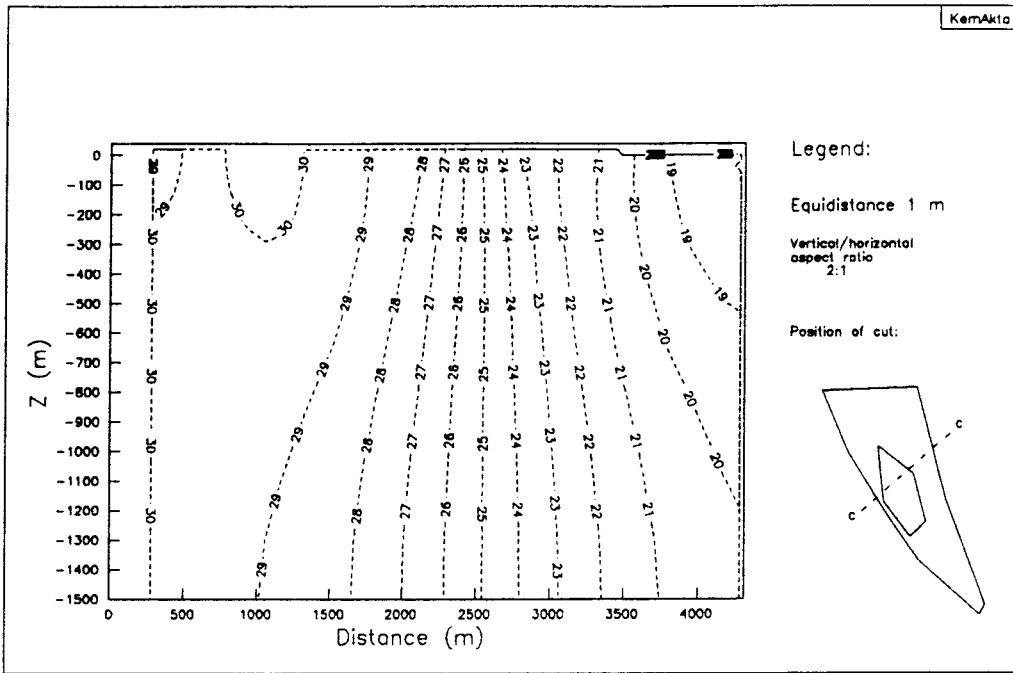


Figure A43 Pressure distribution in vertical cut 3; Case 3DS2.

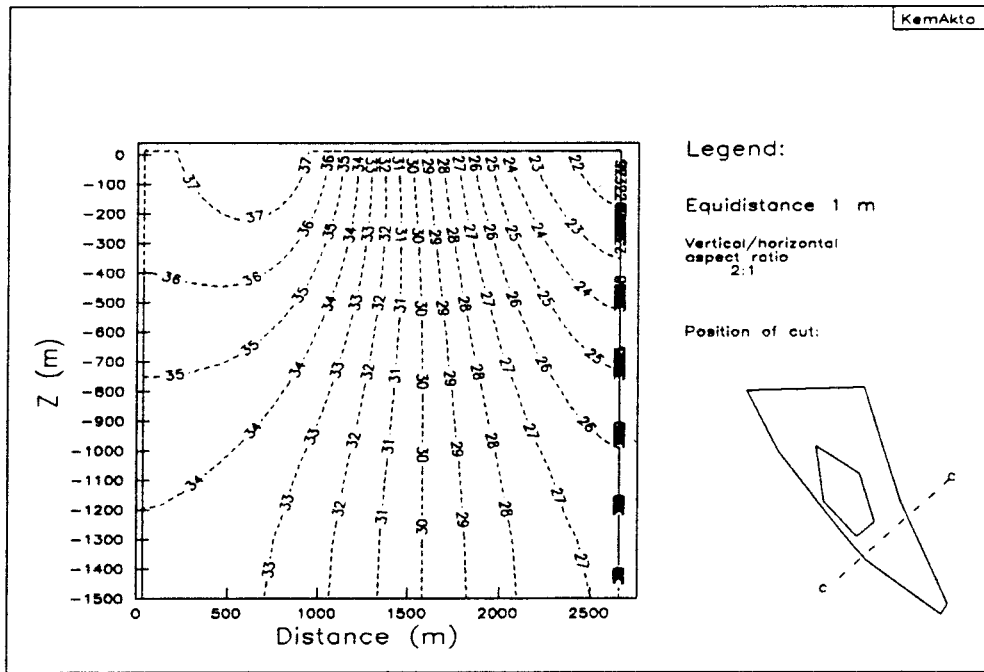


Figure A44 Pressure distribution in vertical cut 4; Case 3DS2.

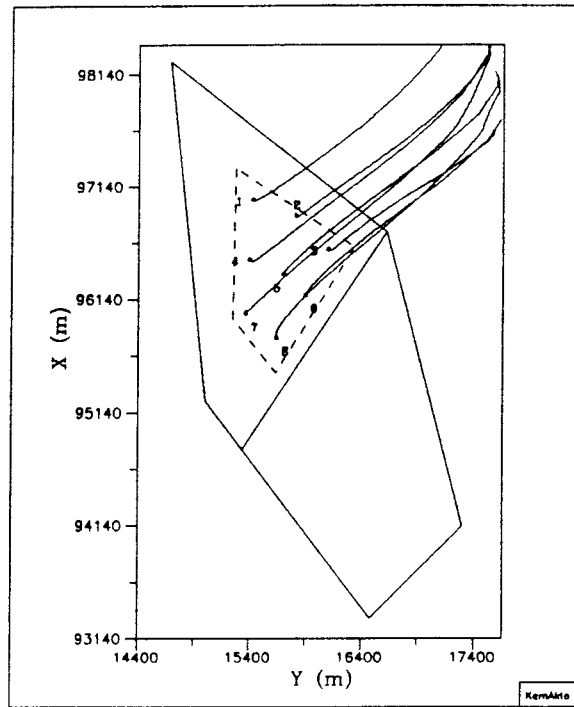


Figure A45 Horizontal projection of pathlines; Case 3DS2.

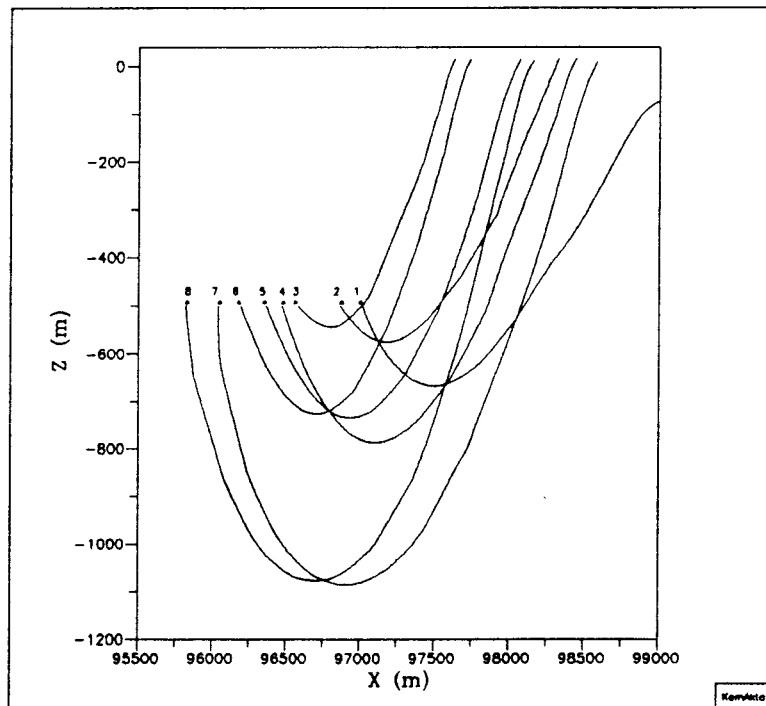


Figure A46 Vertical projection (xz-plane) of pathlines; Case 3DS2.

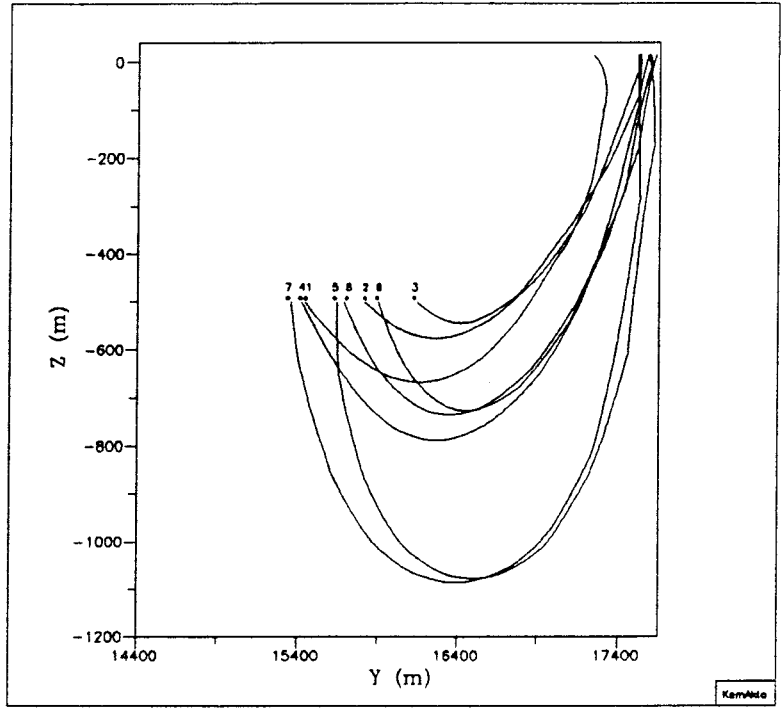


Figure A47 Vertical projection (yz-plane) of pathlines; Case 3DS2.

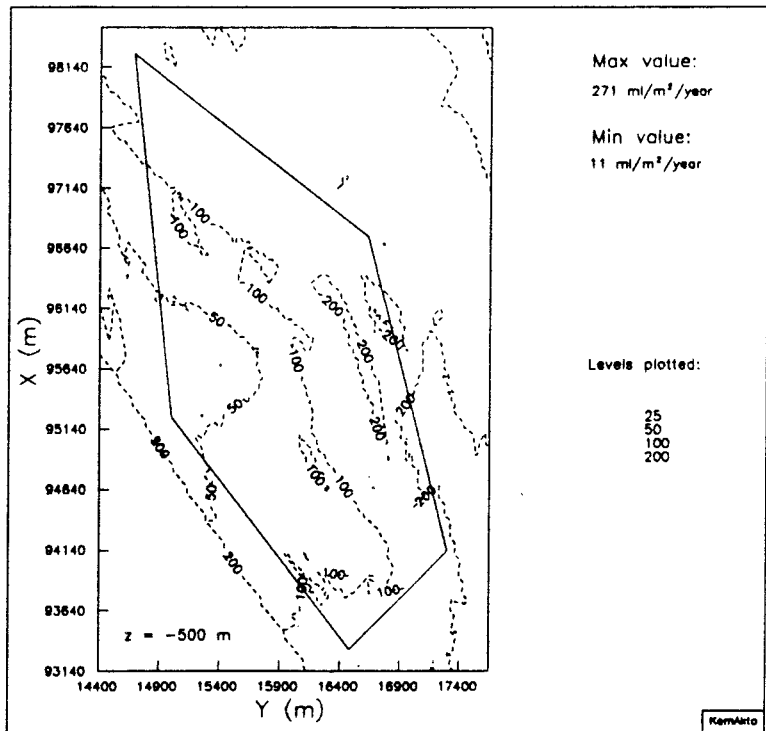


Figure A48 Flux distribution at z=-500 m; Case 3DS2.

APPENDIX B

The figures presented in this appendix are organised so that the different cases considered on the local scale are presented consecutively. The evaluation figures start with the pressure distribution in horizontal cuts, pressure distribution in vertical cuts, particle tracking, and end with the flux distribution. The results from the different cases appear in the following order: Case 3DLSR, Case 3DLSB, Case 3DLS1, Case 3DL1, and Case 3DL2. Note, that the evaluation for Case 3DLSR was reduced compared to the other cases, since this was regarded as a reference-case.

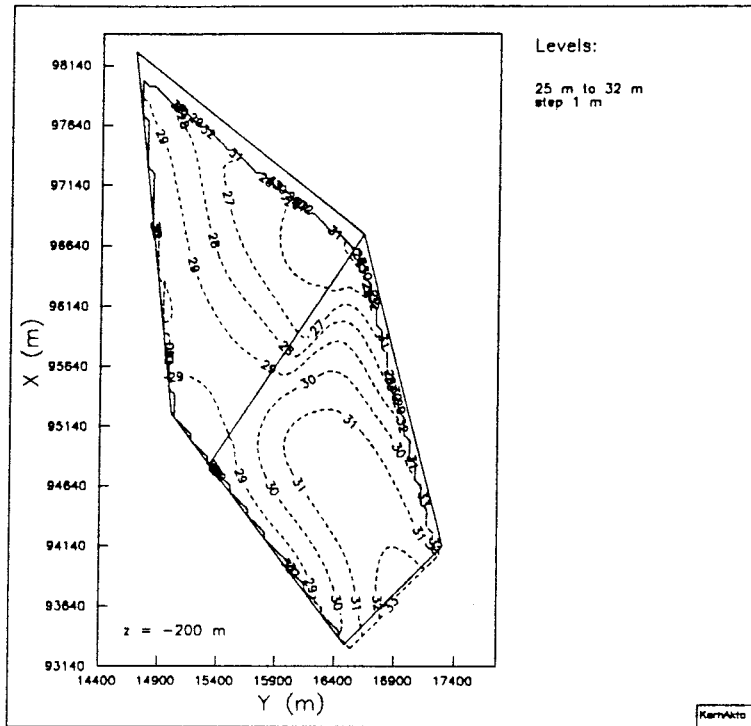


Figure B1 Pressure distribution at $z=-200$ m; Case 3DLSR.

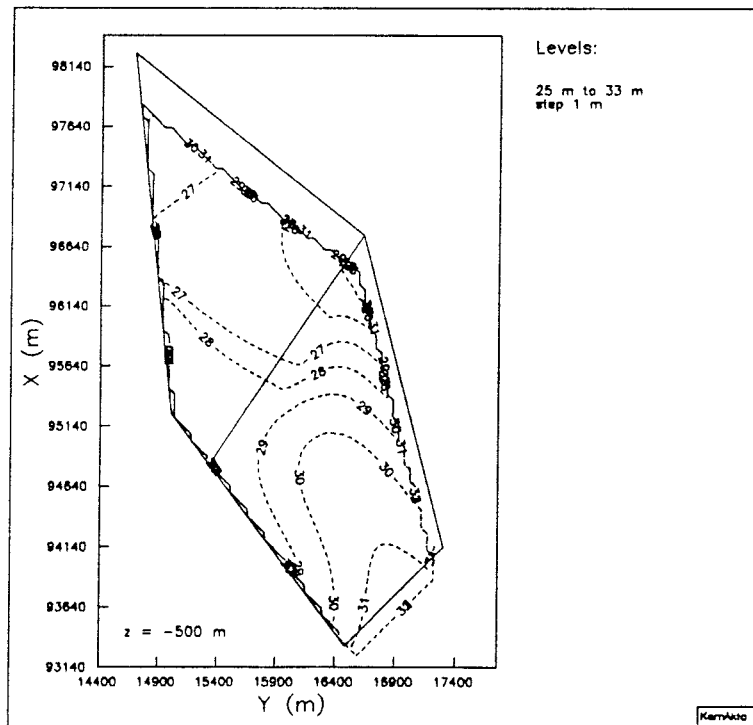


Figure B2 Pressure distribution at $z=-500$ m; Case 3DLSR.

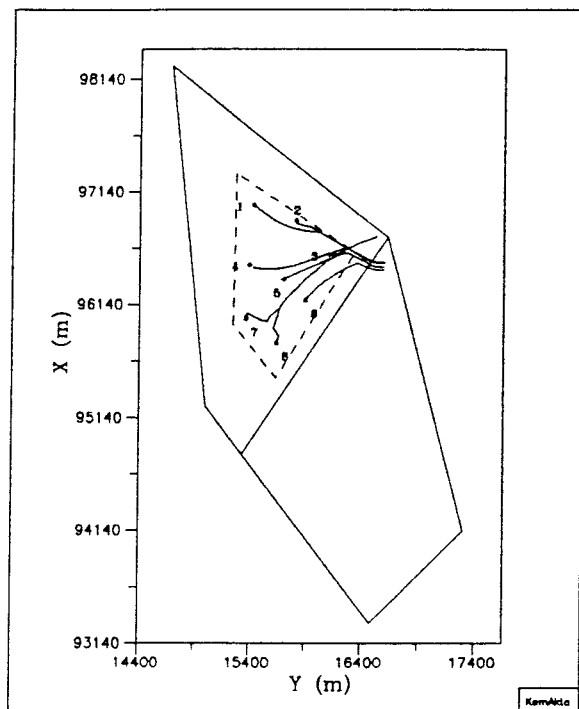


Figure B3 Horizontal projection of pathlines; Case 3DLSR.

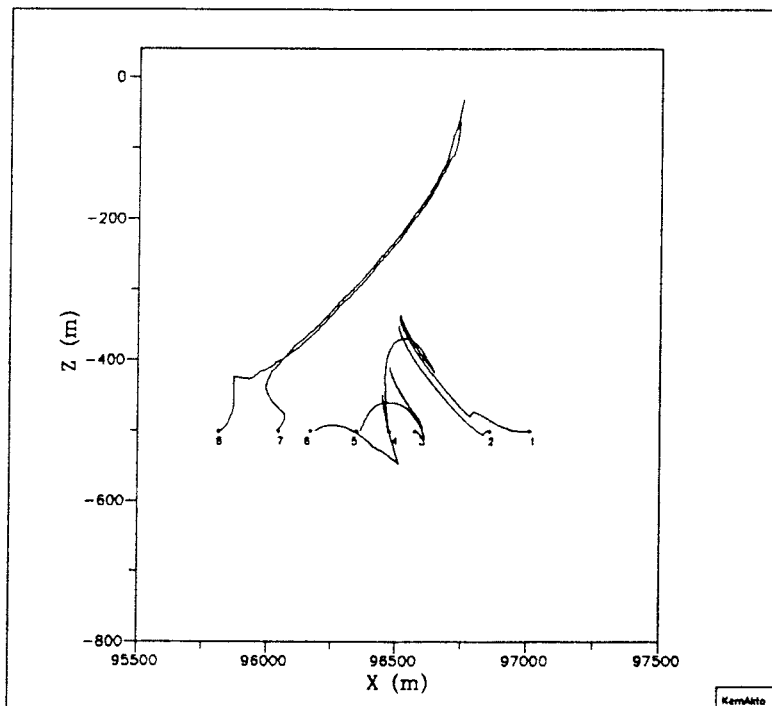


Figure B4 Vertical projection (xz-plane) of pathlines; Case 3DLSR.

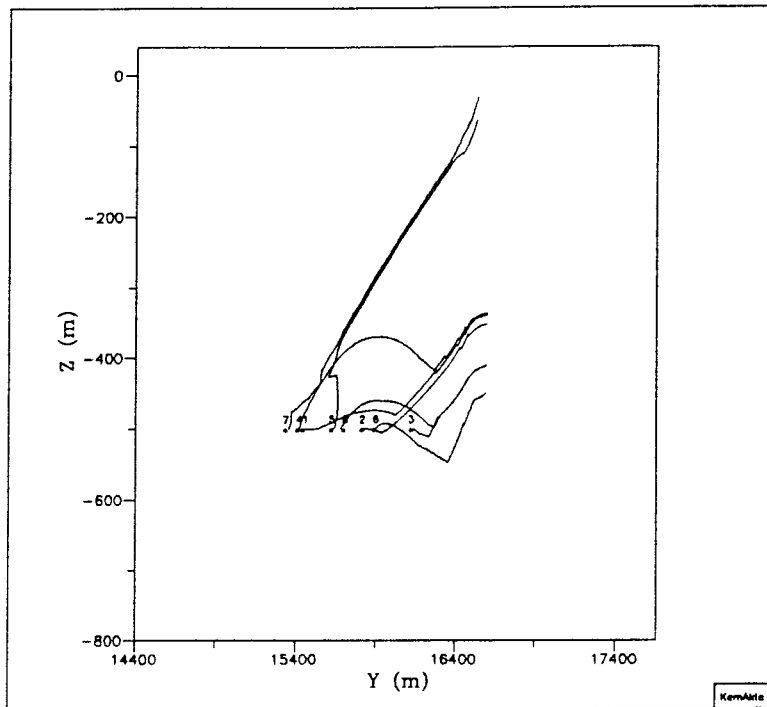


Figure B5 Vertical projection (yz-plane) of pathlines; Case 3DLSR.

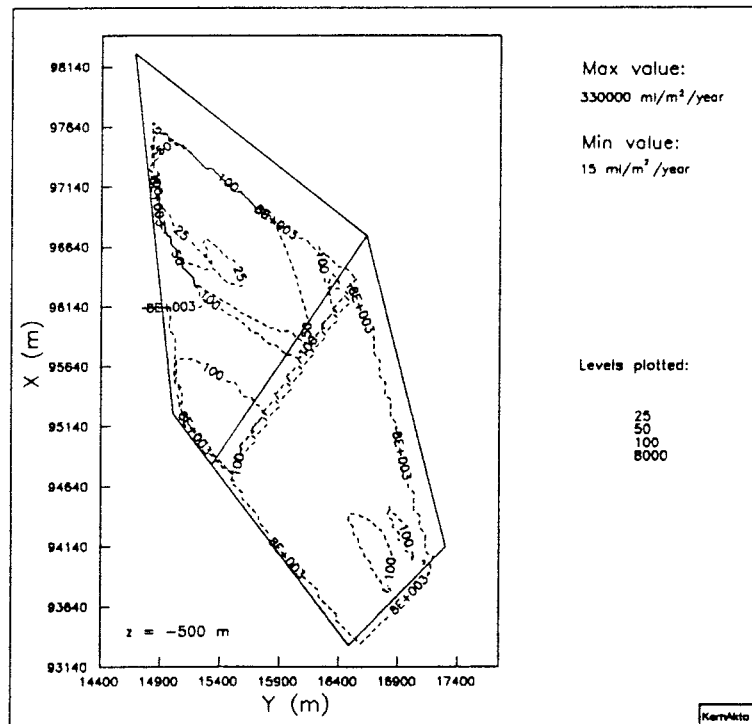


Figure B6 Flux distribution at z=-500 m; Case 3DLSR.

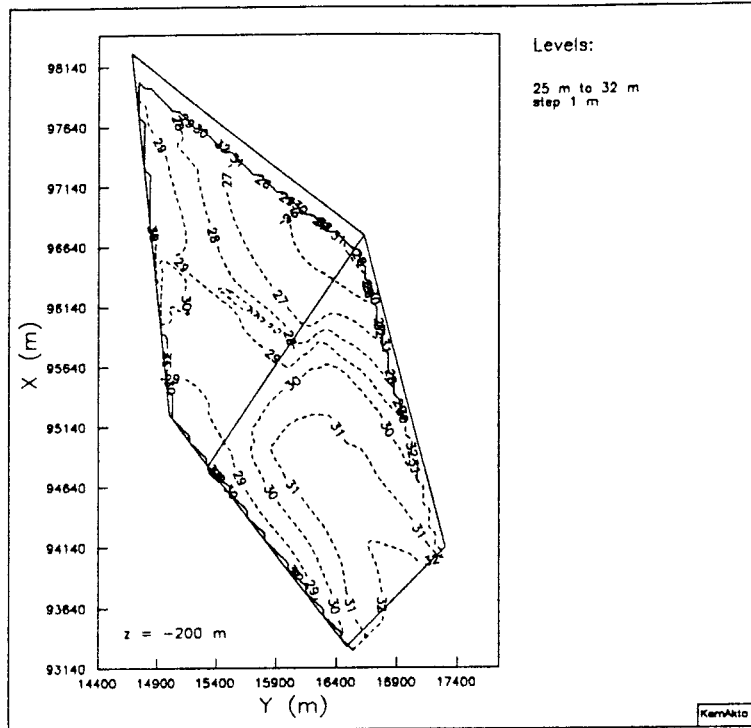


Figure B7 Pressure distribution at $z=-200$ m; Case 3DLSB.

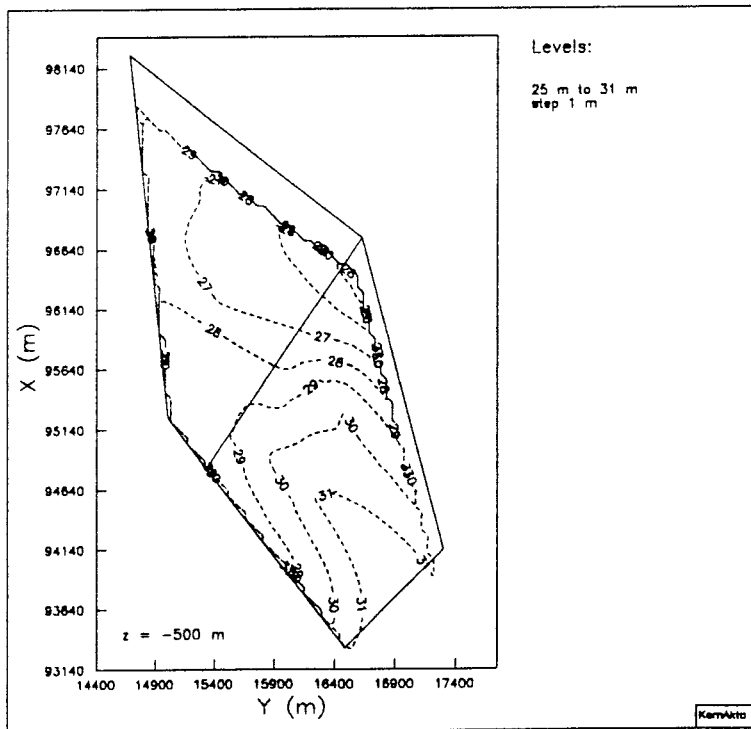


Figure B8 Pressure distribution at $z=-500$ m; Case 3DLSB.

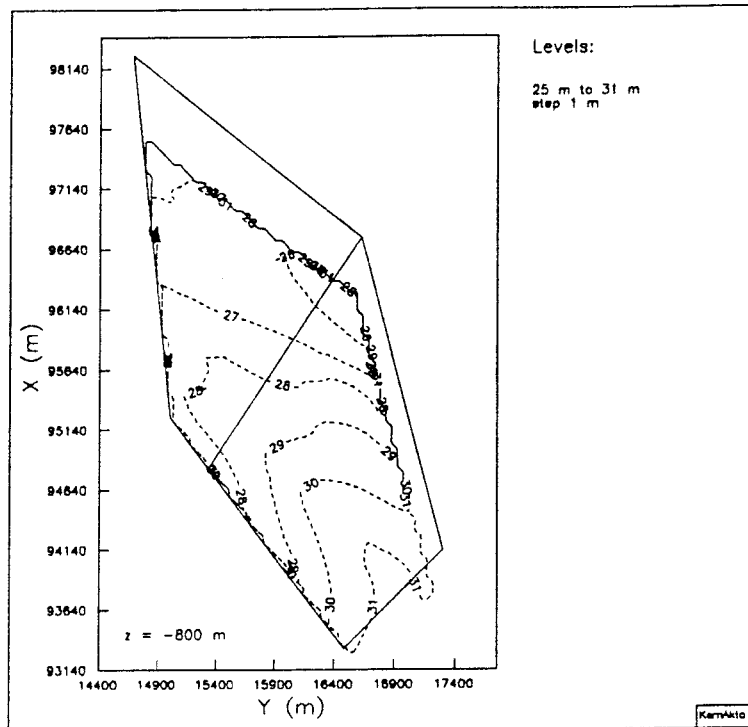


Figure B9 Pressure distribution at $z = -800$ m; Case 3DLSB.

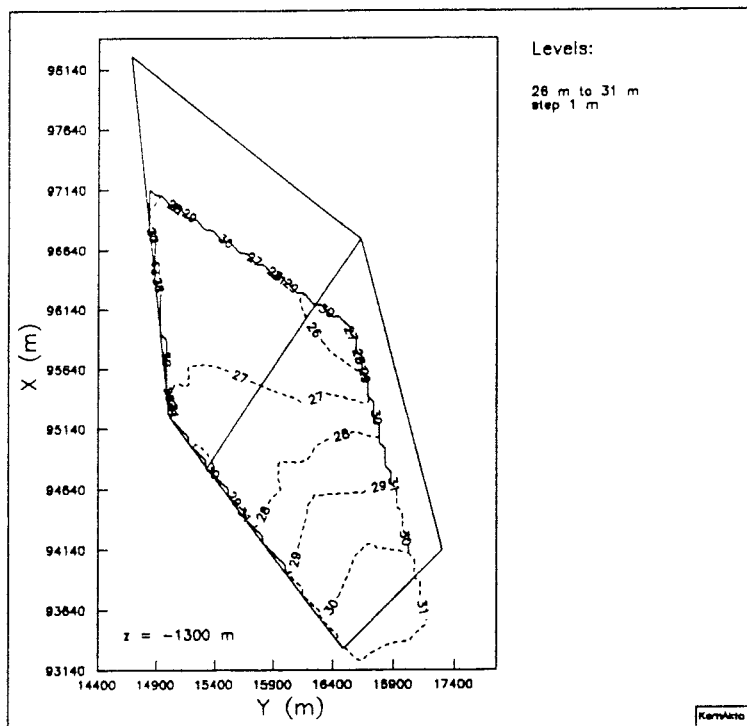


Figure B10 Pressure distribution at $z = -1300$ m; Case 3DLSB.

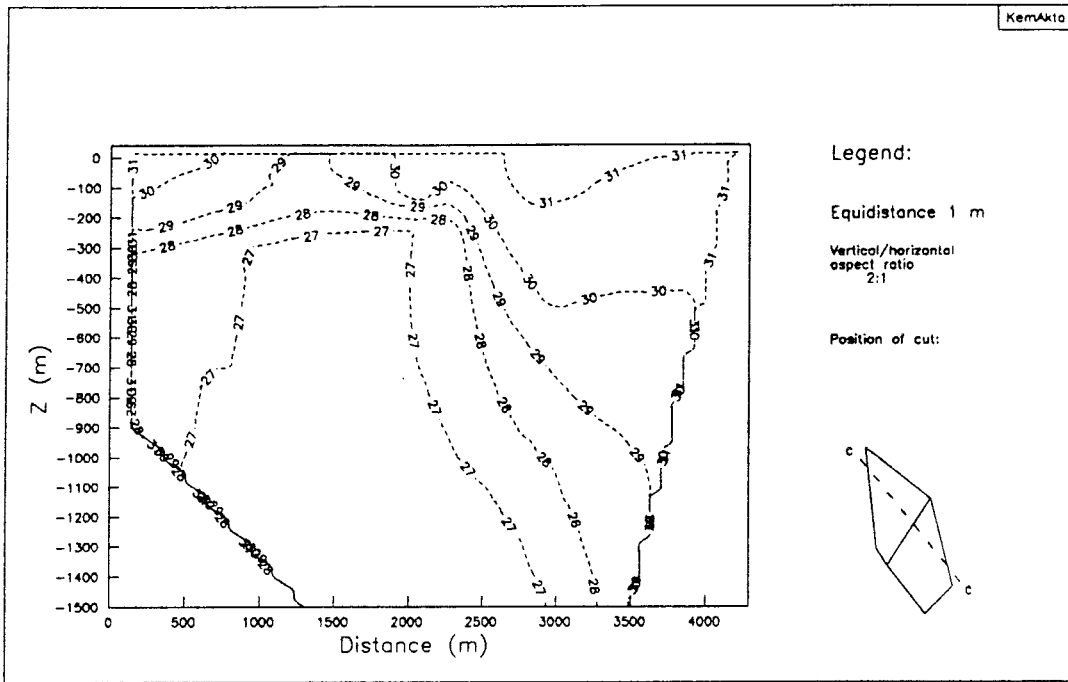


Figure B11 Pressure distribution in vertical cut 1; Case 3DLSB.

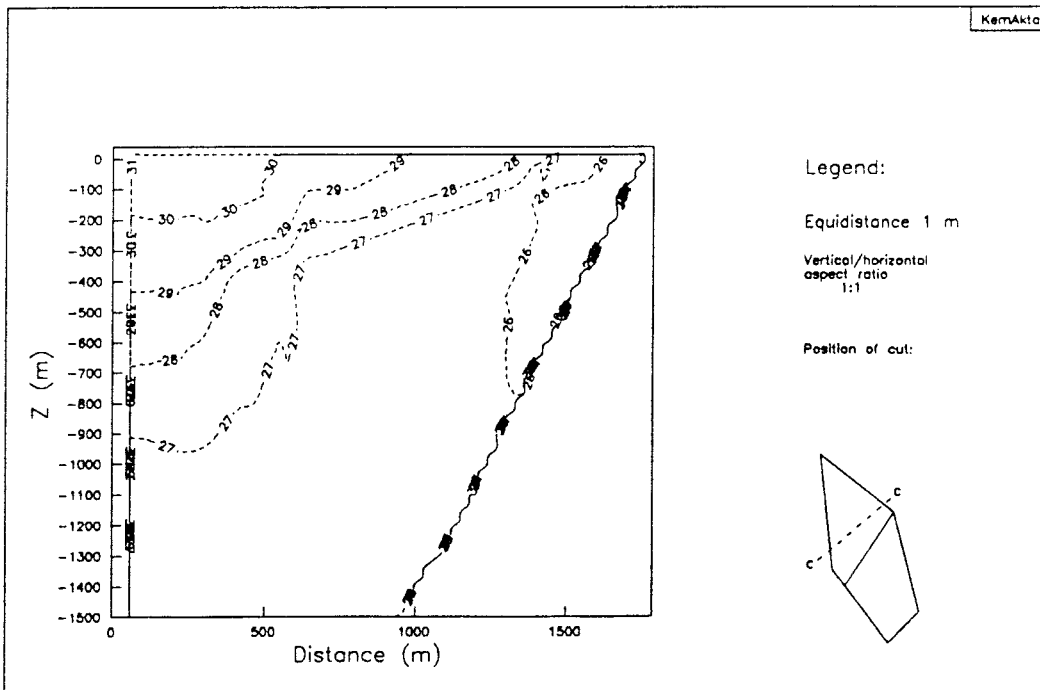


Figure B12 Pressure distribution in vertical cut 2; Case 3DLSB.

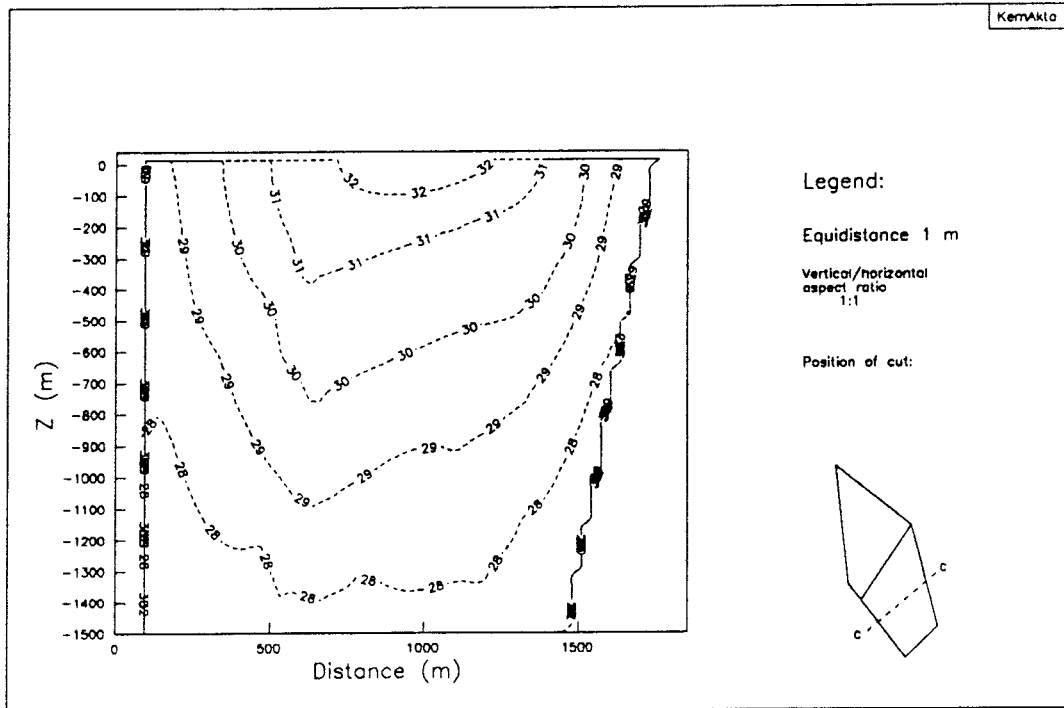


Figure B13 Pressure distribution in vertical cut 3; Case 3DLSB.

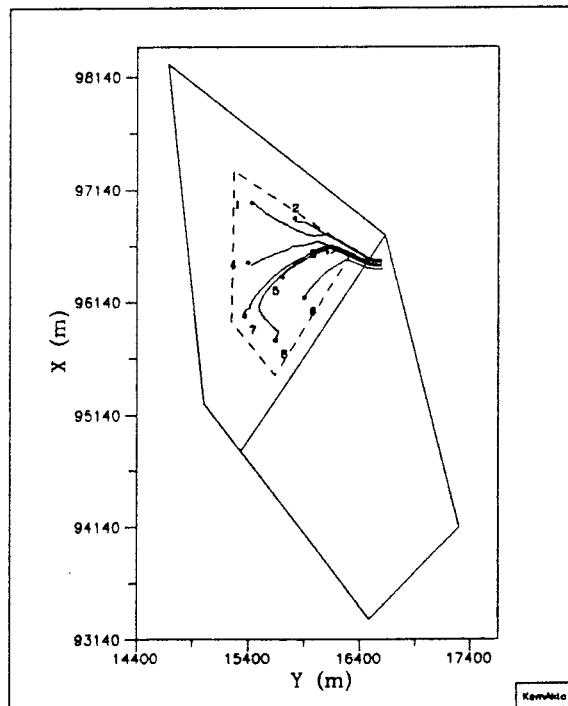


Figure B14 Horizontal projection of pathlines; Case 3DLSB.

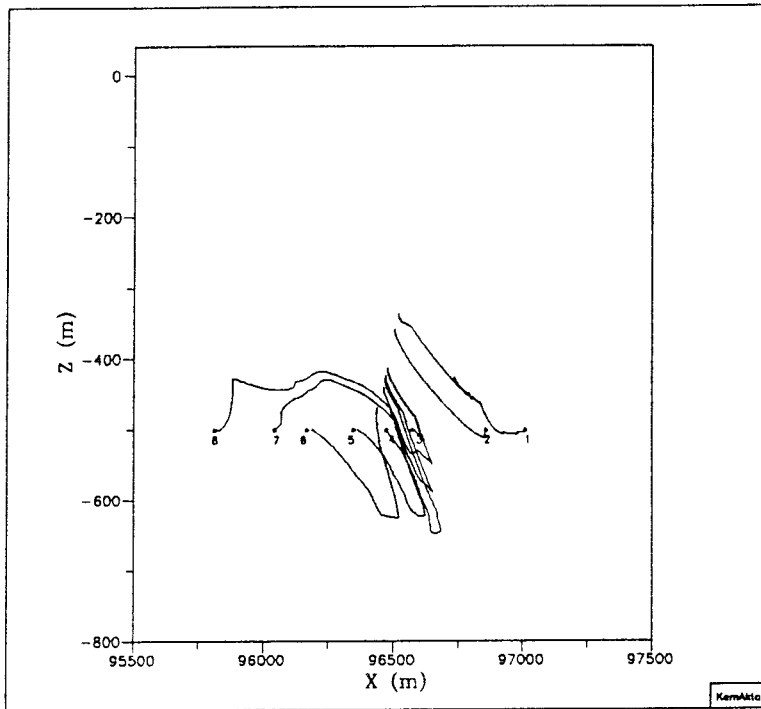


Figure B15 Vertical projection (xz-plane) of pathlines; Case 3DLSB.

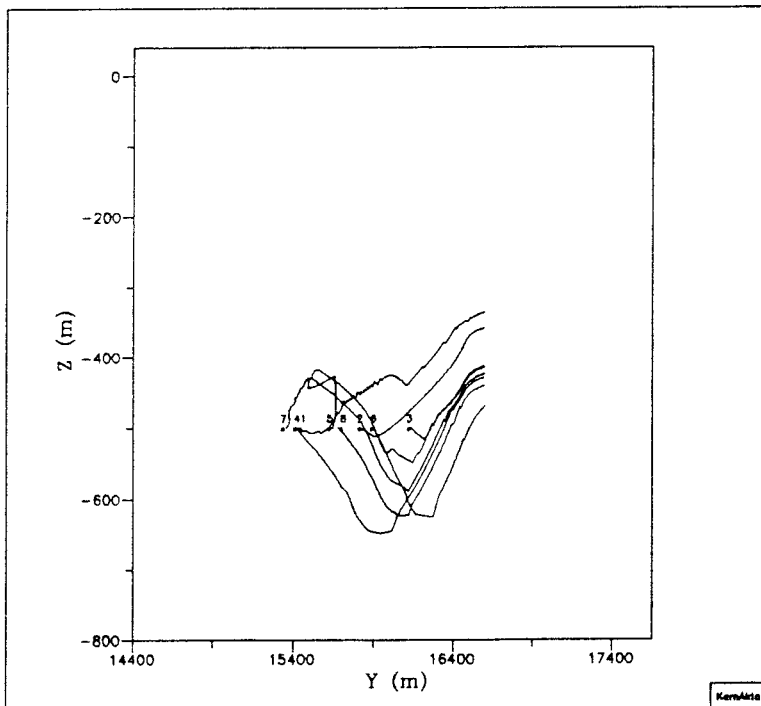


Figure B16 Vertical projection (yz-plane) of pathlines; Case 3DLSB.

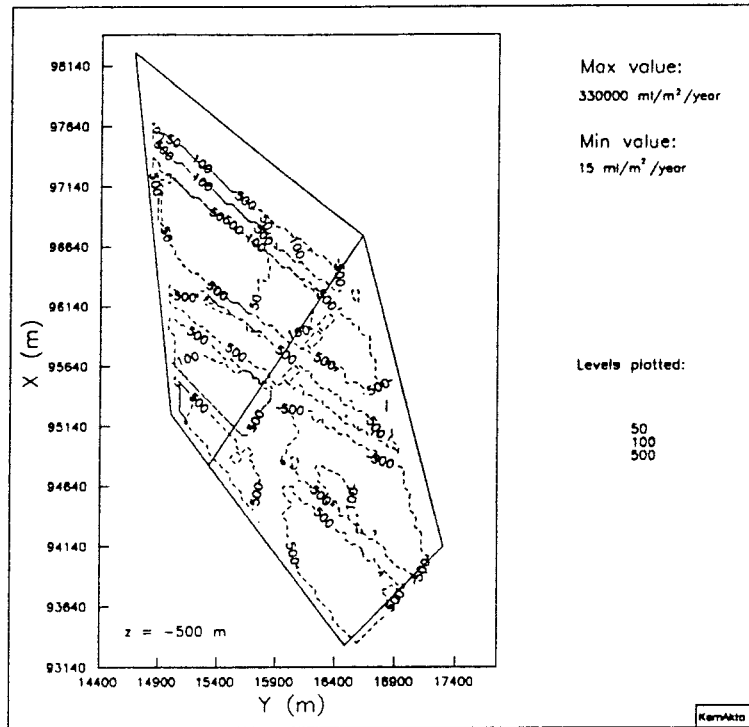


Figure B17 Flux distribution at z=-500 m; Case 3DLSB.

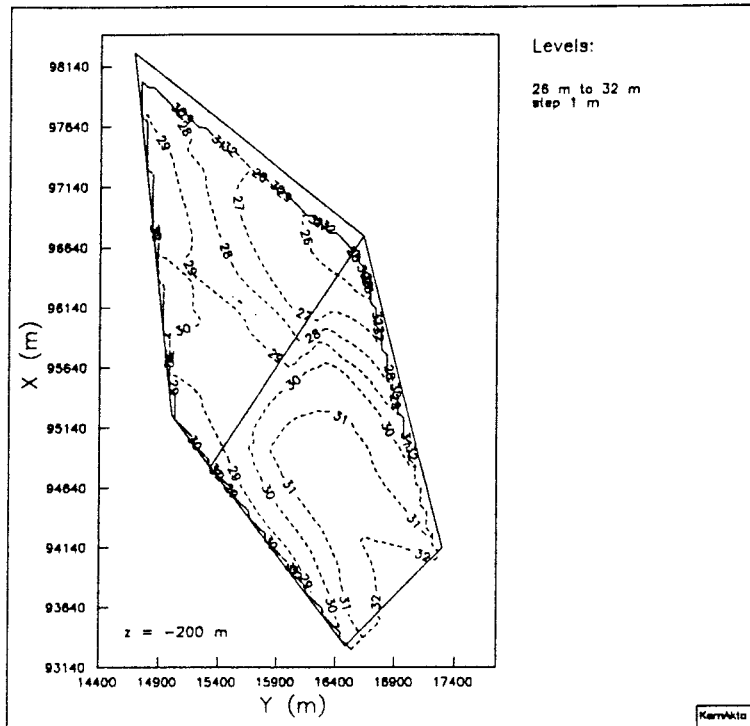


Figure B18 Pressure distribution at $z=-200$ m; Case 3DLS1.

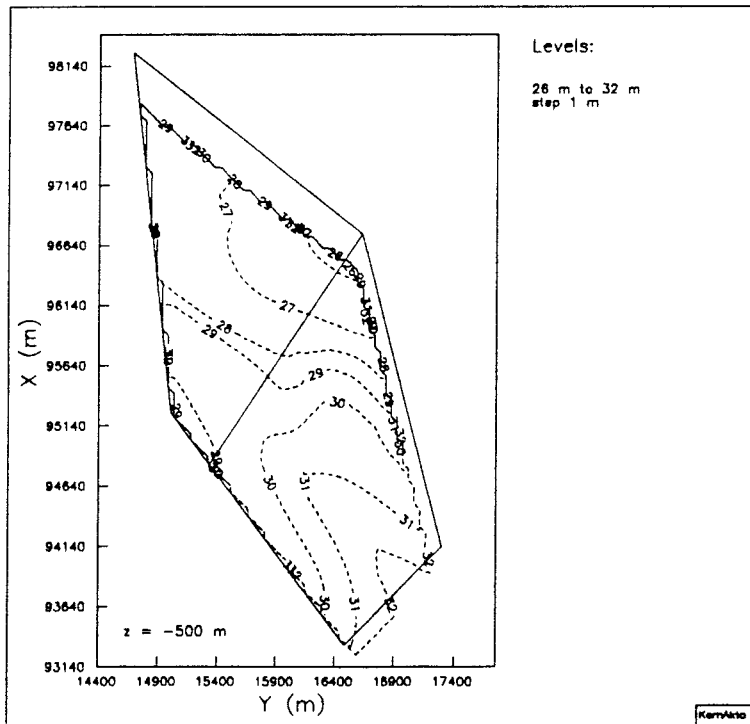


Figure B19 Pressure distribution at $z=-500$ m; Case 3DLS1.

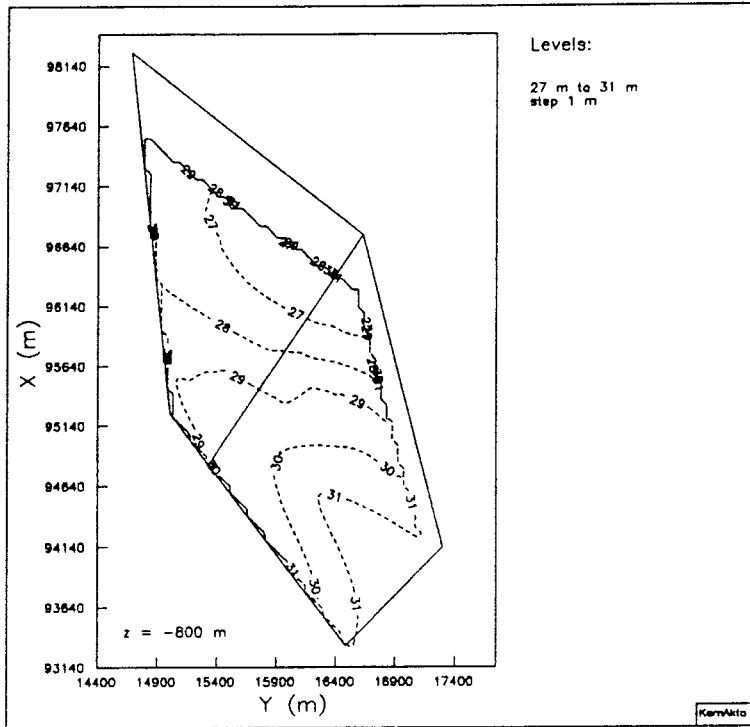


Figure B20 Pressure distribution at $z = -800 \text{ m}$; Case 3DLS1.

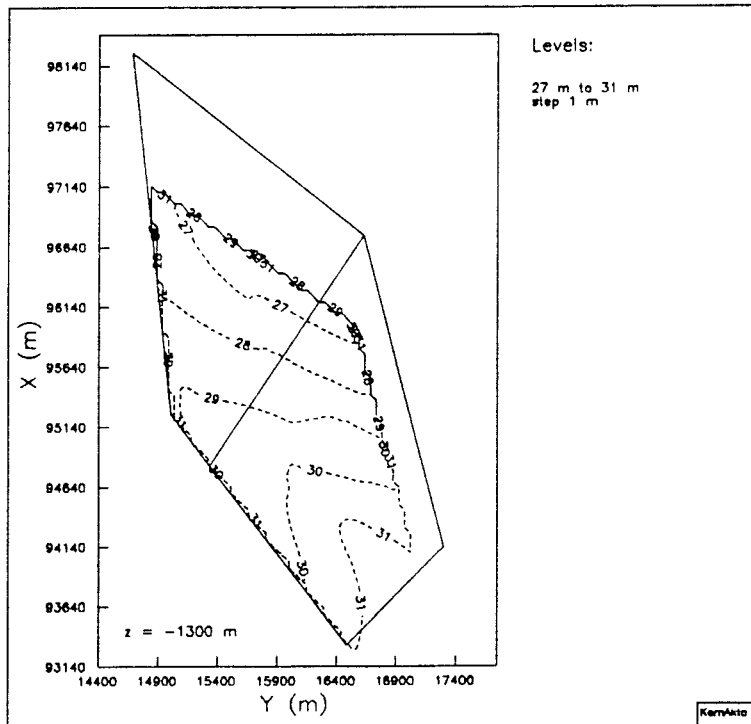


Figure B21 Pressure distribution at $z = -1300 \text{ m}$; Case 3DLS1.

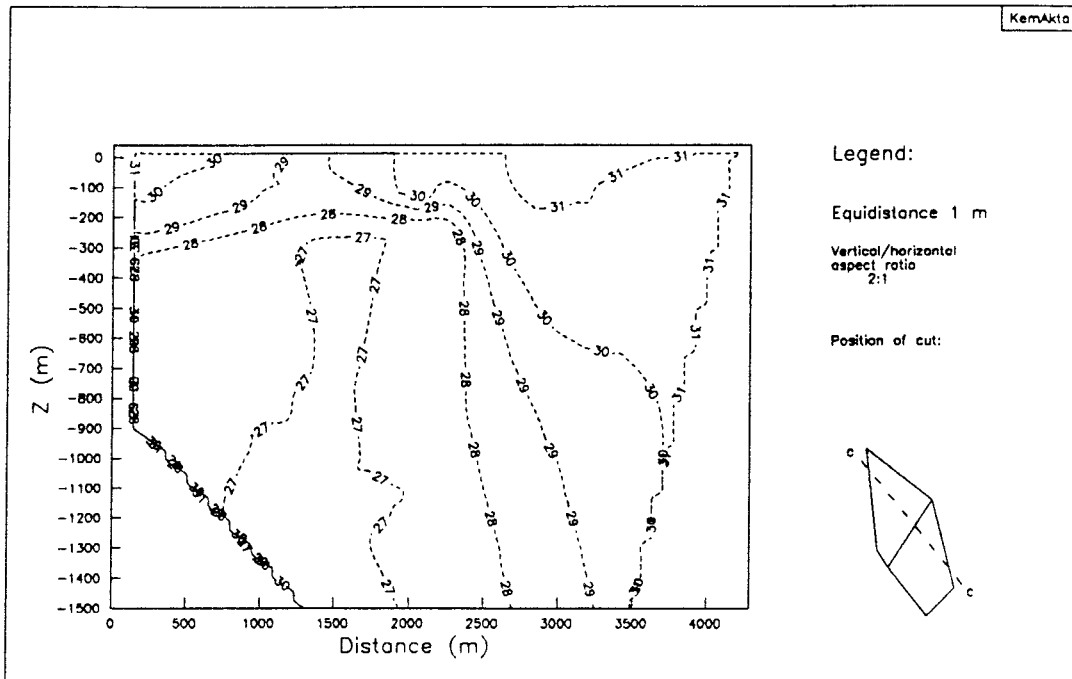


Figure B22 Pressure distribution in vertical cut 1; Case 3DLS1.

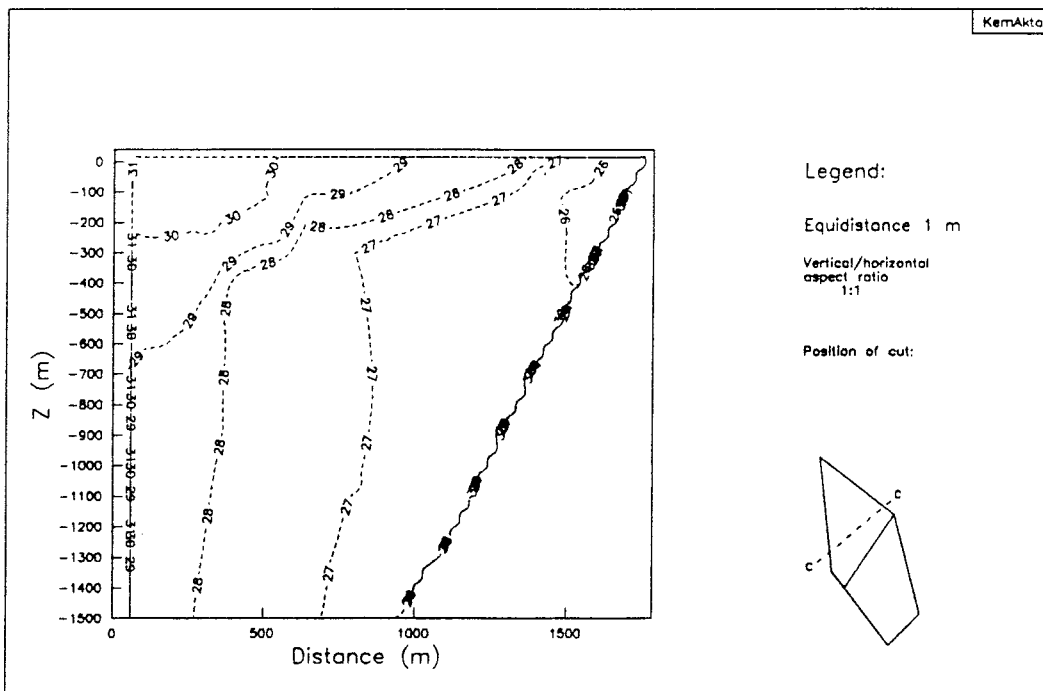


Figure B23 Pressure distribution in vertical cut 2; Case 3DLS1.

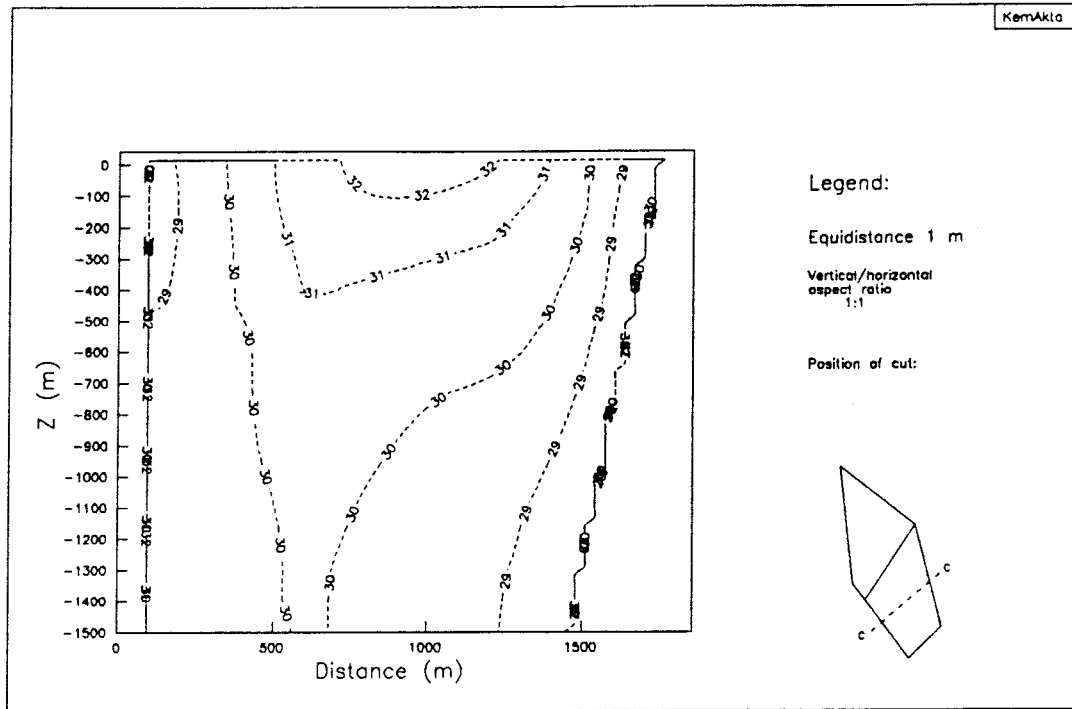


Figure B24 Pressure distribution in vertical cut 3; Case 3DLS1.

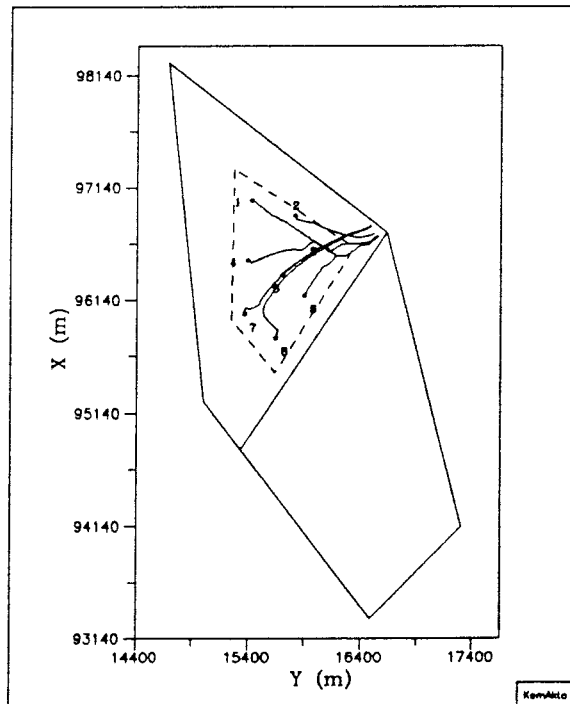


Figure B25 Horizontal projection of pathlines; Case 3DLS1.

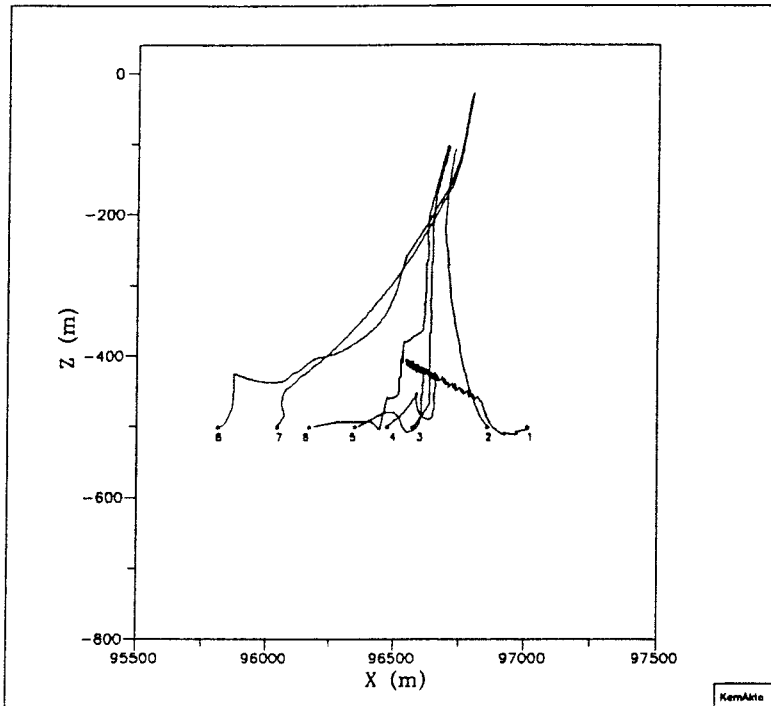


Figure B26 Vertical projection (xz-plane) of pathlines; Case 3DLS1.

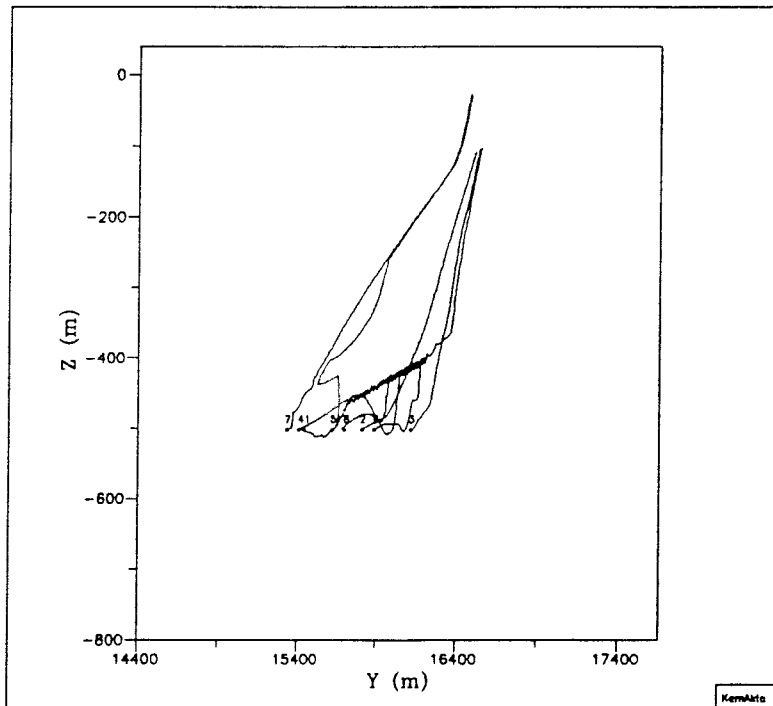


Figure B27 Vertical projection (yz-plane) of pathlines; Case 3DLS1.

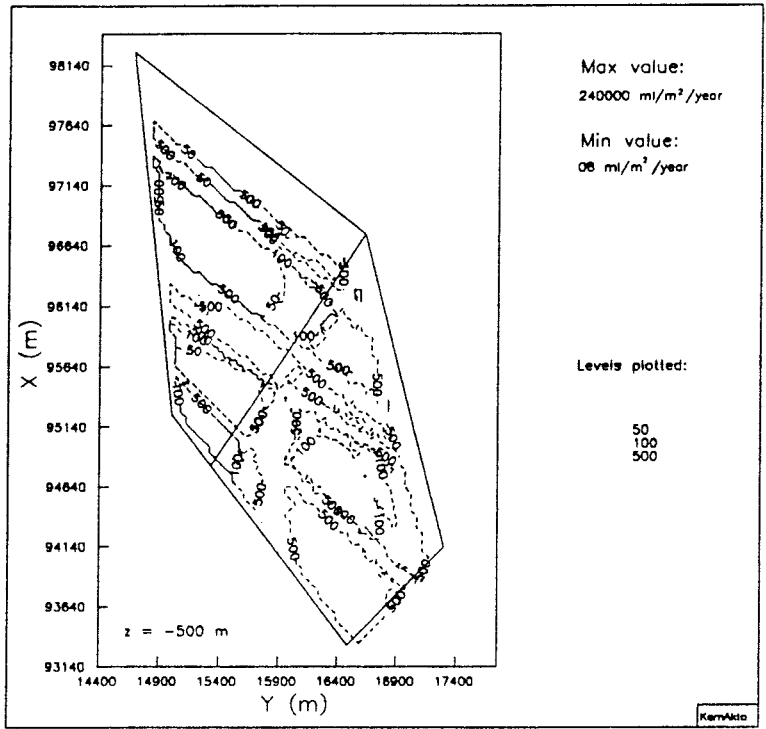


Figure B28

Flux distribution at z=-500 m; Case 3DLS1.

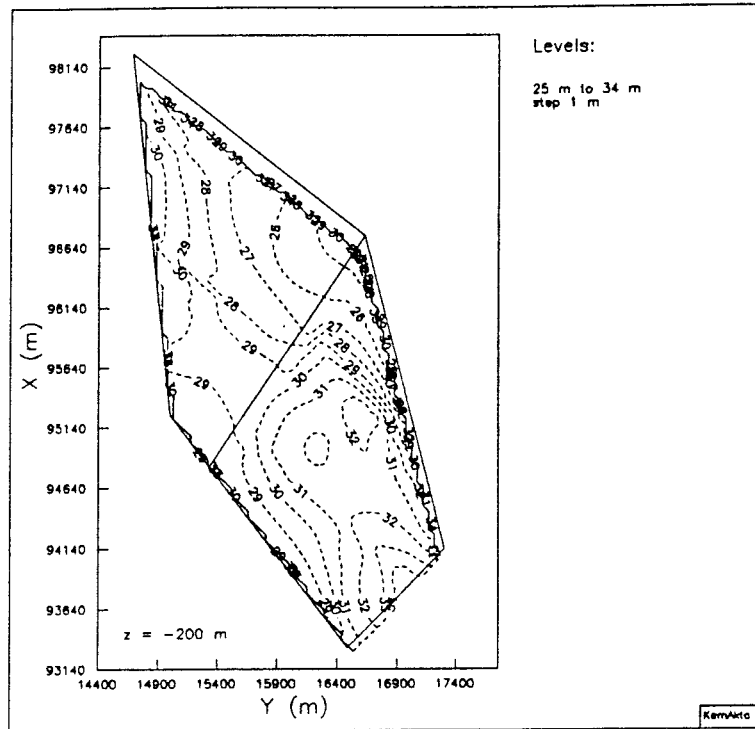


Figure B29 Pressure distribution at $Z=-200$ m; Case 3DL1.

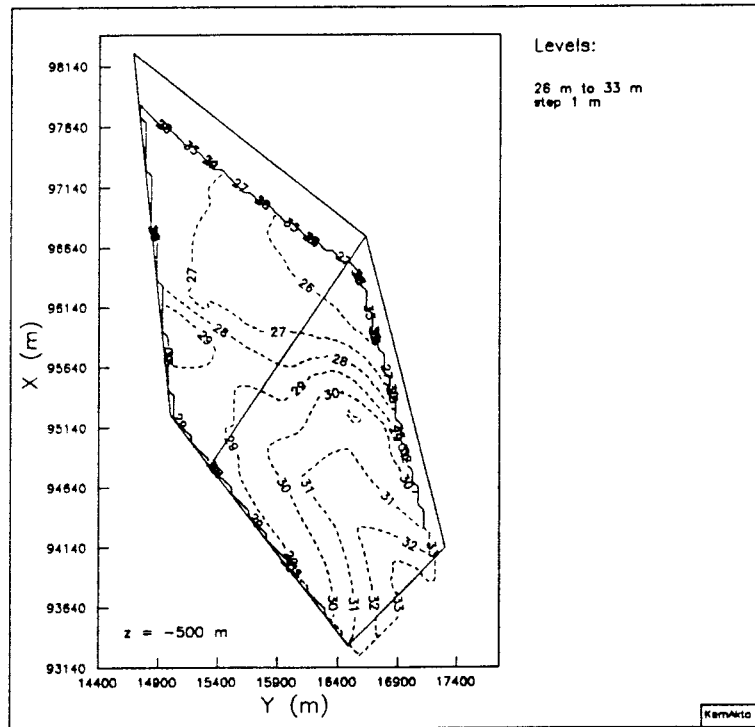


Figure B30 Pressure distribution at $z=-500$ m; Case 3DL1.

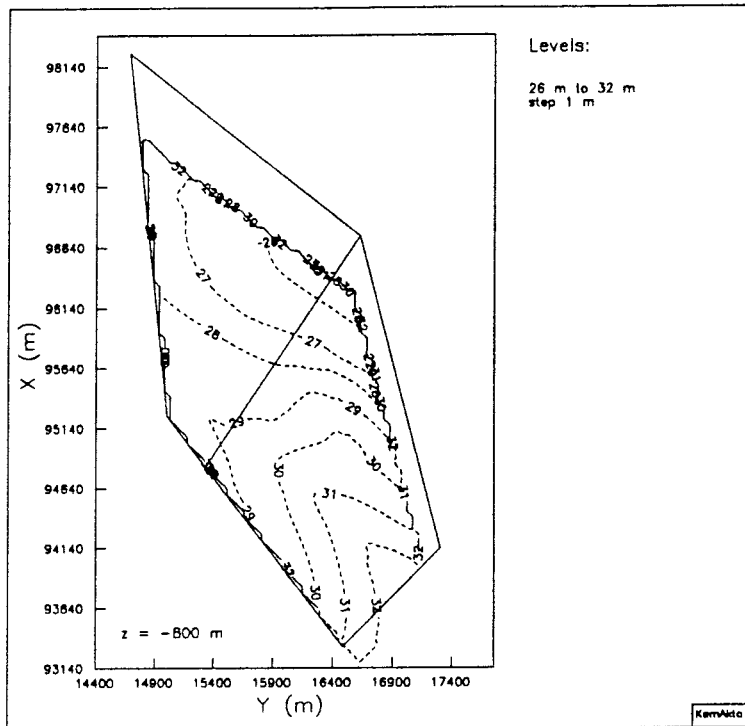


Figure B31 Pressure distribution at $z=-800$ m; Case 3DL1.

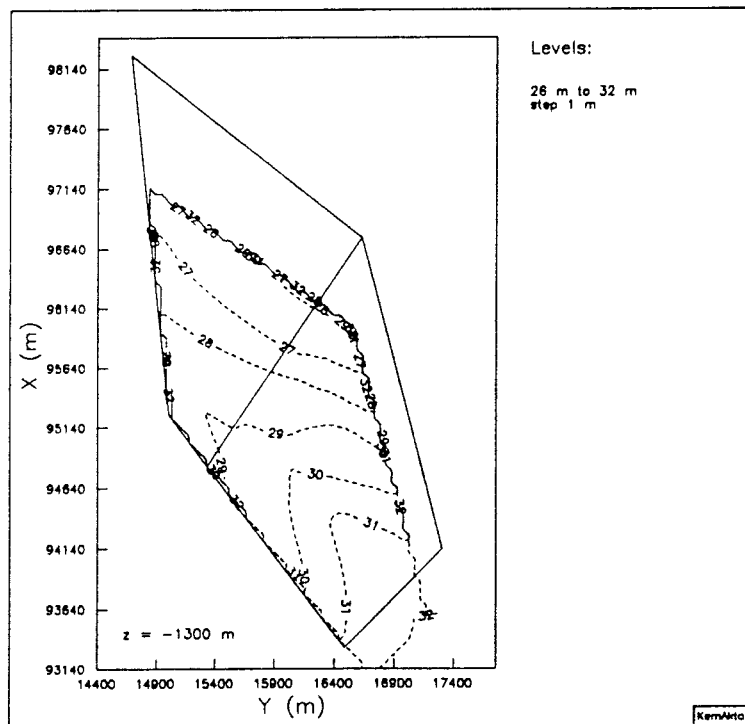


Figure B32 Pressure distribution at $z=-1300$ m; Case 3DL1.

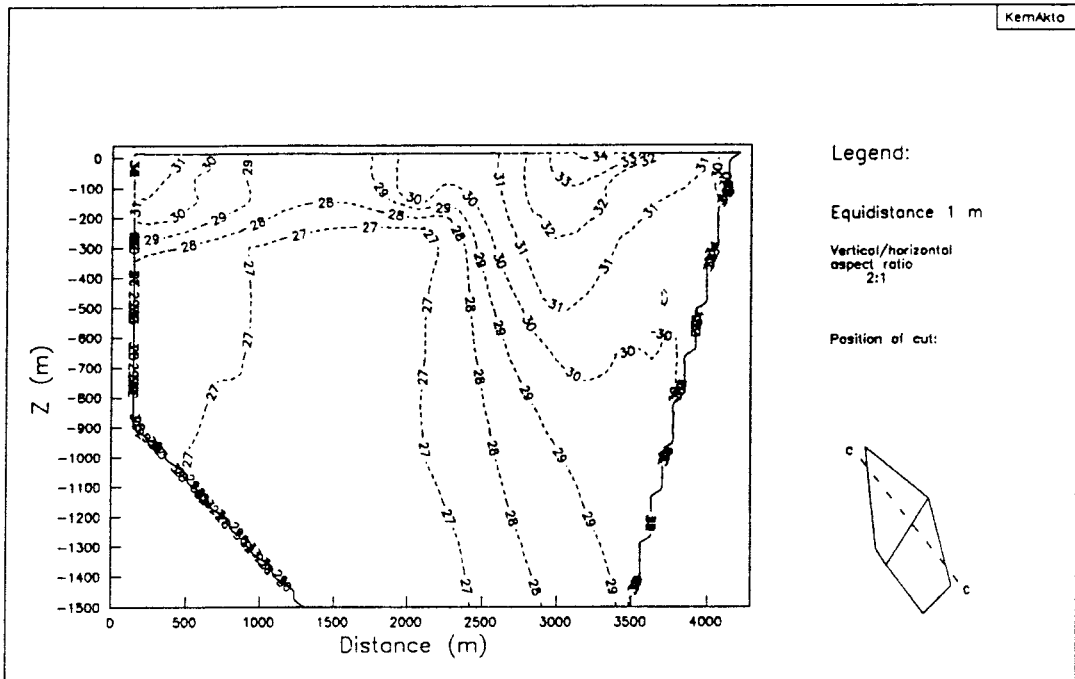


Figure B33 Pressure distribution in vertical cut 1; Case 3DL1.

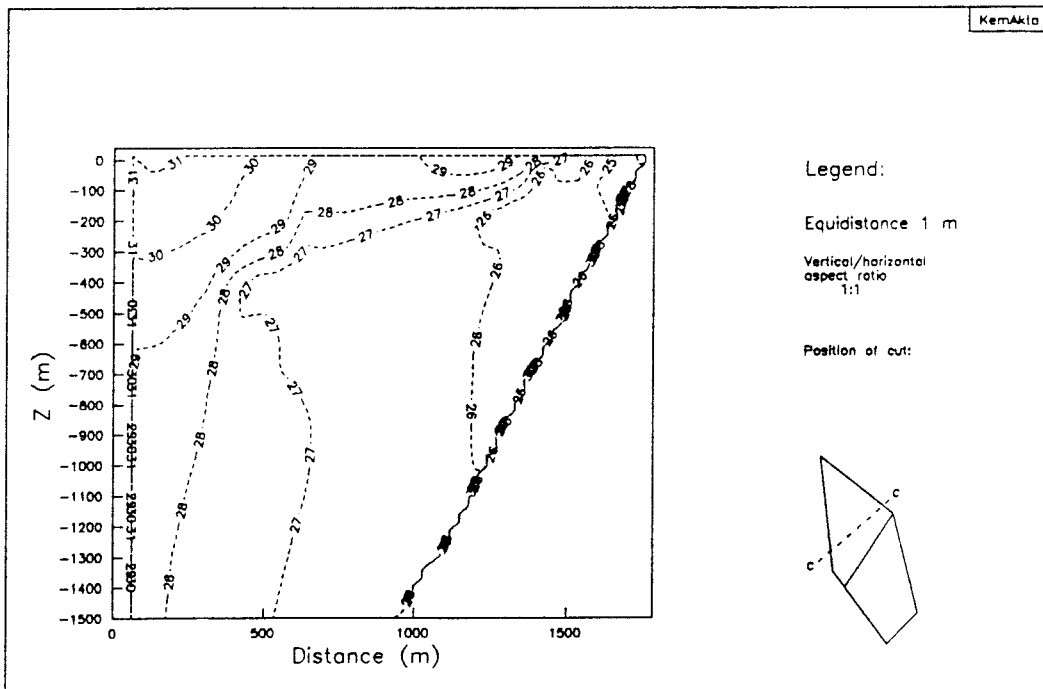


Figure B34 Pressure distribution in vertical cut 2; Case 3DL1.

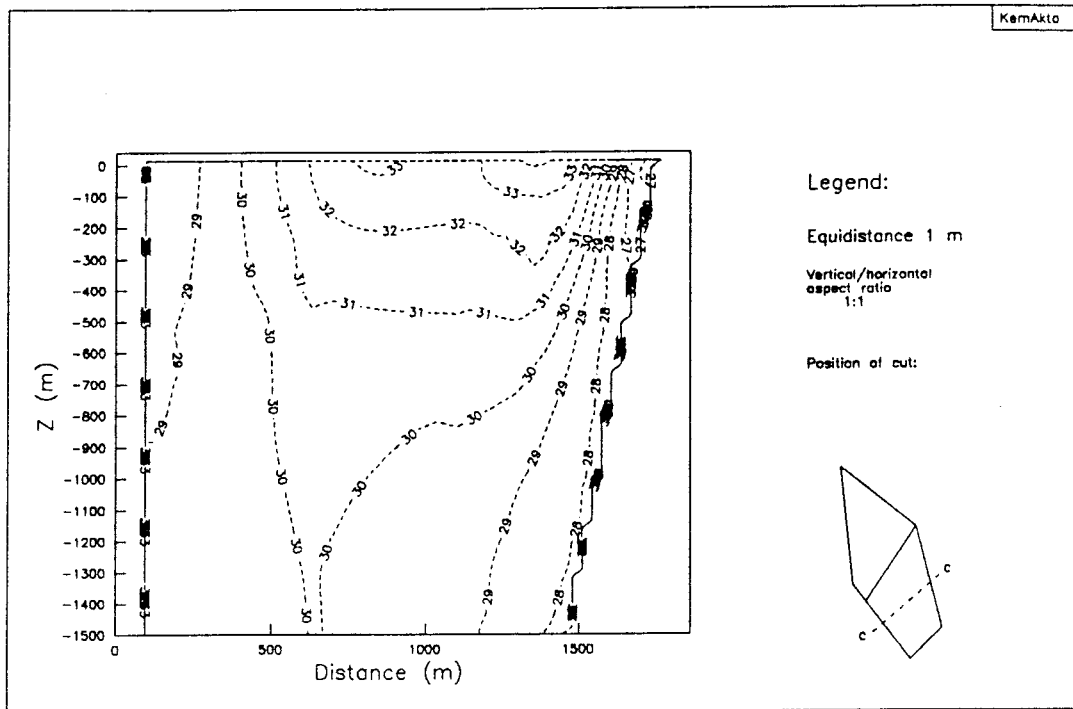


Figure B35 Pressure distribution in vertical cut 3; Case 3DL1.

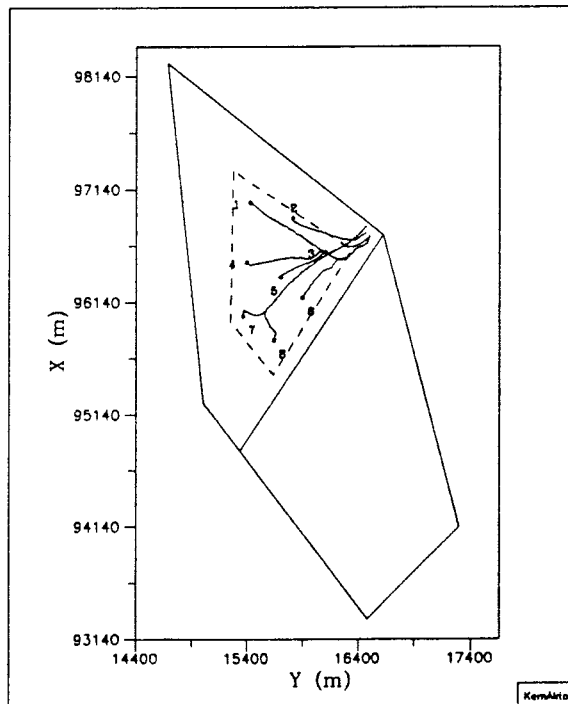


Figure B36 Horizontal projection of pathlines; Case 3DL1.

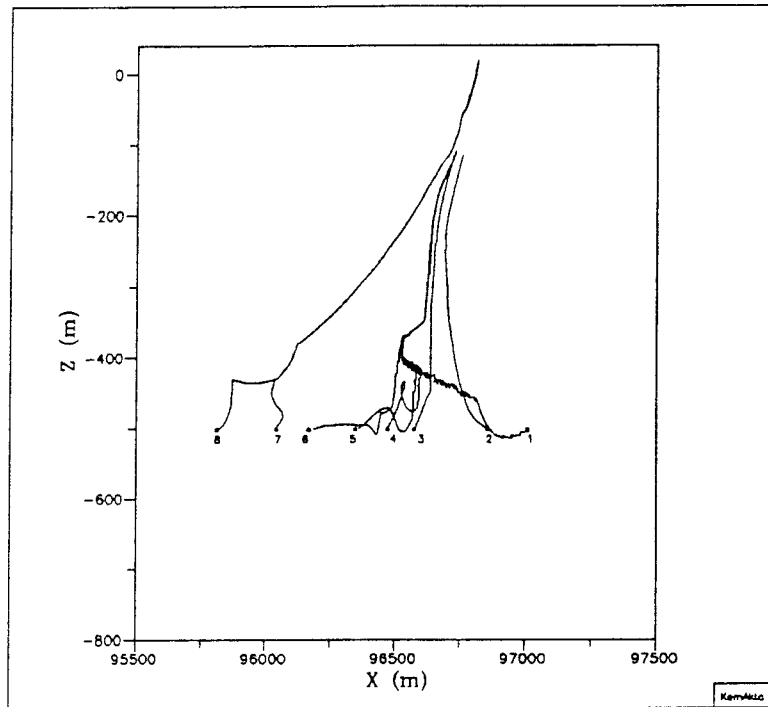


Figure B37 Vertical projection (xz-plane) of pathlines; Case 3DL1.

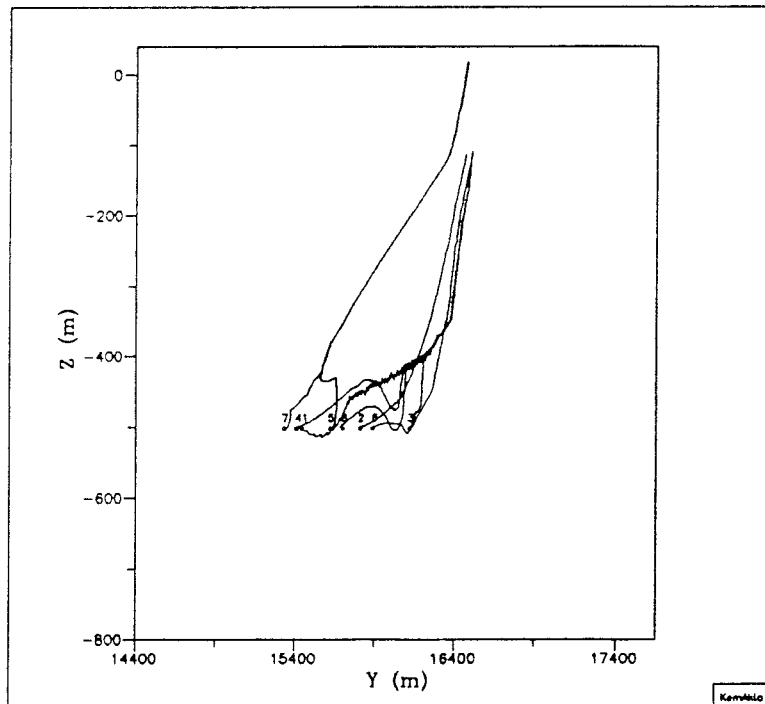


Figure B38 Vertical projection (yz-plane) of pathlines; Case 3DL1.

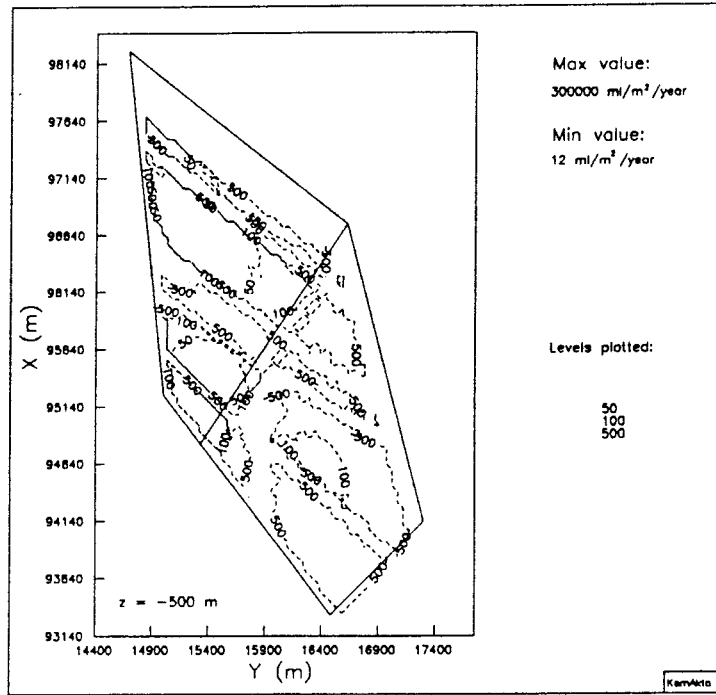


Figure B39 Flux distribution at a level of $z=-500$ m; Case 3DL1.

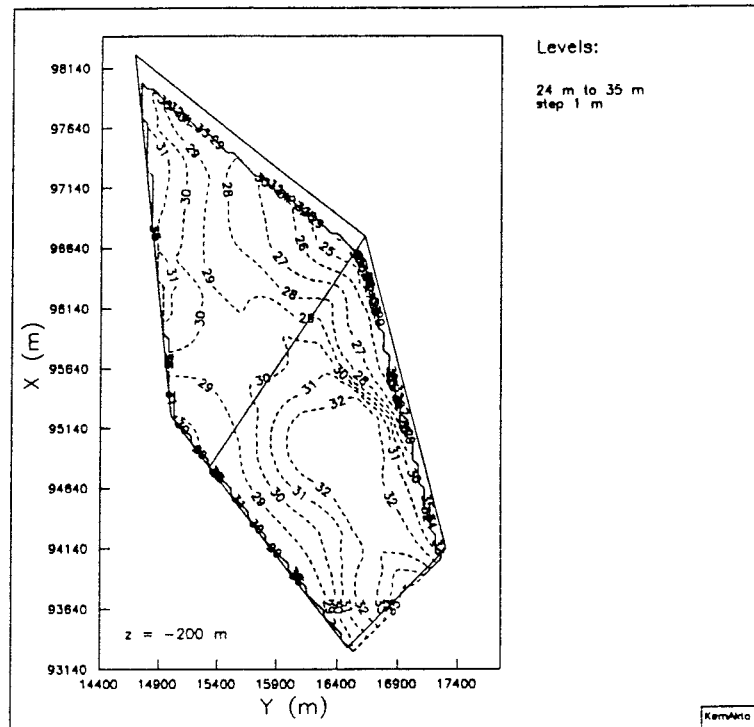


Figure B40 Pressure distribution at $z=-200$ m; Case 3DL2.

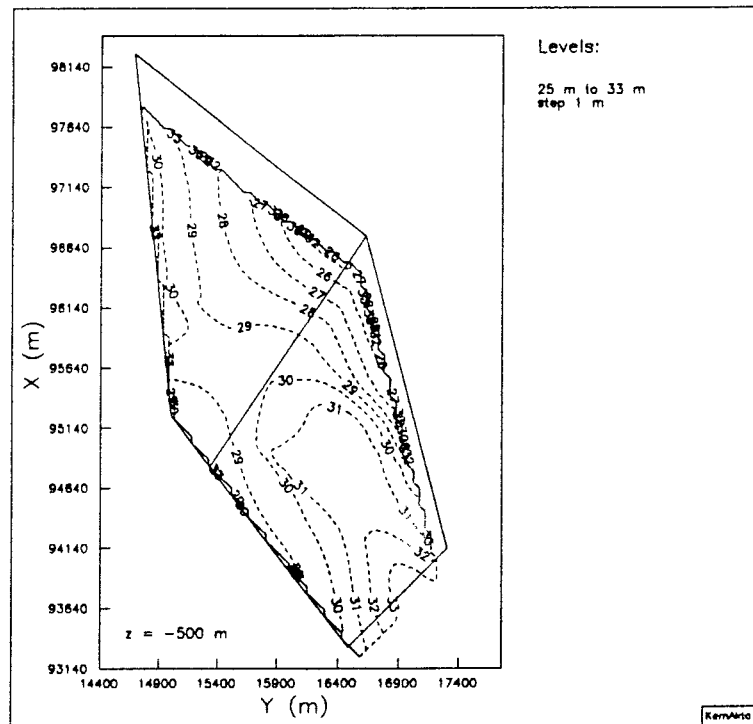


Figure B41 Pressure distribution at $z=-500$ m; Case 3DL2.

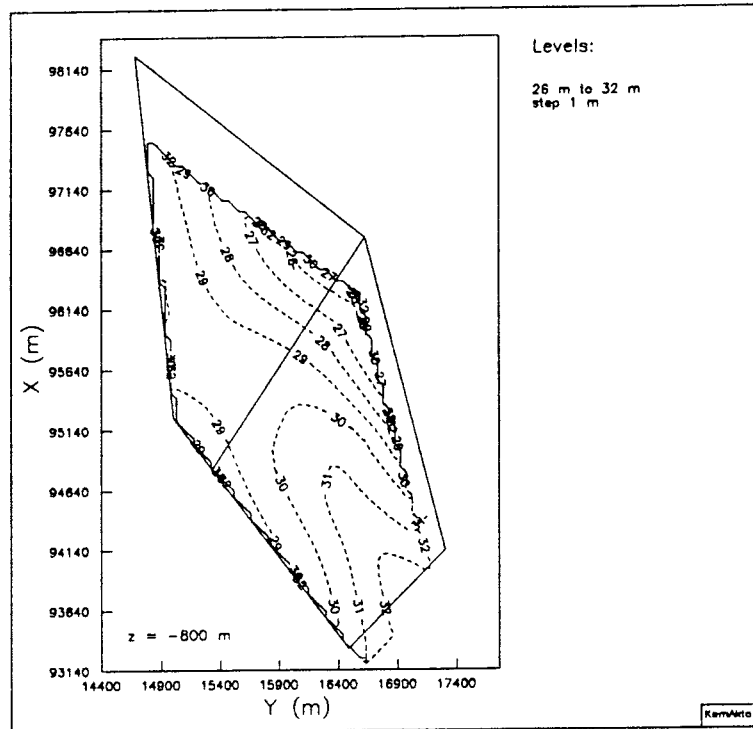


Figure B42 Pressure distribution at $z=-800$ m; Case 3DL2.

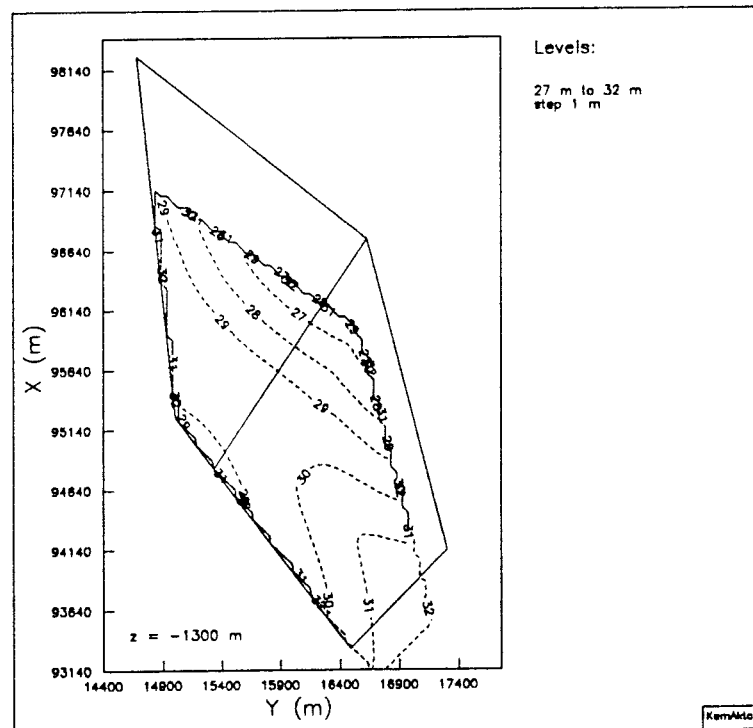


Figure B43 Pressure distribution at $z=-1300$ m; Case 3DL2.

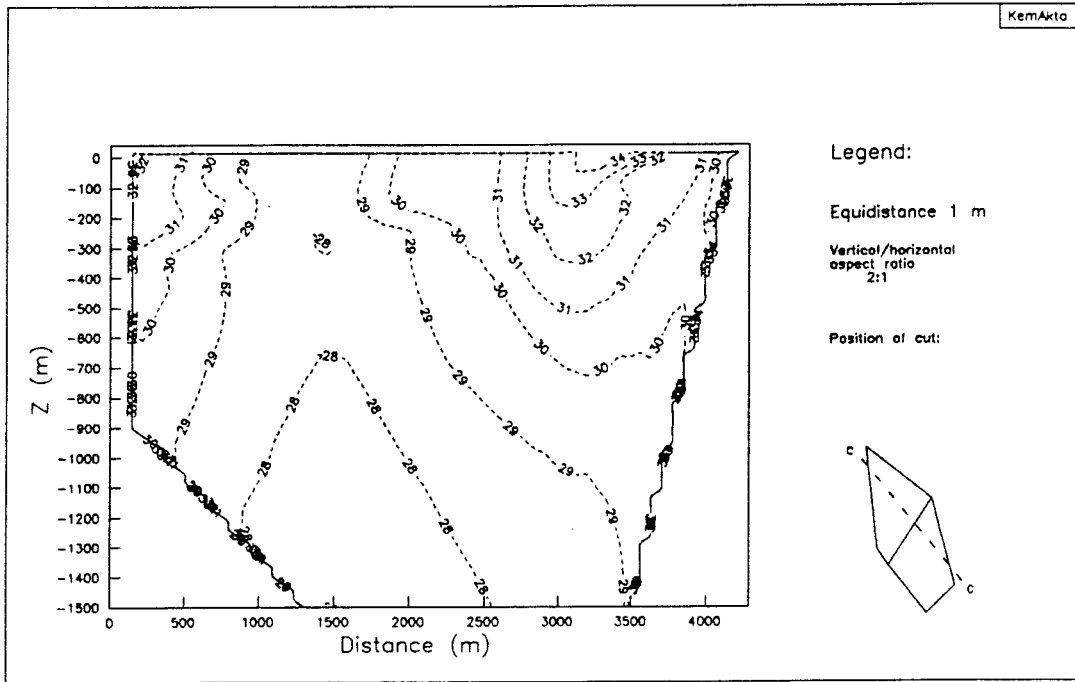


Figure B44 Pressure distribution in vertical cut 1; Case 3DL2.

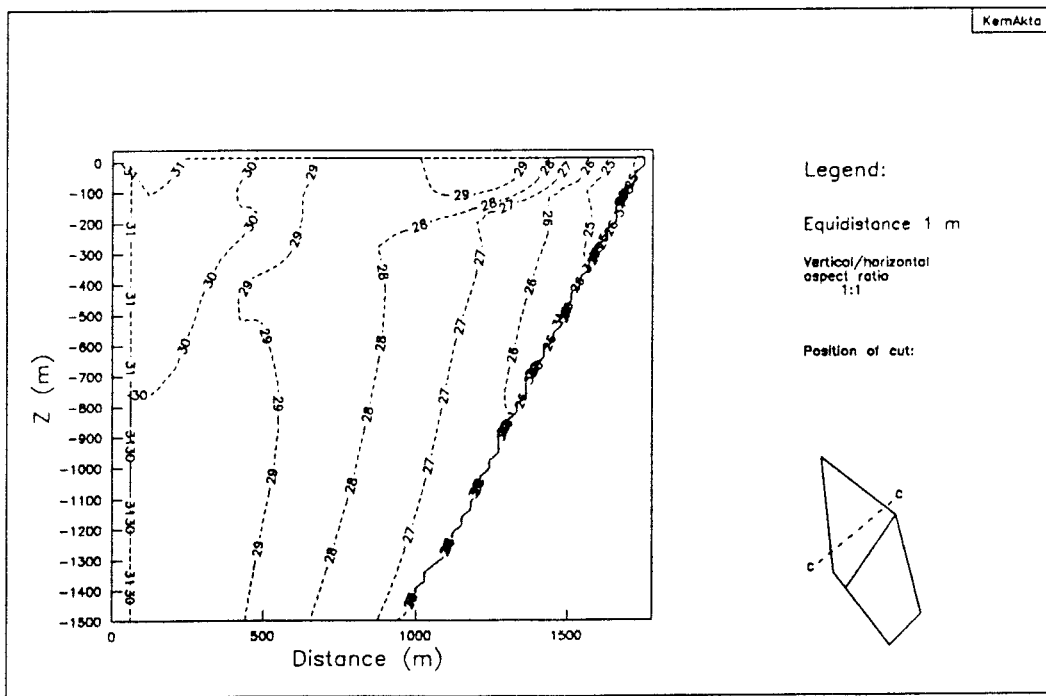


Figure B45 Pressure distribution in vertical cut 2; Case 3DL2.

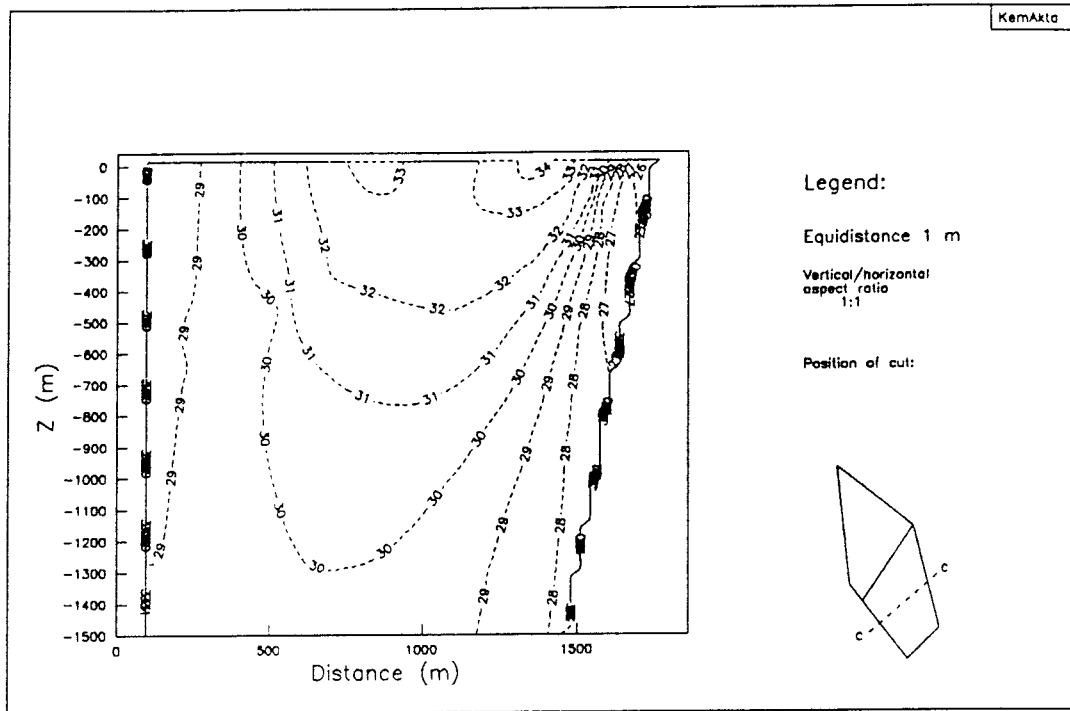


Figure B46 Pressure distribution in vertical cut 3; Case 3DL2.

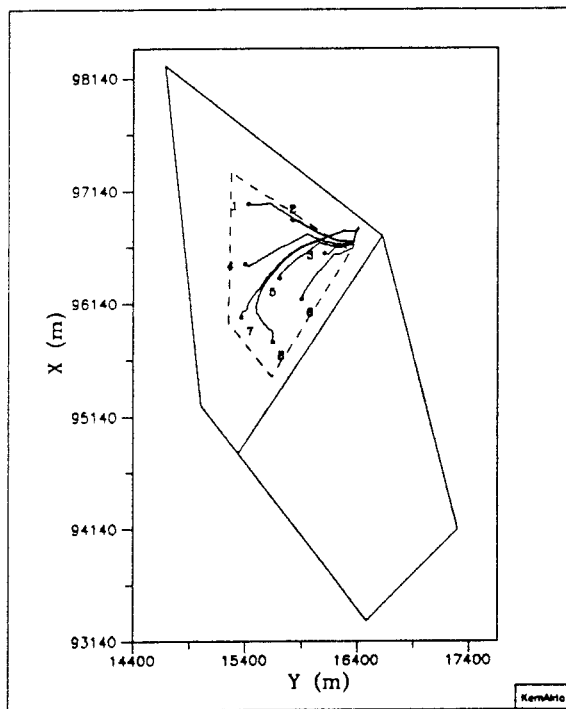


Figure B47 Horizontal projection of pathlines; Case 3DL2.

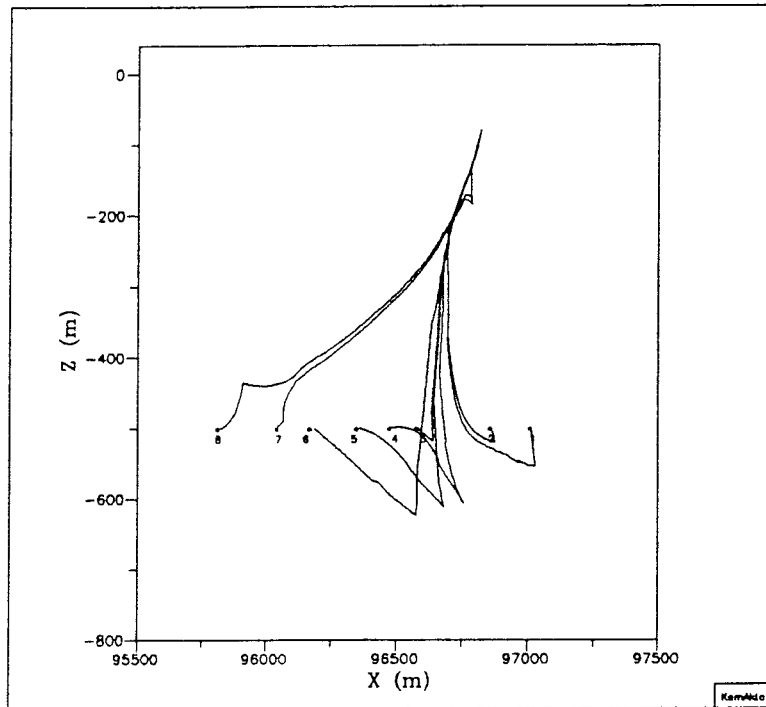


Figure B48 Vertical projection (xz-plane) of pathlines; Case 3DL2.

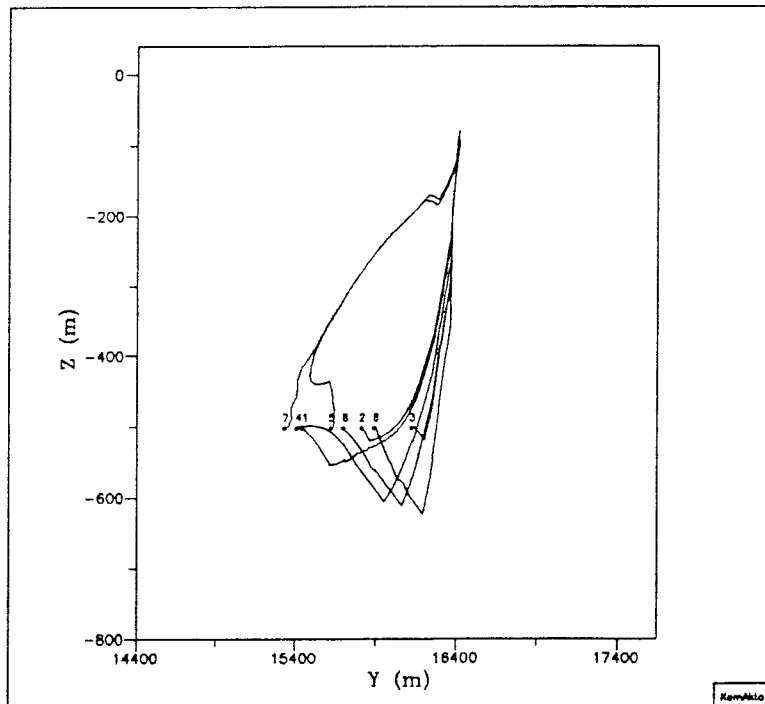


Figure B49 Vertical projection (yz-plane) of pathlines; Case 3DL2.

APPENDIX C

Quality Assurance

Files created and processed during the project

For further information with regard to file-name conventions and the contents on the files referred to in this Appendix, see "HYPAC User's Guide", B. Grundfelt, et al, Kemakta Report AR 89-18, Kemakta Consultants Co., Stockholm, Sweden, 1989.

All files listed on the following pages have been stored on tape on the SKB Sun computer, except those files within parenthesis. The superscripts T1,T2 etc denote the tape number that the files have been stored on. Notations within brackets refer to program names.

Semiregional model

File creation flow on cvx:

All files are stored on /files/home/users/kemanb/0274/fis/

Mesh-generation

The input files to femgen have been stored on 3 inch disks. The files are called PLANx where x runs from A to H, designating the 8 different layers in the model.

neu/fiag.neu^{T2} --> [EMC]

[PFG] <-- neu/fiag.dup^{T2}

pfg/fiag.pfg^{T2}
pfg/fiag.pfc^{T2}

...
...
...

The operation above is repeated for figb, fibc, fich, fihd, fide, fief

fiag.pfg ^{T2} fiag.pfc ^{T2}	[JTM]	jtm/fiab.jtg ^{T2} jtm/fiab.jtc ^{T2}
figb.pfg ^{T2} figb.pfc ^{T2}
...
...
fiae.pfg ^{T2} fiae.pfc ^{T2}	[JTM]	jtm/fiaf.jtg ^{T2} jtm/fiaf.jtc ^{T2}
fief.jtg ^{T2} fief.jtc ^{T2}		

Rest of preprocessing

fiaf.jtg ^{T2} fiaf.jtc ^{T2} fis.ssf ^{T2}	[AMT]	amt/fis.amg ^{T2}
---	-------	---------------------------

amt/fis.amg ^{T2}	[EMC]	
fis.amg ^{T2} fis.jtc ^{T2}	[OPT]	opt/fis.opg ^{T2} opt/fis.opc ^{T2}
fis.opg ^{T2} fis.opc ^{T2}	[BCA]	bca/fis.bcg ^{T2}

Preprocessing finished :
 Mesh : **bca/fis.bcg^{T2}**
 Code : **opt/fis.opc^{T2}**

Base Case and Variations

Note that the following notations have been used for file identification of the various variations made :

Notation in report	File notation		
3DSB	fisB		
3DS1A	fisv1a		
3DS1B	fisv1b		
3DS2	fisv2		
3DS3	fisx		
fis.bcg ^{T2} fis.opc ^{T2}	[PEA]	pea/fisB.peg pea/fisv1a.peg pea/fisv1b.peg pea/fisv2.peg pea/fisx.peg	Base case V1a V1b V2 V3
			T3 T3 T3 T3 T3

All resultfiles from NAMMU have the extension .res, hence, fisB.res is the resultfile from the base case run. The result files along with the Nammu input files have been stored on T3.

The numbers of the bodies outlining the various fracture zones in the model are listed in the files peaBrun, pealarun, pea1brun, pea2run and peaxrun. These files have been stored on T3.

Local model

File creation flow on cvx :

All files are stored on `/files/home/users/kemanb/0274/fil`

Mesh-generation

The input files to femgen have been stored on 3 inch disks. The files are called **PL_xy** where **x** and **y** runs from **A** to **H**, designating the 8 different layers in the model. Unfortunately, four of the files have been lost since these files was not originally intended to be saved for the quality assurance. The files lost are **AG**, **BC**, **CH** and **DE**.

neu/planag.NEU^{T1} --> [EMC]

[PFG] <--- emc/planag.DUP^{T1}

pfg/planag.PFC^{T3}
pfg/planag.PFG^{T3}

This is repeated for all 7 layers. (The pfg-files have been stored on T3 and the rest on T1)

neu/planag.neu	----> pfg/planag.PFG >I		
	--> pfg/planag.PFC >---> [JTM]	---> jtm/plangb.JTG	
neu/plangb.neu	----> pfg/plangb.PFG >I	---> jtm/plangb.JTC	
	--> pfg/plangb.PFC >I		
neu/planbc.neu	----> pfg/planbc.PFG >-----I		
	--> pfg/planbc.PFC >-----> [JTM]		
neu/planch.neu	----> pfg/planch.PFG		
	--> pfg/planch.PFC		
neu/planhd.neu	----> pfg/planhd.PFG		
	--> pfg/planhd.PFC		
neu/plande.neu	----> pfg/plande.PFG		
	--> pfg/plande.PFC		
neu/planef.neu	----> pfg/planef.PFG		
	--> pfg/planef.PFC		
		jtm/planef.JTG ^{T1}	
		jtm/planef.JTC ^{T1}	

Rest of preprocessing

jtm/planef.JTG^{T1}
jtm/planef.JTC^{T1}

[OPT]

opt/planef.OPG^{T1}

opt/planef.OPC^{T1}

[PEA] ;Assigning rock.perm
(pea/planef.PEG)
[IFZ] ;Assigning imp.frc.zones
(ifz/planef.IFG) (ifz/planef.IFP)
[PEA] ;Assigning exp.frc.zones
ssf/fil.ssf^{T3} **pea/planef.PEP^{T3}**
[AMT]
amt/planef.AMG^{T3}
[BCA] ;Assigning Pt zero on topsurface
bca/planef.BCG^{T3}

Preprocessing finished. Start to prepare for variations using files

Mesh : bca/planef.BCG^{T3}
Code : opt/planef.OPC^{T1}
Perm : pea/planef.PEP^{T3}

Base-Case and Variations

Note that the following notations have been used for file identification of the various variations made :

Notation in report	File notation
3DLSR	filsr
3DLSB	filsb
3DLS1	filsv
3DL1	filv1
3DL2	filv4

Base-Case :

opt/planef.OPG^{T1} [AMT] (amt/filsr.AMG) [PEA] (pea/filsr.PEG) ...
fis/ssf/fis.ssf^{T2}

... [BCA] bca/filsr.BCG^{T3} [TBC] tbc/filsr.TBG^{T3}
fis/pea/fisB.peg^{T3}
fis/nammu/fisb.res^{T3}

M : tbc/filsr.TBG^{T3}
P : pea/planef.PEP^{T3}

Reference-Case :

M : tbc/filsr.TBG^{T3}
P : Not used

SV (Subregional topography, Noflow lateral boundaries) :

M : bca/filsr.BCG^{T3}
P : pea/planef.PEP^{T3}

V1 (Noflow lateral boundaries) :

M : bca/planef.BCG^{T3}
P : pea/planef.PEP^{T3}

V4 (Hydraulic conductivities approximately corresponding to KBS3-values) :

bca/planef.BCG^{T3} [PEA] (pea/filv4a.PEG) [IFZ] (ifz/filv4.IFG) [PEA] ...
pea/planef.PEP^{T3} (ifz/filv4a.PEP) (ifz/filv4.IFP)

... [PEA] (pea/filv4.PEG)
pea/filv4.PEP^{T3}

Mesh : bca/planef.BCG^{T3}
Perm : pea/filv4.PEP^{T3}

All resultfiles from NAMMU have the extension .res, hence, fisb.res is the resultfile from the base case run. All result files along with the Nammu input files have been stored on T3.

The numbers of the bodies outlining the various fracture zones in the model are listed in the files z1214.bod, z113.bod, z4.bod, z3.bod, z2.bod and z2e.bod. The file z2e.bod holds the extended zone 2. These have been stored on tape T3.

Two-Dimensional model

File creation flow on Kemakta-Net :

All files are stored on **USR:0274\2D**

Mesh-generation

FIN2D.STP	[FEMGEN]	FIN.NEU
FIN.NEU	[PFG]	(FIN.PFG) (FIN.PFC)
(FIN.PFG)	[PEA]	(FIN.PEG)
(FIN.PEG)	[BCA]	(FIN.BCG)

Variations

Note that the following notations have been used for file identification of the various variations made :

Notation in report	File notation
2D1	TUS
2D2	TMS
2D3	HUS
2D4	HMS

The mesh-files for the variations was named FITUS.PEG, FITMS.PEG, FIHUS.BCG and FIHMS.BCG. These have been stored along with the Nammu input files (*.NAM).

No resultfiles have been stored since these are of no interest when having varying density (NAMMU post-processing facilities have been used). Instead files holding the results from the velocity field and pathline calculations have been stored. These have the extensions .VEL and .PTH respectively.

The files used for the two-dimensional calculations have been stored on 3 inch floppy disks and sent to SKB.

APPENDIX D

Description of the technique for modelling fracture zones implicitly.

General.

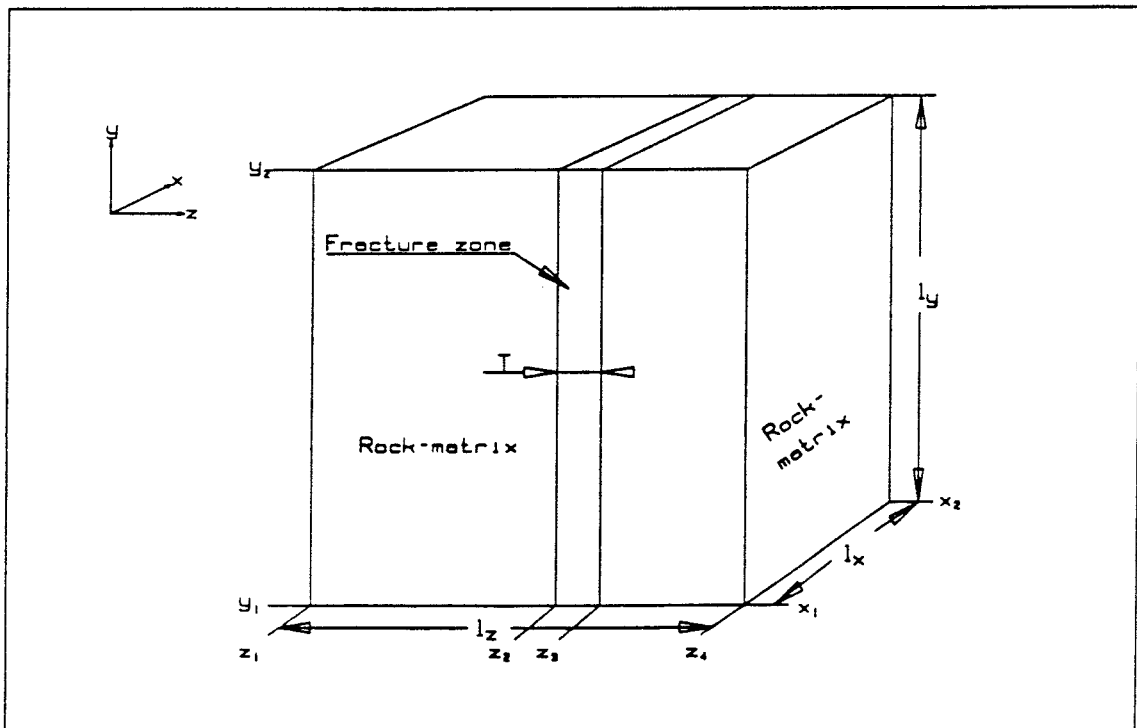
In this Appendix, a technique for averaging hydraulic conductivities is presented. A few assumptions are necessary to make. These assumptions, some simplifications, and the associated introduction of errors, are described. The method is based on the fact that the flow through a rectangular box with a fracture zone orthogonally crossing the box, easily can be computed analytically when some assumptions are made. How this technique is applied to the finite elements being used is also presented, as well as the introduction of an anisotropic medium in elements where a fracture zone is crossing the elements. The method is named "implicit fracture zones".

Computing flows and mean-conductivities through a rectangular box.

Consider the following flow problem. Define a rectangular box of rock with a fracture zone orthogonally crossing the box. The box is of the size $(l_x \cdot l_y \cdot l_z)$ and the fracture zone width is T . The following assumptions are made:

1. The fracture zone is of constant width throughout the box.
2. The hydraulic head takes constant values on each face of the box and on the surfaces of the fracture zone.
3. Both the rock-matrix and fracture zone have constant conductivity and are isotropic media.

Now a coordinate system parallel to the principal directions of the fracture zone (and rock-matrix) is defined. The direction of z is oriented in the normal direction to the fracture zone plane. The figure below illustrates the situation together with distances and coordinates used in the formulae.



The flow through the box in the z-direction is computed through the Darcy law.

$$\begin{aligned} Q_z &= K_z \cdot l_x \cdot l_y \cdot \frac{\Phi_{z1} - \Phi_{z4}}{l_z} = K_m \cdot l_x \cdot l_y \cdot \frac{\Phi_{z1} - \Phi_{z2}}{z_2 - z_1} = K_f \cdot l_x \cdot l_y \cdot \frac{\Phi_{z2} - \Phi_{z3}}{z_3 - z_2} = \\ &= K_m \cdot l_x \cdot l_y \cdot \frac{\Phi_{z3} - \Phi_{z4}}{z_4 - z_3}, \end{aligned} \quad (D.1)$$

where

- Q_z = flow in the z-direction,
- K_z = conductivity in the z-direction,
- K_m = conductivity for the rock-matrix,
- K_f = conductivity for the fracture zone,
- Φ_z = hydraulic head at the point z.

This leads to

$$\Phi_{z1} - \Phi_{z2} = \frac{Q_z \cdot (z_2 - z_1)}{K_m \cdot l_x \cdot l_y}, \quad (D.2)$$

$$\Phi_{z2} - \Phi_{z3} = \frac{Q_z \cdot (z_3 - z_2)}{K_f \cdot l_x \cdot l_y}, \quad (D.3)$$

$$\Phi_{z3} - \Phi_{z4} = \frac{Q_z \cdot (z_4 - z_3)}{K_m \cdot l_x \cdot l_y}. \quad (D.4)$$

Adding the equations (D.2)–(D.4) we obtain

$$\begin{aligned} \Phi_{z1} - \Phi_{z4} &= \frac{Q_z \cdot ((z_2 - z_1) + (z_4 - z_3))}{K_m \cdot l_x \cdot l_y} + \frac{Q_z \cdot (z_3 - z_2)}{K_f \cdot l_x \cdot l_y} = \\ &= \frac{Q_z \cdot (l_z - T)}{K_m \cdot l_x \cdot l_y} + \frac{Q_z \cdot T}{K_f \cdot l_x \cdot l_y} = \frac{Q_z \cdot l_z}{K_z \cdot l_x \cdot l_y}. \end{aligned} \quad (D.5)$$

The last step in (D.5) was derived from the first step in (D.1). Solving for K_z we arrive with

$$K_z = l_z \cdot \left[\frac{1}{\frac{(l_z - T)}{K_m} + \frac{T}{K_f}} \right]. \quad (D.6)$$

The flow in the x-direction is derived in a similar way (notations as above):

$$\begin{aligned} Q_x &= K_x \cdot l_z \cdot l_y \cdot \frac{\Phi_{x1} - \Phi_{x2}}{l_x} = K_f \cdot (T \cdot l_y) \cdot \frac{\Phi_{x1} - \Phi_{x2}}{l_x} + K_m \cdot (l_z \cdot l_y - T \cdot l_y) \cdot \frac{\Phi_{x1} - \Phi_{x2}}{l_x} = \\ &= (K_f \cdot (T \cdot l_y) + K_m \cdot (l_z \cdot l_y - T \cdot l_y)) \cdot \frac{\Phi_{x1} - \Phi_{x2}}{l_x}. \end{aligned} \quad (D.7)$$

Solving for K_x we obtain

$$K_x = \frac{K_f \cdot T + K_m \cdot (l_z - T)}{l_z} \quad (D.8)$$

The flow in the y-direction is defined analogously.

$$\begin{aligned} Q_y &= K_y \cdot l_z \cdot l_x \cdot \frac{\Phi_{y1} - \Phi_{y2}}{l_y} = K_f \cdot (T \cdot l_x) \cdot \frac{\Phi_{y1} - \Phi_{y2}}{l_y} + K_m \cdot (l_z \cdot l_x - T \cdot l_x) \cdot \frac{\Phi_{y1} - \Phi_{y2}}{l_y} = \\ &= (K_f \cdot (T \cdot l_x) + K_m \cdot (l_z \cdot l_x - T \cdot l_x)) \cdot \frac{\Phi_{y1} - \Phi_{y2}}{l_y}, \end{aligned} \quad (D.9)$$

thus

$$K_y = \frac{K_f \cdot T + K_m \cdot (l_z - T)}{l_z} \quad (D.10)$$

As noted K_x, K_y , and K_z all depend on K_f, K_m, l_z , and T , but not on l_x and l_y . In the direction of the fracture zone a mean conductivity is computed as a weighted arithmetic mean, and in the direction of the normal to the fracture zone plane a weighted harmonic mean is used.

Using mean conductivities on finite elements.

In ground-water flow calculations when finite elements are used, the elements are usually not shaped as boxes and the fracture zones cross the computational domain arbitrarily. The averaging technique above can still be used in an approximate manner. The following procedure is used for each element.

1. Check which fracture zone that crosses the element.
2. Calculate an approximation to the volume of the element E_v .
3. Calculate an approximation to the volume of the fracture zone inside the element F_v .
4. The volume fraction part is defined $V_{fp} = \frac{F_v}{E_v}$
5. In the formulas for K_x, K_y , and K_z , the values T and l_z are used. Since the element is of arbitrary shape, two such values must be set up. The spatial discretizations in the physical (sub) horizontal plane are assumed to be of the same magnitude, and this is true in most cases. Further, the fracture zones are settled to be horizontal or vertical (just for the mean calculations). If the fracture zone is horizontal, l_z is set equal to the spatial difference in the vertical direction for the element, and if the fracture zone is vertical, l_z is set to the spatial difference in one of the other directions. Since nothing is known about the way the fracture zone cuts the element (just the volume is known), the new fracture zone width is set as $T_n = V_{fp} \cdot l_z$. In such a procedure the most important information is retained.

6. $K_x, K_y,$ and K_z are computed with the formulas derived above (note that $x, y,$ and z correspond to the principal directions of the fracture zone).
7. Rotate the conductivity tensor $\begin{bmatrix} K_x & 0 & 0 \\ 0 & K_y & 0 \\ 0 & 0 & K_z \end{bmatrix}$ into the physical coordinate system, and the tensor will now become full unless the principal directions of the fracture zone coincide with the principal directions of the physical coordinate system.

A problem will arise when two or more fracture zones are crossing the same element. The average procedure will be much more complex in such a case. This is simplified by calculating the average as if the fracture zone with the highest conductivity of the crossing fracture zones is the only crossing fracture zone.

Errors introduced by the method.

The method described in the previous sections can sometimes introduce numerical errors compared with traditional finite element generation, where fracture zones are introduced in the rock by elements that are shaped as the fracture zones. However, by increasing the spatial discretization i.e. increasing the number of elements that are placed completely within the fracture zones, the errors will be limited. Another way of limiting the errors, is to use traditional finite element generation for those fracture zones that are assumed to be very significant for the flow. On the other hand, elements that are shaped as the fracture zones will model the flow with high contrasts of the conductivities along the boundaries of the fracture zones, while the implicit method will make the contrasts more smooth. The implicit method may therefore in some sense be a more correct modelling. Further, the explicit method may distort the geometry of the elements. The method described above allows the use of a combination of both explicitly and implicitly modelled fracture zones.

List of SKB reports

Annual Reports

1977-78

TR 121

KBS Technical Reports 1 – 120

Summaries

Stockholm, May 1979

1979

TR 79-28

The KBS Annual Report 1979

KBS Technical Reports 79-01 – 79-27

Summaries

Stockholm, March 1980

1980

TR 80-26

The KBS Annual Report 1980

KBS Technical Reports 80-01 – 80-25

Summaries

Stockholm, March 1981

1981

TR 81-17

The KBS Annual Report 1981

KBS Technical Reports 81-01 – 81-16

Summaries

Stockholm, April 1982

1982

TR 82-28

The KBS Annual Report 1982

KBS Technical Reports 82-01 – 82-27

Summaries

Stockholm, July 1983

1983

TR 83-77

The KBS Annual Report 1983

KBS Technical Reports 83-01 – 83-76

Summaries

Stockholm, June 1984

1984

TR 85-01

Annual Research and Development Report 1984

Including Summaries of Technical Reports Issued during 1984. (Technical Reports 84-01 – 84-19)

Stockholm, June 1985

1985

TR 85-20

Annual Research and Development Report 1985

Including Summaries of Technical Reports Issued during 1985. (Technical Reports 85-01 – 85-19)

Stockholm, May 1986

1986

TR 86-31

SKB Annual Report 1986

Including Summaries of Technical Reports Issued during 1986

Stockholm, May 1987

1987

TR 87-33

SKB Annual Report 1987

Including Summaries of Technical Reports Issued during 1987

Stockholm, May 1988

1988

TR 88-32

SKB Annual Report 1988

Including Summaries of Technical Reports Issued during 1988

Stockholm, May 1989

1989

TR 89-40

SKB Annual Report 1989

Including Summaries of Technical Reports Issued during 1989

Stockholm, May 1990

Technical Reports

List of SKB Technical Reports 1991

TR 91-01

Description of geological data in SKB's database GEOTAB

Version 2

Stefan Sehlstedt, Tomas Stark

SGAB, Luleå

January 1991

TR 91-02

Description of geophysical data in SKB database GEOTAB

Version 2

Stefan Sehlstedt

SGAB, Luleå

January 1991

TR 91-03

1. The application of PIE techniques to the study of the corrosion of spent oxide fuel in deep-rock ground waters

2. Spent fuel degradation

R S Forsyth

Studsvik Nuclear

January 1991

TR 91-04

Plutonium solubilities

I Puigdomènech¹, J Bruno²

¹Environmental Services, Studsvik Nuclear,
Nyköping, Sweden

²MBT Tecnologia Ambiental, CENT, Cerdanyola,
Spain

February 1991

TR 91-11

Impact from the disturbed zone on nuclide migration – a radioactive waste repository study

Akke Bengtsson¹, Bertil Grundfelt¹,

Anders Markström¹, Anders Rasmuson²

¹KEMAKTA Konsult AB

²Chalmers Institute of Technology

January 1991

TR 91-05

Description of tracer data in the SKB database GEOTAB

SGAB, Luleå

April, 1991

TR 91-06

Description of background data in the SKB database GEOTAB

Version 2

Ebbe Eriksson, Stefan Sehlstedt

SGAB, Luleå

March 1991

TR 91-07

Plutonium solubilities

Margareta Gerlach¹, Bengt Gentzschein²

¹SGAB, Luleå

²SGAB, Uppsala

April 1991

TR 91-08

Overview of geologic and geohydrologic conditions at the Finnsjön site and its surroundings

Kaj Ahlbom¹, Sven Tirén²

¹Conterra AB

²Sveriges Geologiska AB

January 1991

TR 91-09

Long term sampling and measuring program. Joint report for 1987, 1988 and 1989. Within the project: Fallout studies in the Gideå and Finnsjö areas after the Chernobyl accident in 1986

Thomas Ittner

SGAB, Uppsala

December 1990

TR 91-10

Sealing of rock joints by induced calcite precipitation. A case study from Bergeforsen hydro power plant

Eva Hakami¹, Anders Ekstav², Ulf Qvarfort²

¹Vattenfall HydroPower AB

²Golder Geosystem AB

January 1991